

OFFICIAL DOCUMENT

DO NOT REMOVE FROM
THE RESEARCH OFFICE

INVESTIGATION OF CULVERT HYDRAULICS RELATED TO JUVENILE FISH PASSAGE

WA-RD 388.2

Final Technical Report
January 1996



**Washington State
Department of Transportation**

Washington State Transportation Commission
Planning and Programming Service Center
in cooperation with the U.S. Department of Transportation
Federal Highway Administration

TECHNICAL REPORT STANDARD TITLE PAGE

1. REPORT NO. WA-RD 388.2	2. GOVERNMENT ACCESSION NO.	3. RECIPIENT'S CATALOG NO.	
4. TITLE AND SUBTITLE Investigation of Culvert Hydraulics Related to Juvenile Fish Passage		5. REPORT DATE January 1996	
		6. PERFORMING ORGANIZATION CODE	
7. AUTHOR(S) Michael E. Barber and Randall Craig Downs		8. PERFORMING ORGANIZATION REPORT NO.	
9. PERFORMING ORGANIZATION NAME AND ADDRESS Washington State Transportation Center (TRAC) Civil and Environmental Engineering; Sloan Hall, Room 101 Washington State University Pullman, Washington 99164-2910		10. WORK UNIT NO.	
		11. CONTRACT OR GRANT NO. T9902-07	
12. SPONSORING AGENCY NAME AND ADDRESS Washington State Department of Transportation Transportation Building, MS 7370 Olympia, Washington 98504-7370		13. TYPE OF REPORT AND PERIOD COVERED Technical Report	
		14. SPONSORING AGENCY CODE	
15. SUPPLEMENTARY NOTES This study was conducted in cooperation with the U.S. Department of Transportation, Federal Highway Administration.			
16. ABSTRACT <p style="text-align: center;"> Culverts often create barriers to the upstream migration of juvenile fish. Fish will not travel upstream under high water velocity conditions. It is hypothesized that low velocity regions exist near culvert boundaries. Therefore, the objective of this study was to determine hydraulic characteristics of culverts with different flow conditions. Methods of predicting flow profiles were developed by both Chiu and Mountjoy. Two equations were compared to experimental results. The Mountjoy equation proved to yield better results for velocity profile predictions. An area of flow corresponding to a predetermined allowable velocity can be calculated using the Mountjoy equation. This can then be used in the design of culverts as fish passage guidelines. The following technical report contains a detailed description of background information, experimental methodology, the results of experimental tests, and an analysis of both the Chiu and Mountjoy equations. </p>			
17. KEY WORDS Key words: Culvert, velocity profile, fish passage, hydraulics		18. DISTRIBUTION STATEMENT No restrictions. This document is available to the public through the National Technical Information Service, Springfield, VA 22616	
19. SECURITY CLASSIF. (of this report) <p style="text-align: center;">None</p>	20. SECURITY CLASSIF. (of this page) <p style="text-align: center;">None</p>	21. NO. OF PAGES <p style="text-align: center;">172</p>	22. PRICE

Technical Report

Research Project T9902, Task 7
Fish Passage Culvert Design

**INVESTIGATION OF CULVERT HYDRAULICS
RELATED TO JUVENILE FISH PASSAGE**

by

Michael E. Barber
Assistant Professor of Civil Engineering
Washington State University

Randall Craig Downs
Graduate Research Assistant
Washington State University

Washington State Transportation Center (TRAC)
Washington State University
Department of Civil and Environmental Engineering
Pullman, WA 99164-2910

Washington State Department of Transportation
Technical Monitor
J.A. Schafer
Chief Biologist

Prepared for

Washington State Transportation Commission
Department of Transportation
and in cooperation with
U.S. Department of Transportation
Federal Highway Administration

January 1996

DISCLAIMER

The contents of this report reflect the views of the authors, who are responsible for the facts and the accuracy of the data presented herein. The contents do not necessarily reflect the official views or policies of the Washington State Transportation Commission, Department of Transportation, or the Federal Highway Administration. This report does not constitute a standard, specification, or regulation.

Table of Contents

	Page
List of Tables	vi
List of Figures	vii
Executive Summary	xviii
Chapter	
1. Introduction	1
1.1 Problem Statement	1
1.2 Objectives	3
2. Literature Review / Background Information	4
2.1 General Background	4
2.2 Literature Review	4
2.2.1 Fish Passage in Culverts: Problems and Requirements	5
2.2.2 Modeling Flow in Culverts	11
2.2.3 Typical Gradually Varied Flow Profiles	17
2.2.4 Velocity Profiles	19
2.2.5 Field Observations and Experimental Data	24
2.3 Discussion of Existing Knowledge	29
2.3.1 Limitations of Existing Knowledge	31
2.3.2 Extension of Existing Knowledge	32
3. Methodology	33
3.1 Experimental Setup	33
3.1.1 Flume	33
3.1.2 Nixon Model 403 Low Speed Probe w/ Streamflo Model 422 Digital Indicator	36
3.1.3 Apple Macintosh Quadra 650 w/ I/O Board	37
3.2 Calibration and Verification of Experimental Setup	38
3.3 Experimental Procedure	40
3.3.1 Culvert Selection	40
3.3.2 Testing Procedure	43
4. Results	51

4.1	Tabulation of Results.....	53
4.2	Effective Cross-Section.....	53
4.3	Scaling Theory.....	56
4.3.1	Application of Chiu Equation.....	58
4.3.2	Application of Mountjoy Equation.....	66
4.4	Observation and Discussion.....	68
4.4.1	Qualitative Observations	68
4.4.2	Gradually Varied Flow.....	72
4.4.3	Discussion	73
4.5	Sensitivity Analysis of Equation Fits.....	74
4.5.1	Chiu Equation Sensitivity Analysis.....	74
4.5.2	Mountjoy Equation Sensitivity Analysis	81
4.6	Horizontal Velocity Profiles.....	83
4.6.1	Effective Width Calculation.....	83
5.	Summary and Conclusions	87
5.1	Summary	87
5.2	Conclusions	88
5.2.1	Limitations of Conclusions	88
5.3	Recommendations for Further Studies.....	89
	References.....	90
Appendix		
A.	Manning Roughness Coefficient Plots.....	93
B.	Velocity Contour Plots.....	96
C.	Plots of One-Dimensional Velocity Contour Plots for: Experimental Data, Chiu Equation, and Mountjoy Equation	123
D.	Horizontal Velocity Profiles.....	141
E.	Example Problem	168

LIST OF TABLES

	Page
3.1 Experimental Culverts.....	41
3.2 Experimental Runs.....	49
4.1 Continuity Check	52
4.2 Parameters for Experimental Runs.....	54
4.3 Band Widths for Effective Cross-Section.....	57
4.4 Calculated Entropy Parameters.....	62
4.5 Statistical Parameters for Chiu Equation Fit	65
4.6 Statistical Parameters for Mountjoy Equation Fit	67
4.7 Computation of the Flow Profile by the Direct Step Method.....	72

LIST OF FIGURES

		Page
2.1	Relationship between fork length and ability to move 100 meters in 10 minutes in water velocities up to 80 cm/s for fish from the MacKenzie River (from Jones et al. 1974).....	8
2.2	Relative length versus relative swimming velocity for fish based on grayling data (from MacPhee and Watts, 1976).	9
2.3	Swimming capability of migration salmon (Alaska curve, from Ziemer, 1965; and Evans and Johnston, 1980).....	10
2.4	Sustained speed versus fork length for juvenile salmon (from USDA Forest Service, 1978).....	11
2.5	Diagram of circular culvert cross-section flowing partially full.....	13
2.6	Manning n versus diameter for 6.8 x 1.3 cm (2 2/3 x 1/2 in) and 7.6 x 2.3 cm (3 x 1 in) annular corrugated metal pipe.	14
2.7	Classifications of culvert flow (from Chow, 1959).....	18
2.8(a-b)	Distribution of normal and lateral velocity components in a straight rectangular channel (Modified from Chow, 1959).	26
2.9	Relative velocity profile for 13.3 cm diameter steel pipe with a flow rate of 0.0014 m ³ /s, slope of 0.2%, and relative depth of 0.33*D _o	27
2.10	Relative velocity profile for 13.3 cm diameter steel pipe with a flow rate of 0.0034 m ³ /s, slope of 0.2%, and relative depth of 0.50*D _o	27
2.11	Relative velocity profile for 13.3 cm diameter steel pipe with a flow rate of 0.0049 m ³ /s, slope of 0.2%, and relative depth of 0.68*D _o	28
2.12	Relative velocity profile for 13.3 cm diameter steel pipe with a flow rate of 0.0106 m ³ /s, slope of 0.8%, and relative depth of 0.65*D _o	28
2.13(a-b)	Velocity profiles at upstream and downstream stations with a flow rate of 12.2 m ³ /s (Modified from Katopodis et al. 1978).	30
2.14(a-b)	Velocity profiles at upstream and downstream stations with a flow rate of 3.8 m ³ /s (Modified from Katopodis et al. 1978).....	30
2.15	Velocity cross-section from 2.9 meter diameter culvert, with 15.2 x 3.5 cm annular corrugations, in Fish Creek Denali Highway, Alaska. Flow rate was 3.06 m ³ /s. (Modified from Behlke et al. 1989).....	31
3.1	Schematic drawing of flume.	34
3.2	Schematic drawing of tailgate.....	35
3.3	Honeycomb flow aligner.....	35
3.4	Schematic drawing of transitional entrance structure.....	36
3.5	Schematic drawing of Nixon probe mounting.....	38

3.6	Shapes of Annular Corrugations for 6.8 x 1.3 cm and 7.6 x 2.5 cm corrugations.....	42
3.7	Diagram of corrugated coupling band and band angle connector.....	43
3.8	Centerline velocity profiles at 0.113 m ³ /s, slope = 0.5%, relative depth = 0.5*D ₀ , with no downstream control.....	45
4.1	Example of non-symmetrical relative velocity contour plot for Culvert #2. Discharge = 0.0850 m ³ /s, Slope = 0.5%, V _{max} = 69.1 cm/s, taken at L/D = 12.....	55
4.2	Illustration of effective area concept.....	56
4.3	Plot of V _{max} versus V _{avg} for Culvert #1 with linear regression line and equation.....	59
4.4	Plot of V _{max} versus V _{avg} for Culvert #2 with linear regression line and equation.....	59
4.5	Plot of V _{max} versus V _{avg} for Culvert #3 with linear regression line and equation.....	60
4.6	Plot of V _{max} versus V _{avg} for Culvert #4 with linear regression line and equation.....	60
4.7	Plot of $\frac{V_{avg}}{V_{max}}$ versus $\frac{CorrugationHeight}{PipeDiameter}$ with linear regression line and equation.....	61
4.8	Plot of best fit entropy parameter (M) versus velocity head coefficient (α)....	63
4.9	Plot of best fit entropy parameter (M) versus momentum coefficient (β).....	63
4.10	Velocity profile from Culvert #1 at Q=0.0527 m ³ /s, 3% slope, 14 Diameters from the entrance, with no downstream control, and V _{max} = 159.6 cm/s.....	68
4.11	Velocity profile from Culvert #2 at Q=0.0566 m ³ /s; 1% slope, 14 Diameters from the entrance, with downstream control, and V _{max} = 37.6 cm/s.	69
4.12	Velocity profile from Culvert #3 at Q=0.0153 m ³ /s, 0.5% slope, 8 Diameters from the entrance, with downstream control, and V _{max} = 29.1 cm/s.....	70
4.13	Velocity profile from Culvert #4 at Q=0.0850 m ³ /s, 1% slope, 7 Diameters from the entrance, with downstream control, and V _{max} = 54.2 cm/s.....	71
4.14	Illustration of gradually varied flow through a culvert approaching normal depth. (Modified from Chow, 1959).	73
4.15	Absolute value of Bias for Chiu and Mountjoy equations plotted for each run.....	76

4.16	Plot of MAE for Chiu and Mountjoy equations for each run.....	77
4.17	Plot of RMSE for Chiu and Mountjoy equations for each run.....	78
4.18	Plot of % error in relative velocity versus relative depth for Culvert #1.....	79
4.19	Plot of % error in relative velocity versus relative depth for Culvert #2.....	79
4.20	Plot of % error in relative velocity versus relative depth for Culvert #3.....	80
4.21	Plot of % error in relative velocity versus relative depth for Culvert #4.....	80
4.22	Plot of % error in velocity versus relative depth for a typical experimental run in Culvert #1.....	81
4.23	Plot of % error in velocity versus relative depth for a typical experimental run in Culvert #2.....	82
4.24	Plot of % error in velocity versus relative depth for a typical experimental run in Culvert #3.....	82
4.25	Plot of % error in velocity versus relative depth for a typical experimental run in Culvert #4.....	83
4.26	Migration zones for juvenile fish passage.....	85
4.27	Downs Correction Factor for width adjustment.....	86
A2.1	Manning roughness coefficient (n) versus Diameter for 14.9 x 2.5 cm annular corrugated metal pipe.....	94
A2.2	Manning roughness coefficient (n) versus Diameter for 14.9 x 5.0 cm annular structural plate corrugated metal pipe.....	94
A2.3	Manning roughness coefficient (n) versus Diameter for 22.3 x 6.2 cm annular structural plate corrugated metal pipe.....	95
B4.1	Velocity contour plot for Culvert #1 at $Q = 0.0052 \text{ m}^3/\text{s}$, 5% slope, $0.17D_o$, $L/D = 14$, no downstream control, $V_{\max} = 101.9 \text{ cm/s}$	97
B4.2	Velocity contour plot for Culvert #1 at $Q = 0.0064 \text{ m}^3/\text{s}$, 3% slope, $0.23D_o$, $L/D = 14$, no downstream control, $V_{\max} = 82.0 \text{ cm/s}$	97
B4.3	Velocity contour plot for Culvert #1 at $Q = 0.0082 \text{ m}^3/\text{s}$, 1% slope, $0.34D_o$, $L/D = 14$, no downstream control, $V_{\max} = 61.2 \text{ cm/s}$	98
B4.4	Velocity contour plot for Culvert #1 at $Q = 0.0094 \text{ m}^3/\text{s}$, 0.5% slope, $0.34D_o$, $L/D = 14$, no downstream control, $V_{\max} = 59.9 \text{ cm/s}$	98
B4.5	Velocity contour plot for Culvert #1 at $Q = 0.0124 \text{ m}^3/\text{s}$, 0.5% slope, $0.68D_o$, $L/D = 14$, downstream control, $V_{\max} = 34.5 \text{ cm/s}$	99
B4.6	Velocity contour plot for Culvert #1 at $Q = 0.0124 \text{ m}^3/\text{s}$, 1% slope, $0.76D_o$, $L/D = 14$, downstream control, $V_{\max} = 33.2 \text{ cm/s}$	99
B4.7	Velocity contour plot for Culvert #1 at $Q = 0.0142 \text{ m}^3/\text{s}$, 5% slope, $0.49D_o$, $L/D = 14$, downstream control, $V_{\max} = 63.1 \text{ cm/s}$	100
B4.8	Velocity contour plot for Culvert #1 at $Q = 0.0213 \text{ m}^3/\text{s}$, 0.5% slope, $0.56D_o$, $L/D = 14$, downstream control, $V_{\max} = 85.1 \text{ cm/s}$	100

B4.9	Velocity contour plot for Culvert #1 at $Q = 0.0278 \text{ m}^3/\text{s}$, 3% slope, $0.43D_o$, $L/D = 14$, no downstream control, $V_{\text{max}} = 125.9 \text{ cm/s}$	101
B4.10	Velocity contour plot for Culvert #1 at $Q = 0.0284 \text{ m}^3/\text{s}$, 1% slope, $0.52D_o$, $L/D = 14$, no downstream control, $V_{\text{max}} = 92.7 \text{ cm/s}$	101
B4.11	Velocity contour plot for Culvert #1 at $Q = 0.0290 \text{ m}^3/\text{s}$, 5% slope, $0.39D_o$, $L/D = 14$, no downstream control, $V_{\text{max}} = 169.3 \text{ cm/s}$	102
B4.12	Velocity contour plot for Culvert #1 at $Q = 0.0438 \text{ m}^3/\text{s}$, 5% slope, $0.46D_o$, $L/D = 14$, no downstream control, $V_{\text{max}} = 178.0 \text{ cm/s}$	102
B4.13	Velocity contour plot for Culvert #1 at $Q = 0.0456 \text{ m}^3/\text{s}$, 0.5% slope, $0.72D_o$, $L/D = 14$, no downstream control, $V_{\text{max}} = 108.5 \text{ cm/s}$	103
B4.14	Velocity contour plot for Culvert #1 at $Q = 0.0527 \text{ m}^3/\text{s}$, 3% slope, $0.62D_o$, $L/D = 14$, no downstream control, $V_{\text{max}} = 159.6 \text{ cm/s}$	103
B4.15	Velocity contour plot for Culvert #1 at $Q = 0.0539 \text{ m}^3/\text{s}$, 1% slope, $0.79D_o$, $L/D = 14$, no downstream control, $V_{\text{max}} = 124.4 \text{ cm/s}$	104
B4.16	Velocity contour plot for Culvert #2 at $Q = 0.0153 \text{ m}^3/\text{s}$, 0.5% slope, $0.38D_o$, $L/D = 14$, downstream control, $V_{\text{max}} = 26.4 \text{ cm/s}$	104
B4.17	Velocity contour plot for Culvert #2 at $Q = 0.0153 \text{ m}^3/\text{s}$, 0.5% slope, $0.33D_o$, $L/D = 8$, downstream control, $V_{\text{max}} = 29.2 \text{ cm/s}$	105
B4.18	Velocity contour plot for Culvert #2 at $Q = 0.0153 \text{ m}^3/\text{s}$, 1% slope, $0.39D_o$, $L/D = 14$, downstream control, $V_{\text{max}} = 25.2 \text{ cm/s}$	105
B4.19	Velocity contour plot for Culvert #2 at $Q = 0.0283 \text{ m}^3/\text{s}$, 0.5% slope, $0.58D_o$, $L/D = 14$, downstream control, $V_{\text{max}} = 22.8 \text{ cm/s}$	106
B4.20	Velocity contour plot for Culvert #2 at $Q = 0.0283 \text{ m}^3/\text{s}$, 0.5% slope, $0.56D_o$, $L/D = 8$, downstream control, $V_{\text{max}} = 26.6 \text{ cm/s}$	106
B4.21	Velocity contour plot for Culvert #2 at $Q = 0.0396 \text{ m}^3/\text{s}$, 0.5% slope, $0.25D_o$, $L/D = 14$, no downstream control, $V_{\text{max}} = 90.1 \text{ cm/s}$	107
B4.22	Velocity contour plot for Culvert #2 at $Q = 0.0396 \text{ m}^3/\text{s}$, 0.5% slope, $0.25D_o$, $L/D = 8$, downstream control, $V_{\text{max}} = 84.9 \text{ cm/s}$	107
B4.23	Velocity contour plot for Culvert #2 at $Q = 0.0515 \text{ m}^3/\text{s}$, 1% slope, $0.25D_o$, $L/D = 14$, no downstream control, $V_{\text{max}} = 108.0 \text{ cm/s}$	108
B4.24	Velocity contour plot for Culvert #2 at $Q = 0.0566 \text{ m}^3/\text{s}$, 0.5% slope, $0.50D_o$, $L/D = 1$, downstream control, $V_{\text{max}} = 51.3 \text{ cm/s}$	108
B4.25	Velocity contour plot for Culvert #2 at $Q = 0.0566 \text{ m}^3/\text{s}$, 0.5% slope, $0.55D_o$, $L/D = 12$, downstream control, $V_{\text{max}} = 46.3 \text{ cm/s}$	109
B4.26	Velocity contour plot for Culvert #2 at $Q = 0.0566 \text{ m}^3/\text{s}$, 0.5% slope, $0.57D_o$, $L/D = 14$, downstream control, $V_{\text{max}} = 41.8 \text{ cm/s}$	109
B4.27	Velocity contour plot for Culvert #2 at $Q = 0.0566 \text{ m}^3/\text{s}$, 0.5% slope, $0.56D_o$, $L/D = 8$, downstream control, $V_{\text{max}} = 44.9 \text{ cm/s}$	110

B4.28 Velocity contour plot for Culvert #2 at $Q = 0.0566 \text{ m}^3/\text{s}$, 1% slope, $0.62D_o$, $L/D = 14$, downstream control, $V_{\max} = 37.6 \text{ cm/s}$110

B4.29 Velocity contour plot for Culvert #2 at $Q = 0.0850 \text{ m}^3/\text{s}$, 0.5% slope, $0.54D_o$, $L/D = 12$, downstream control, $V_{\max} = 69.1 \text{ cm/s}$111

B4.30 Velocity contour plot for Culvert #2 at $Q = 0.0850 \text{ m}^3/\text{s}$, 0.5% slope, $0.54D_o$, $L/D = 14$, downstream control, $V_{\max} = 64.2 \text{ cm/s}$111

B4.31 Velocity contour plot for Culvert #2 at $Q = 0.0850 \text{ m}^3/\text{s}$, 0.5% slope, $0.54D_o$, $L/D = 8$, downstream control, $V_{\max} = 69.8 \text{ cm/s}$112

B4.32 Velocity contour plot for Culvert #2 at $Q = 0.0850 \text{ m}^3/\text{s}$, 0.5% slope, $0.50D_o$, at entrance, downstream control, $V_{\max} = 71.5 \text{ cm/s}$112

B4.33 Velocity contour plot for Culvert #2 at $Q = 0.0850 \text{ m}^3/\text{s}$, 1% slope, $0.63D_o$, $L/D = 14$, downstream control, $V_{\max} = 58.2 \text{ cm/s}$113

B4.34 Velocity contour plot for Culvert #2 at $Q = 0.1274 \text{ m}^3/\text{s}$, 0.5% slope, $0.50D_o$, $L/D = 8$, no downstream control, $V_{\max} = 118.4 \text{ cm/s}$113

B4.35 Velocity contour plot for Culvert #3 at $Q = 0.0153 \text{ m}^3/\text{s}$, 0.5% slope, $0.31D_o$, $L/D = 8$, downstream control, $V_{\max} = 22.2 \text{ cm/s}$114

B4.36 Velocity contour plot for Culvert #3 at $Q = 0.0153 \text{ m}^3/\text{s}$, 1% slope, $0.62D_o$, $L/D = 8$, downstream control, $V_{\max} = 9.9 \text{ cm/s}$114

B4.37 Velocity contour plot for Culvert #3 at $Q = 0.0153 \text{ m}^3/\text{s}$, 0.5% slope, $0.33D_o$, $L/D = 8$, downstream control, $V_{\max} = 20.5 \text{ cm/s}$115

B4.38 Velocity contour plot for Culvert #3 at $Q = 0.0566 \text{ m}^3/\text{s}$, 0.5% slope, $0.57D_o$, $L/D = 8$, downstream control, $V_{\max} = 31.2 \text{ cm/s}$115

B4.39 Velocity contour plot for Culvert #3 at $Q = 0.0566 \text{ m}^3/\text{s}$, 1% slope, $0.58D_o$, $L/D = 8$, downstream control, $V_{\max} = 33.9 \text{ cm/s}$116

B4.40 Velocity contour plot for Culvert #3 at $Q = 0.0575 \text{ m}^3/\text{s}$, 0.5% slope, $0.24D_o$, $L/D = 8$, no downstream control, $V_{\max} = 120.8 \text{ cm/s}$116

B4.41 Velocity contour plot for Culvert #3 at $Q = 0.0664 \text{ m}^3/\text{s}$, 1% slope, $0.25D_o$, $L/D = 8$, no downstream control, $V_{\max} = 135.1 \text{ cm/s}$117

B4.42 Velocity contour plot for Culvert #3 at $Q = 0.0850 \text{ m}^3/\text{s}$, 0.5% slope, $0.57D_o$, $L/D = 8$, downstream control, $V_{\max} = 46.6 \text{ cm/s}$117

B4.43 Velocity contour plot for Culvert #3 at $Q = 0.0850 \text{ m}^3/\text{s}$, 1% slope, $0.59D_o$, $L/D = 8$, downstream control, $V_{\max} = 44.2 \text{ cm/s}$118

B4.44 Velocity contour plot for Culvert #4 at $Q = 0.0153 \text{ m}^3/\text{s}$, 0.5% slope, $0.28D_o$, $L/D = 7$, downstream control, $V_{\max} = 27.4 \text{ cm/s}$118

B4.45 Velocity contour plot for Culvert #4 at $Q = 0.0153 \text{ m}^3/\text{s}$, 0.5% slope, $0.33D_o$, $L/D = 7$, downstream control, $V_{\max} = 23.1 \text{ cm/s}$119

B4.46 Velocity contour plot for Culvert #4 at $Q = 0.0500 \text{ m}^3/\text{s}$, 0.5% slope, $0.23D_o$, $L/D = 7$, no downstream control, $V_{\max} = 127.2 \text{ cm/s}$119

B4.47	Velocity contour plot for Culvert #4 at $Q = 0.0563 \text{ m}^3/\text{s}$, 1% slope, 0.22 D_o , $L/D = 7$, no downstream control, $V_{\text{max}} = 140.2 \text{ cm/s}$	120
B4.48	Velocity contour plot for Culvert #4 at $Q = 0.0566 \text{ m}^3/\text{s}$, 0.5% slope, 0.57 D_o , $L/D = 7$, downstream control, $V_{\text{max}} = 38.9 \text{ cm/s}$	120
B4.49	Velocity contour plot for Culvert #4 at $Q = 0.0566 \text{ m}^3/\text{s}$, 1% slope, 0.59 D_o , $L/D = 7$, downstream control, $V_{\text{max}} = 36.8 \text{ cm/s}$	121
B4.50	Velocity contour plot for Culvert #4 at $Q = 0.0850 \text{ m}^3/\text{s}$, 0.5% slope, 0.56 D_o , $L/D = 7$, downstream control, $V_{\text{max}} = 59.7 \text{ cm/s}$	121
B4.51	Velocity contour plot for Culvert #4 at $Q = 0.0850 \text{ m}^3/\text{s}$, 1% slope, 0.58 D_o , $L/D = 7$, downstream control, $V_{\text{max}} = 54.2 \text{ cm/s}$	122
C4.1	Centerline velocity plots for Culvert #1 at $Q = 0.0052 \text{ m}^3/\text{s}$, 5% slope, 0.17 D_o , $L/D = 14$, no downstream control, $V_{\text{max}} = 101.9 \text{ cm/s}$	124
C4.2	Centerline velocity plots for Culvert #1 at $Q = 0.0064 \text{ m}^3/\text{s}$, 3% slope, 0.23 D_o , $L/D = 14$, no downstream control, $V_{\text{max}} = 82.0 \text{ cm/s}$	124
C4.3	Centerline velocity plots for Culvert #1 at $Q = 0.0082 \text{ m}^3/\text{s}$, 1% slope, 0.34 D_o , $L/D = 14$, no downstream control, $V_{\text{max}} = 61.2 \text{ cm/s}$	124
C4.4	Centerline velocity plots for Culvert #1 at $Q = 0.0094 \text{ m}^3/\text{s}$, 0.5% slope, 0.34 D_o , $L/D = 14$, no downstream control, $V_{\text{max}} = 59.9 \text{ cm/s}$	125
C4.5	Centerline velocity plots for Culvert #1 at $Q = 0.0124 \text{ m}^3/\text{s}$, 0.5% slope, 0.68 D_o , $L/D = 14$, downstream control, $V_{\text{max}} = 34.5 \text{ cm/s}$	125
C4.6	Centerline velocity plots for Culvert #1 at $Q = 0.0124 \text{ m}^3/\text{s}$, 1% slope, 0.76 D_o , $L/D = 14$, downstream control, $V_{\text{max}} = 33.2 \text{ cm/s}$	125
C4.7	Centerline velocity plots for Culvert #1 at $Q = 0.0142 \text{ m}^3/\text{s}$, 5% slope, 0.49 D_o , $L/D = 14$, downstream control, $V_{\text{max}} = 63.1 \text{ cm/s}$	126
C4.8	Centerline velocity plots for Culvert #1 at $Q = 0.0213 \text{ m}^3/\text{s}$, 0.5% slope, 0.56 D_o , $L/D = 14$, downstream control, $V_{\text{max}} = 85.1 \text{ cm/s}$	126
C4.9	Centerline velocity plots for Culvert #1 at $Q = 0.0278 \text{ m}^3/\text{s}$, 3% slope, 0.43 D_o , $L/D = 14$, no downstream control, $V_{\text{max}} = 125.9 \text{ cm/s}$	126
C4.10	Centerline velocity plots for Culvert #1 at $Q = 0.0284 \text{ m}^3/\text{s}$, 1% slope, 0.52 D_o , $L/D = 14$, no downstream control, $V_{\text{max}} = 92.7 \text{ cm/s}$	127
C4.11	Centerline velocity plots for Culvert #1 at $Q = 0.0290 \text{ m}^3/\text{s}$, 5% slope, 0.39 D_o , $L/D = 14$, no downstream control, $V_{\text{max}} = 169.3 \text{ cm/s}$	127
C4.12	Centerline velocity plots for Culvert #1 at $Q = 0.0438 \text{ m}^3/\text{s}$, 5% slope, 0.46 D_o , $L/D = 14$, no downstream control, $V_{\text{max}} = 178.0 \text{ cm/s}$	127
C4.13	Centerline velocity plots for Culvert #1 at $Q = 0.0456 \text{ m}^3/\text{s}$, 0.5% slope, 0.72 D_o , $L/D = 14$, no downstream control, $V_{\text{max}} = 108.5 \text{ cm/s}$	128
C4.14	Centerline velocity plots for Culvert #1 at $Q = 0.0527 \text{ m}^3/\text{s}$, 3% slope, 0.62 D_o , $L/D = 14$, no downstream control, $V_{\text{max}} = 159.6 \text{ cm/s}$	128

C4.15	Centerline velocity plots for Culvert #1 at $Q = 0.0539 \text{ m}^3/\text{s}$, 1% slope, $0.79D_o$, $L/D = 14$, no downstream control, $V_{\text{max}} = 124.4 \text{ cm/s}$	128
C4.16	Centerline velocity plots for Culvert #2 at $Q = 0.0153 \text{ m}^3/\text{s}$, 0.5% slope, $0.38D_o$, $L/D = 14$, downstream control, $V_{\text{max}} = 26.4 \text{ cm/s}$	129
C4.17	Centerline velocity plots for Culvert #2 at $Q = 0.0153 \text{ m}^3/\text{s}$, 0.5% slope, $0.33D_o$, $L/D = 8$, downstream control, $V_{\text{max}} = 29.2 \text{ cm/s}$	129
C4.18	Centerline velocity plots for Culvert #2 at $Q = 0.0153 \text{ m}^3/\text{s}$, 1% slope, $0.39D_o$, $L/D = 14$, downstream control, $V_{\text{max}} = 25.2 \text{ cm/s}$	129
C4.19	Centerline velocity plots for Culvert #2 at $Q = 0.0283 \text{ m}^3/\text{s}$, 0.5% slope, $0.58D_o$, $L/D = 14$, downstream control, $V_{\text{max}} = 22.8 \text{ cm/s}$	130
C4.20	Centerline velocity plots for Culvert #2 at $Q = 0.0283 \text{ m}^3/\text{s}$, 0.5% slope, $0.56D_o$, $L/D = 8$, downstream control, $V_{\text{max}} = 26.6 \text{ cm/s}$	130
C4.21	Centerline velocity plots for Culvert #2 at $Q = 0.0396 \text{ m}^3/\text{s}$, 0.5% slope, $0.25D_o$, $L/D = 14$, no downstream control, $V_{\text{max}} = 90.1 \text{ cm/s}$	130
C4.22	Centerline velocity plots for Culvert #2 at $Q = 0.0396 \text{ m}^3/\text{s}$, 0.5% slope, $0.25D_o$, $L/D = 8$, downstream control, $V_{\text{max}} = 84.9 \text{ cm/s}$	131
C4.23	Centerline velocity plots for Culvert #2 at $Q = 0.0515 \text{ m}^3/\text{s}$, 1% slope, $0.25D_o$, $L/D = 14$, no downstream control, $V_{\text{max}} = 108.0 \text{ cm/s}$	131
C4.24	Centerline velocity plots for Culvert #2 at $Q = 0.0566 \text{ m}^3/\text{s}$, 0.5% slope, $0.50D_o$, $L/D = 1$, downstream control, $V_{\text{max}} = 51.3 \text{ cm/s}$	131
C4.25	Centerline velocity plots for Culvert #2 at $Q = 0.0566 \text{ m}^3/\text{s}$, 0.5% slope, $0.55D_o$, $L/D = 12$, downstream control, $V_{\text{max}} = 46.3 \text{ cm/s}$	132
C4.26	Centerline velocity plots for Culvert #2 at $Q = 0.0566 \text{ m}^3/\text{s}$, 0.5% slope, $0.57D_o$, $L/D = 14$, downstream control, $V_{\text{max}} = 41.8 \text{ cm/s}$	132
C4.27	Centerline velocity plots for Culvert #2 at $Q = 0.0566 \text{ m}^3/\text{s}$, 0.5% slope, $0.56D_o$, $L/D = 8$, downstream control, $V_{\text{max}} = 44.9 \text{ cm/s}$	132
C4.28	Centerline velocity plots for Culvert #2 at $Q = 0.0566 \text{ m}^3/\text{s}$, 1% slope, $0.62D_o$, $L/D = 14$, downstream control, $V_{\text{max}} = 37.6 \text{ cm/s}$	133
C4.29	Centerline velocity plots for Culvert #2 at $Q = 0.0850 \text{ m}^3/\text{s}$, 0.5% slope, $0.54D_o$, $L/D = 12$, downstream control, $V_{\text{max}} = 69.1 \text{ cm/s}$	133
C4.30	Centerline velocity plots for Culvert #2 at $Q = 0.0850 \text{ m}^3/\text{s}$, 0.5% slope, $0.54D_o$, $L/D = 14$, downstream control, $V_{\text{max}} = 64.2 \text{ cm/s}$	133
C4.31	Centerline velocity plots for Culvert #2 at $Q = 0.0850 \text{ m}^3/\text{s}$, 0.5% slope, $0.54D_o$, $L/D = 8$, downstream control, $V_{\text{max}} = 69.8 \text{ cm/s}$	134
C4.32	Centerline velocity plots for Culvert #2 at $Q = 0.0850 \text{ m}^3/\text{s}$, 0.5% slope, $0.50D_o$, at entrance, downstream control, $V_{\text{max}} = 71.5 \text{ cm/s}$	134
C4.33	Centerline velocity plots for Culvert #2 at $Q = 0.0850 \text{ m}^3/\text{s}$, 1% slope, $0.63D_o$, $L/D = 14$, downstream control, $V_{\text{max}} = 58.2 \text{ cm/s}$	134

C4.34	Centerline velocity plots for Culvert #2 at $Q = 0.1274 \text{ m}^3/\text{s}$, 0.5% slope, $0.50D_o$, $L/D = 8$, no downstream control, $V_{\max} = 118.4 \text{ cm/s}$	135
C4.35	Centerline velocity plots for Culvert #3 at $Q = 0.0153 \text{ m}^3/\text{s}$, 0.5% slope, $0.31D_o$, $L/D = 8$, downstream control, $V_{\max} = 22.2 \text{ cm/s}$	135
C4.36	Centerline velocity plots for Culvert #3 at $Q = 0.0153 \text{ m}^3/\text{s}$, 1% slope, $0.62D_o$, $L/D = 8$, downstream control, $V_{\max} = 9.9 \text{ cm/s}$	135
C4.37	Centerline velocity plots for Culvert #3 at $Q = 0.0153 \text{ m}^3/\text{s}$, 0.5% slope, $0.33D_o$, $L/D = 8$, downstream control, $V_{\max} = 20.5 \text{ cm/s}$	136
C4.38	Centerline velocity plots for Culvert #3 at $Q = 0.0566 \text{ m}^3/\text{s}$, 0.5% slope, $0.57D_o$, $L/D = 8$, downstream control, $V_{\max} = 31.2 \text{ cm/s}$	136
C4.39	Centerline velocity plots for Culvert #3 at $Q = 0.0566 \text{ m}^3/\text{s}$, 1% slope, $0.58D_o$, $L/D = 8$, downstream control, $V_{\max} = 33.9 \text{ cm/s}$	136
C4.40	Centerline velocity plots for Culvert #3 at $Q = 0.0575 \text{ m}^3/\text{s}$, 0.5% slope, $0.24D_o$, $L/D = 8$, no downstream control, $V_{\max} = 120.8 \text{ cm/s}$	137
C4.41	Centerline velocity plots for Culvert #3 at $Q = 0.0664 \text{ m}^3/\text{s}$, 1% slope, $0.25D_o$, $L/D = 8$, no downstream control, $V_{\max} = 135.1 \text{ cm/s}$	137
C4.42	Centerline velocity plots for Culvert #3 at $Q = 0.0850 \text{ m}^3/\text{s}$, 0.5% slope, $0.57D_o$, $L/D = 8$, downstream control, $V_{\max} = 46.6 \text{ cm/s}$	137
C4.43	Centerline velocity plots for Culvert #3 at $Q = 0.0850 \text{ m}^3/\text{s}$, 1% slope, $0.59D_o$, $L/D = 8$, downstream control, $V_{\max} = 44.2 \text{ cm/s}$	138
C4.44	Centerline velocity plots for Culvert #4 at $Q = 0.0153 \text{ m}^3/\text{s}$, 0.5% slope, $0.28D_o$, $L/D = 7$, downstream control, $V_{\max} = 27.4 \text{ cm/s}$	138
C4.45	Centerline velocity plots for Culvert #4 at $Q = 0.0153 \text{ m}^3/\text{s}$, 0.5% slope, $0.33D_o$, $L/D = 7$, downstream control, $V_{\max} = 23.1 \text{ cm/s}$	138
C4.46	Centerline velocity plots for Culvert #4 at $Q = 0.0500 \text{ m}^3/\text{s}$, 0.5% slope, $0.23D_o$, $L/D = 7$, no downstream control, $V_{\max} = 127.2 \text{ cm/s}$	139
C4.47	Centerline velocity plots for Culvert #4 at $Q = 0.0563 \text{ m}^3/\text{s}$, 1% slope, $0.22D_o$, $L/D = 7$, no downstream control, $V_{\max} = 140.2 \text{ cm/s}$	139
C4.48	Centerline velocity plots for Culvert #4 at $Q = 0.0566 \text{ m}^3/\text{s}$, 0.5% slope, $0.57D_o$, $L/D = 7$, downstream control, $V_{\max} = 38.9 \text{ cm/s}$	139
C4.49	Centerline velocity plots for Culvert #4 at $Q = 0.0566 \text{ m}^3/\text{s}$, 1% slope, $0.59D_o$, $L/D = 7$, downstream control, $V_{\max} = 36.8 \text{ cm/s}$	140
C4.50	Centerline velocity plots for Culvert #4 at $Q = 0.0850 \text{ m}^3/\text{s}$, 0.5% slope, $0.56D_o$, $L/D = 7$, downstream control, $V_{\max} = 59.7 \text{ cm/s}$	140
C4.51	Centerline velocity plots for Culvert #4 at $Q = 0.0850 \text{ m}^3/\text{s}$, 1% slope, $0.58D_o$, $L/D = 7$, downstream control, $V_{\max} = 54.2 \text{ cm/s}$	140
D4.1	Velocity profile for Culvert #1 at $Q = 0.0052 \text{ m}^3/\text{s}$, 5% slope, $0.17D_o$, $L/D = 14$, no downstream control, $V_{\max} = 101.9 \text{ cm/s}$	142

D4.2	Velocity profile for Culvert #1 at $Q = 0.0064 \text{ m}^3/\text{s}$, 3% slope, $0.23D_o$, $L/D = 14$, no downstream control, $V_{\text{max}} = 82.0 \text{ cm/s}$	142
D4.3	Velocity profile for Culvert #1 at $Q = 0.0082 \text{ m}^3/\text{s}$, 1% slope, $0.34D_o$, $L/D = 14$, no downstream control, $V_{\text{max}} = 61.2 \text{ cm/s}$	143
D4.4	Velocity profile for Culvert #1 at $Q = 0.0094 \text{ m}^3/\text{s}$, 0.5% slope, $0.34D_o$, $L/D = 14$, no downstream control, $V_{\text{max}} = 59.9 \text{ cm/s}$	143
D4.5	Velocity profile for Culvert #1 at $Q = 0.0124 \text{ m}^3/\text{s}$, 0.5% slope, $0.68D_o$, $L/D = 14$, downstream control, $V_{\text{max}} = 34.5 \text{ cm/s}$	144
D4.6	Velocity profile for Culvert #1 at $Q = 0.0124 \text{ m}^3/\text{s}$, 1% slope, $0.76D_o$, $L/D = 14$, downstream control, $V_{\text{max}} = 33.2 \text{ cm/s}$	144
D4.7	Velocity profile for Culvert #1 at $Q = 0.0142 \text{ m}^3/\text{s}$, 5% slope, $0.49D_o$, $L/D = 14$, downstream control, $V_{\text{max}} = 63.1 \text{ cm/s}$	145
D4.8	Velocity profile for Culvert #1 at $Q = 0.0213 \text{ m}^3/\text{s}$, 0.5% slope, $0.56D_o$, $L/D = 14$, downstream control, $V_{\text{max}} = 85.1 \text{ cm/s}$	145
D4.9	Velocity profile for Culvert #1 at $Q = 0.0278 \text{ m}^3/\text{s}$, 3% slope, $0.43D_o$, $L/D = 14$, no downstream control, $V_{\text{max}} = 125.9 \text{ cm/s}$	146
D4.10	Velocity profile for Culvert #1 at $Q = 0.0284 \text{ m}^3/\text{s}$, 1% slope, $0.52D_o$, $L/D = 14$, no downstream control, $V_{\text{max}} = 92.7 \text{ cm/s}$	146
D4.11	Velocity profile for Culvert #1 at $Q = 0.0290 \text{ m}^3/\text{s}$, 5% slope, $0.39D_o$, $L/D = 14$, no downstream control, $V_{\text{max}} = 169.3 \text{ cm/s}$	147
D4.12	Velocity profile for Culvert #1 at $Q = 0.0438 \text{ m}^3/\text{s}$, 5% slope, $0.46D_o$, $L/D = 14$, no downstream control, $V_{\text{max}} = 178.0 \text{ cm/s}$	147
D4.13	Velocity profile for Culvert #1 at $Q = 0.0456 \text{ m}^3/\text{s}$, 0.5% slope, $0.72D_o$, $L/D = 14$, no downstream control, $V_{\text{max}} = 108.5 \text{ cm/s}$	148
D4.14	Velocity profile for Culvert #1 at $Q = 0.0527 \text{ m}^3/\text{s}$, 3% slope, $0.62D_o$, $L/D = 14$, no downstream control, $V_{\text{max}} = 159.6 \text{ cm/s}$	148
D4.15	Velocity profile for Culvert #1 at $Q = 0.0539 \text{ m}^3/\text{s}$, 1% slope, $0.79D_o$, $L/D = 14$, no downstream control, $V_{\text{max}} = 124.4 \text{ cm/s}$	149
D4.16	Velocity profile for Culvert #2 at $Q = 0.0153 \text{ m}^3/\text{s}$, 0.5% slope, $0.38D_o$, $L/D = 14$, downstream control, $V_{\text{max}} = 26.4 \text{ cm/s}$	149
D4.17	Velocity profile for Culvert #2 at $Q = 0.0153 \text{ m}^3/\text{s}$, 0.5% slope, $0.33D_o$, $L/D = 8$, downstream control, $V_{\text{max}} = 29.2 \text{ cm/s}$	150
D4.18	Velocity profile for Culvert #2 at $Q = 0.0153 \text{ m}^3/\text{s}$, 1% slope, $0.39D_o$, $L/D = 14$, downstream control, $V_{\text{max}} = 25.2 \text{ cm/s}$	150
D4.19	Velocity profile for Culvert #2 at $Q = 0.0283 \text{ m}^3/\text{s}$, 0.5% slope, $0.58D_o$, $L/D = 14$, downstream control, $V_{\text{max}} = 22.8 \text{ cm/s}$	151
D4.20	Velocity profile for Culvert #2 at $Q = 0.0283 \text{ m}^3/\text{s}$, 0.5% slope, $0.56D_o$, $L/D = 8$, downstream control, $V_{\text{max}} = 26.6 \text{ cm/s}$	151

D4.21	Velocity profile for Culvert #2 at $Q = 0.0396 \text{ m}^3/\text{s}$, 0.5% slope, $0.25D_o$, $L/D = 14$, no downstream control, $V_{\max} = 90.1 \text{ cm/s}$	152
D4.22	Velocity profile for Culvert #2 at $Q = 0.0396 \text{ m}^3/\text{s}$, 0.5% slope, $0.25D_o$, $L/D = 8$, downstream control, $V_{\max} = 84.9 \text{ cm/s}$	152
D4.23	Velocity profile for Culvert #2 at $Q = 0.0515 \text{ m}^3/\text{s}$, 1% slope, $0.25D_o$, $L/D = 14$, no downstream control, $V_{\max} = 108.0 \text{ cm/s}$	153
D4.24	Velocity profile for Culvert #2 at $Q = 0.0566 \text{ m}^3/\text{s}$, 0.5% slope, $0.50D_o$, $L/D = 1$, downstream control, $V_{\max} = 51.3 \text{ cm/s}$	153
D4.25	Velocity profile for Culvert #2 at $Q = 0.0566 \text{ m}^3/\text{s}$, 0.5% slope, $0.55D_o$, $L/D = 12$, downstream control, $V_{\max} = 46.3 \text{ cm/s}$	154
D4.26	Velocity profile for Culvert #2 at $Q = 0.0566 \text{ m}^3/\text{s}$, 0.5% slope, $0.57D_o$, $L/D = 14$, downstream control, $V_{\max} = 41.8 \text{ cm/s}$	154
D4.27	Velocity profile for Culvert #2 at $Q = 0.0566 \text{ m}^3/\text{s}$, 0.5% slope, $0.56D_o$, $L/D = 8$, downstream control, $V_{\max} = 44.9 \text{ cm/s}$	155
D4.28	Velocity profile for Culvert #2 at $Q = 0.0566 \text{ m}^3/\text{s}$, 1% slope, $0.62D_o$, $L/D = 14$, downstream control, $V_{\max} = 37.6 \text{ cm/s}$	155
D4.29	Velocity profile for Culvert #2 at $Q = 0.0850 \text{ m}^3/\text{s}$, 0.5% slope, $0.54D_o$, $L/D = 12$, downstream control, $V_{\max} = 69.1 \text{ cm/s}$	156
D4.30	Velocity profile for Culvert #2 at $Q = 0.0850 \text{ m}^3/\text{s}$, 0.5% slope, $0.54D_o$, $L/D = 14$, downstream control, $V_{\max} = 64.2 \text{ cm/s}$	156
D4.31	Velocity profile for Culvert #2 at $Q = 0.0850 \text{ m}^3/\text{s}$, 0.5% slope, $0.54D_o$, $L/D = 8$, downstream control, $V_{\max} = 69.8 \text{ cm/s}$	157
D4.32	Velocity profile for Culvert #2 at $Q = 0.0850 \text{ m}^3/\text{s}$, 0.5% slope, $0.50D_o$, at entrance, downstream control, $V_{\max} = 71.5 \text{ cm/s}$	157
D4.33	Velocity profile for Culvert #2 at $Q = 0.0850 \text{ m}^3/\text{s}$, 1% slope, $0.63D_o$, $L/D = 14$, downstream control, $V_{\max} = 58.2 \text{ cm/s}$	158
D4.34	Velocity profile for Culvert #2 at $Q = 0.1274 \text{ m}^3/\text{s}$, 0.5% slope, $0.50D_o$, $L/D = 8$, no downstream control, $V_{\max} = 118.4 \text{ cm/s}$	158
D4.35	Velocity profile for Culvert #3 at $Q = 0.0153 \text{ m}^3/\text{s}$, 0.5% slope, $0.31D_o$, $L/D = 8$, downstream control, $V_{\max} = 22.2 \text{ cm/s}$	159
D4.36	Velocity profile for Culvert #3 at $Q = 0.0153 \text{ m}^3/\text{s}$, 1% slope, $0.62D_o$, $L/D = 8$, downstream control, $V_{\max} = 9.9 \text{ cm/s}$	159
D4.37	Velocity profile for Culvert #3 at $Q = 0.0153 \text{ m}^3/\text{s}$, 0.5% slope, $0.33D_o$, $L/D = 8$, downstream control, $V_{\max} = 20.5 \text{ cm/s}$	160
D4.38	Velocity profile for Culvert #3 at $Q = 0.0566 \text{ m}^3/\text{s}$, 0.5% slope, $0.57D_o$, $L/D = 8$, downstream control, $V_{\max} = 31.2 \text{ cm/s}$	160
D4.39	Velocity profile for Culvert #3 at $Q = 0.0566 \text{ m}^3/\text{s}$, 1% slope, $0.58D_o$, $L/D = 8$, downstream control, $V_{\max} = 33.9 \text{ cm/s}$	161

D4.40	Velocity profile for Culvert #3 at $Q = 0.0575 \text{ m}^3/\text{s}$, 0.5% slope, 0.24 D_o , $L/D = 8$, no downstream control, $V_{\text{max}} = 120.8 \text{ cm/s}$	161
D4.41	Velocity profile for Culvert #3 at $Q = 0.0664 \text{ m}^3/\text{s}$, 1% slope, 0.25 D_o , $L/D = 8$, no downstream control, $V_{\text{max}} = 135.1 \text{ cm/s}$	162
D4.42	Velocity profile for Culvert #3 at $Q = 0.0850 \text{ m}^3/\text{s}$, 0.5% slope, 0.57 D_o , $L/D = 8$, downstream control, $V_{\text{max}} = 46.6 \text{ cm/s}$	162
D4.43	Velocity profile for Culvert #3 at $Q = 0.0850 \text{ m}^3/\text{s}$, 1% slope, 0.59 D_o , $L/D = 8$, downstream control, $V_{\text{max}} = 44.2 \text{ cm/s}$	163
D4.44	Velocity profile for Culvert #4 at $Q = 0.0153 \text{ m}^3/\text{s}$, 0.5% slope, 0.28 D_o , $L/D = 7$, downstream control, $V_{\text{max}} = 27.4 \text{ cm/s}$	163
D4.45	Velocity profile for Culvert #4 at $Q = 0.0153 \text{ m}^3/\text{s}$, 0.5% slope, 0.33 D_o , $L/D = 7$, downstream control, $V_{\text{max}} = 23.1 \text{ cm/s}$	164
D4.46	Velocity profile for Culvert #4 at $Q = 0.0500 \text{ m}^3/\text{s}$, 0.5% slope, 0.23 D_o , $L/D = 7$, no downstream control, $V_{\text{max}} = 127.2 \text{ cm/s}$	164
D4.47	Velocity profile for Culvert #4 at $Q = 0.0563 \text{ m}^3/\text{s}$, 1% slope, 0.22 D_o , $L/D = 7$, no downstream control, $V_{\text{max}} = 140.2 \text{ cm/s}$	165
D4.48	Velocity profile for Culvert #4 at $Q = 0.0566 \text{ m}^3/\text{s}$, 0.5% slope, 0.57 D_o , $L/D = 7$, downstream control, $V_{\text{max}} = 38.9 \text{ cm/s}$	165
D4.49	Velocity profile for Culvert #4 at $Q = 0.0566 \text{ m}^3/\text{s}$, 1% slope, 0.59 D_o , $L/D = 7$, downstream control, $V_{\text{max}} = 36.8 \text{ cm/s}$	166
D4.50	Velocity profile for Culvert #4 at $Q = 0.0850 \text{ m}^3/\text{s}$, 0.5% slope, 0.56 D_o , $L/D = 7$, downstream control, $V_{\text{max}} = 59.7 \text{ cm/s}$	166
D4.51	Velocity profile for Culvert #4 at $Q = 0.0850 \text{ m}^3/\text{s}$, 1% slope, 0.58 D_o , $L/D = 7$, downstream control, $V_{\text{max}} = 54.2 \text{ cm/s}$	167

EXECUTIVE SUMMARY

Cross-sectional velocity distributions were measured by performing laboratory tests on four metal culverts, with inside diameters ranging from 30.5 cm (12 in) to 73.7 cm (29 in), with the objective of developing a method of predicting the percentage amount of cross-sectional area of a large diameter culvert with velocities sufficiently low enough to pass juvenile fish. Fifty-one experimental runs were conducted under varying flow, slope, relative depth, and downstream control conditions. Because measured velocity distributions were often non-symmetrical about the centerlines of the culverts, it was not possible to predict exact two-dimensional velocity distributions. Instead, the areas between adjacent velocity contour lines were converted to symmetrical ring-shaped bands which were then used to create an "effective" two-dimensional velocity distribution. This effective velocity distribution represents average band widths of a given velocity range that could be expected in the culvert. The band widths allow the amount of cross-sectional area with acceptable velocities to be determined, which is an important design parameter in the design of culverts to provide juvenile fish passage.

Two existing equations were used to predict the centerline velocity distribution for the conditions that were tested. The first equation was taken from Chiu (1993), and the second equation was taken from Mountjoy (1986). The curves resulting from the two equations were compared to an "effective" symmetrical velocity distribution obtained from the experimental data. Based on a statistical analysis, the Mountjoy equation was the more accurate method of predicting the "effective" velocity distribution for the highway culverts. It was concluded that the Mountjoy equation provides a means of predicting "effective" cross-sectional velocity distributions in large diameter highway culverts.

Chapter 1

INTRODUCTION

1.1 Problem Statement

Barriers to upstream migration of juvenile fish have been recognized for their negative impact on the long-term preservation of fish populations. For many species of fish, this migration is essential for survival (Baker and Votapka, 1990). Juvenile salmonids as well as many resident fish species migrate both upstream and downstream. Upstream migration of juvenile anadromous fish has been documented by several authors, including Skeesick (1970) and Cederholm and Scarlett (1981). Juvenile sockeye salmon are particularly vulnerable to upstream blockages in stream systems that require upstream migration to reach suitable habitat (Dane, 1978). According to the Washington Department of Fish and Wildlife (WDFW), juvenile fish may migrate upstream in response to water conditions, predation, or population pressures (WDFW, 1990). It is noted, however, that some studies have not clearly shown there to be an upstream migration of juvenile salmon. Therefore, it is not a clear fact that upstream juvenile fish migration will always occur, only that it can and does occur on some occasions (Baker and Votapka, 1990).

Barriers to juvenile fish passage exist in many forms. There are natural barriers such as waterfalls, debris jams, and temperature barriers. There are also artificial barriers such as log jams, dams, roadway crossings, and pollution (Evans and Johnston, 1980). There is a potential for an artificial barrier to occur when corrugated or smooth metal culverts are used at roadway crossings. The use of culverts is often a cost-effective method to provide roadway overcrossing of a stream. Excessive velocities within the culvert barrel however, can pose a barrier to juvenile, as well as adult fish migration (Bates, 1992).

There are currently culvert fish passage design standards which dictate the maximum average flow velocity ($Velocity_{avg} = \text{Discharge}/\text{Cross-Sectional Area}$) through the culvert barrel. The WDFW currently uses this approach for juvenile fish passage through culverts. These

standards assume open channel flow, as dictated by Manning's equation, and are often based on the swimming capabilities of adult migrating fish. Juvenile fish have lower swimming capabilities than do adult fish (Gebhards and Fisher, 1972). Consequently, a culvert that may be passable by adult fish may pose a barrier to juvenile fish. This would seem to suggest using a lower average velocity criteria for culverts where it is necessary to provide passage for juvenile fish. On the other hand, it has also been observed that juvenile fish are sensitive to variations in hydraulic conditions and will use the low velocity regions of the culvert's boundary layer for passage. Thus, a culvert designed to meet the maximum average flow velocity criteria for juvenile fish passage may be overly conservative.

In response to endangered species legislation, as well as the growing concern for the survival of salmon and other resident fish species in Washington, the Washington State Department of Transportation (WSDOT) has begun studying the issue of providing acceptable passage to juvenile salmon at culvert roadway crossings. The WSDOT has proposed that if an adequate low velocity region is provided through the culvert, juvenile fish will use this layer for passage. This will eliminate the need for an overly conservative average flow velocity criteria for juvenile fish to be applied to culverts at roadway crossings.

Research into the hydraulic conditions of culverts with particular interest in the low velocity region near the wall has been conducted. The results of this research will be used to develop a method of predicting relative velocity distributions in highway culverts of any diameter. Research is also being performed by the Washington Department of Fish and Wildlife to determine if fish will use the low velocity boundary layer near the edge of the pipe, how large of a low velocity region is necessary, and what are the limiting velocity and slope to allow upstream passage of juvenile salmon and trout. By combining the two studies, designers will be able to examine if upstream migrating juvenile salmon and trout use the low velocity region near the wall of a culvert for passage.

1.2 Objectives

The primary objectives of this research are to:

1. Measure the velocity distributions and examine the low velocity region near the wall in smooth and corrugated pipes.
2. Derive an empirical method that will predict areas of low velocity based on traditional hydraulic parameters.

The development of a scaling theory will provide a means of predicting the percentage amount of cross-sectional area of a large diameter highway culvert with velocities sufficiently low enough to pass juvenile fish. The empirical method will allow the size of the low velocity region in any large diameter culvert to be extrapolated from experimental test results on smaller diameter culverts. The ability to predict the size of the low velocity region in a highway culvert will provide a valuable tool in the design of culverts for juvenile fish passage. Thus, given the design flow (Q), the desired corrugations (n), and the desired slope (S_o), tail water condition and assuming Manning's equation to be valid, a designer will be able to pick the minimum pipe diameter which would produce an adequate low velocity region that will allow for juvenile fish passage. In this way, the empirical method, in conjunction with existing culvert design criteria, can be used by the WSDOT and the WDFW in the process of designing circular culvert roadway crossings that provide acceptable juvenile fish passage at minimal costs.

Chapter 2

LITERATURE REVIEW / BACKGROUND INFORMATION

2.1 General Background

A culvert is any conduit or waterway used to allow passage of flow underneath a roadway or embankment. Culverts are available in a variety of shapes, including those of circular, square, arch, and horseshoe cross-sections. Culverts are also constructed from various materials such as corrugated metal and concrete. Corrugated metal is far more popular for use at roadway crossings because it is more cost effective than concrete in many cases. As requested by WSDOT, corrugated metal culverts were selected for this research. The driving mechanism behind this research project is the desire to provide passage for juvenile fish at roadway culvert crossings. To design for juvenile fish passage, the following two questions must ultimately be answered:

1. What is the swimming capability of the juvenile fish, and
2. If it is found that juvenile fish do in fact use the low velocity region near the wall, is a sufficient region present to provide passage?

It is the latter portion of these issues to which the research presented here is directed.

2.2 Literature Review

An extensive literature review was conducted as part of this research project in order to examine the current standards and state-of-the-art approaches that exist. In an effort to provide a comprehensive background for this report on the subject of juvenile fish passage in culverts, three areas of previous works were emphasized in this search. These areas were:

1. Fish Passage in Culverts: Problems and requirements.
2. Open Channel Flow: Application to culverts flowing partially full.
3. Velocity Profiles: Attempts at one-dimensional and two-dimensional modeling of velocity distributions.

2.2.1 Fish Passage in Culverts: Problems and Requirements.

There have been numerous studies and papers written on the subject of fish passage through culverts (i.e. Baker and Votapka, 1990; Behlke et al. 1989; Kane and Wellen, 1985). Culverts, which are often used at roadway crossings, are potential barriers to upstream migration of juvenile, as well as adult fish because of the high velocity of flow in the culvert barrel. In the State of Washington, juvenile salmonid passage must be provided in reaches of streams where migration to seasonal rearing habitat occurs (WDFW, 1990). The design of a roadway culvert must take into account the magnitude of the design flow as well as provide adequate fish passage. To accomplish these tasks, culvert roadway crossing designs must specifically look at the biological criteria of the design fish to be passed and the hydraulics of the culvert which must pass the design storm.

Biological Criteria. - Fish use two separate muscle systems to propel themselves through the water. Red muscles (aerobic) are used by fish for long periods of steady swimming, and white muscles (anaerobic) are used for short periods of sprint swimming (Behlke et al. 1989). The swimming capabilities of fish can be broken down into three categories: (1) sustained (cruising) speed; (2) prolonged speed; and (3) burst speed. Sustained speed is a speed fish can maintain for an extended period of time without fatigue. Prolonged speed is a speed fish can maintain for a considerable length of time (between 10 and 500 minutes) but ultimately will result in fatigue. And finally, fish can maintain burst speed for only a very short period of time (nominally 7 seconds although sometimes considered to be between 5 and 60 seconds).

Bell (1973) provides a listing of the cruising speed, sustained speed, and burst speed of several fish species. The data from Bell is based on average size adult fish. Bell suggests that migrating fish normally swim at cruising speed and use sustained speed to pass through difficult areas. For culvert passage the capability of interest is the sustained speed.

A report prepared for the State of Alaska by Kane and Wellen (1985) discusses fish swimming capability. The discussion is based on studies performed by Jones et al. (1974) and

MacPhee and Watts (1976). The authors also suggest that the sustained speed of a fish be used for culvert design.

The data and guidelines that exist for juvenile fish passage are not entirely consistent from state to state. In the State of Washington, a maximum average velocity of 122 cm/s (4 ft/s) is given by the WDFD for juvenile salmonids. This is based on an assumption that the culvert being passed is less than 18.3 meters (60 feet) in length and that the roughness of the corrugations provides a low velocity region near the wall of the culvert. This is assumed to be the maximum limit of the swimming capability of the juvenile salmon under these conditions.

In addition to state guidelines there have been independent studies of the swimming capabilities of juvenile fish. Several authors have developed relationships between fork length, which is the length of the fish, and swimming capability for various fish species. The United States Department of Transportation (USDOT) (Baker and Votapka, 1990) provides a graph of fork length versus water velocity for several types of adult fish. This graph is taken from a study by Jones et al. (1974) and is illustrated in Figure 2.1. This graph shows that as the fork length of a fish increases so does its ability to pass through higher velocities of flow. To relate this graph for adult fish to juvenile fish, the USDOT provides an additional plot which was taken from work done by MacPhee and Watts (1976). This plot, which is shown in Figure 2.2, relates the relative length of a juvenile fish to a relative swimming velocity by a non-linear curve. The applicability of the information is questionable, however, since it requires extrapolation to use a reasonable ratio of fork lengths between juvenile salmonids and adult salmon ($L/L_{adult} = 0.1$). The USDOT report also includes a plot of the swimming capability of migrating salmon (see Figure 2.3). Water velocity is plotted versus the maximum allowable distance between resting pools in this figure. This upper curve on the plot was taken from Ziemer (1965) of the Alaska Department of Fish and Game and the lower curve was prepared by Evans and Johnston (1980).

In 1978, the U.S. Department of Agriculture (USDA) Forest Service in Alaska took a similar approach to determining the swimming capability of juvenile salmon. A graph is provided in the USDA report (see Figure 2.4) which shows sustained speed versus fork length.

The WDFW (1995) report these values are too high for coho and are more representative of prolonged speed. This plot indicates a linear relationship between the sustained speed capability of a juvenile fish and its fork length. For this plot, it is assumed that the jumping capability of juvenile fish is non-existent (USDA Forest Service, 1978). As was pointed out by WDFW (1995), this assumption is not true.

In 1972 a report to the Idaho Fish and Game Department (IFGD) provided fish passage guidelines currently still used in Idaho (Gebhards and Fischer, 1972). The authors note in the paper that the swimming ability of a fish is a function of its size. Therefore, a larger fish has a higher swimming capability. The report states that the sustained speed capability for juvenile salmonids is approximately four body lengths per second depending on water temperature. This estimate is based on a study performed in Rome, Italy by Blaxter (1969).

Considerably more biological information regarding the fish response is available. For example, studies documenting swimming ability as a function of water temperature or the consequences of the timing of juvenile fish migration or the response to the first fall freshet are available (WDFW, 1995). Because this report focuses on the hydraulic factors involved with fish migration, only an overview of the biological criteria has been provided.

Culvert Hydraulic Considerations.- The installation of a highway culvert creates changes in the hydraulic characteristics of the stream. For example, a culvert often constricts the flow to form a special type of contraction. Often these changes are detrimental to the passage of both adult and juvenile fish. The primary factor of importance is that of the cross-sectional area with velocities less than or equal to those acceptable for passage. Historically, the most important design consideration has been the culverts' ability to pass the design flow. However, for fish passage consideration, the factor that this research is interested in is the velocity distribution through the culvert barrel.

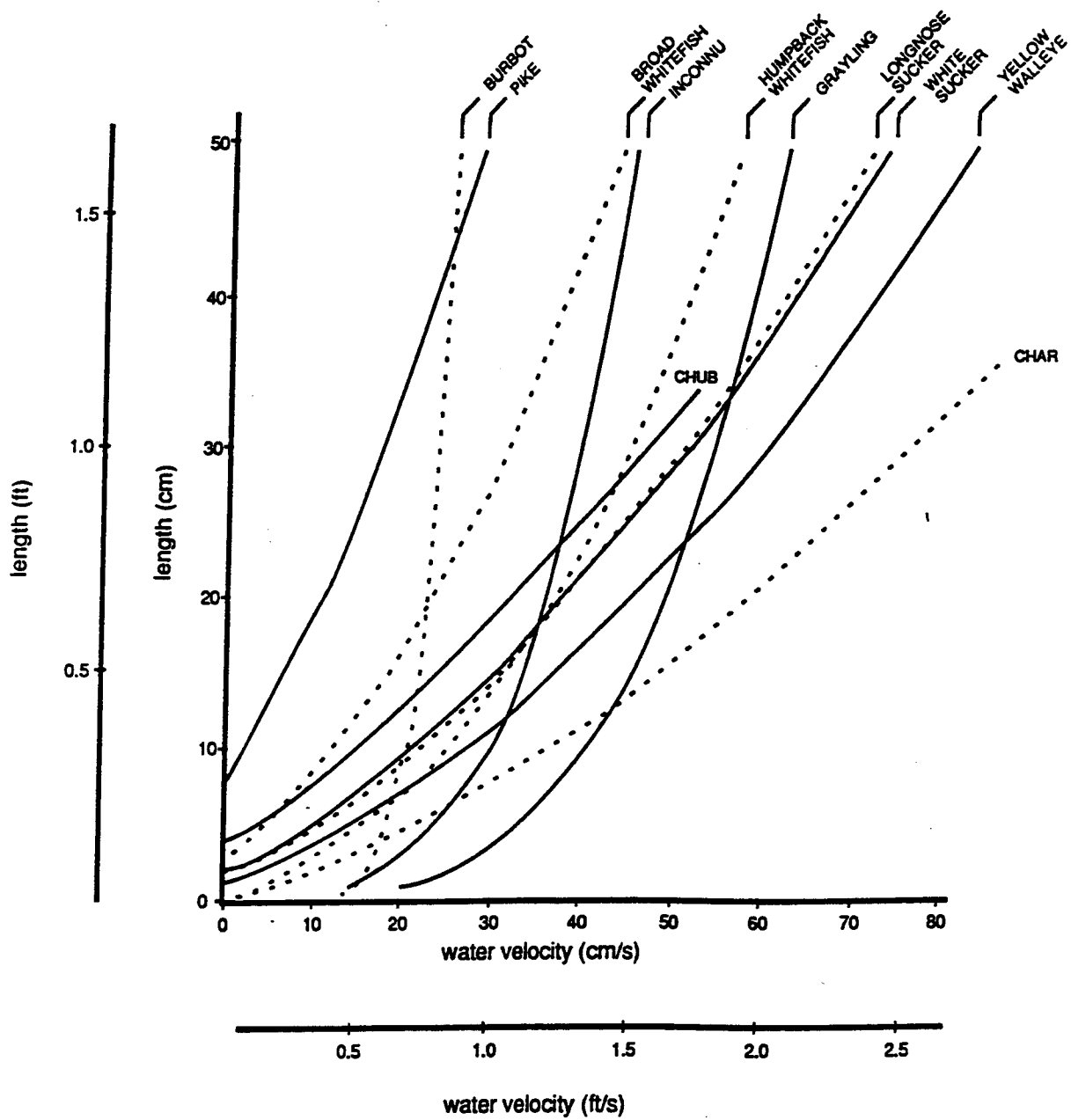


Figure 2.1. Relationship between fork length and ability to move 100 meters in 10 minutes in water velocities up to 80 cm/s for fish from the MacKenzie River (from Jones et al. 1974).

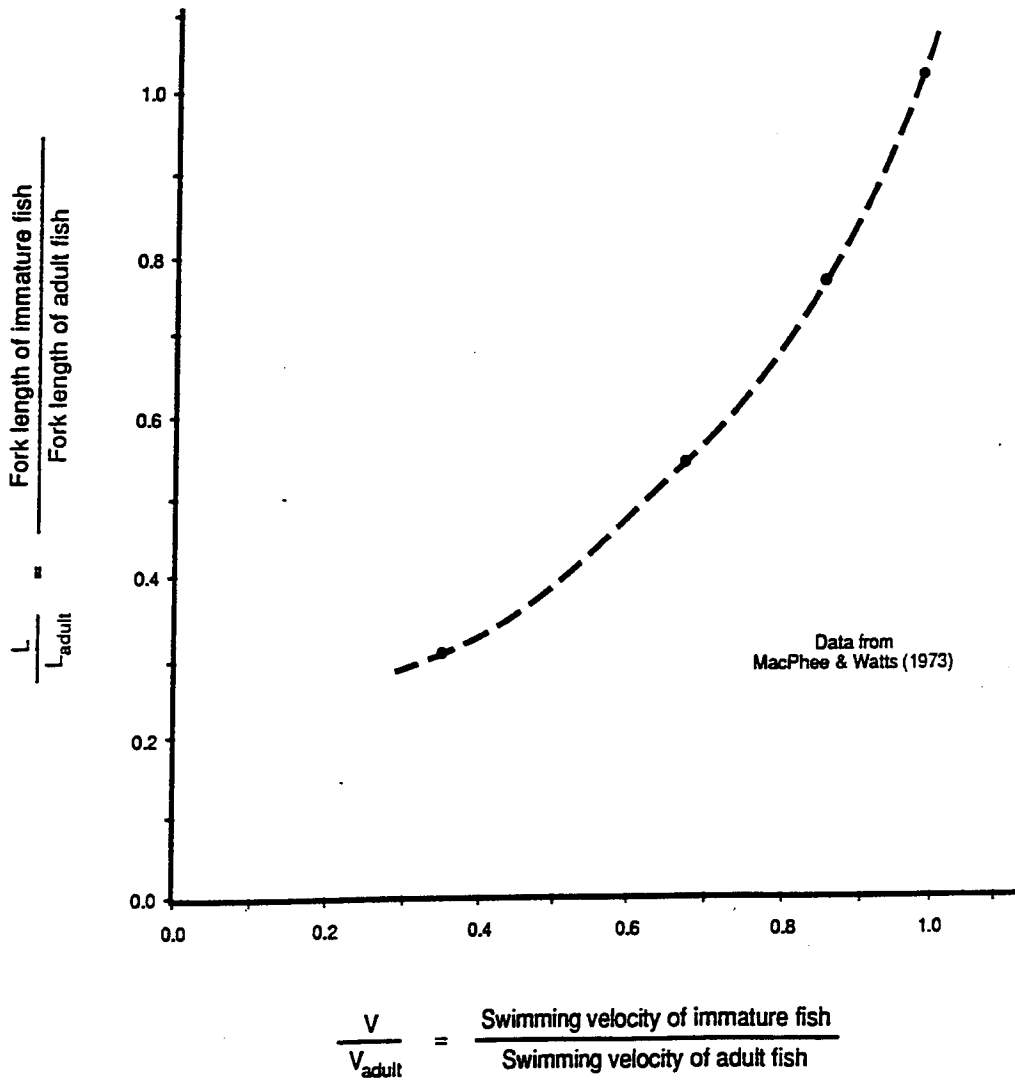


Figure 2.2. Relative length versus relative swimming velocity for fish based on grayling data (from MacPhee and Watts, 1976).

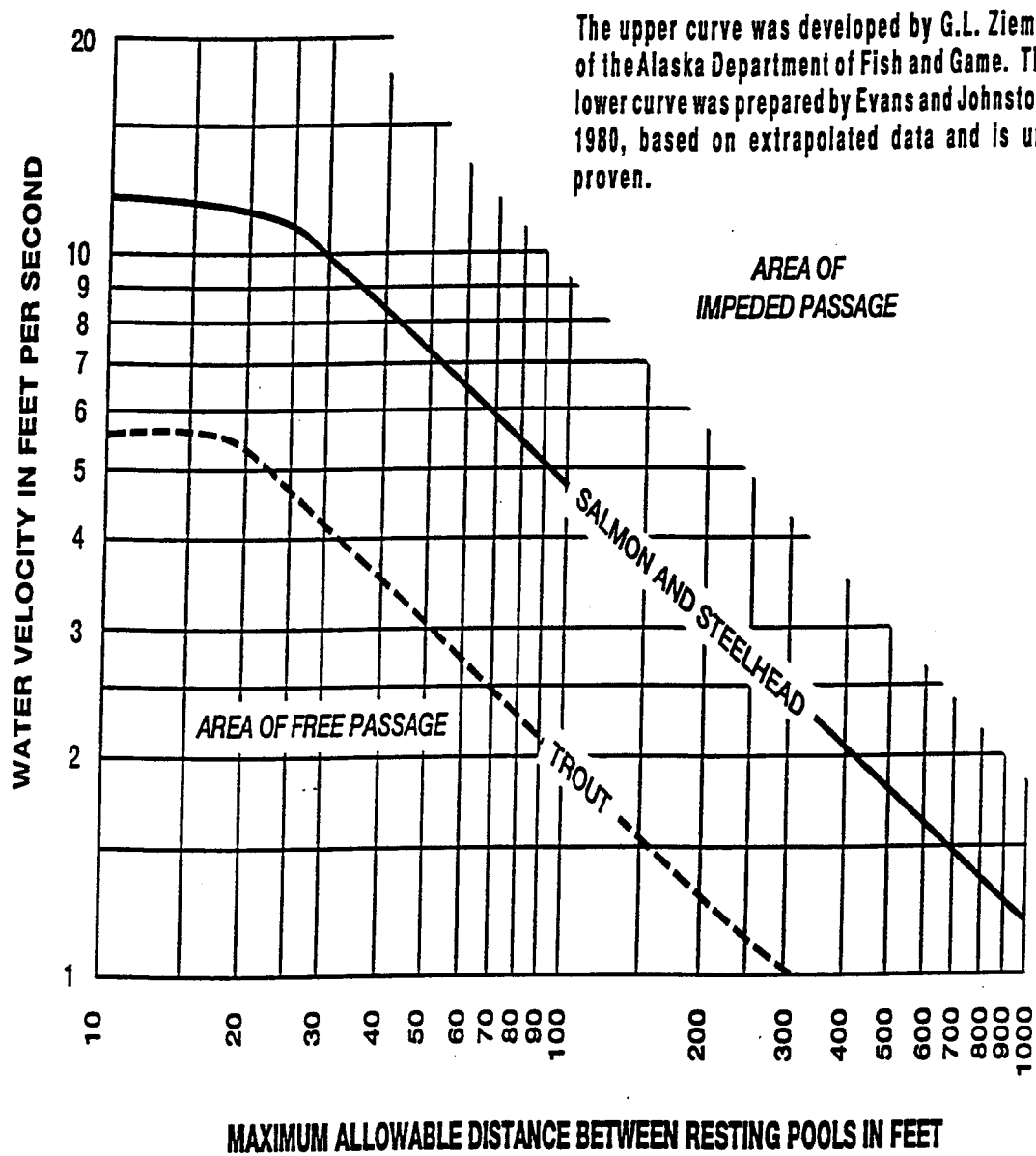


Figure 2.3. Swimming capability of migration salmon (Alaska curve, from Ziemer, 1965; and Evans and Johnston, 1980).

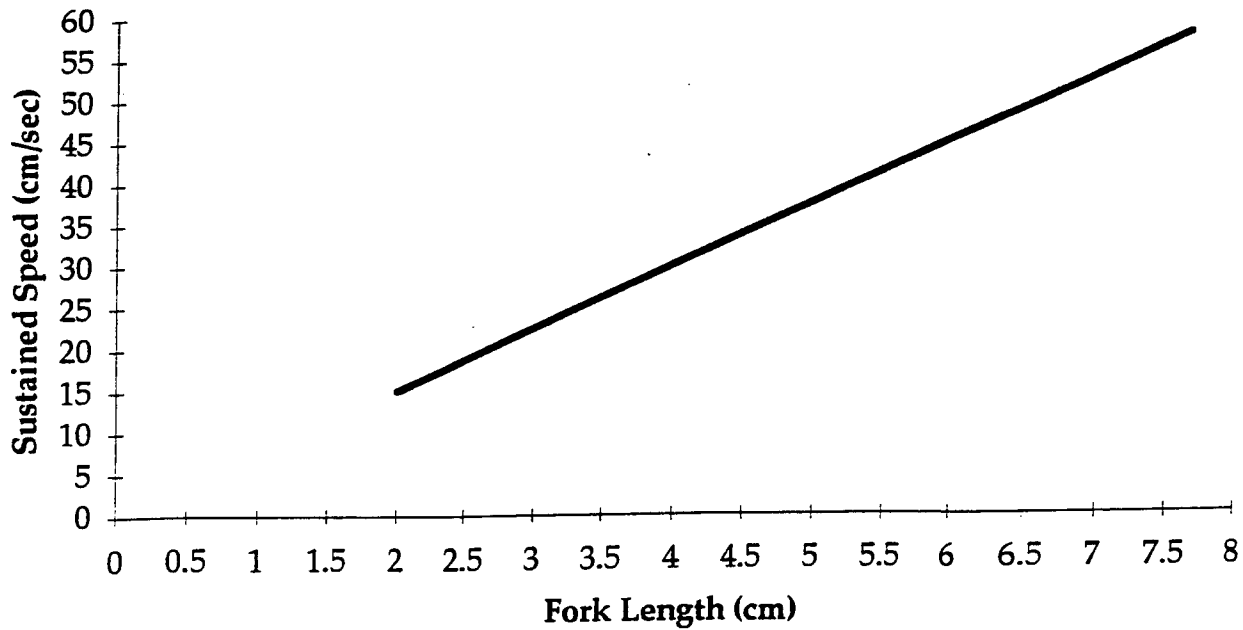


Figure 2.4. Sustained speed versus fork length for juvenile salmon (Modified from USDA Forest Service, 1978).

2.2.2 Modeling Flow in Culverts

Flow Characterization.- As a subclass of open channel flow, the flow in culverts can be classified based on temporal and spatial descriptors. For partially full pipes, the flow is referred to as being *steady* if the flow velocity (or depth) does not change at a given point with respect to time and *unsteady* if these properties are changing. These descriptors represent the temporal characterization of the flow. By contrast, in spatial terms, the flow is either *uniform* if the velocity (distribution) and depth are not changing as a function of location (along an axes representing the primary direction of flow) and *non-uniform* if the velocity and depth are changing at different locations. These descriptors are typically used in combination to provide a spatial and temporal characterization of the flow, e.g. steady, non-uniform flow (Chaudhry, 1993).

Non-uniform flow can be further classified based on the rate of variation with respect to distance. A non-uniform flow that varies at a slow rate (i.e. across a relatively long distance) is

called *gradually varied* flow, and a flow that varies over a short distance is called *rapidly varied* flow. Classic examples of: (i) gradually varied flow are those of backwater profiles created by some obstruction in the stream; and (ii) rapidly varied flow that of a hydraulic jump.

Relevant Governing Equations.- In classic terms, the modeling of the flow in culverts must adhere to the laws of conservation of mass, momentum, and energy. Two flow variables, for example the depth of flow and the velocity, or the depth of flow and the discharge rate are sufficient to define the flow conditions at a cross-section of the channel. Therefore, any two of the three governing equations can be used to investigate a given open channel flow (Chaudhry, 1993). Often the continuity equation, which is derived from the conservation of mass law, is used in combination with either the momentum or energy equation to provide the two governing equations that are necessary. For applications in this research and for a constant density fluid, the form of the continuity equation used is as follows:

$$V_1A_1 = V_2A_2 \quad (2.1)$$

where V_1 is the mean flow velocity at section 1; V_2 is the mean flow velocity at section 2; A_1 is the cross-sectional area at section 1; and A_2 is the cross-sectional area at section 2.

To estimate total discharge, Manning's equation is the most widely used formula in the world (Chow, 1959; Henderson, 1966). Despite the typically non-uniform flow through culverts, the Manning equation is often used for hydraulic design because the equation can be used easily and provides acceptable results. The Manning equation for velocity is as follows:

$$V = \frac{1}{n} R^{2/3} S_f^{1/2} \quad (\text{SI Units}) \quad (2.2)$$

where V is the average flow velocity [m/s]; n is the Manning roughness coefficient; R is the hydraulic radius [m], and S_f is the friction slope.

The constant, 1, contains unit conversion factors which allow n to be dimensionless. For english units this constant becomes 1.486.

Manning's equation can also be solved for the discharge (Q) by multiplying both sides of Equation 2.2 by the cross-sectional area of flow (A). This yields:

$$Q = VA = \frac{1}{n} AR^{2/3} S_f^{1/2} \quad (\text{SI Units}) \quad (2.3)$$

The hydraulic radius (R) and cross-sectional area (A) for a circular conduit (such as a highway culvert) are given by:

$$R = \frac{1}{4} \left(1 - \frac{\sin \theta}{\theta} \right) D_o \quad (2.4)$$

$$A = \frac{1}{8} (\theta - \sin \theta) D_o^2 \quad (2.5)$$

where θ is the angle shown in Figure 2.5; and D_o is the diameter of the culvert [m].

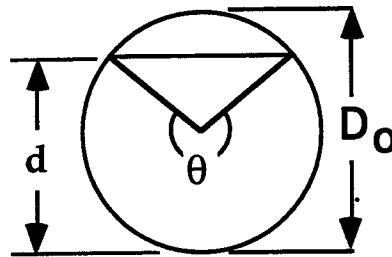


Figure 2.5. Diagram of circular culvert cross-section flowing partially full.

The Manning roughness coefficients (n) have been determined experimentally for a large number of channel surfaces. The Federal Highway Administration (FHWA) (Normann, 1980) has produced a series of plots showing Manning roughness coefficients versus pipe diameter for a number of corrugated metal pipes (CMP). The plot for 6.8 x 1.3 cm and 7.6 x 2.3 cm annular corrugated culverts is shown in Figure 2.6. Given the discharge (Q), pipe diameter (D), and relative depth (d/D_0), the Manning roughness coefficient can be found off the plot. The USFHWA only provides Manning n values for relative depths between $0.7 \cdot D_0$ and $1.0 \cdot D_0$. Additional plots for other corrugations are included in Appendix A of this report (see Figures A2.1, A2.2, and A2.3). The American Iron and Steel Institute (1980) also has published a table which gives Manning n values for a wide variety of culverts.

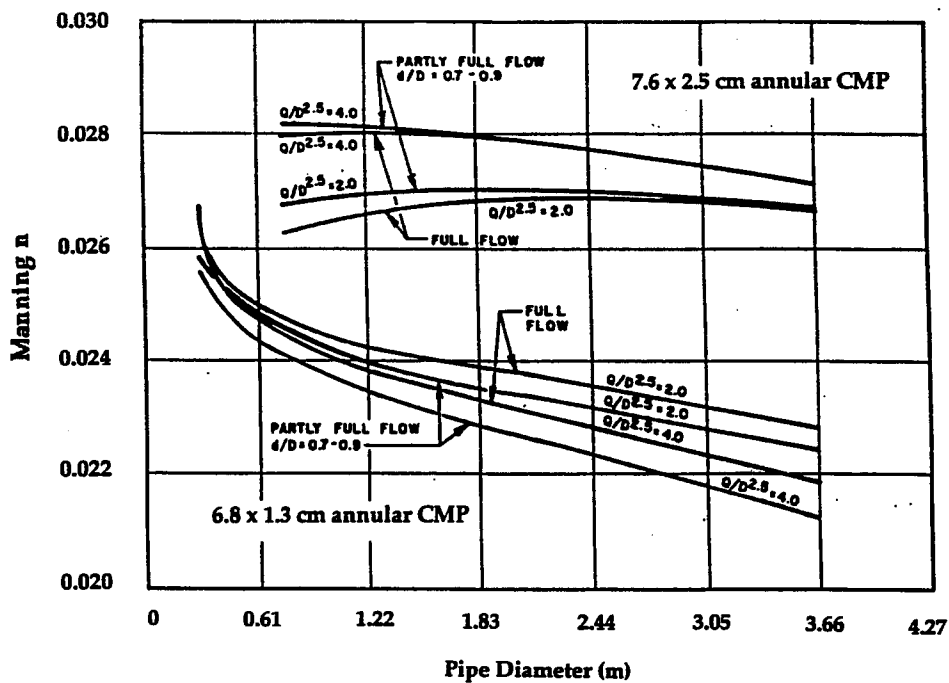


Figure 2.6. Manning n versus diameter for 6.8 x 1.3 cm (2 2/3 x 1/2 in) and 7.6 x 2.3 cm (3 x 1 in) annular corrugated metal pipe.

Boundary Layer and Shear Stress.- The boundary layer is the region of fluid near the wall of the conduit. The flow has undergone a change in velocity because of the shear stress at the wall boundary (Roberson and Crowe, 1990). The shear stress at the wall is the stress created by the intermolecular forces between the water and the wall material. For juvenile fish passage considerations, it has been proposed that fish will use the lower velocity of the boundary layer to pass through a highway culvert. Research to test this hypothesis is currently underway by WDFW. Existing methods of predicting the velocity distribution in open channel flow are discussed in Section 2.2.4.

Energy and Momentum Coefficients.- As was stated earlier, two governing equations can be used to analyze a typical flow situation (Chaudhry, 1993). Two coefficients, the energy coefficient, α , and the momentum coefficient, β , are necessary in the analysis of velocity distributions in open channel flow through a culvert. The energy coefficient, α , is necessary because the flow velocity varies from one point to another in the cross-section. The velocity head of an open channel flow is usually greater than the value computed from the equation $V_m^2/2g$ where V_m is the mean velocity of the cross-section. The true velocity head may be expressed as $\alpha V_m^2/2g$ (Chow, 1959). The energy coefficient is given by the following equation:

$$\alpha = \frac{\int V^3 dA}{V_m^3 \int dA} = \frac{\left(\sum_{i=1}^N V_i^3 A_i\right) \cdot \left(\sum_{i=1}^N A_i\right)^2}{\left(\sum_{i=1}^N V_i A_i\right)^3} \quad (2.6)$$

where V_i is the velocity in subarea A_i [m/s]; and V_m is the mean velocity in the cross-section [m/s].

The second velocity distribution coefficient necessary was the momentum coefficient, β , which accounts for non-uniform distribution of velocities in open channel flow in the computation of momentum. The momentum coefficient is found from the following expression:

$$\beta = \frac{\int V^2 dA}{V_m^2 \int dA} = \frac{\left(\sum_{i=1}^N V_i^2 A_i\right) \cdot \left(\sum_{i=1}^N A_i\right)}{\left(\sum_{i=1}^N V_i A_i\right)^2} \quad (2.7)$$

where V_i , A_i , and V_m have been previously defined.

Flow through highway culverts is generally considered turbulent, with the liquid particles moving in irregular paths which are not fixed with respect to either time or space. The parameter that was considered for turbulence was the Reynolds number (R_e). For flows through culverts the Reynolds number is generally in excess of 1×10^4 . The Reynolds number is a ratio of viscous and inertial forces and is defined as:

$$R_e = \frac{V \cdot L}{\nu} \quad (2.8)$$

where V is the mean flow velocity [m/s]; L is the characteristic length [m]; and ν is the kinematic viscosity of the liquid [m²/s].

The hydraulic radius is defined as the flow area (A) divided by the wetted perimeter (P). The hydraulic radius for a circular conduit was given previously in Equation 2.4. The hydraulic radius was used in this research.

An interesting aspect of the boundary layer process is the concept of turbulence. The flow velocity is assumed to be zero at the wall and close to zero in a thin layer very near the pipe wall causing the flow to be laminar in this thin region. Outside this layer, as velocities increase, flow travels in random arrangements with the actual flow paths constantly changing. This flow regime is referred to as turbulent. While not exactly defined, turbulent flow occurs when the Reynolds number exceeds approximately 2000-4000. Since the kinematic viscosity of water is on the order of 10^{-6} , the flow velocity does not have to be very large before turbulence can occur. Turbulence is a totally random process. In culverts, the amount of turbulence will vary dramatically from point to point depending on the location of measurement.

2.2.3 Typical Gradually Varied Flow Profiles

As was discussed earlier, uniform flow occurs when the flow depth does not change with distance. Although theoretically important, uniform flows seldom occurs in nature, this due to the physical irregularity found in most natural channels (Henderson, 1966). In fact, the most common flow occurrence in culverts would be that of gradually varied flow generated by a potential combination of various entrance/tail water conditions and an undulating boundary throughout its length.

The typical flow control will either be an inlet or outlet feature. Inlet control occurs when the barrel of the culvert is capable of passing more flow than the inlet will accept. Outlet control occurs when the culvert barrel is not capable of passing the amount of flow that the inlet will accept. Chow (1959) classifies culvert flow into six types, which are shown in Figure 2.7. According to Chow, the classification of each type of culvert flow is explained by the following:

- | | |
|--------|--|
| Type 1 | Outlet Submerged |
| Type 2 | Outlet unsubmerged, headwater greater than the critical value, full flow through the culvert. |
| Type 3 | Outlet unsubmerged, headwater greater than the critical value, partially full flow through the culvert. |
| Type 4 | Outlet unsubmerged, headwater less than the critical value, tailwater higher than the critical depth. |
| Type 5 | Outlet unsubmerged, headwater less than the critical value, tailwater lower than the critical depth, slope is subcritical. |
| Type 6 | Outlet unsubmerged, headwater less than the critical value, tailwater lower than the critical depth, slope is supercritical. |

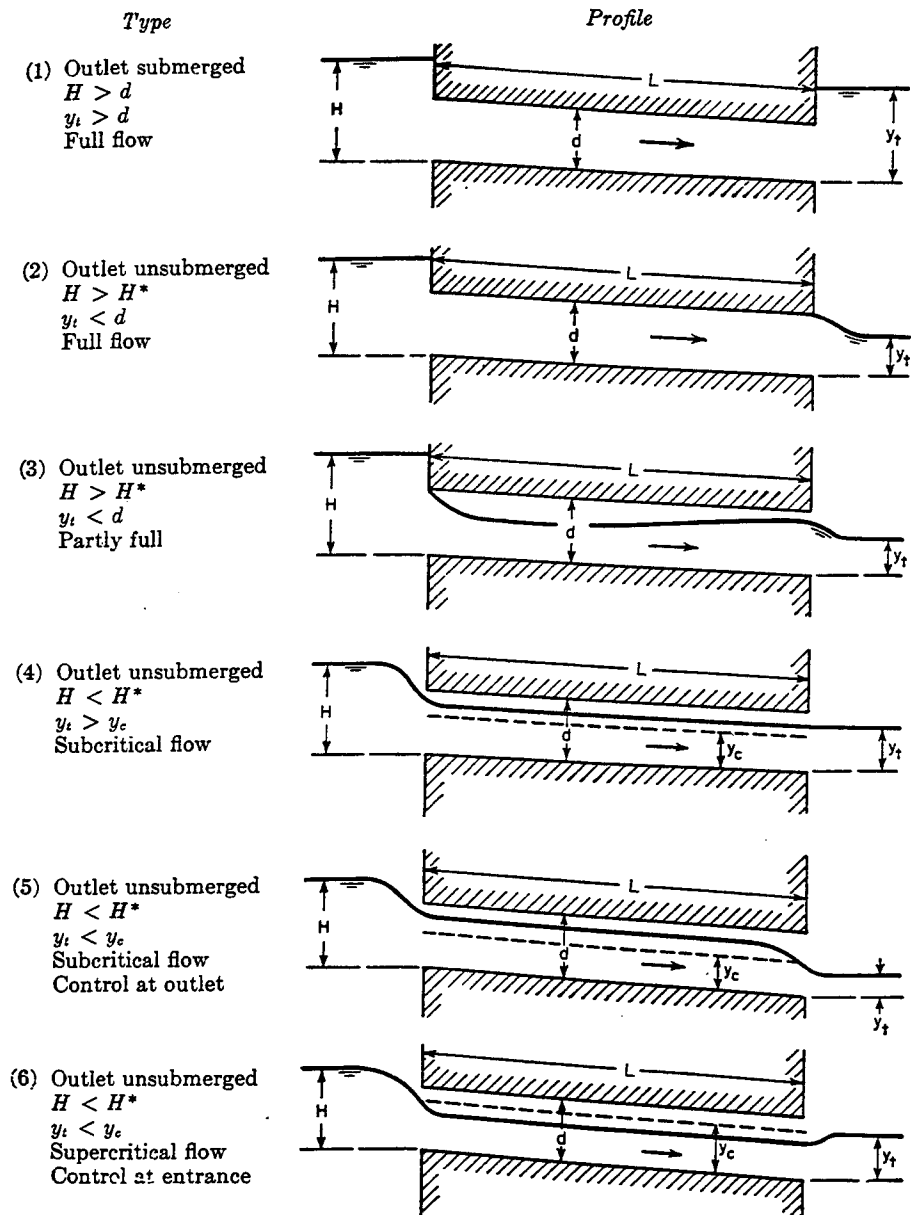


Figure 2.7. Classifications of culvert flow (Modified from Chow, 1959).

The headwater critical value is given as H^* and is usually between 1.2 and 1.5 times the diameter of the culvert. The critical depth is the depth of flow which corresponds to the minimum specific energy. For small slopes, the specific energy, E , is defined by:

$$E = y + \frac{V^2}{2g} \quad (2.9)$$

where y is the depth of the flow [m]; V is the velocity of the flow [m/s]; g is the gravitational acceleration [m/s²].

A slope which results in a flow depth greater than critical depth is referred to as a subcritical slope, while that resulting in a flow depth less than the critical depth is known as a supercritical slope.

2.2.4 Velocity Profiles

There have been numerous attempts to mathematically model velocity distributions for open channel flow (i.e. Prandtl-von Kármán Universal Law, 1979; Morsel et al. 1981; Chiu et al. 1988). These attempts can be divided into two types: (1) one-dimensional models which predict velocity as a function of depth; and (2) two-dimensional models which predict velocity throughout the cross-section.

One Dimensional Velocity Profiles.- The one-dimensional models for velocity distribution that were examined make use of a logarithmic relationship to predict the velocity. Roberson and Crowe (1990) detail the following two methods of determining the one-dimensional velocity distribution in the turbulent boundary layer: (1) The logarithmic velocity distribution; and (2) the Power-Law formula for velocity distribution.

The logarithmic velocity distribution of the turbulent boundary layer is given by:

$$\frac{u}{u^*} = 5.75 \log \left(\frac{yu^*}{\nu} \right) + 5.56 \quad (2.10)$$

where \mathbf{u} is the velocity [$\mathbf{m/s}$]; \mathbf{u}^* is the shear velocity ($\gamma R S_f$) [$\mathbf{m/s}$]; \mathbf{g} is the specific weight of the fluid [$\mathbf{N/m}^3$]; \mathbf{R} is the hydraulic radius [\mathbf{m}]; \mathbf{S}_f is the friction slope; \mathbf{y} is the depth [\mathbf{m}], and \mathbf{v} is the kinematic viscosity [\mathbf{m}^2/\mathbf{s}].

According to Roberson and Crowe (1990), the Power-Law formula has been shown to reasonably approximate the velocity distribution in the turbulent boundary layer for Reynolds numbers ranging from $10^5 < \mathbf{Re} < 10^7$. Moreover, the Power-Law formula has been shown to compare reasonably with experimental results for the range of $0.1 < \mathbf{y/d} < 1$. (Roberson and Crowe, 1990). The Power-Law Formula is:

$$\frac{u}{u_o} = \left(\frac{y}{\delta} \right)^{1/7} \quad (2.11)$$

where \mathbf{u} is the velocity [$\mathbf{m/s}$]; \mathbf{u}_o is the mean velocity [$\mathbf{m/s}$]; \mathbf{y} is the depth [\mathbf{m}]; and \mathbf{d} is the thickness of the boundary layer [\mathbf{m}].

Both of these methods are limited to the boundary layer thickness and require knowledge of the boundary layer thickness in order for them to be applied.

Chiu (1993) presents the Prandtl-von Kármán Universal Law interpreted for axial symmetric pipe flow taken from Schlichting (1979). For axis symmetric turbulent flow in a pipe, the Prandtl-von Kármán Universal Law is as follows:

$$\frac{u_{max} - u}{u_*} = -\frac{1}{k} \ln \left(1 - \frac{r}{D} \right) \quad (2.12)$$

where \mathbf{u} is the flow velocity [$\mathbf{m/s}$]; \mathbf{u}_{max} is the maximum velocity that occurs at the center of the pipe [$\mathbf{m/s}$]; \mathbf{u}_* is the shear velocity [$\mathbf{m/s}$], which has been previously defined; \mathbf{k} is the von Kármán constant; \mathbf{r} is the radial distance from the center of the pipe cross-section [\mathbf{m}]; and \mathbf{D} is the diameter of the pipe [\mathbf{m}].

Chiu (1993) discusses the following limitations of the Prandtl-von Kármán Universal Law. The Universal Law does not satisfy the boundary condition that $u=0$ at $r=R$. Therefore the model is inaccurate at the pipe wall. The Universal law also goes to infinity at $r=R$, so it is also inaccurate at the center of the pipe.

Kane and Wellen (1985) make use of an equation from Chow (1964) to predict the one-dimensional velocity distribution in highway culverts. The equation depends on average flow velocity, relative depth, and a roughness coefficient. Chow (1964) specifies that the equation is applicable to turbulent flow in a wide channel and that the equation does not apply near the bed or near the water surface. The equation is as follows:

$$\frac{(v-V)C}{V\sqrt{8g}} = 2 \log\left(\frac{y}{y_0}\right) + 0.88 \quad (2.13)$$

where v is the velocity at a point [m/s]; V is the mean velocity; C is the Chezy roughness coefficient; and $\frac{y}{y_0}$ is the relative depth.

The Chezy roughness coefficient (C) can be related to the Manning roughness coefficient (n) which was used previously. This relationship is given as:

$$C = \frac{R^{1/6}}{n} \quad (2.14)$$

where R is the hydraulic radius which was previously defined.

This relationship is substituted into Equation 2.13 and rearranged yielding the following expression for n :

$$v = \frac{(32g)^{1/2}(V_{avg})n}{R^{1/6}} \log_{10}\left(\frac{y}{y_0}\right) + \frac{0.88(8g)^{1/2}(V_{avg})n}{R^{1/6}} + V_{avg} \quad (2.15)$$

Mountjoy (1986) rewrites the above equation as:

$$v = A \log_{10} \left(\frac{y}{y_0} \right) + B \quad (2.16)$$

where $A = \frac{(32g)^{1/2} (V_{avg})n}{R^{1/6}}$, and $B = \frac{0.88(8g)^{1/2} (V_{avg})n}{R^{1/6}} + V_{avg}$. Mountjoy then develops a method

of predicting the coefficients **A** and **B** during the design phase of the culvert. The method of prediction involves using the correlation between the velocity at $\frac{y}{D_0} = 0.6$ and the coefficient **B**.

The correlation between the coefficient **B** and the coefficient **A** is then used to predict **A**. Based on a study of 49 sites throughout Alaska, Mountjoy developed prediction equations for the coefficients **A** and **B**. For circular culverts, values for the coefficient **A** were typically between -1 and 10, and values for coefficient **B** were typically between 0.5 and 13.

Two-Dimensional Velocity Distributions.- Morsel et al. (1981) proposed the concept of an occupied zone to address fish passage through culverts. Based on observations that fish use the low velocity region near the wall of the culvert for passage, the authors developed equations to predict **V_{occupied}**, which is the velocity in this occupied zone. The equations that Morsel et al. (1981) developed are as follows:

$$V_{occupied} = V_{skin} + 0.25(V_{avg} - V_{skin}) \quad (2.17)$$

where **V_{skin}** is the water velocity adjacent to the culvert wall [**m/s**]; and **V_{avg}** is the average water velocity in the culvert barrel [**m/s**].

Morsel et al. (1981) arbitrarily define the following:

$$V_{skin} = 0.4 V_{max} \quad (2.18)$$

$$V_{avg} = 0.8 V_{max} \quad (2.19)$$

Kane and Wellen (1985) make mention of the approach proposed by Morsel et al. (1981). They make some algebraic substitutions and present the following relationships which allow **V_{occupied}** to be determined directly from **V_{avg}**. For example:

$$V_{\text{occupied}} = 1.25 V_{\text{skin}} = 0.625 V_{\text{avg}} = 0.5 V_{\text{max}} \quad (2.20)$$

where **V_{occupied}**, **V_{skin}**, **V_{avg}**, and **V_{max}** have been previously defined. Measurements by the WDFW found $V_{\text{skin}} = 0.2 V_{\text{max}}$ rather than the value reported by Morsel et al. (WDFW, 1995).

Manning's equation is often used to calculate **V_{avg}** and **V_{occupied}** can be approximated through the use of Equation 2.20. Kane and Wellen (1985) state reservations about the form of the equations presented by Morsel et al. (1981). They suggest that first the size of the occupied zone be defined by the design fish and then established equations be used to determine the velocity in the occupied zone.

Chiu (1988) has developed a state-of-the-art approach for predicting two-dimensional velocity distributions in open channel cross-sections based on probability and entropy. Chiu (1993) further developed this approach and applied it to pipe flow studies. Chiu recommends the use of the following velocity distribution equation for pipe flow as an alternative to existing one-dimensional equations:

$$\frac{u}{u_{\text{max}}} = \frac{1}{M} \ln \left[1 + (e^M - 1) \frac{\xi - \xi_0}{\xi_{\text{max}} - \xi_0} \right] \quad (2.21)$$

where **u** is the velocity at a point [m/s]; **u_{max}** is the maximum velocity [m/s]; **M** is the dimensionless entropy parameter; and **ξ** is a dimensionless, independent variable used for the coordinate system. According to Chiu (1988), the entropy parameter, **M**, is a measure of the uniformity of the probability and velocity distributions. A value of **M** equal to zero represents a uniform distribution and corresponds to the (theoretical) maximum value of entropy. A value of

M approaching infinity represents an invariant velocity distribution and corresponds to the minimum entropy situation.

For the case of open channel culvert flow with axial symmetry, at the centerline the variable ξ is given by:

$$\xi = \frac{y}{d-h} \exp\left(1 - \frac{y}{d-h}\right) \quad (2.22)$$

where y is the vertical distance from the bottom of the culvert [m]; d is the depth of flow [m]; and h is the depth below the water surface where V_{\max} occurs [m].

Chiu (1988) derives an equation which relates the entropy parameter, M , to the ratio of $\frac{u_{avg}}{u_{max}}$. The equation is as follows:

$$\frac{u_{avg}}{u_{max}} = e^M (e^M - 1)^{-1} - \frac{1}{M} \quad (2.23)$$

where u_{avg} is the average velocity of the flow cross-section.

2.2.5 Field Observations and Experimental Data

While there has not been extensive research into the velocity distribution of culvert cross-sections, several papers were found to contain relevant information. Chow (1959) discusses the impact of secondary currents and states that careful laboratory investigations have revealed that flow in a straight prismatic channel is three-dimensional, exhibiting a spiral motion. According to Shukry (1950), a small disturbance at the entrance, which is usually unavoidable, can result in the shift of the zone of highest water level to one side and cause single spiral motion to occur. Two plots of the distribution of the velocity components in a straight rectangular channel are also given by Shukry and were used by Chow. The first plot shows the shift of the velocity component normal to the cross-section to one side of the channel (see Figure 2.8a). The second

plot shows the direction lines and the magnitude of the lateral velocity components and illustrates the spiral motion that is occurring in the channel (see Figure 2.8b).

Replogle and Chow (1966) examined circular pipes flowing partially full to determine the tractive-force distribution. Two test pipes were used in the experiment, a 10.2 cm (4.0 in) inside diameter copper pipe and a 13.3 cm (5.2 in) inside diameter cold-rolled steel pipe. Conical pipe entrance sections were used to provide a smooth transition of flow from the reservoir into the pipes. Velocity distribution data was taken for three depths of flow in the pipes, at approximately one-third, one-half, and two-thirds of the diameter of the culvert, D_0 . The authors mention that no attempt was made to examine a range of velocities because Kennedy and Fulton (1961) reported that the magnitude of the velocity had an insignificant effect on the velocity distribution for the range of velocities normally encountered. Four cross-sectional velocity distributions for the steel pipe are shown (see Figure 2.9, Figure 2.10, Figure 2.11, and Figure 2.12). The first cross-sectional velocity distribution (Figure 2.9) is at a relative depth of $0.33 \cdot D_0$, and appears to be very nearly symmetrical. The second cross-sectional velocity distribution (Figure 2.10) is at a relative depth of $0.5 \cdot D_0$, and shows a slight skew of the higher velocities to the left side of the pipe. The third cross-sectional velocity distribution (Figure 2.11) is at a relative depth of $0.68 \cdot D_0$, and shows a very slight skew of the higher velocities to the left side of the pipe. The final velocity distribution (Figure 2.12) is at a relative depth of 0.65 and at a slope of 0.8% which differs from the 0.2% slope that was used on the first three velocity cross-sections. This cross-section shows a distinct skew of the higher velocities to the left side of the pipe. The channel geometry is theorized to play a major role in triggering and establishing secondary currents which are believed to impact the location of maximum velocity in the pipe cross-section.

The most pertinent study was performed by Katopodis et al. (1978). A technical report was written on a study of model and prototype culvert baffles. To determine the effects of the baffles, a 4.27 meter (14 ft) diameter, 44.5 (146 ft) meter-long control culvert was tested without baffles at various discharges and relative depths. Cross-section velocity distributions were taken

at two stations within the culvert. The velocity distributions were plotted from the perspective of looking upstream with the flow coming out of the paper. This differs from the other velocity plots shown in this paper which are referenced as looking downstream with the flow going into the paper. One station was located approximately 13 meters (42.7 ft) ($L/D=3.0$) from the inlet of the culvert and the second station was located approximately 37 meters (121.4 ft) ($L/D=8.7$) from the inlet. The upstream station was tested at relative depths ranging from $0.38 \cdot D_0$ to $0.10 \cdot D_0$. The downstream station was tested at relative depths ranging from $0.32 \cdot D_0$ to $0.07 \cdot D_0$. The relative depth at the upstream station was greater than the relative depth at the downstream station which indicated gradually varied flow.

For relative depths greater than about $0.30 \cdot D_0$, the velocity distribution was skewed to the right side looking upstream. As the relative depth decreased, the velocity distribution became approximately symmetrical. Two sets of the cross-sectional velocity distributions are shown. The first set is for the highest flow condition observed of $12.2 \text{ m}^3/\text{s}$ (430.8 cfs) and a cross-sectional velocity distribution is given for both the downstream and upstream stations (see Figure 2.13). Figure 2.13a shows the velocity distribution for the upstream station at a relative depth of $0.38 \cdot D_0$, and there is a noticeable skew of the velocity distribution to the lower right side of the culvert. Figure 2.13b shows the velocity distribution for the downstream station at a relative depth of $0.32 \cdot D_0$, and there is a slight skew in the distribution to the right side of the culvert.

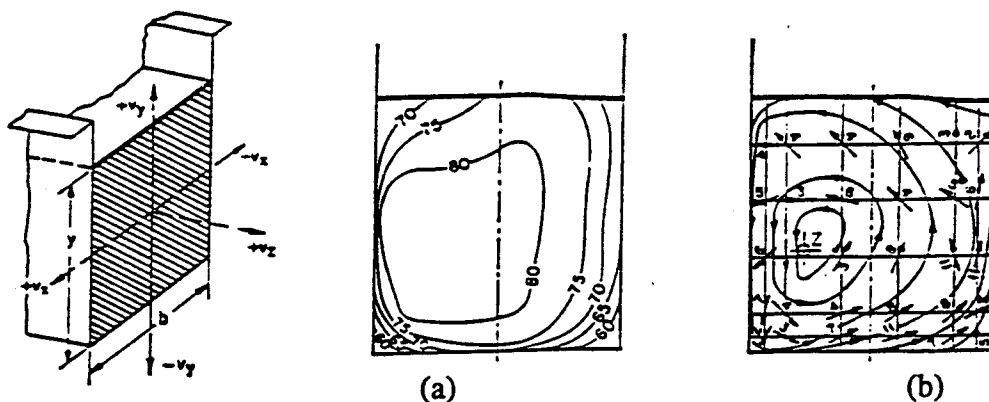


Figure 2.8. Distribution of normal and lateral velocity components in a straight rectangular channel (Modified from Chow, 1959). Velocity magnitudes shown are in cm/s.

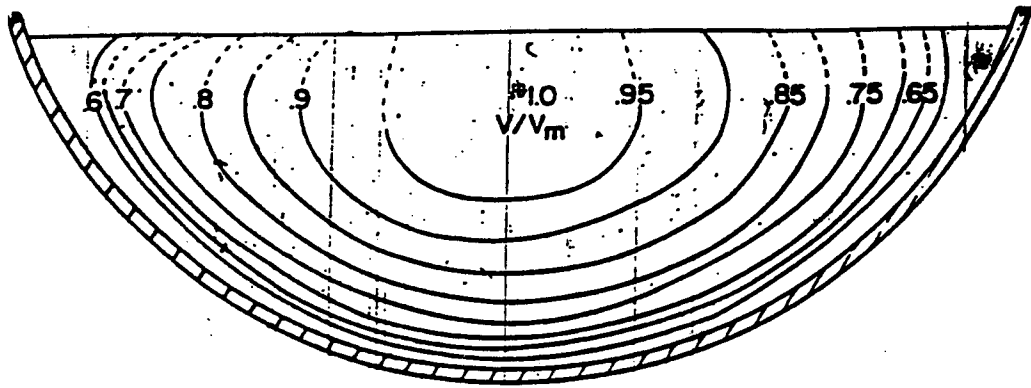


Figure 2.9. Relative velocity distribution for 13.3 cm diameter steel pipe with a flow rate of $0.0014 \text{ m}^3/\text{s}$, slope of 0.2%, and relative depth of $0.33 \cdot D_0$. Looking downstream.

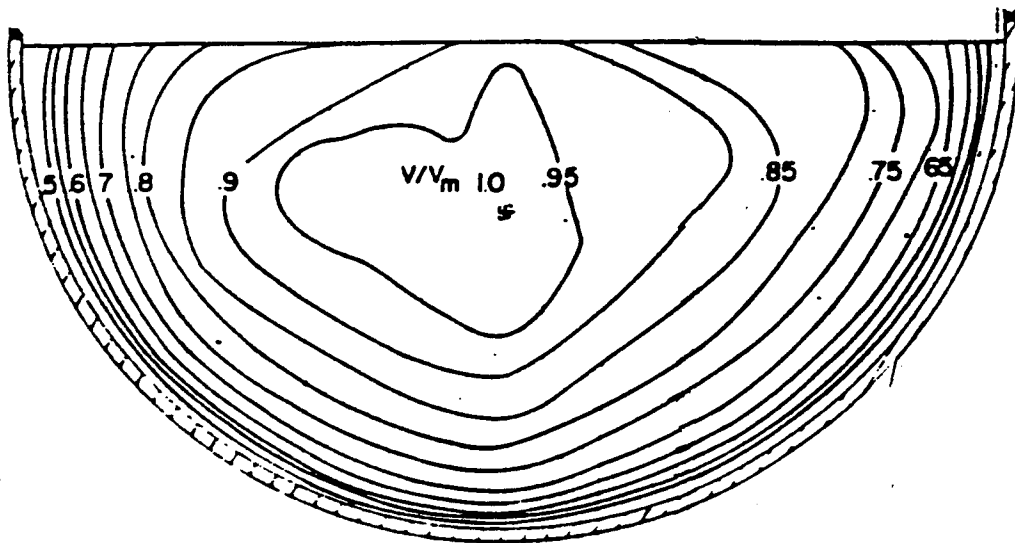


Figure 2.10. Relative velocity distribution for 13.3 cm diameter steel pipe with a flow rate of $0.0034 \text{ m}^3/\text{s}$, slope of 0.2%, and relative depth of $0.50 \cdot D_0$. Looking downstream.

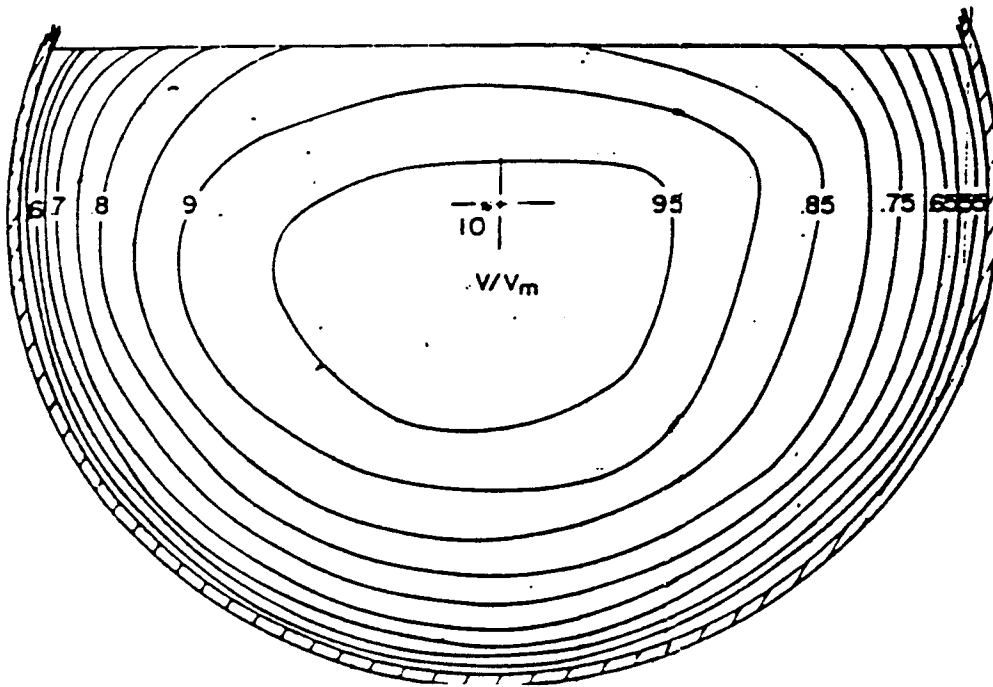


Figure 2.11. Relative velocity distribution for 13.3 cm diameter steel pipe with a flow rate of $0.0049 \text{ m}^3/\text{s}$, slope of 0.2%, and relative depth of $0.68 \cdot D_0$. Looking downstream.

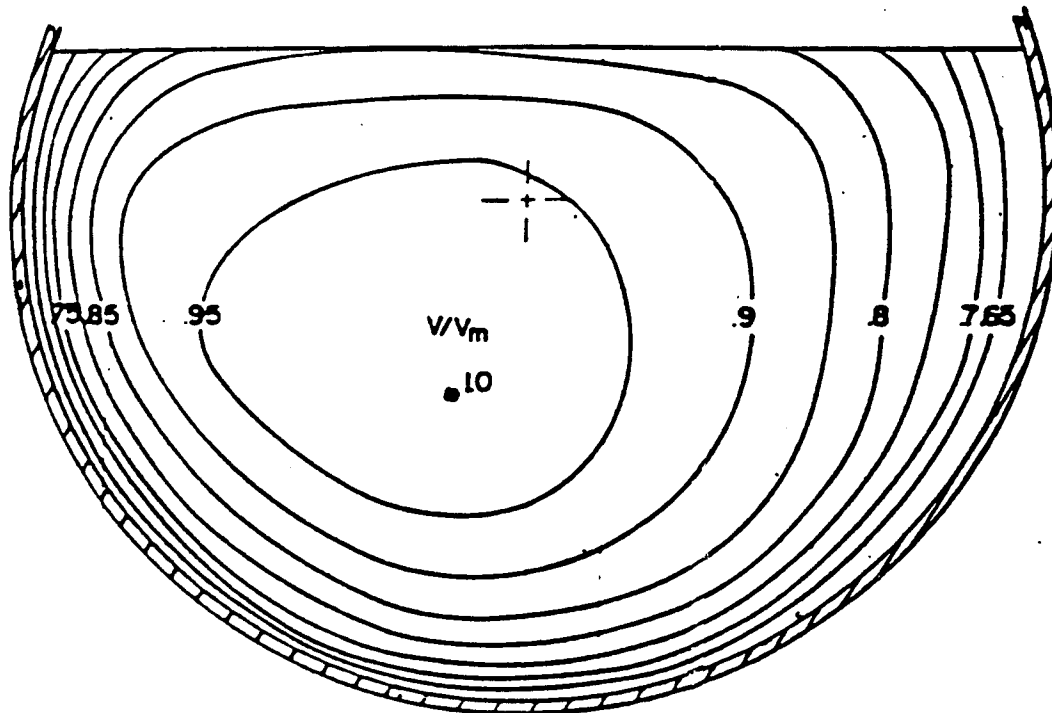


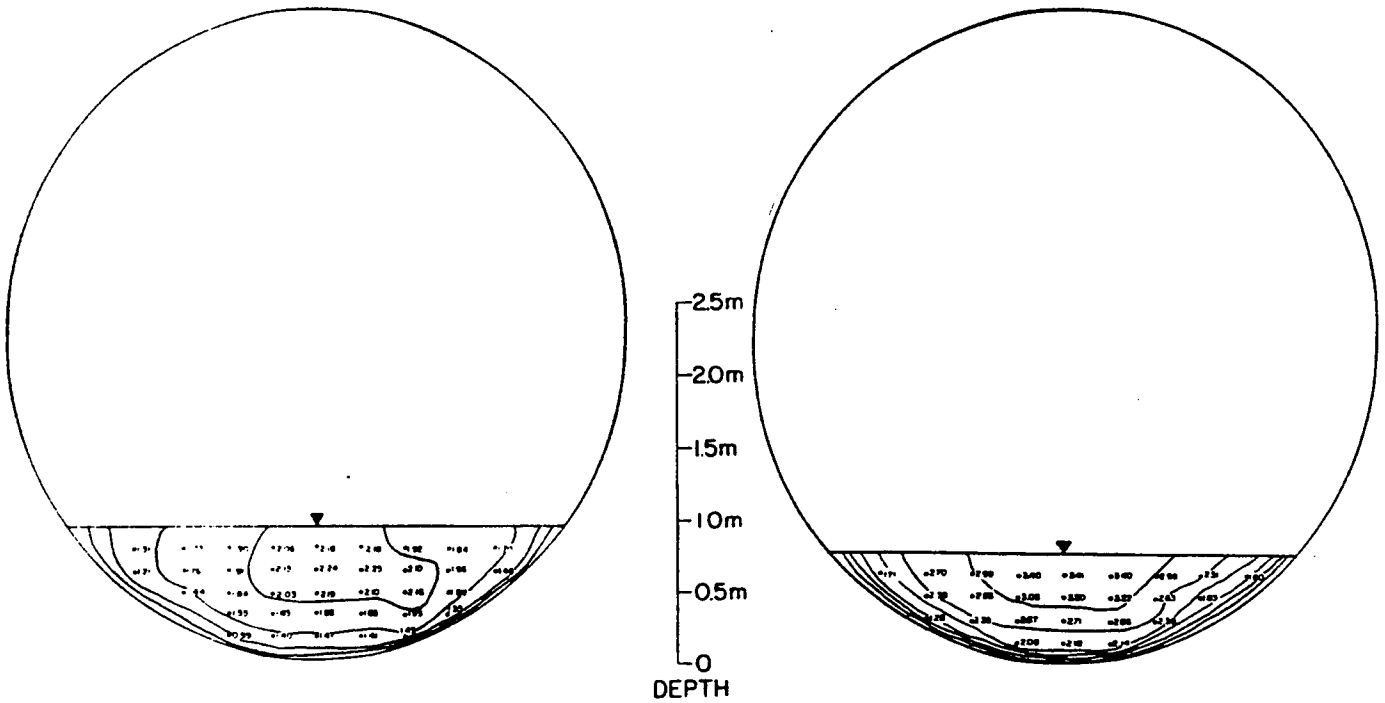
Figure 2.12. Relative velocity distribution for 13.3 cm diameter steel pipe with a flow rate of $0.0106 \text{ m}^3/\text{s}$, slope of 0.8%, and relative depth of $0.65 \cdot D_0$. Looking downstream.

The second set of cross-sectional velocity distributions is for a lower flow rate of $3.8 \text{ m}^3/\text{s}$ (134.2 cfs) with lower relative depths. A cross-sectional velocity distribution is shown for both the downstream and upstream stations (see Figure 2.14). Figure 2.14a shows the velocity distribution for the upstream station at a relative depth of $0.21 \cdot D_0$, and the velocity distribution is fairly symmetrical about the centerline of the culvert with a slight skew to the right side of the culvert. Figure 2.14b shows the velocity distribution for the downstream station at a relative depth of $0.17 \cdot D_0$, and the velocity distribution is nearly symmetrical about the centerline.

Behlke et al. (1989) made field observations of fish passage through a culvert in Fish Creek which is located in Alaska. The culvert tested in the study was a 2.9 meter (9.5 ft) diameter culvert with $15.2 \times 3.5 \text{ cm}$ ($6 \times 1.4 \text{ in}$) annular corrugations. At the cross section taken 9.14 meters (30 ft) ($L/D=3.2$) from the inlet, where the flow was assumed to be fully developed, the relative depth was approximately $0.25 \cdot D_0$. The discharge through the pipe was $3.06 \text{ m}^3/\text{s}$ (108.06 cfs). The velocity distribution that was generated is shown in Figure 2.15 and the velocity distribution exhibits a skew to the right side of the culvert. This skew is attributed to the fact that the culvert was not installed parallel to the flow of the stream. It should be noted that observations of other researchers, as well as from this research, do not support the assumption of Behlke et al. (1989) that the flow was fully developed at the sampling point.

2.3 Discussion of Existing Knowledge

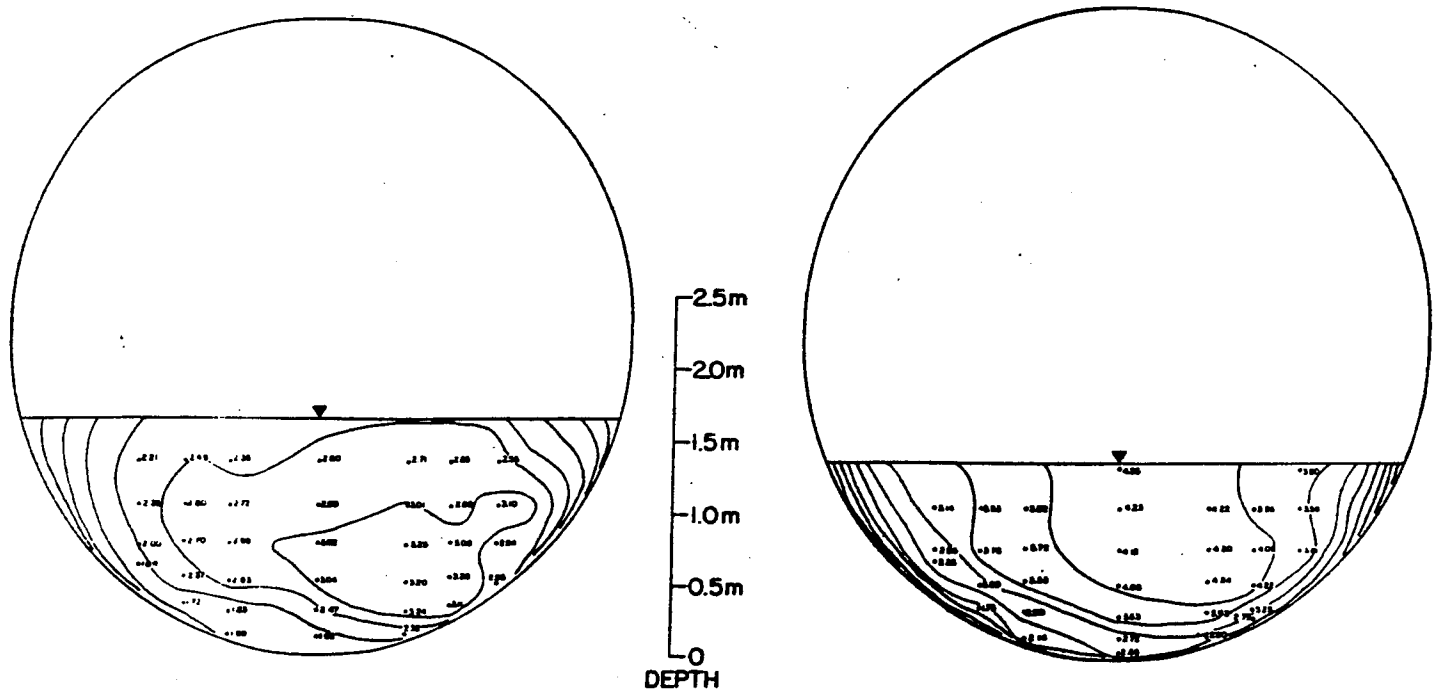
The following section presents a discussion concerning the limitations of the existing knowledge related to the two-dimensional velocity distributions in highway culverts and the resulting impact on juvenile fish passage. A discussion of the extenuation of existing knowledge that will be produced by this research is also included in this section.



(a) Upstream station

(b) Downstream Station

Figure 2.13 Velocity distributions at upstream and downstream stations with a flow rate of 12.2 m³/s. Looking upstream. (Modified from Katopodis et al. 1978).



(a) Upstream station

(b) Downstream Station

Figure 2.14 Velocity distributions at upstream and downstream stations with a flow rate of 3.8 m³/s. Looking upstream (Modified from Katopodis et al. 1978).

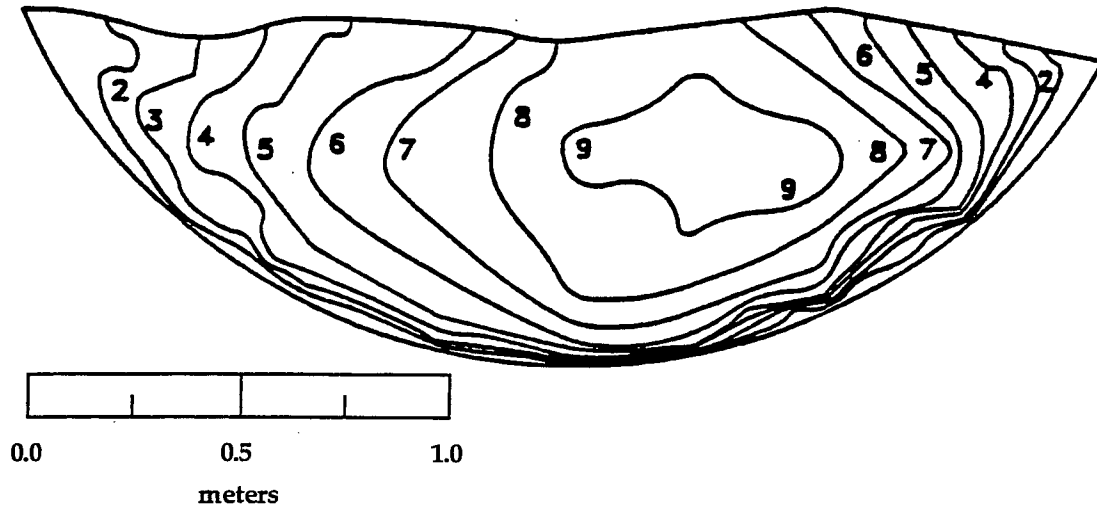


Figure 2.15. Velocity cross-section from 2.9 meter diameter culvert, with 15.2 x 3.5 cm annular corrugations, in Fish Creek Denali Highway, Alaska. Flow rate was 3.06 m³/s. (Modified from Behlke et al. 1989).

2.3.1 Limitations of Existing Knowledge

The goal of this research is to provide passage to juvenile fish through highway culverts. One step that would go a long way in reaching this objective is being able to accurately predict the two-dimensional velocity distribution in a highway culvert. The problem with even the state of the art two-dimensional model proposed by Chiu (1993) is that it will predict a velocity distribution that is symmetrical about the centerline. However, culverts are not smooth-walled pipes, and the corrugations create turbulent and chaotic flow in the boundary layer. As has been illustrated by field observations of culverts and experimental data on smooth pipes, there is currently no accurate method of predicting the velocity distribution in corrugated culverts. Entrance conditions, depth of flow, and irregularities of the culvert or its corrugations can all cause the cross-sectional velocity distribution to become non-symmetrical. The problems encountered in obtaining symmetrical velocity distributions even under laboratory conditions are

further complicated by current road construction practices. It is likely that culverts installed in the field will not be placed perfectly parallel to the natural stream flow and that little notice will be given to whether or not the culvert is truly round with no irregular corrugations or dents. Furthermore, another limitation is that none of the existing work has proposed an adequate method of predicting velocity distributions in corrugated highway culverts.

2.3.2 Extension of Existing Knowledge

Based on preliminary results obtained from experiments on the first test culvert and results from other researchers, this research focused on determining a method of predicting the size of the low velocity zone and the low velocity in this zone. This research proposes to extend the existing knowledge through the development of a method of predicting the velocity distribution. The ability to characterize the velocity distribution will provide the hydraulic engineer with a valuable tool that will help to insure juvenile fish passage. The intention of this research is not to attempt to account for every molecule of water flowing through a culvert, but rather to provide an empirical approach that will predict the amount of cross-sectional area in a culvert that has velocities which are sufficiently low to provide passage for juvenile fish. The data generated from this research may also be used to extend the knowledge of the hydraulic characteristics of flow through corrugated highway culverts. It must be noted that this research dealt exclusively with circular culverts with annular corrugations. It also must be noted that only hydraulic characteristics of flow were considered related to juvenile fish passage. The prediction of the velocity distributions must be combined with considerations of other factors that may impact juvenile fish passage, such as high sediment load and temperature.

Chapter 3

METHODOLOGY

As previously stated, the primary objectives of this research were to measure the velocity distributions in small-diameter highway culverts and to develop a means of extrapolating these results to large-diameter highway culverts. To help reach these objectives, both an experimental setup and an experimental procedure were developed. The following chapter describes these methodologies and, where appropriate, the rationale behind them.

3.1 Experimental Setup

The research for this project was conducted at the R.L. Albrook Hydraulic Laboratory operated by the Department of Civil and Environmental Engineering at Washington State University in Pullman, Washington. Whenever possible, existing laboratory facilities were used in the research.

3.1.1 Flume

Individually, each of the experimental culverts was placed in an existing 22.3 meter (73.2 ft) long flume. A schematic diagram of the flume setup is shown in Figure 3.1. The walls of the flume are 57.8 cm (22.8 in) high walls and the flume is 90.8 cm (35.7 in) wide. The flume can be tilted through the use of a screw jack to provide slope of up to 2.5%. The head box of the flume is supplied by a maximum of four pumps through two feed pipes. Without modification, the flume allows for culverts up to 76.2 cm (30 in) in diameter to be tested with flow rates up to 0.14 m³/s (4.94 cfs) (as measured by a magnetic flow meter). Although the pumps were capable of much higher flow rates (up to 0.850 m³/s (30 cfs)) the allowable pressure in the feed pipes was limited to 103.4 kPa (15 psi). The flume is also equipped with a tailgate that allows for downstream control (see Figure 3.2). To provide straight flow that was normal to the cross-section of the flume, two honeycomb flow aligners (see Figure 3.3) were placed immediately

after the head box. And finally, to reduce the effect of the contraction created by the culvert entrance, an transitional entrance structure was built out of plywood and a lightweight concrete compound. This entrance structure provides a transition from the rectangular flume to the circular culvert. A schematic drawing showing the dimensions of the entrance transition is provided in Figure 3.4.

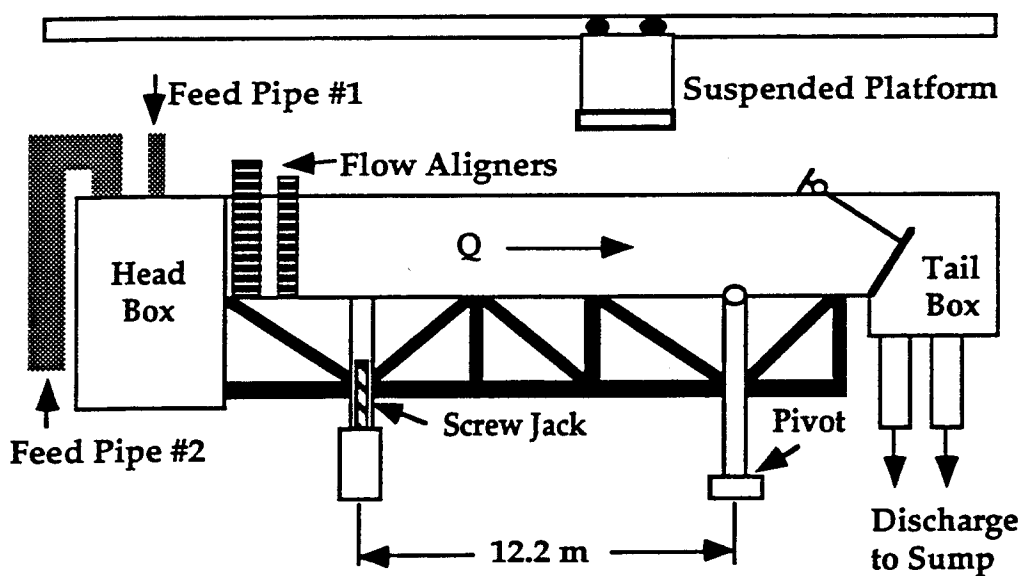


Figure 3.1 Schematic drawing of flume.

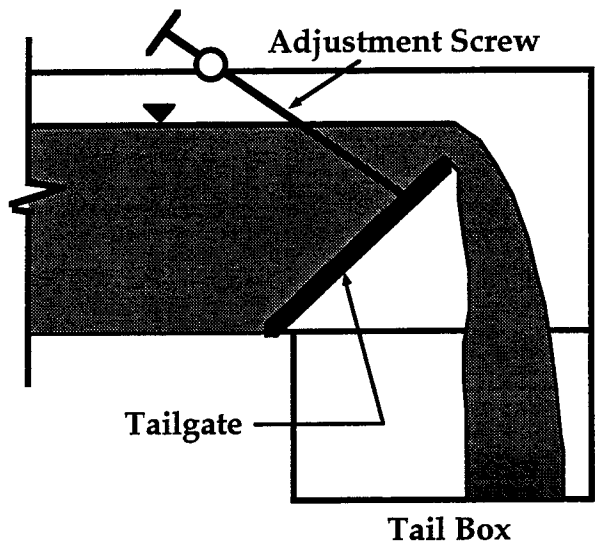


Figure 3.2 Schematic drawing of tailgate.

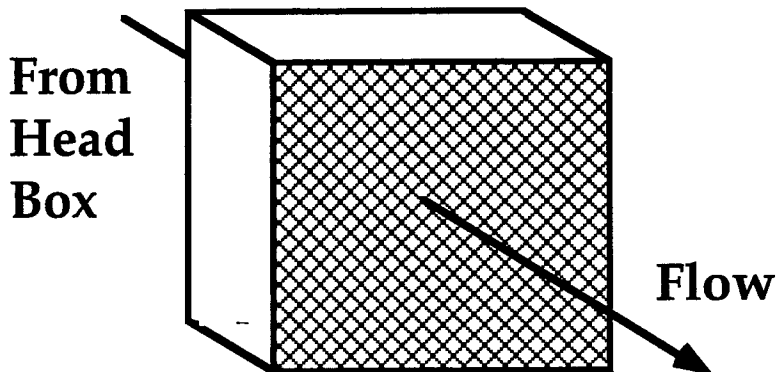


Figure 3.3 Honeycomb flow aligner.

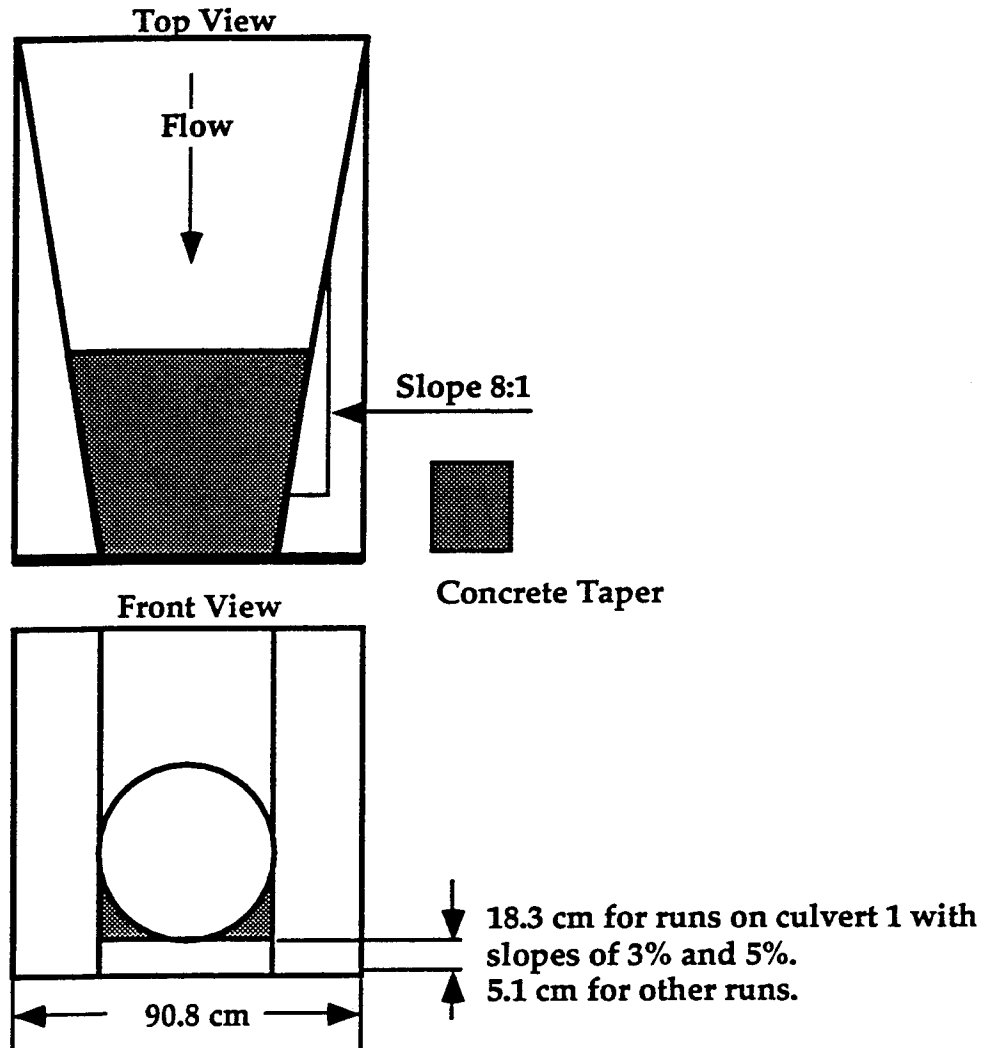


Figure 3.4 Schematic drawing of transitional entrance structure.

3.1.2 Nixon Model 403 Low Speed Probe w/ Streamflo Model 422 Digital Indicator

The velocity measurements were taken by a Nixon Model 403 Low Speed Probe. The Nixon probe is a propeller flow meter designed for measuring velocities from 2.5 to 150 cm/s (0.98 to 59 in/s). The probe has a $\pm 5\%$ accuracy for velocities between 2.5 and 7.5 cm/s (0.98 and 2.95 in/s), a $\pm 2\%$ accuracy for velocities between 7.5 and 15.0 cm/s (2.95 and 5.90 in/s),

and a $\pm 1\%$ accuracy for velocities between 15.0 and 150 cm/s (5.90 and 59.0 in/s). The Nixon probe generates an analog signal which is read by a battery powered Streamflo Model 422 Digital Indicator and is read in units of Hertz. The units of Hertz are then converted to a velocity in cm/s via a calibration chart supplied by the manufacturer. The Nixon probe was attached to a point gage which in turn was mounted on a horizontal slide bar (see Figure 3.5). The slide bar was attached to a suspended platform which was able to be moved along the length of the flume. The point gage allowed for the vertical movement of the probe to be measured and the horizontal slide bar allowed for the horizontal movement of the probe to be measured.

To take velocity measurements near the sides of the pipe, the Nixon probe was attached to the point gage via a rotation joint. The joint allowed for the probe to be angled at 45 degrees to reach the sides of the culvert. Two Nixon probes were used in this research. The first probe (#1858) was purchased new for this research project. The second probe (#881) had been purchased for use on earlier research projects.

3.1.3 Apple Macintosh Quadra 650 w/ I/O Board

Collection of the probes output signal was done via an Apple Macintosh Quadra 650 equipped with a Lab-NB I/O board. The software LabVIEW was installed on the computer and allowed for the voltage being read in by the I/O board to be calibrated to the frequency reading generated by the Nixon Probe. The Quadra was used as a data logger and allowed an average velocity to be taken from a large number of readings.

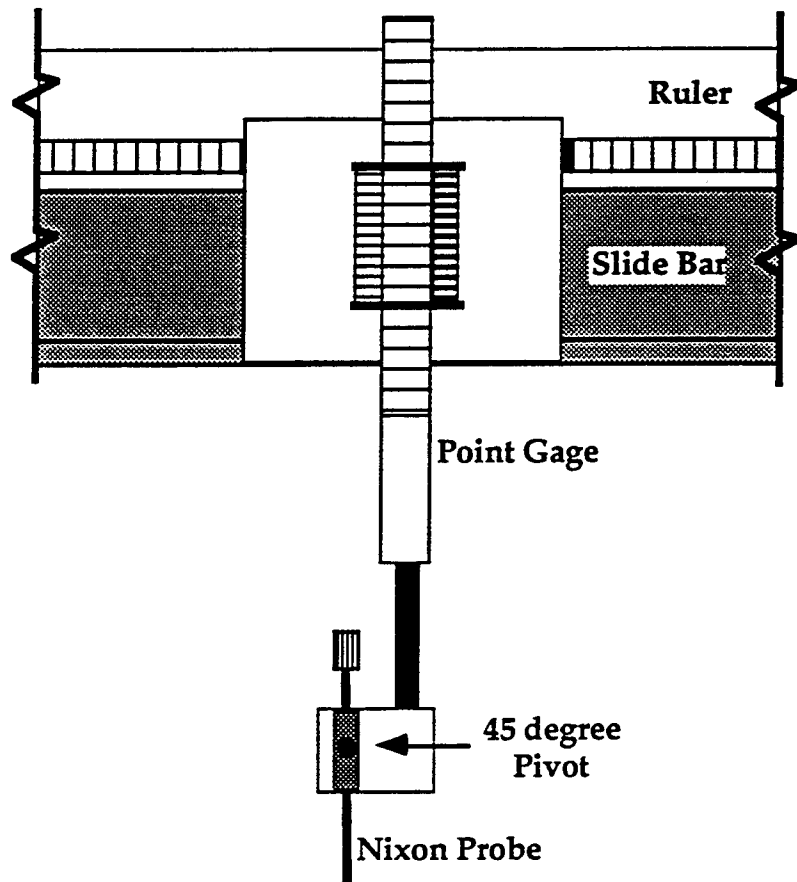


Figure 3.5 Diagram of Nixon probe mounting.

3.2 Calibration and Verification of Experimental Setup

The slope of the flume was verified through the use of a surveyors level. The screw jacks were calibrated to a ruler that was mounted on the support of the jack. The distance between the screw jack and pivot was 12.2 m (40.0 ft), so in order to provide 1% slope, the screw jack raised the flume 12.2 cm (4.8 in).

The magnetic flow meters were calibrated by using a trapezoidal (Cipolletti) weir with end inclinations of 4V:1H (Grant, 1979). The flow rate over a range of discharges was measured manually using the weir. The flow rate was then plotted versus the flow gage reading

for each gage. A linear regression was performed using KaleidaGraph software and the equations for flow gages #1 and #2 are as follows:

$$Q = 0.0020 + 0.0007 * G \quad R^2=0.99 \quad (\text{Gage \#1}) \quad (3.1)$$

$$Q = -0.0019 + 0.0012 * G \quad R^2=0.98 \quad (\text{Gage \#2}) \quad (3.2)$$

where **Q** is the flow rate [**m³/sec**]; and **G** is the magnetic flow gage reading.

Probe 1858 was compared with Probe 881 to insure it was yielding accurate velocity measurements. A linear regression was performed on the calibration charts for each of the probes which were supplied by the manufacturer. An equation was derived for each Nixon probe and the two resulting two equations are:

$$V = 4.8 + 0.53 * R \quad R^2=0.99 \quad (\text{Probe 1858}) \quad (3.3)$$

$$V = 5.4 + 0.51 * R \quad R^2=0.99 \quad (\text{Probe 881}) \quad (3.4)$$

where **V** is the velocity of the flow [**cm/s**]; and **R** is the frequency reading generated by the Nixon probe [**Hz**].

It should be noted that Probe 1858 was only used on runs for Culvert #2. During an experimental run the probe was damaged and it became necessary to use Probe 881 for the remaining experimental runs.

On a number of experimental runs the flow velocity readings from the Nixon probe were widely scattered for measurements taken near the corrugations. An average of several readings was taken to yield the average flow velocity at the location being tested. The Streamflo Model 422 Digital Indicator that was used with the Nixon probe allowed for a 10-second average to be taken provided that the average was below 100 Hz. For averages greater than 100 Hz, the average had to be taken manually. For a time during the experimental runs, the Macintosh Quadra 650 mentioned earlier was available for use as a data logger. Through the use of the I/O

board in the computer and the LabVIEW software the computer was configured to read a large number of inputs from the Nixon probe and provide the mean and standard deviation for the readings. The voltage signal imputed to the computer was calibrated to the frequency signal read by the Streamflo display unit, by taking measurements in areas of steady flow where the Nixon probe readings varied only slightly (± 2 Hz). A plot was made of the frequency reading from the Nixon probe versus the voltage read by the I/O board. A linear regression was performed on this plot and the equation of the best fit line is:

$$P = 2.24 + 1.13 \cdot V_t \quad R^2 = 0.99 \quad (3.5)$$

where P is the Nixon probe reading from the Streamflo display unit [Hz]; and V_t is the voltage read by the computer [mV].

3.3 Experimental Procedure

The development of an experimental procedure for this project seemed at times to be a never ending evolution. The first task that had to be undertaken was to select the culverts that would be tested. The second and more difficult task was to develop a procedure for testing the culverts.

3.3.1 Culvert Selection

One of the primary goals of this research is to provide a means of extrapolating results from small-diameter experimental culverts to any size diameter culverts used for fish passage. Ideally, the results of one of the small-diameter culverts would be compared directly to results from a large-diameter fish passage culvert, with both of the culverts tested in the laboratory under controlled conditions. Unfortunately the flume that was available for this research could only accommodate culverts up to 76 cm (30 in).

Based on logistic constraints, it was decided to test three corrugated culverts and one smooth steel pipe. Since large-diameter culverts used for fish passage have annular corrugations, all of the corrugated culverts tested had annular corrugations. Based on requests from the WSDOT, it was decided that one culvert would have 7.6 x 2.5 cm (3 x 1 in) corrugations. This culvert had to be custom made with an inside diameter of 73.7 cm (29.0 in) since the minimum standard diameter available was 91.4 cm (36 in). It was decided the other two culverts would both have 6.8 x 1.3 cm (2.7 x 0.5 in) corrugations and would be of different diameters. One culvert had an inside diameter of 30.5 cm (12 in) and the other culvert had an inside diameter of 61.0 cm (24 in). The non-corrugated pipe was selected to have an inside diameter of 61.0 cm (24 in). Table 3.1 provides the diameter, length, and corrugation properties for each of the three culverts that was selected. Diagrams of the 6.8 x 1.3 cm (2.7 x 0.5 in) and the 7.6 x 2.5 (3 x 1 in) annular corrugations are shown in Figure 3.6 and provide a comparison between the two corrugations.

Table 3.1 Experimental Culverts

Culvert #	Inside Diameter	Length	Corrugation
1	30.5 cm (12 inch)	6.10 m	6.8 x 1.3 cm
2	61.0 cm (24 inch)	12.20 m	6.8 x 1.3 cm
3	73.7 cm (30 inch)	9.74 m	7.6 x 2.5 cm
4	61.0 cm (24 inch)	6.10 m	none

The three highway culverts were constructed of 16-gage steel in several shorter sections that were overlapped and plug welded together to form the culvert. Culvert #1 was assembled from ten shorter pipe sections, Culvert #2 was assembled from two lengths of culverts, each comprised of ten shorter pipe sections, and Culvert #3 was also assembled from two lengths of culvert with eight shorter pipe sections in one length and six pipe sections in the second length. Each of the shorter pipe sections was plug welded along its longitudinal axis to form a

cylindrical section. When the shorter pipe sections were assembled and welded together, the welds that ran along the longitudinal axis of each pipe section were not lined up. The non-corrugated steel pipe (Culvert #4) was also constructed of 16-gage steel in four welded pipe sections which were then welded together. As was the case for the corrugated culverts, the welds that ran along the axis of each pipe section were not lined up when the four sections were welded together.

For Culvert #2 and Culvert #3 a corrugated coupling band with a band angle connector (see Figure 3.7) was used to joint together the two lengths of culvert. The coupling band was made from the same corrugated steel as each of the culverts and was tightened by bolts passing through the band angle connector. Culvert #2 consisted of two 6.10 meter long lengths of culvert and Culvert #3 was jointed 4.17 meters (13.7 ft) from the entrance of the culvert. The coupling bands for each culvert were sealed with silicone caulking to prevent water from leaking out of the joints.

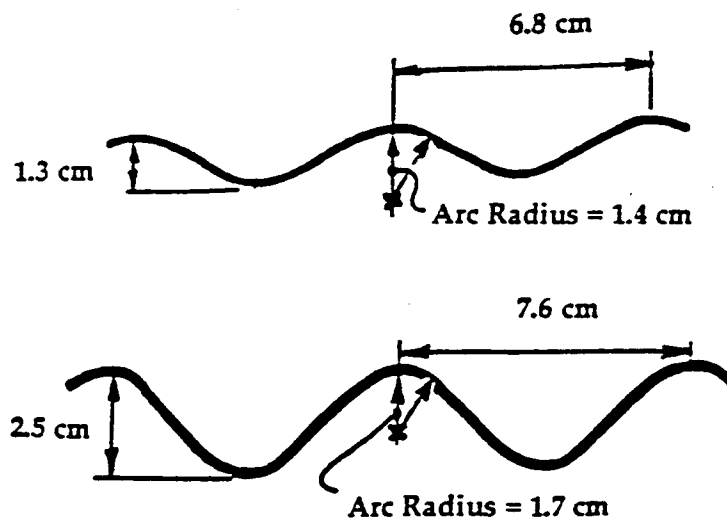


Figure 3.6 Shapes of Annular Corrugations for 6.8 x 1.3 cm (2.7 x 0.5 in) and 7.6 x 2.5 cm (3 x 1 in) corrugations.

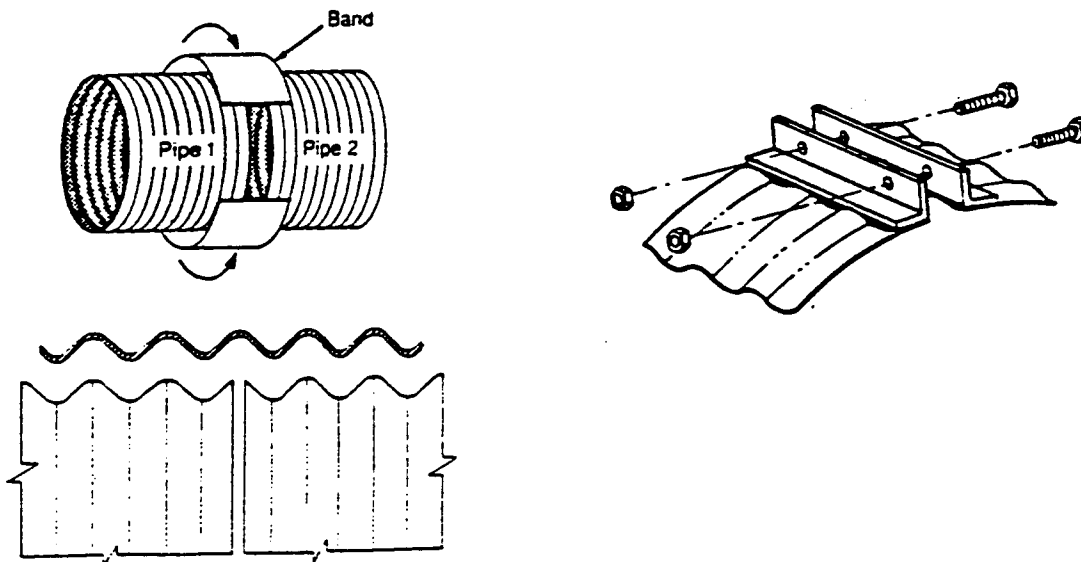


Figure 3.7 Diagram of corrugated coupling band and band angle connector.

3.3.2 Testing Procedure

The first experimental culvert was placed in the flume and secured by semi-circular templates that supported the culvert 5.1 cm (2 in) above the bottom of the channel and held the culvert in the center of the flume. The entrance of the culvert was fitted with a flat plate made of plywood. Extensive testing was performed on this culvert in order to develop a testing procedure for the remaining culverts.

Small access holes were cut along the top centerline of the culvert at intervals of 1 diameter (61.0 cm (24.0 in), $L/D=1$). At three different flow rates and two different slopes the centerline velocity distributions were taken at several stations along the culvert in an attempt to find the point where flow in the culvert became uniform and "typical". The centerline velocity plot for a flow rate of $0.113 \text{ m}^3/\text{s}$ (4 cfs) at one-half percent slope with a relative depth of $0.5 \cdot D_0$ is shown in Figure 3.8. This plot shows the centerline velocity distribution continuing to change

at stations along the culvert. This plot is typical of the centerline distributions that were taken and demonstrates the inability to find a "typical" cross-section for the selected culverts. Because the location of a typical cross-section was not determined, it was decided to take cross-sectional velocity distributions at two stations in the culvert. This allowed for a two-dimensional investigation of how the velocity distribution of the flow developed as it traveled down the culvert. The two stations selected were one at a distance of 8 diameters (4.9 m (16.1 ft), $L/D=8$) from the entrance and one at a distance of 14 diameters (8.5 m (27.9 ft), $L/D=14$) from the entrance.

The velocity measurements were taken at data points in a grid that covered the cross-section of the flow. The centerline of the culvert was determined, and the Nixon probe was placed at the bottom of the culvert, along the centerline, at the top of the corrugation. This was the origin of the cross-sectional grid. As the Nixon probe was moved vertically, the point gage yielded a Y-axis component. After the velocity readings had been taken at the centerline, the probe was moved horizontally along the slide bar and the process was repeated until all areas of the culvert cross-section were covered. A meter stick mounted behind the slide bar yielded the X-axis component. The velocity measurements were recorded along with the X and Y coordinates. For the first several cross-sections a considerable number of data points were taken throughout the cross-section. Nearly 400 data points were taken on a few of the initial experimental runs. Because of the time required to take this many data points, it was decided that it was not feasible to take as many data points on later runs. Depending on the relative depth and the culvert diameter, the number of data points for subsequent runs was usually between fifty and one hundred and twenty. Because of the interest in the region near the wall for this research, more data points were taken near the boundary of the culvert than in the center of the flow.

At the eight diameter station ($L/D=8$), a large access slot was cut in the top of the culvert to allow for the Nixon probe to take velocity measurements at points throughout the cross-section. A flow rate of $0.127 \text{ m}^3/\text{s}$ (4.48 cfs) was used with a slope of one-half percent with no downstream control. The velocity readings from the Nixon probe were consistently higher on

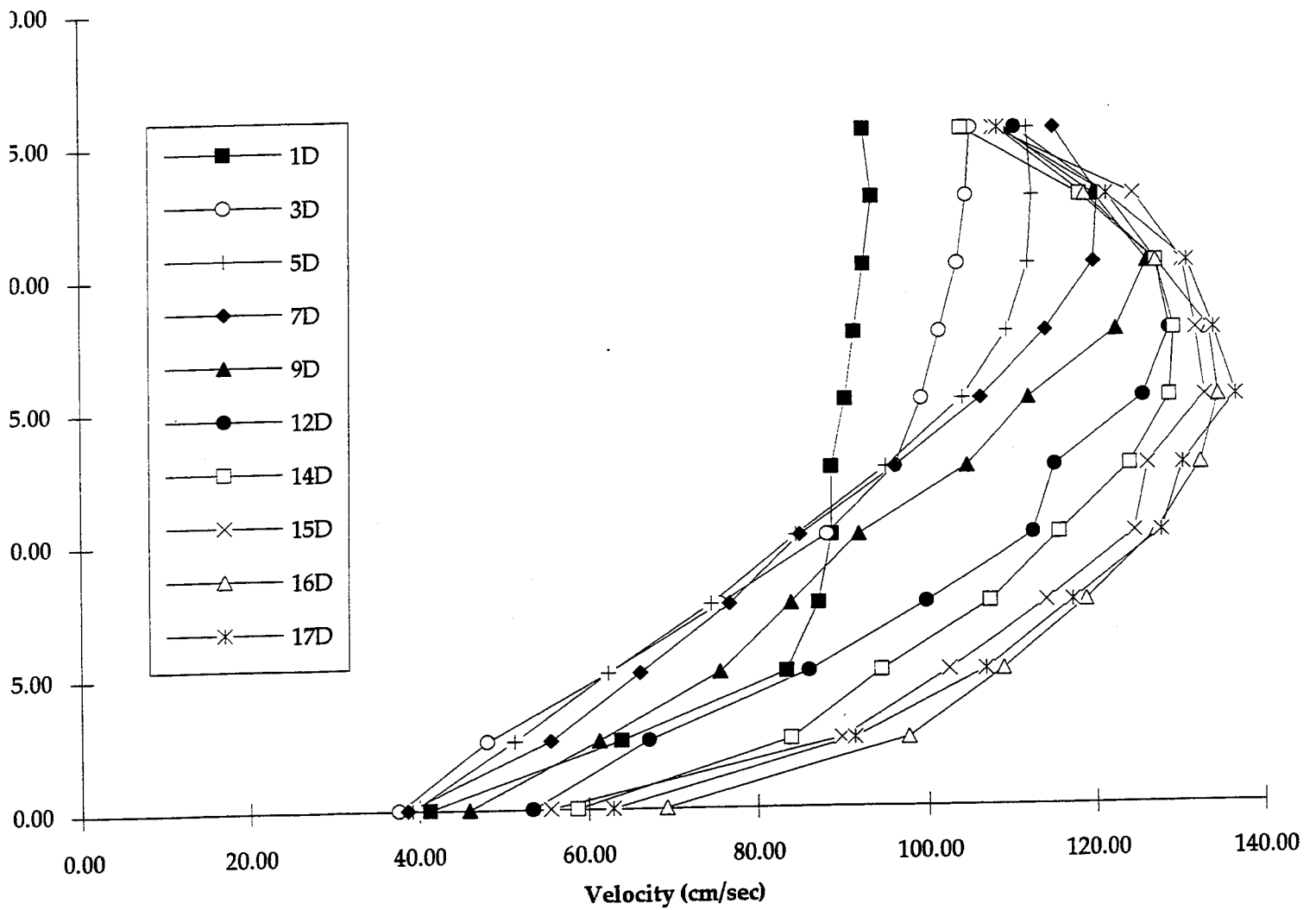


Figure 3.8 Centerline velocity distributions for culvert #1 at 0.113 m³/sec, slope = 1/2%, relative depth = 0.5*D_O, with no downstream control.

the left side of the culvert (looking downstream) and the velocity distribution was not symmetrical about the centerline. A standing wave was also observed throughout the length of the culvert that appeared to originate at the culvert entrance. The wave seemed to be caused by the sudden contraction caused by the flat plate at the entrance. It was theorized that the flow in the culvert was behaving similar to a ricocheting bullet as it traveled through the culvert with the maximum velocity shifting from side to side and not traveling along the centerline of the culvert as expected. Because of the unexpected results obtained from the first cross-section, the data collection was repeated under the same conditions and the results were again the same. At this point it was decided to build the entrance region to provide a gradual transition from the rectangular flume to the circular culvert.

The decision was also made to use the tailgate on the flume as a downstream control device to control the depth of flow in the culvert. The tailgate and lower flow rates were used, in addition to the entrance region, in an attempt to provide more symmetrical velocity distributions. Velocity distributions were taken at the 8 diameter station and the 14 diameter station under the new conditions. These distributions were to be taken at a relative depth of $0.5 \cdot D_0$. However, because the tailgate caused a backwater effect, the depth at the 8 diameter station was different than the depth at the 14 diameter station. To preserve continuity at both stations for each testing condition, the relative depth of flow at the entrance was set to be $0.5 \cdot D_0$. This resulted in relative depths that ranged from $0.52 \cdot D_0$ to $0.56 \cdot D_0$ for the station at $L/D=8$, and from $0.54 \cdot D_0$ to $0.62 \cdot D_0$ for the station at $L/D=14$, depending on flow rate and slope. The velocity distributions generated for the stations at $L/D=8$ and $L/D=14$ still showed a skew to the left side of the culvert despite the honeycomb aligners, entrance region, and lower flow rates.

Two more slots were cut in the culvert in order to measure the velocity distributions at a distance of 1 diameter (0.6 m (2 ft), $L/D=1$) and a distance of 12 diameters (7.3 m (24 ft), $L/D=12$) from the entrance. The velocity distribution taken at $L/D=1$ was nearly symmetrical, but it was slightly skewed to the left side of the culvert. The velocity distribution taken at $L/D=12$ was similar to the velocity distributions taken at the $L/D=14$ station, and showed a skew

to the left side of the culvert. On the basis of the results obtained from the velocity distributions taken at various stations through the culvert, the decision was made to test each of the culverts at a distance approximately 70% of the length of the culvert from the entrance. This was done to try and minimize the impact of the entrance and the exit of the culverts. For Culvert #1 the testing station was selected at $L/D=14$ (14 m (46 ft) from the entrance), for Culvert #3 the testing station was selected at $L/D=8$ (20 m (66 ft) from the entrance), and for Culvert #4 the testing station was selected at $L/D=7$ (14m from the entrance).

The WDFW requested that experimental runs be performed at relative depths other than $0.5 \cdot D_0$. It was also of interest to investigate the effect of the backwater caused by the tailgate. A relative depth of $0.25 \cdot D_0$ provided the opportunity to test the flow through the culvert with and without the tailgate. The decision was made to scale the flow rate down from the flow rate used for the relative depth of $0.5 \cdot D_0$. From Manning's equation (Equation 2.3) it was assumed that the roughness coefficient, n , and the friction slope, S_f , were constant for the culvert and that $AR^{2/3}$ was the term that varied. Based on this assumption it was decided to scale the flow rate by the ratio $\frac{AR_{0.25D_0}^{2/3}}{AR_{0.5D_0}^{2/3}}$. The culvert was first run with a relative depth at the entrance of $0.25 \cdot D_0$, with the tailgate and a scaled flow rate, and then the culvert was run again at a relative depth of $0.25 \cdot D_0$ with no tailgate and at the flow rate required to make the relative depth $0.25 \cdot D_0$ at the entrance.

The selection of the 30.5 cm (12 in) diameter culvert provided the opportunity to test a culvert under conditions that were not possible for the other two culverts. The culvert was tested at relative depths greater than $0.5 \cdot D_0$ without the tailgate. The WDFW requested that experimental runs be made with slopes up to five percent, so the culvert was installed at a slope of three percent relative to the floor of the flume for a number of runs. This allowed for the culvert to be tested at slopes of three and five percent.

Based on the preliminary testing results and the previous work discussed in Section 2.2.5, it was concluded that it was not possible to predict the exact shapes of the velocity cross-

sections. This conclusion was reached because of the skew that was experienced in several of the velocity cross-sections. The decision was made to experimentally determine the percentage of area of the cross-section with various relative velocities. The contours of the velocity distribution plots were at relative velocities of $0.2*V_{max}$, $0.4*V_{max}$, $0.5*V_{max}$, $0.6*V_{max}$, $0.8*V_{max}$, $0.9*V_{max}$, and $0.95*V_{max}$. The percentage of area in the cross-section that was within the boundary of each contour line was determined for each of the velocity distribution plots that was taken. A total of 51 cross-sections were taken in the four culverts. The station, flow rate, slope, relative depth, and downstream control testing conditions for each of the 51 runs is detailed in Table 3.2. These testing conditions were selected based on requests from the WSDOT and the WDFW, and to allow for an investigation of the impact on the velocity distribution of change in diameter, use of corrugation, change in corrugation, change in slope, change in flow rate, and use of downstream control. The results from these 51 runs were then used to develop an empirical method of predicting the percentage of area in the cross-section with velocities acceptable for juvenile fish passage.

Table 3.2 Experimental Runs

Culvert	Station (L/D)	Slope (%)	Flow Rate (m ³ /sec)	Relative Depth at Entrance	Downstream Control
1	14 Diam	0.5	Variable	0.33	N
1	14 Diam	0.5	0.0124	0.50	Y
1	14 Diam	0.5	0.0213	0.50	Y
1	14 Diam	0.5	Variable	0.75	N
1	14 Diam	1.0	Variable	0.33	N
1	14 Diam	1.0	0.0124	0.50	Y
1	14 Diam	1.0	Variable	0.50	N
1	14 Diam	1.0	Variable	0.75	N
1	14 Diam	3.0	Variable	0.25	N
1	14 Diam	3.0	Variable	0.50	N
1	14 Diam	3.0	Variable	0.75	N
1	14 Diam	5.0	Variable	0.25	N
1	14 Diam	5.0	0.0142	0.50 [‡]	Y
1	14 Diam	5.0	Variable	0.50	N
1	14 Diam	5.0	Variable	0.66	N
2	Entrance	0.5	0.0850	0.50	Y
2	1 Diam	0.5	0.0566	0.50	Y
2	8 Diam	0.5	Scaled*	0.25	Y
2	8 Diam	0.5	Variable	0.25	N
2	8 Diam	0.5	0.0283	0.50	Y
2	8 Diam	0.5	0.0566	0.50	Y
2	8 Diam	0.5	0.0850	0.50	Y
2 [†]	8 Diam	0.5	Variable	0.50	N
2	12 Diam	0.5	0.0566	0.50	Y
2	12 Diam	0.5	0.0850	0.50	Y
2	14 Diam	0.5	Scaled*	0.25	Y
2	14 Diam	0.5	Variable	0.25	N
2	14 Diam	0.5	0.0566	0.50	Y
2	14 Diam	0.5	0.0850	0.50	Y
2	14 Diam	1.0	Scaled*	0.25	Y
2	14 Diam	1.0	Variable	0.25	N
2	14 Diam	1.0	0.0283	0.50	Y
2	14 Diam	1.0	0.0566	0.50	Y
2	14 Diam	1.0	0.0850	0.50	Y

Culvert	Station (L/D)	Slope (%)	Flow Rate (m ³ /sec)	Relative Depth at Entrance	Downstream Control
3	8 Diam	0.5	Scaled*	0.25	Y
3	8 Diam	0.5	Variable	0.25	N
3	8 Diam	0.5	0.0566	0.50	Y
3	8 Diam	0.5	0.0850	0.50	Y
3	8 Diam	1.0	Scaled*	0.25	Y
3	8 Diam	1.0	Variable	0.25	N
3	8 Diam	1.0	0.0153	0.50	Y
3	8 Diam	1.0	0.0566	0.50	Y
3	8 Diam	1.0	0.0850	0.50	Y
4	7 Diam	0.5	Scaled*	0.25	Y
4	7 Diam	0.5	Variable	0.25	N
4	7 Diam	0.5	0.0566	0.50	Y
4	7 Diam	0.5	0.0850	0.50	Y
4	7 Diam	1.0	Scaled*	0.25	Y
4	7 Diam	1.0	Variable	0.25	N
4	7 Diam	1.0	0.0566	0.50	Y
4	7 Diam	1.0	0.0850	0.50	Y

*Scaled from 0.0566 m³/s by the ratio: $\frac{AR_{0.25D_0}^{2/3}}{AR_{0.5D_0}^{2/3}}$.

‡Relative depth of 0.50*D₀ at station.

†Experimental run made with no entrance transition region.

Chapter 4

RESULTS

A considerable amount of data was recorded at numerous locations in the flow cross-section throughout this research project due to the need to examine variations in flow, location, culvert diameter, slope, corrugation size, and other variables. In addition to solving for relevant parameters, this information was used to develop a method of predicting velocity distributions. Discrete velocity measurements were recorded with their respective X-Y coordinates and the software Spyglass Transform was used to generate cross-sectional contour plots of the velocity. Transform translated the inputted data into a X-Y matrix with magnitudes of velocity. Velocity values at the inputted points were preserved and the software interpolated between these known points by using a Kriging fill method, which provided a weighted value which minimized the statistical variance of the array. This was the most accurate method available from the software.

The resulting contour plots were digitized and the areas between adjacent contour isovel lines were determined. For each of the experimental runs, a comparison was made between the discharge measured by the magnetic flow meters and the discharge calculated from the cross-sectional contour plots. The calculated discharge (Q_{Total}) was determined by the following equation:

$$Q_{Total} = \sum_{i=1}^n A_i \left(\frac{V_i + V_{i+1}}{2} \right) \quad (4.1)$$

where A is the area between adjacent contour lines [m^2]; and V is the velocity at the contour line [m/s]. This check was to verify that continuity was preserved. The continuity check for each of the runs is included in Table 4.1.

In addition, these areas were used to determine the velocity distribution coefficients α and β . These areas were also used to calculate "effective" cross-sectional areas, which are

Table 4.1. Continuity Check

Run #	Culvert	Calculated Discharge (cms)	Measured Discharge (cms)	% Difference of Calculated Discharge
1	1	0.0057	0.0052	8.1%
2	1	0.0067	0.0064	4.8%
3	1	0.0089	0.0082	7.8%
4	1	0.0085	0.0094	-10.2%
5	1	0.0131	0.0124	5.2%
6	1	0.0136	0.0124	8.6%
7	1	0.0141	0.0142	-0.7%
8	1	0.0233	0.0213	8.4%
9	1	0.0260	0.0278	-6.8%
10	1	0.0277	0.0284	-2.5%
11	1	0.0289	0.0290	-0.4%
12	1	0.0434	0.0438	-1.0%
13	1	0.0418	0.0456	-9.0%
14	1	0.0504	0.0527	-4.6%
15	1	0.0514	0.0539	-4.9%
16	2	0.0167	0.0153	8.6%
17	2	0.0163	0.0153	6.0%
18	2	0.0171	0.0153	10.3%
19	2	0.0290	0.0283	2.5%
20	2	0.0300	0.0283	5.8%
21	2	0.0372	0.0396	-6.5%
22	2	0.0380	0.0396	-4.3%
23	2	0.0489	0.0515	-5.2%
24	2	0.0596	0.0566	5.1%
25	2	0.0569	0.0566	0.6%
26	2	0.0536	0.0566	-5.5%
27	2	0.0545	0.0566	-3.9%
28	2	0.0525	0.0566	-7.9%
29	2	0.0784	0.0850	-8.3%
30	2	0.0812	0.0850	-4.7%
31	2	0.0815	0.0850	-4.3%
32	2	0.0851	0.0850	0.2%
33	2	0.0818	0.0850	-3.9%
34	2	0.1222	0.1274	-4.2%
35	3	0.0165	0.0153	7.3%
36	3	0.0196	0.0153	22.1%
37	3	0.0150	0.0153	-1.7%
38	3	0.0575	0.0566	1.6%
39	3	0.0612	0.0566	7.6%
40	3	0.0578	0.0575	0.5%
41	3	0.0698	0.0664	4.9%
42	3	0.0809	0.0850	-5.0%
43	3	0.0798	0.0850	-6.5%
44	4	0.0153	0.0153	-0.2%
45	4	0.0162	0.0153	5.3%
46	4	0.0542	0.0527	2.8%
47	4	0.0586	0.0563	3.9%
48	4	0.0583	0.0566	3.0%
49	4	0.0572	0.0566	1.0%
50	4	0.0868	0.0850	2.1%
51	4	0.0829	0.0850	-2.5%

discussed in Section 4.2. Prediction of these "effective" cross-sectional areas and subsequent development of a method of predicting velocity distributions through the use of the Chiu equation (Equation 2.21) and the Mountjoy equation (Equation 2.16) are discussed in Section 4.3. Qualitative observations and discussion of the flow through each of the four test culverts are presented in Section 4.4. Finally, sensitivity analysis and discussion for both the Chiu and the Mountjoy equations are included in Section 4.5.

4.1 Tabulation of Results

Velocity measurements were made on three corrugated and one non-corrugated steel culverts. Several parameters were measured or calculated for each of the fifty-one experimental runs. These parameters include the discharge, slope, existence of downstream control, depth, relative depth, maximum velocity, average velocity, hydraulic radius, α , β , Reynolds number, and shear velocity. The methods used to determine the calculated parameters are discussed in Chapter 2. A tabulation of these parameters for each experimental run is given in Table 4.2.

4.2 Effective Cross-Sections

Cross-sectional contour plots of the relative velocity (V/V_{\max}) were generated for each of the fifty-one experimental runs. The contours were based on the discrete velocity measurements made at various points in the cross-section. The contour plots are shown looking downstream. Because of space requirements, the contour plots are not shown here. Instead, each one of these contour plots is presented in Appendix B. Also shown in appendix figures are the maximum velocity, discharge, relative depth of the flow, and the location of cross-section for each of the contour plots.

Often the contour plots were irregularly shaped with respect to the theoretical, symmetrical shape about the centerline. A typical example of a non-symmetrical velocity distribution is shown in Figure 4.1. The reasons for the asymmetry were discussed in Sections 2.2.5 and 2.3.1. In terms of fish passage, evidence suggests the non-symmetric nature of the

Table 4.2. Parameters for Experimental Runs.

Run #	Culvert	Discharge (cms)	Slope (%)	Downstream Control	Depth (cm)	Relative Depth	Vmax (cm/sec)	Vavg (cm/sec)	Hyd. Radius (cm)	α	β	Reynold's No.** Re	Shear Velocity (v*) (cm/sec)
1	1	0.0052	5.0%	N	5.1	0.17	101.9	65.0	3.1	1.39	1.13	2.26E+04	12.4
2	1	0.0064	3.0%	N	7.0	0.23	82.0	55.3	4.2	1.32	1.11	2.35E+04	11.1
3	1	0.0082	1.0%	N	10.4	0.34	61.2	41.2	5.8	1.36	1.13	2.41E+04	7.5
4	1	0.0094	0.5%	N	10.4	0.34	59.9	38.0	5.8	1.40	1.15	2.77E+04	5.3
5	1	0.0124	0.5%	Y	20.7	0.68	34.5	23.9	8.9	1.37	1.14	2.35E+04	6.6
6	1	0.0124	1.0%	Y	23.1	0.76	33.2	22.5	9.2	1.41	1.15	2.16E+04	9.5
7	1	0.0142	5.0%	Y	15.0	0.49	63.1	38.6	7.5	1.41	1.15	3.35E+04	19.2
8	1	0.0213	0.5%	Y	17.0	0.56	85.1	56.2	8.1	1.38	1.14	4.64E+04	6.3
9	1	0.0278	3.0%	N	13.2	0.43	125.9	84.9	6.9	1.32	1.12	7.10E+04	14.3
10	1	0.0284	1.0%	N	16.0	0.52	92.7	70.2	7.9	1.22	1.08	6.43E+04	8.8
11	1	0.0290	5.0%	N	12.0	0.39	169.3	106.8	6.4	1.51	1.19	7.85E+04	17.8
12	1	0.0438	5.0%	N	14.0	0.46	178.0	129.9	7.2	1.18	1.07	1.08E+05	18.8
13	1	0.0456	0.5%	N	22.0	0.72	108.5	74.6	9.1	1.44	1.17	8.25E+04	6.7
14	1	0.0527	3.0%	N	19.0	0.62	159.6	103.6	8.6	1.43	1.16	1.06E+05	15.9
15	1	0.0539	1.0%	N	24.0	0.79	124.4	83.2	9.3	1.34	1.13	9.07E+04	9.5
16	2	0.0153	0.5%	Y	23.3	0.38	26.4	16.0	12.6	1.34	1.12	2.11E+04	7.9
17	2	0.0153	0.5%	Y	20.4	0.33	29.2	18.5	11.4	1.33	1.12	2.28E+04	7.5
18	2	0.0153	1.0%	Y	24.0	0.39	25.2	15.5	12.9	1.38	1.14	2.07E+04	11.2
19	2	0.0283	0.5%	Y	35.2	0.58	22.8	16.2	16.6	1.29	1.11	3.01E+04	9.0
20	2	0.0283	0.5%	Y	34.4	0.56	26.6	17.4	16.4	1.34	1.13	3.06E+04	9.0
21	2	0.0396	0.5%	N	15.7	0.26	90.1	60.8	9.2	1.31	1.11	6.83E+04	6.7
22	2	0.0396	0.5%	N	15.9	0.26	84.9	60.7	9.3	1.44	1.16	6.78E+04	6.7
23	2	0.0515	1.0%	N	15.7	0.26	108.0	80.3	9.2	1.28	1.10	8.88E+04	9.5
24	2	0.0566	0.5%	Y	30.9	0.51	51.3	39.6	15.4	1.14	1.05	6.56E+04	8.7
25	2	0.0566	0.5%	Y	33.5	0.55	46.3	33.9	16.1	1.21	1.08	6.22E+04	8.9
26	2	0.0566	0.5%	Y	34.5	0.57	41.8	30.7	16.4	1.18	1.07	6.10E+04	9.0
27	2	0.0566	0.5%	Y	34.3	0.56	44.9	31.7	16.4	1.20	1.07	6.12E+04	9.0
28	2	0.0566	1.0%	Y	38.1	0.62	37.6	26.5	17.3	1.27	1.10	5.70E+04	13.0
29	2	0.0850	0.5%	Y	33.1	0.54	69.1	47.4	16.0	1.24	1.09	9.42E+04	8.9
30	2	0.0850	0.5%	Y	33.2	0.54	64.2	49.1	16.0	1.15	1.05	9.40E+04	8.9
31	2	0.0850	0.5%	Y	32.9	0.54	69.8	49.9	16.0	1.15	1.06	9.46E+04	8.8
32	2	0.0850	1.0%	Y	30.9	0.51	71.5	56.6	15.4	1.16	1.06	9.85E+04	12.3
33	2	0.0850	0.5%	Y	38.5	0.63	58.2	41.2	17.3	1.24	1.09	8.49E+04	9.2
34	2	0.1274	0.5%	N	30.7	0.50	118.4	81.3	15.3	1.15	1.05	1.48E+05	8.7
35	3	0.0153	0.5%	Y	23.0	0.31	22.2	14.6	13.0	1.38	1.14	1.96E+04	8.0
36	3	0.0153	1.0%	Y	45.4	0.62	9.9	7.3	20.7	1.19	1.07	1.29E+04	14.3
37	3	0.0153	1.0%	Y	24.5	0.33	20.5	12.5	13.7	1.47	1.16	1.89E+04	11.6
38	3	0.0566	0.5%	Y	42.3	0.57	31.2	22.5	20.0	1.30	1.11	5.00E+04	9.9
39	3	0.0566	1.0%	Y	43.0	0.58	33.9	23.6	20.2	1.30	1.11	4.94E+04	14.1
40	3	0.0575	0.5%	N	17.5	0.24	120.8	76.7	10.3	1.52	1.19	8.57E+04	7.1
41	3	0.0664	1.0%	N	18.2	0.25	135.1	87.9	10.7	1.50	1.18	9.69E+04	10.2
42	3	0.0850	0.5%	Y	42.0	0.57	46.6	32.2	19.9	1.39	1.14	7.54E+04	9.9
43	3	0.0850	1.0%	Y	43.2	0.59	44.2	30.4	20.2	1.36	1.13	7.40E+04	14.1
44	4	0.0153	0.5%	Y	17.3	0.28	27.4	21.4	9.9	1.16	1.06	2.50E+04	7.0
45	4	0.0153	1.0%	Y	20.4	0.33	23.1	18.2	11.4	1.16	1.06	2.28E+04	10.6
46	4	0.0527	0.5%	N	14.0	0.23	127.2	104.5	8.3	1.14	1.05	9.68E+04	6.4
47	4	0.0563	1.0%	N	13.4	0.22	140.2	117.6	8.0	1.15	1.06	1.06E+05	8.9
48	4	0.0566	0.5%	Y	35.0	0.57	38.9	34.0	16.5	1.08	1.03	6.04E+04	9.0
49	4	0.0566	1.0%	Y	36.0	0.59	36.8	31.4	16.8	1.09	1.03	5.93E+04	12.8
50	4	0.0850	0.5%	Y	34.3	0.56	59.7	50.9	16.4	1.09	1.03	9.20E+04	9.0
51	4	0.0850	1.0%	Y	35.2	0.58	54.2	47.0	16.6	1.08	1.03	9.04E+04	12.8

** Hydraulic radius (R) used as characteristic length for Reynold's number (Re).

velocity distribution is not significant since the fish appear capable of finding low velocity passage zones. Consequently, when considerations are being made for juvenile fish passage, it is important to be able to predict the thickness of the region of the velocity distribution with acceptable velocities. For this reason, the areas between isovel lines in the contour plots were converted to "effective" areas. That is to say, a given digitized area was converted to an equivalent, symmetrical ring-shaped band having the same area. This concept is illustrated in Figure 4.2. The thickness of each additional band represents an average thickness that could be expected with relative velocities below a certain level. This means given a desired relative velocity, the average thickness of the boundary layer with velocities below this desired level can be predicted.

The effective band widths for each of the fifty-one experimental runs were calculated for relative velocities of $0.2 \cdot V_{max}$, $0.4 \cdot V_{max}$, $0.5 \cdot V_{max}$, $0.6 \cdot V_{max}$, $0.8 \cdot V_{max}$, $0.9 \cdot V_{max}$, and $0.95 \cdot V_{max}$. These effective band widths are tabulated in Table 4.3.

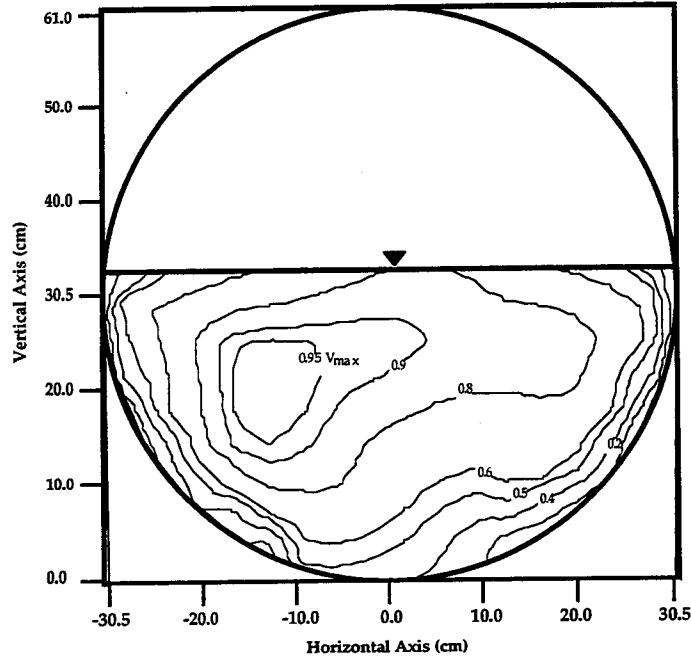


Figure 4.1. Example of non-symmetrical relative velocity contour plot for Culvert #2, looking downstream. Discharge = $0.0850 \text{ m}^3/\text{s}$, Slope = $1/2\%$, $V_{max} = 69.1 \text{ cm/s}$, taken at $L/D = 12$.

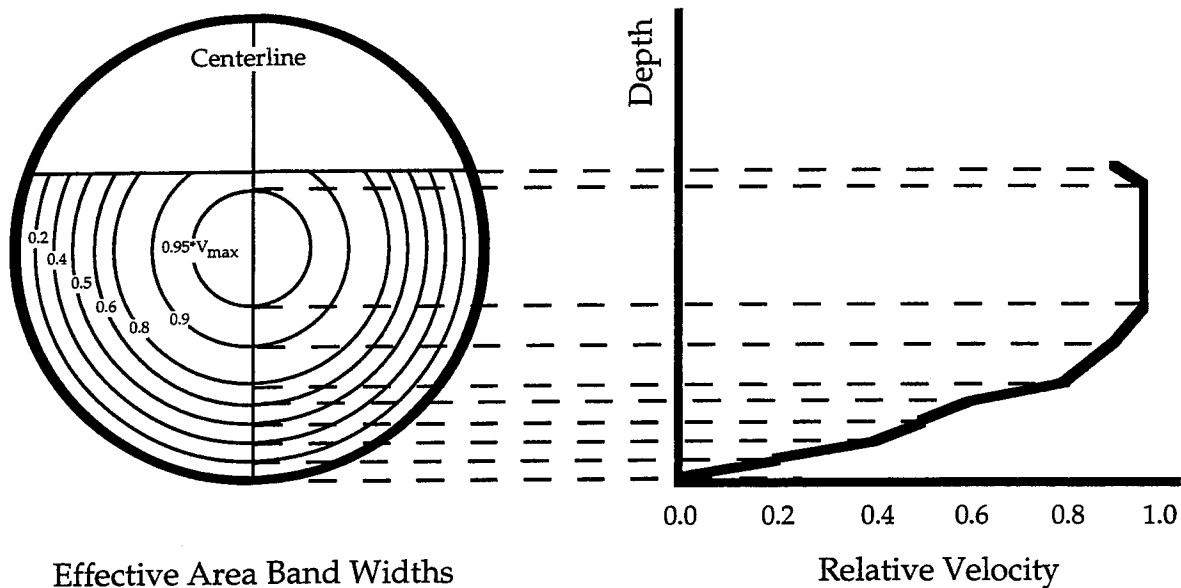


Figure 4.2 Illustration of effective area concept.

4.3 Prediction of Velocity Distributions in Culverts

One of the primary objectives of this research was to develop a means of predicting cross-sectional velocity distributions in any large diameter circular corrugated culvert based on experimental test results on smaller diameter circular corrugated culverts. Because of the irregular and non-symmetrical velocity cross-sections observed, and also because the maximum velocity often did not occur at the centerline, it was decided that the effective cross-section area discussed in Section 4.2 would be acceptable and useful for fish passage considerations. A centerline plot of the relative velocities taken from the effective cross-section was used as the experimental data to be fitted to an appropriate one-dimensional velocity distribution equation. By finding a one-dimensional equation that would adequately predict the centerline velocity distribution, this equation could be used to scale up to larger diameter culverts and predict the effective band widths, and thus the effective cross-section for the culvert.

Table 4.3 Band Widths for Effective Cross-Section

Run #	Band Width 0.0*Vmax (cm)	Band Width 0.2*Vmax (cm)	Band Width 0.4*Vmax (cm)	Band Width 0.5*Vmax (cm)	Band Width 0.6*Vmax (cm)	Band Width 0.8*Vmax (cm)	Band Width 0.9*Vmax (cm)	Band Width 0.95*Vmax (cm)
1	0.0	0.1	0.6	1.0	1.6	2.5	3.5	4.2
2	0.0	0.1	0.3	1.2	2.0	3.0	4.2	5.0
3	0.0	0.4	0.8	1.4	2.4	4.0	6.0	8.2
4	0.0	0.4	1.1	1.8	2.6	4.8	7.2	8.7
5	0.0	0.6	1.5	2.1	2.9	5.6	8.4	10.3
6	0.0	0.7	1.8	2.4	3.3	5.6	8.4	11.0
7	0.0	0.6	1.3	2.3	3.9	7.6	9.7	12.1
8	0.0	0.7	1.5	2.0	3.0	5.7	10.0	13.8
9	0.0	0.3	0.9	1.7	2.5	5.4	7.6	9.7
10	0.0	0.1	0.7	1.2	1.8	3.7	6.8	8.8
11	0.0	0.7	1.6	2.2	2.8	4.8	7.6	9.2
12	0.0	0.2	0.4	0.8	1.6	4.9	8.0	9.9
13	0.0	0.9	1.9	2.4	3.1	5.1	7.8	10.1
14	0.0	0.8	1.7	2.5	3.4	6.2	10.1	12.3
15	0.0	0.6	1.3	2.1	3.2	6.6	9.5	12.5
16	0.0	0.6	1.9	3.4	6.4	11.5	18.0	21.3
17	0.0	0.5	1.6	2.8	4.9	9.9	13.0	16.9
18	0.0	0.8	2.3	3.7	6.3	13.4	16.4	20.2
19	0.0	0.7	2.2	3.2	4.9	10.1	16.4	23.8
20	0.0	0.9	2.4	3.5	5.5	10.5	15.3	19.9
21	0.0	0.4	1.1	2.1	3.6	7.0	9.9	12.3
22	0.0	0.6	1.8	2.8	4.2	7.2	9.3	10.9
23	0.0	0.4	0.7	1.7	3.6	7.0	9.9	12.3
24	0.0	0.3	0.6	1.5	2.3	4.9	8.2	16.9
25	0.0	0.4	0.9	2.4	4.3	9.9	15.7	21.0
26	0.0	0.2	0.8	2.2	4.3	10.9	16.9	24.2
27	0.0	0.3	1.0	2.7	4.8	12.5	21.7	27.4
28	0.0	0.7	1.4	3.5	5.5	11.4	18.1	22.3
29	0.0	0.3	1.5	3.2	5.4	12.3	20.5	24.9
30	0.0	0.1	0.6	1.3	2.8	9.3	15.0	19.2
31	0.0	0.2	0.9	1.8	3.5	11.5	22.7	28.9
32	0.0	0.2	0.8	1.5	2.9	6.0	10.9	17.7
33	0.0	0.7	1.8	2.6	4.8	11.3	19.3	25.4
34	0.0	0.2	0.7	2.1	4.3	13.9	25.2	27.7
35	0.0	0.7	2.0	3.6	5.6	10.2	14.2	16.8
36	0.0	0.3	1.4	2.4	5.0	13.4	19.3	25.7
37	0.0	0.9	3.2	4.8	7.5	12.3	16.9	19.8
38	0.0	1.0	2.6	4.0	5.7	11.7	16.4	24.8
39	0.0	0.7	2.5	4.3	7.0	13.6	20.3	27.5
40	0.0	1.2	2.3	2.9	4.7	7.8	10.6	13.1
41	0.0	1.0	2.4	3.5	4.5	7.5	10.4	12.5
42	0.0	1.2	3.5	5.0	7.0	12.7	18.1	23.6
43	0.0	1.3	3.1	4.5	7.0	13.6	19.7	25.0
44	0.0	0.0	0.4	1.0	2.3	4.3	7.6	11.1
45	0.0	0.2	0.5	1.1	1.9	5.1	8.6	12.2
46	0.0	0.1	0.1	0.8	1.4	2.8	4.3	6.9
47	0.0	0.1	0.4	0.8	1.2	2.0	3.3	5.9
48	0.0	0.0	0.2	0.6	1.2	3.5	6.5	10.9
49	0.0	0.2	0.4	0.6	1.2	4.3	8.5	14.9
50	0.0	0.1	0.3	0.9	1.7	3.6	7.4	16.3
51	0.0	0.1	0.3	0.7	1.3	3.5	7.0	12.7

Two equations were examined for use in predicting the one-dimensional centerline velocity distribution of the effective cross-sections. The first equation was the Chiu (1995) equation (Equation 2.21) which was derived for describing two-dimensional velocity distributions in an open channel cross-section. The Chiu equation was used only to predict the one-dimensional velocity distribution along the centerline. The second equation used was the Mountjoy (1986) equation (Equation 2.16) which was taken from Chow (1964). Each of these equations are discussed in Section 2.2.4.

4.3.1 Application of Chiu Equation

The Chiu equation (Equation 2.21) was used to predict the centerline velocity distribution. It was necessary to determine the entropy parameter, M , for each of the culverts. As was stated in Section 2.2.4, the entropy parameter (M) can be calculated from $\frac{V_{avg}}{V_{max}}$.

The data for the four culverts used in this research displayed a linear relationship between V_{max} and V_{avg} . This relationship was noted by Chiu (1995) and is discussed in Section 2.2.4. The linear relationships between V_{max} and V_{avg} for the four culverts tested in this research are illustrated in Figures 4.3, 4.4, 4.5, and 4.6. The coefficient of determination (R^2) is given for each of the linear fits. The coefficient of determination is a statistical parameter which illustrates the quality of a linear fit to a set of data. The coefficient of determination can be between 0 and 1 with a perfect fit having $R^2 = 1$.

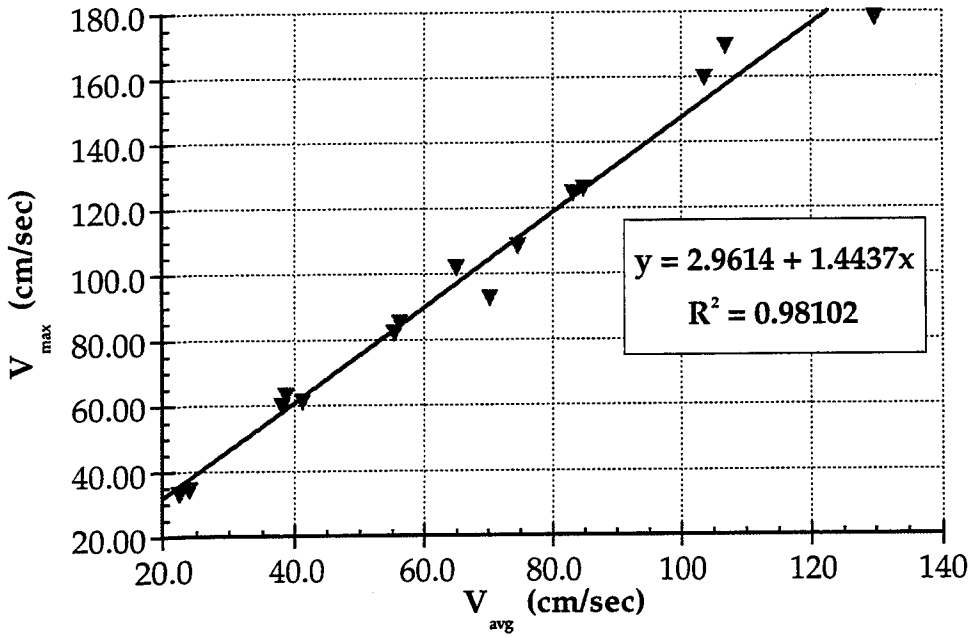


Figure 4.3 Plot of V_{max} versus V_{avg} for Culvert #1 with linear regression line and equation.

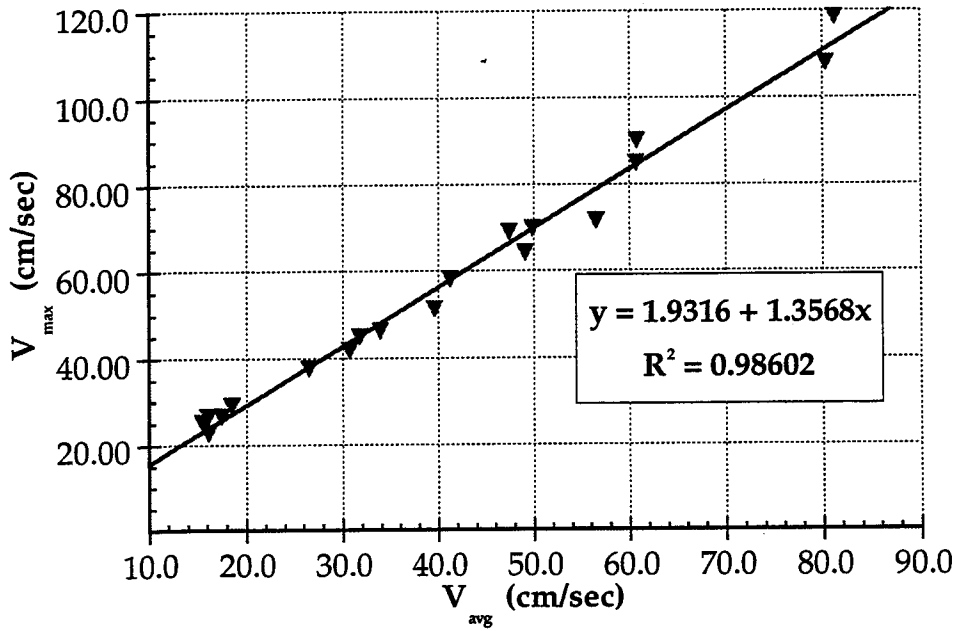


Figure 4.4 Plot of V_{max} versus V_{avg} for Culvert #2 with linear regression line and equation.

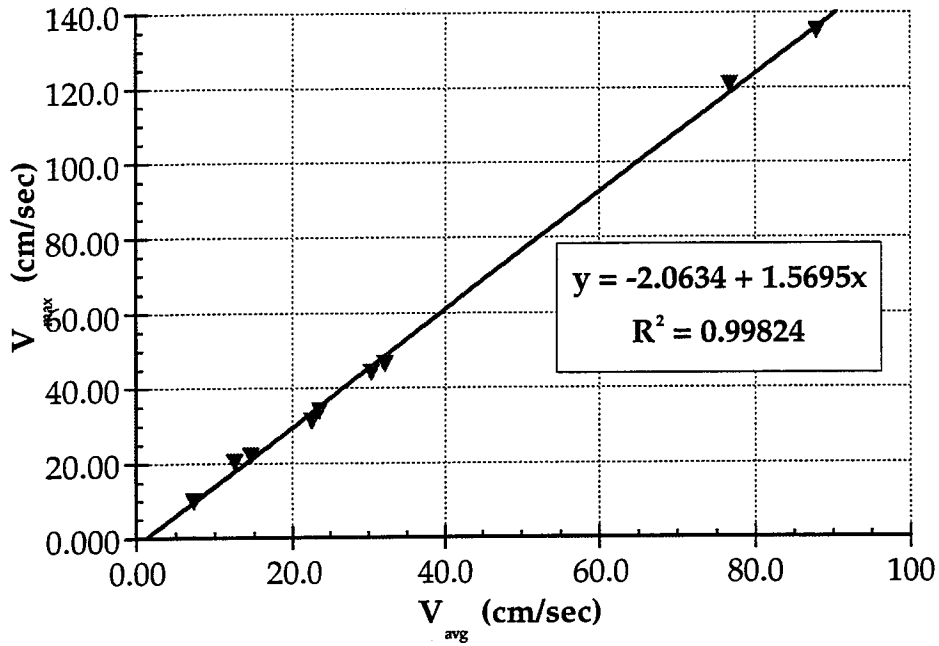


Figure 4.5 Plot of V_{max} versus V_{avg} for Culvert #3 with linear regression line and equation.

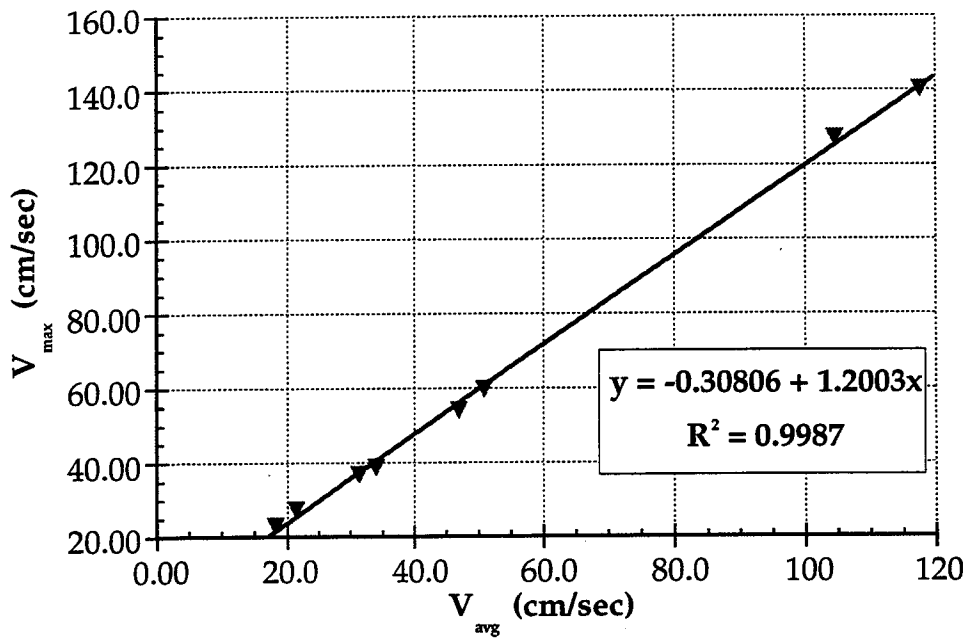


Figure 4.6 Plot of V_{max} versus V_{avg} for Culvert #4 with linear regression line and equation.

Based on data from the four culverts in this research and previous studies on three additional culverts, it was found that there was a linear relationship between $\frac{V_{avg}}{V_{max}}$ and $\frac{CorrugationHeight}{PipeDiameter}$. This relationship is illustrated in Figure 4.7.

The entropy parameter M was calculated for each of the four test culverts using $\frac{V_{avg}}{V_{max}}$ and Equation 2.23. The entropy parameters that were calculated are given in Table 4.4. The Chiu equation was used to predict the centerline velocity distribution for each of the fifty-one experimental runs. In the application of the Chiu equation it was assumed that V_{max} occurred 0.10*Depth below the surface of the flow. The centerline velocity distribution predicted by the Chiu equation was compared to the centerline velocity distribution taken from the effective cross-sections. Plots of the centerline velocity distribution curves predicted by the Chiu equation for each of the conditions examined in the experimental runs are included in Appendix C.

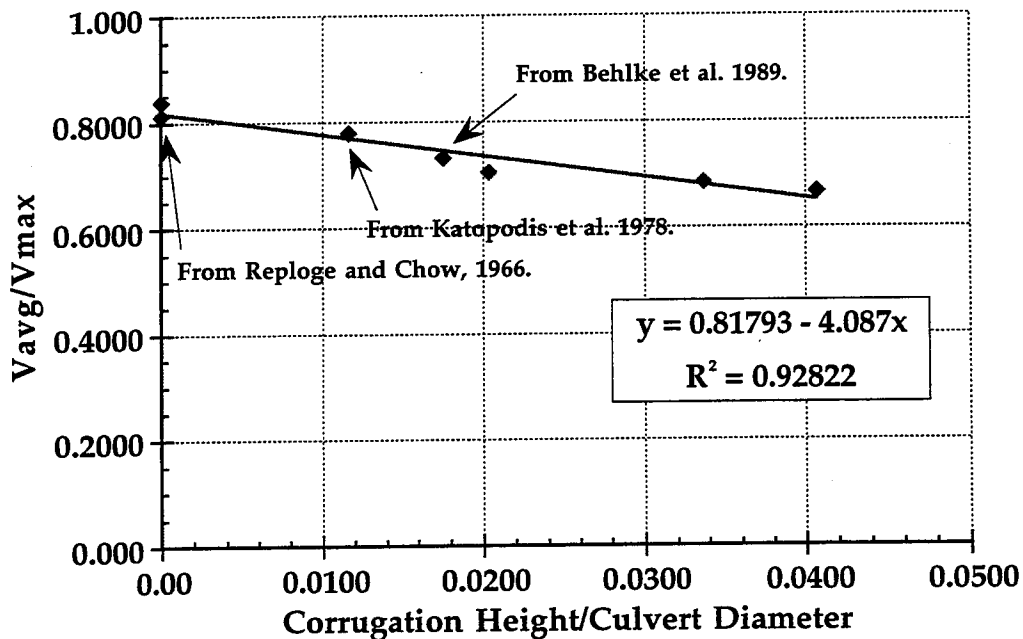


Figure 4.7 Plot of $\frac{V_{avg}}{V_{max}}$ versus $\frac{CorrugationHeight}{PipeDiameter}$ with linear regression line and equation.

Table 4.4. Calculated Entropy Parameters.

<u>Culvert</u>	<u>Entropy Parameter</u>
1	2.14
2	2.76
3	2.43
4	6.13

Because the Chiu equation tended to over predict the relative velocity distribution at the centerline using the calculated entropy parameters, a best fit entropy parameter was calculated for each experimental run. For correlation purposes, Culvert #2 was examined. The calculated entropy parameter for Culvert #2 was 2.76. The best fit entropy parameter varied from 0.49 to 4.33. This seemed to contradict the statement by Chiu (1995) that M is constant for a given channel section. An attempt was made to correlate the variation in the best fit entropy parameter to a property of the flow. Correlation attempts were made for several parameters of the flow including Reynolds number, hydraulic radius, wetted perimeter, shear velocity, friction factor, and relative depth. No significant relationship could be found between the best fit entropy parameter and these variables. A sensitivity analysis of the entropy parameter for each of the culverts is included in Section 4.5. A linear correlation was found between the best fit entropy parameter and the velocity head coefficient, α . This relationship is illustrated in Figure 4.8. A linear relationship was also found between the best fit entropy parameter and the momentum coefficient, β . This relationship is illustrated in Figure 4.9.

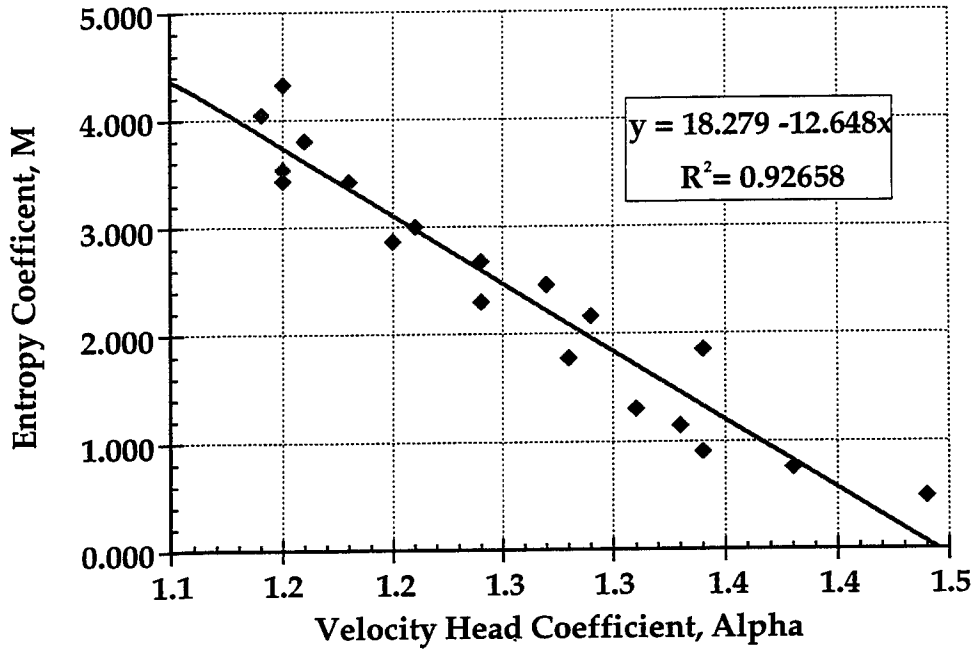


Figure 4.8. Plot of best fit entropy parameter (M) versus velocity head coefficient (α).

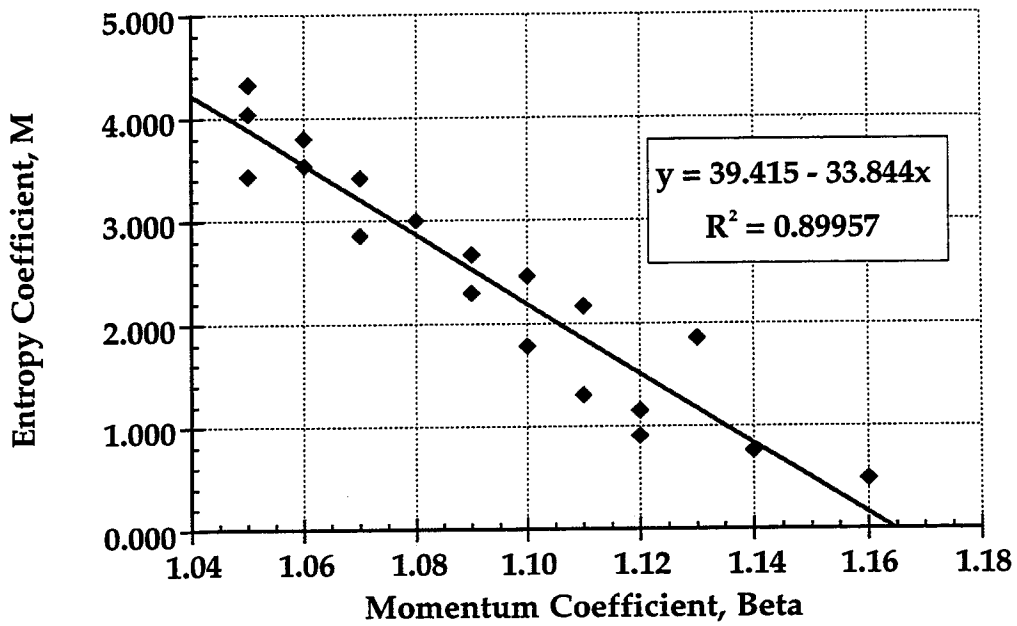


Figure 4.9. Plot of best fit entropy parameter (M) versus momentum coefficient (β).

Chiu (1995) discusses the relationship between M and α stating that because M is directly related to the velocity distribution, the velocity head coefficient, α , can be related to the entropy parameter, M . This statement appears justified given the linear fit of the plots shown in Figure 4.8 and Figure 4.9.

For use in fish passage design, it was determined that the entropy parameter could be calculated from $\frac{V_{avg}}{V_{max}}$, which could be calculated from $\frac{CorrugationHeight}{PipeDiameter}$ for a given culvert. This would provide a constant M for each culvert. Because no correlation could be found between the best fit entropy parameter and a property of the flow that would be known in the case of culvert design, it was determined that for Chiu's equation to be used, the constant calculated entropy parameter must be used.

A statistical analysis of the bias and the error of the experimental data fit to the Chiu equation was performed. The three statistical parameters used were the Bias, the Mean Absolute Error (MAE), and the Root Mean Squared Error (RMSE). These parameters provide a means of comparing different curve fits to experimental data. The Bias indicates the tendency of the equation to over or under predict. A positive Bias indicates a trend of over prediction, a negative Bias indicates a trend of under prediction, and a Bias of zero indicates that the equation shows no tendency to over or under predict. The MAE and RMSE are always positive, and lower values of MAE and RMSE indicate less error in the fit. The magnitudes of MAE and RMSE are a function of the input values, so they are only useful as a comparison between different fits. The Bias, MAE, and RMSE for the Chiu equation are shown in Table 4.4.

To apply the Chiu equation to fish passage culvert design, the $\frac{CorrugationHeight}{PipeDiameter}$ ratio would predict a value of $\frac{V_{avg}}{V_{max}}$ for the culvert. This could then be used to determine the entropy parameter for the culvert. Given the discharge (Q), and the flow depth (D), V_{avg} could be determined by $V_{avg} = Q/A$, and V_{max} could be determined from the value for $\frac{V_{avg}}{V_{max}}$ that had been predicted earlier. The allowable velocity for the design juvenile fish would then be

Table 4.5. Statistical Parameters for Chiu Equation Fit.

RUN #	Bias	MAE	RMSE
1	0.097	0.108	0.052
2	0.060	0.086	0.035
3	0.068	0.068	0.019
4	0.097	0.097	0.038
5	0.023	0.025	0.005
6	0.037	0.051	0.018
7	0.091	0.091	0.034
8	0.063	0.063	0.015
9	0.050	0.054	0.013
10	-0.032	0.046	0.011
11	0.110	0.110	0.050
12	-0.021	0.069	0.021
13	0.027	0.047	0.010
14	0.065	0.065	0.017
15	0.026	0.039	0.016
Separator			
16	0.107	0.107	0.050
17	0.097	0.097	0.040
18	0.119	0.119	0.058
19	0.044	0.044	0.007
20	0.058	0.058	0.013
21	0.089	0.089	0.034
22	0.122	0.122	0.065
23	0.075	0.078	0.028
24	-0.063	0.077	0.026
25	0.007	0.042	0.008
26	-0.007	0.060	0.016
27	0.030	0.063	0.016
28	0.030	0.041	0.007
29	0.041	0.060	0.015
30	-0.046	0.078	0.031
31	0.008	0.067	0.019
32	-0.042	0.057	0.016
33	0.030	0.036	0.007
34	0.012	0.078	0.026
Separator			
35	0.094	0.094	0.037
36	-0.032	0.058	0.018
37	0.126	0.126	0.069
38	0.021	0.022	0.002
39	0.031	0.037	0.006
40	0.131	0.131	0.075
41	0.122	0.122	0.065
42	0.053	0.053	0.012
43	0.047	0.047	0.008
Separator			
44	0.086	0.102	0.047
45	0.115	0.115	0.059
46	0.090	0.090	0.041
47	0.100	0.100	0.053
48	0.000	0.022	0.002
49	0.031	0.031	0.007
50	0.029	0.033	0.006
51	0.019	0.026	0.003

expressed as a fraction of V_{\max} ($V_{\text{allow}}/V_{\max}$). The Chiu equation could then be used to solve for the thickness of the boundary layer with relative velocities (V/V_{\max}) sufficient for fish passage.

4.3.2 Application of Mountjoy Equation

The Mountjoy (1986) equation (Equation 2.16) was the second equation used to predict the one-dimensional centerline velocity distribution. The Mountjoy equation requires knowledge of the average velocity (V_{avg}), hydraulic radius (R), Manning's coefficient (n), and the depth of the flow (y_o). These values can be determined given the diameter and corrugation of the culvert, the discharge (Q), and the depth of flow in the culvert.

The Mountjoy equation was examined as a comparison to the one-dimensional application of the Chiu equation which was discussed in Section 4.3.1. The Manning n values were taken from the American Iron and Steel Institute (1980). Plots of the centerline velocity distribution curves predicted by the Mountjoy equation for each of the experimental runs are included in Appendix C. A sensitivity analysis of the selection of a Manning n value is included in Section 4.5 for a typical run from each of the culverts.

A statistical analysis of the bias and the error of the experimental data fit to the Mountjoy equation was again performed. The three statistical parameters used were the Bias, the Mean Absolute Error (MAE), and the Root Mean Squared Error (RMSE). These parameters provide a means of comparing different curve fits to experimental data. The Bias, MAE, and RMSE for the Mountjoy equation are shown in Table 4.5.

To apply the Mountjoy equation to fish passage, the discharge (Q), properties of the culvert (corrugation and diameter), and the depth of flow (y_o) would be used to determine V_{avg} , hydraulic radius (R), and Manning's coefficient (n). These values would be used in the Mountjoy equation along with the relative depth (y/y_o) to predict a velocity. The allowable velocity for the design juvenile fish would then be used as the target velocity and the relative depth at which this velocity occurs could be determined from the Mountjoy equation.

Table 4.6. Statistical Parameters for Mountjoy Equation Fit.

RUN #	Bias	MAE	RMSE
1	0.001	0.047	0.018
2	-0.038	0.074	0.032
3	-0.010	0.029	0.003
4	0.024	0.025	0.003
5	-0.036	0.065	0.018
6	-0.019	0.073	0.032
7	0.026	0.028	0.004
8	0.007	0.031	0.006
9	-0.031	0.042	0.016
10	-0.101	0.112	0.047
11	0.035	0.047	0.010
12	-0.093	0.104	0.054
13	-0.031	0.070	0.024
14	0.006	0.040	0.008
15	-0.033	0.082	0.031
16	0.038	0.046	0.009
17	0.018	0.031	0.005
18	0.048	0.048	0.010
19	-0.026	0.037	0.006
20	-0.015	0.031	0.006
21	0.000	0.030	0.005
22	0.031	0.045	0.009
23	-0.012	0.038	0.009
24	-0.139	0.150	0.088
25	-0.068	0.079	0.028
26	-0.074	0.085	0.037
27	-0.033	0.062	0.027
28	-0.040	0.051	0.011
29	-0.031	0.042	0.017
30	-0.113	0.124	0.069
31	-0.047	0.084	0.038
32	-0.112	0.123	0.059
33	-0.018	0.048	0.009
34	-0.046	0.082	0.039
35	0.008	0.027	0.004
36	-0.100	0.112	0.051
37	0.045	0.047	0.013
38	-0.052	0.063	0.015
39	-0.044	0.055	0.013
40	0.038	0.050	0.012
41	0.027	0.050	0.010
42	-0.022	0.041	0.008
43	-0.025	0.036	0.007
44	0.055	0.065	0.025
45	0.034	0.081	0.035
46	0.053	0.071	0.027
47	0.057	0.092	0.037
48	0.003	0.052	0.010
49	0.031	0.063	0.021
50	0.028	0.062	0.016
51	0.020	0.064	0.017

4.4 Observations and Discussion

From the analysis of the results obtained from the experimental runs on the four culverts, several important, qualitative observations were made. These are discussed in the following subsection.

4.4.1 Qualitative Observations

CULVERT 1 (30.5 cm (12 in) diameter, 6.8 x 1.3 cm (2.7 x 0.5 in) corrugations)

Cross-sectional velocity distributions were taken at this culvert for relative depths ranging from $0.16 \cdot D_0$ to $0.78 \cdot D_0$, and slopes from 0.5% to 5%. The velocity distributions were, for the most part, nearly symmetrical about the centerline. There were a few exceptions, however, as a few of the contour plots showed a slight shift of the velocity contours to the left side of the culvert, and a couple of plots showed a slight shift to the right side of the culvert. An example of a velocity distribution plot produced from Culvert #1 is shown in Figure 4.10. The figure is shown looking downstream.

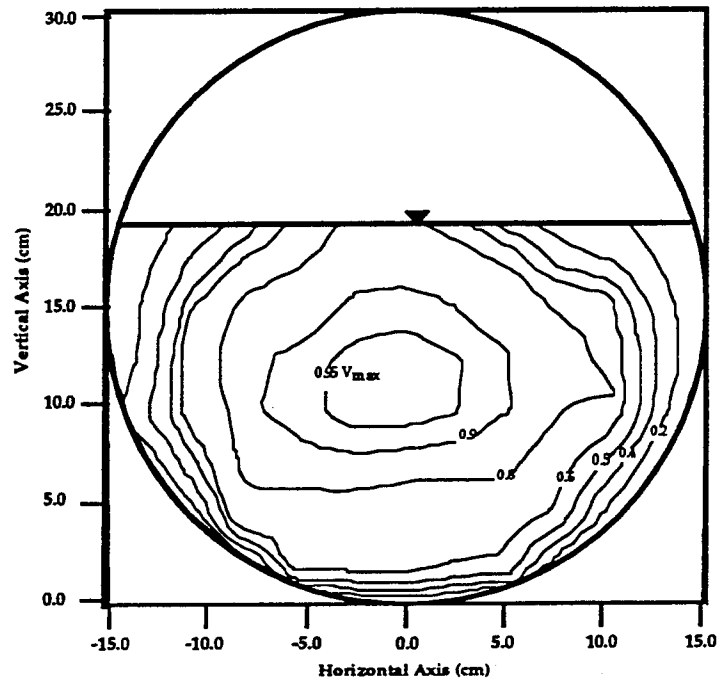


Figure 4.10. Velocity distribution from Culvert #1 looking downstream, at $Q=0.0527 \text{ m}^3/\text{s}$, 3% slope, 14 Diameters from the entrance, with no downstream control, and $V_{\text{max}} = 159.6 \text{ cm/s}$.

CULVERT 2 (61.0 cm (24 in) diameter, 6.8 x 1.3 cm (2.7 x 0.5 in) corrugations)

Cross-sectional velocity distributions for Culvert #2 were taken at several stations along the culvert. These stations were at $L/D = 0, 1, 8, 12,$ and 14 . The velocity distributions were taken on this culvert for a range of relative depths from $0.25 \cdot D_0$ to $0.62 \cdot D_0$, and slopes from 0.5% to 1%. Many of the velocity distribution plots taken at stations along the barrel of the culvert showed a distinct shift toward the left side of the culvert. This shift was less pronounced for relative depths below $0.40 \cdot D_0$, although it still existed. An example of a velocity distribution plot produced from Culvert #2, shown looking downstream, is given in Figure 4.11.

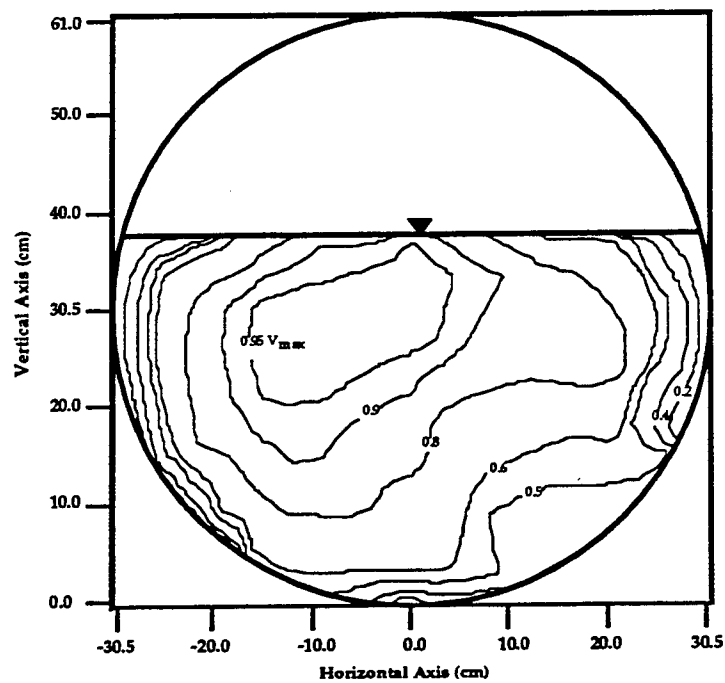


Figure 4.11. Velocity distribution from Culvert #2 looking downstream, at $Q=0.0566 \text{ m}^3/\text{s}$, 1% slope, 14 Diameters from the entrance, with downstream control, and $V_{\text{max}} = 37.6 \text{ cm/s}$.

CULVERT 3 (73.7 cm (29 in) diameter, 7.6 x 2.5 cm (3 x 1 in) corrugations)

Culvert 3 was the largest diameter culvert to be tested and it also had the largest corrugations. This culvert was tested for a range of relative depths from $0.25 \cdot D_0$ to $0.62 \cdot D_0$, and slopes from 0.5% to 1%. Similar to Culvert #1, the velocity distribution plots for Culvert #3 were mostly symmetrical about the centerline with some velocity plots showing a slight skew to either the left or the right side of the culvert. An example of a velocity distribution plot produced from Culvert #3 is shown in Figure 4.12. A noticeable difference is that the V_{max} is closer to the water surface than that shown in Figure 4.11. This figure is shown looking downstream.

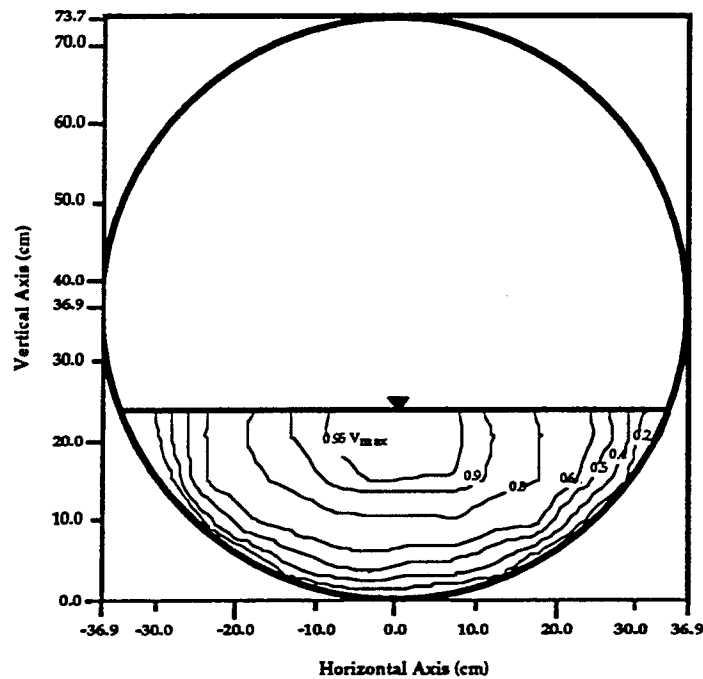


Figure 4.12. Velocity distribution from Culvert #3 looking downstream, at $Q=0.0153 \text{ m}^3/\text{s}$, 0.5% slope, 8 Diameters from the entrance, with downstream control, and $V_{max} = 29.1 \text{ cm/s}$.

CULVERT 4 (61.0 cm 24 in) diameter, non-corrugated)

Culvert 4 was the smooth walled pipe and this culvert was tested for a range of relative depths from $0.20 \cdot D_0$ to $0.57 \cdot D_0$, and slopes from 0.5% to 1%. The velocity distribution plots produced for this culvert were mostly symmetrical about the centerline. The velocity distribution in Culvert 4 was not nearly as varied as the distributions seen in the corrugated culverts. Most of the flow area in Culvert #4 had relative velocities above $0.8 \cdot V_{\max}$. An example of a velocity distribution plot (shown looking downstream) produced from Culvert #4 is given in Figure 4.13. For the contour plot shown in Figure 4.13 over 80% of the flow area has relative velocities greater than $0.8 \cdot V_{\max}$.

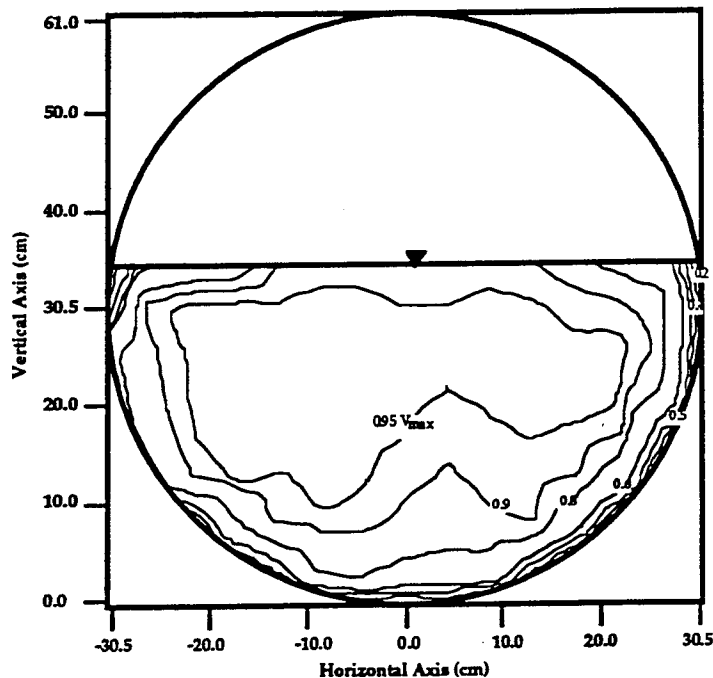


Figure 4.13. Velocity distribution from Culvert #4 looking downstream, at $Q=0.0850 \text{ m}^3/\text{s}$, 1% slope, 7 Diameters from the entrance, with downstream control, and $V_{\max} = 54.2 \text{ cm/s}$.

4.4.2 Gradually Varied Flow

For the experimental runs with no downstream control, the flow through the culvert was gradually varied. Gradually varied flow was discussed earlier in Section 2.2.3. The gradually varied flow in the culverts approached normal depth and uniform flow. However, because of the lengths of the culverts tested, the flow was not able to fully develop into uniform flow before the outlet of the culvert. The flow profile through the culvert can be determined through the use of the Direct Step Method. Further information on the Direct Step Method may be found in Chapter 6 of Open Channel Flow by Chaudhry. An illustration of the application of the Direct Step Method for a culvert was modified from Chow (1959) and is illustrated in Table 4.7 and Figure 4.14.

Table 4.7. Computation of the Flow Profile by the Direct Step Method.

Relative Depth (y/D)	Depth (y) (m)	Theta (degrees)	Area (m ²)	Hyd Radius (R) (m)	R ^{4/3}	Avg Vel (V) (m/sec)	V ^{2/2g}	E (m)	Delta E	Sf	Sf avg	So-Sf	Delta x (m)	x (m)
0.73	1.33	233.5	2.040	0.5474	0.4478	3.50	0.6242	1.950		0.004				
0.70	1.28	227.2	1.964	0.5418	0.4416	3.63	0.6732	1.953	0.003	0.004	0.00412	0.01588	0.20844	0.20844
0.65	1.19	214.9	1.807	0.5270	0.4256	3.95	0.7949	1.984	0.030	0.005	0.00479	0.01521	1.98888	2.19732
0.60	1.10	203.1	1.646	0.5078	0.4051	4.34	0.9590	2.056	0.073	0.007	0.00598	0.01402	5.17971	7.37704
0.55	1.01	191.5	1.480	0.4844	0.3805	4.82	1.1850	2.191	0.135	0.009	0.00774	0.01226	10.9851	18.3621
0.50	0.91	180.0	1.313	0.4572	0.3522	5.43	1.5055	2.420	0.229	0.012	0.01044	0.00956	23.9465	42.3086
0.48	0.88	175.4	1.247	0.4453	0.3400	5.73	1.6713	2.549	0.129	0.014	0.01298	0.00702	18.4217	60.7303
0.47	0.86	173.1	1.213	0.4391	0.3337	5.88	1.7646	2.624	0.075	0.015	0.01441	0.00559	13.4285	74.1588
0.46	0.84	170.8	1.180	0.4327	0.3273	6.05	1.8658	2.707	0.083	0.016	0.01552	0.00448	18.5199	92.6787

Discharge	7.14	m ³ /sec
Manning n	0.012	
So	0.02	
α	1.0	
Diameter	1.83	m
Normal Depth	1.33	m

(Example modified from Chow, 1959)

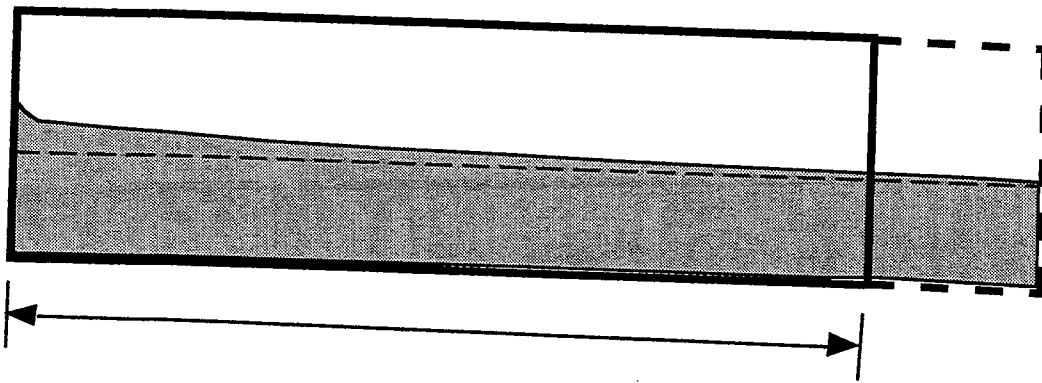


Figure 4.14 Illustration of gradually varied flow through a culvert approaching normal depth. (Modified from Chow, 1959). The figure is not drawn to scale.

4.4.3 Discussion

Based on the ability of the two equations to predict "effective" cross-sectional areas for various combinations of flow, slope, relative depth, downstream control, culvert corrugation, and culvert diameter, it was observed that the parameters important for fish design consideration were discharge, slope, culvert diameter, corrugations, and depth of flow. The two equations predicted the effective cross-section equally well regardless of the use of downstream control.

A comparison of the statistical parameters calculated for each of the two equations shows that the Mountjoy equation provided a better fit to the experimental data for more of the runs. All three of the statistical parameters were found to favor the Mountjoy equation in twenty-six of the runs. The Chiu equation was favored by all three of the statistical parameters for eighteen of the runs. For seven of the runs the statistical parameters did not favor one equation over the other. Although the Chiu equation was favored for eighteen of the runs, on only four of the runs were the magnitudes of all three of the statistical parameters for the Mountjoy equation greater than double the corresponding parameters for the Chiu equation. Therefore for many of the runs that the Chiu equation predicted better, the Mountjoy prediction was not significantly worse. Plots showing comparisons of the Bias, MAE, and RMSE for each of the equations are included in Figure 4.15, Figure 4.16, and Figure 4.17 respectively.

For the Mountjoy equation, the "effective" cross-sections predicted were compared to the actual "effective" cross-sections obtained experimentally. The region with velocities below $0.5*V_{max}$ were considered, because according to preliminary results from the WDFW (Powers, 1995) it was assumed that juvenile fish swimming capabilities were below this level. The Mountjoy equation prediction produced the greatest error for Run #24, which was the cross-section taken at the entrance on Culvert #2. The areas calculated between the band widths had an average of 49% error up to the contour line at $0.5*V_{max}$. The Mountjoy equation provided several very good fits such as the fit on Run #35 which was a velocity distribution taken for Culvert #3. The areas that were calculated between the band widths for this run had an average error of only 13% up to the contour line at $0.5*V_{max}$. These percentages may be slightly different depending on the cross-sectional area of the low velocity region being examined.

The results of the Chiu fit were improved when a best fit entropy parameter was found for each run. However, because no correlation could be found that would enable the best fit entropy parameter to be determined, and also because Chiu states that the entropy parameter is constant for a channel section, the best fit entropy parameter was not used.

4.5 Sensitivity Analysis of Equation Fits

A sensitivity analysis was performed for each of the two equations used for predicting the effective velocity cross-section. For the Chiu equation the impact of the entropy parameter selection was examined, and for the Mountjoy equation the impact of the Manning n selection was examined.

4.5.1 Chiu equation Sensitivity Analysis

A constant calculated entropy parameter (M) was calculated for each culvert. These values were given in Table 4.3. Best fit entropy parameters were calculated for each of the runs. For Culvert #1 the best fit entropy parameters ranged from 0.11 to 3.15. For Culvert #2 the best fit entropy parameters ranged from 0.48 to 4.33. For Culvert #3 the best fit entropy parameters ranged from 0.06 to 3.40. And for Culvert #4 the best fit parameters ranged from 3.30 to 6.24.

Given a depth, the Chiu equation predicts a relative velocity for that depth. The percentage of error in the relative velocity prediction was calculated for the difference between the each of the extreme values of the best fit M and the constant M which was calculated for the culvert. A plot was made for each of the four culverts showing the percent error in the relative velocity versus the relative depth for each of the extreme best fit entropy parameter values. These plots show how much the relative velocity values predicted by the Chiu equation, using best fit values for M , differed from the relative velocity values predicted using the constant value for M . The plots for Culverts #1, #2, #3, and #4 are shown in Figures 4.18, 4.19, 4.20, and 4.21 respectively.

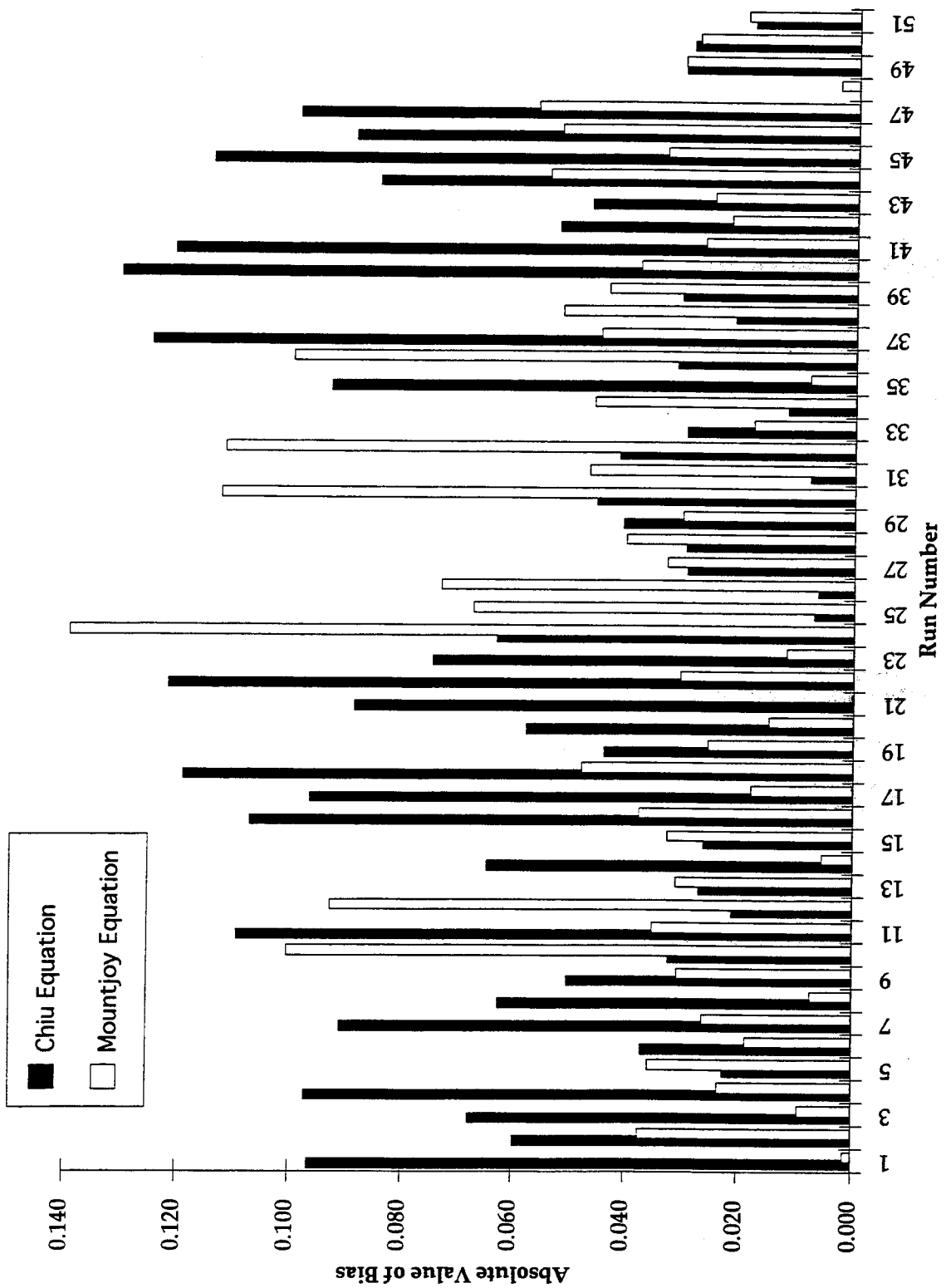


Figure 4.15. Absolute value of Bias for Chiu and Mountjoy equations plotted for each run.

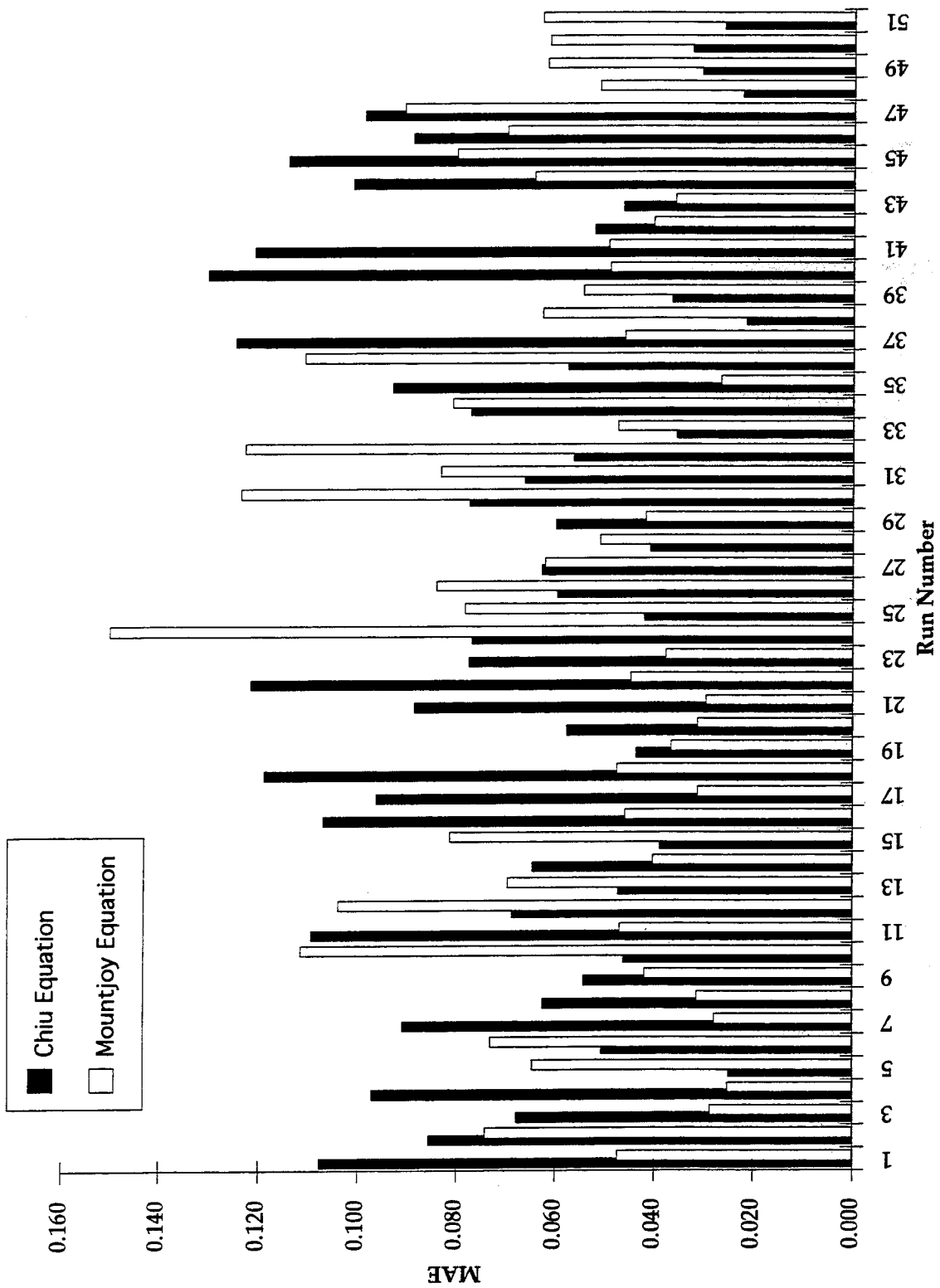


Figure 4.16. Plot of MAE for Chiu and Mountjoy equations for each run.

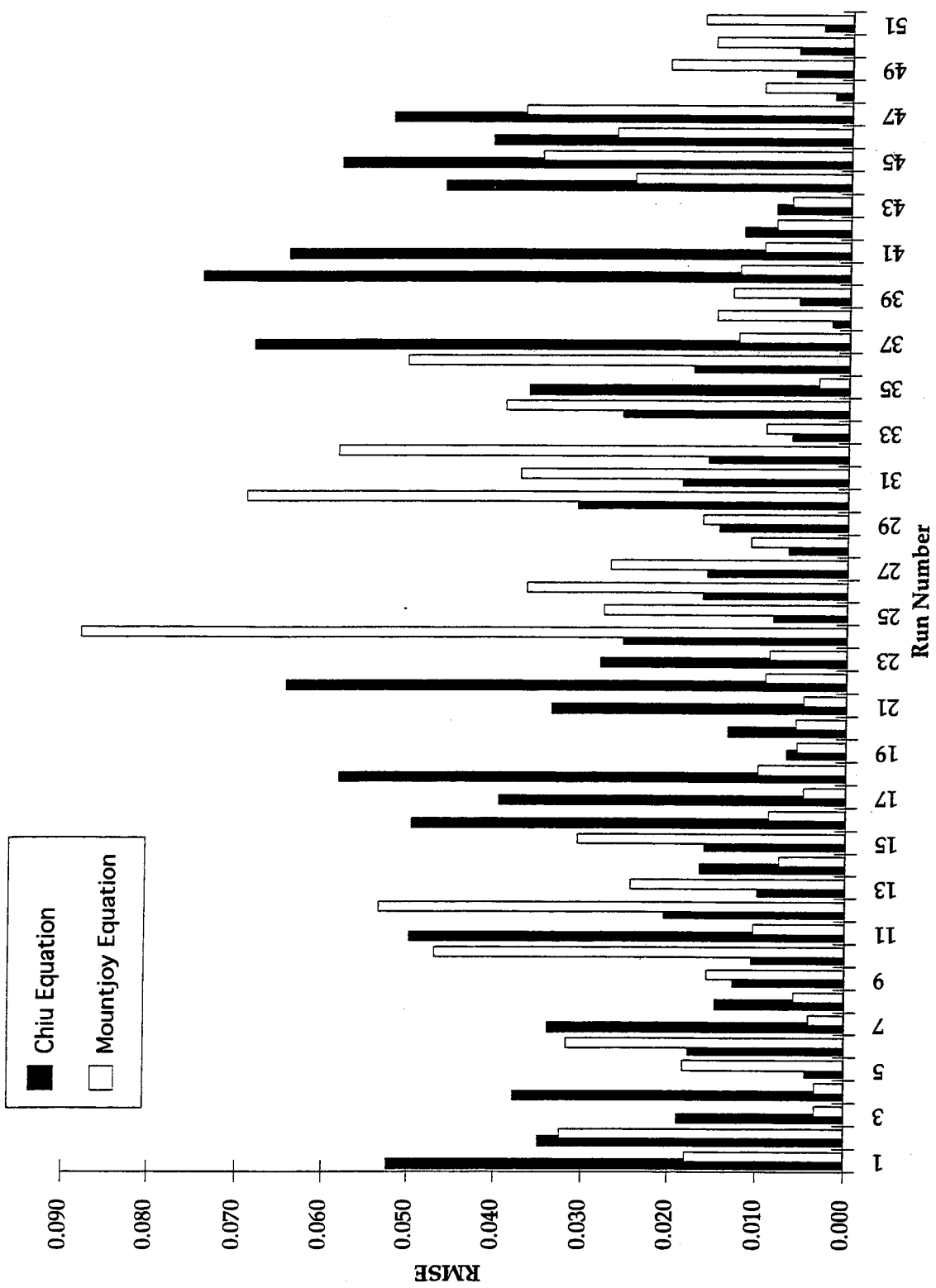


Figure 4.17. Plot of RMSE for Chiu and Mountjoy equations for each run.

**Chiu Equation Sensitivity Analysis for Culvert #1. Calculated
M=2.14.**

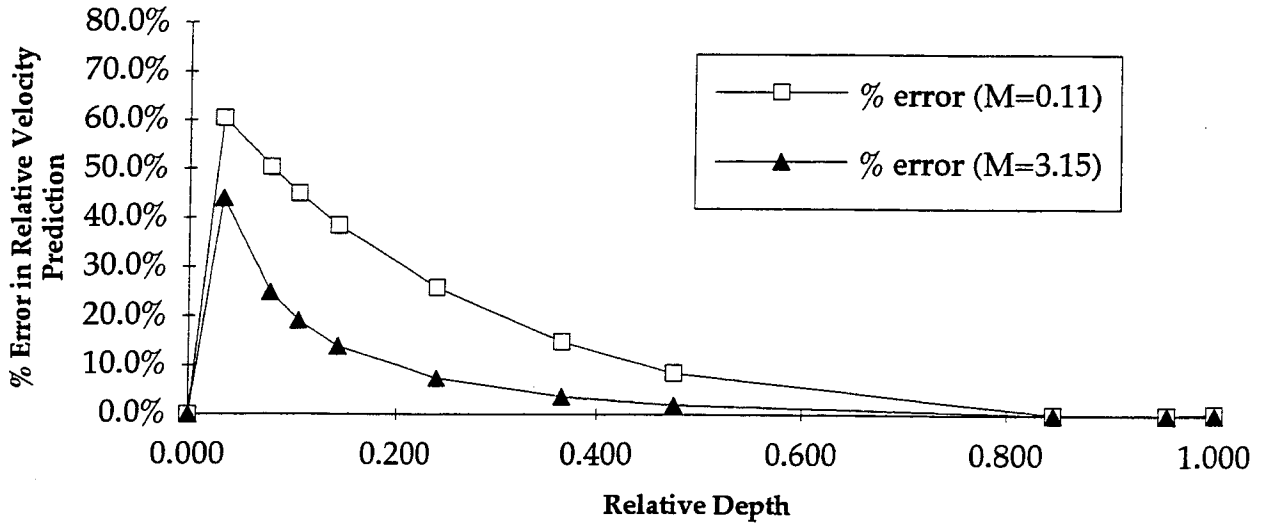


Figure 4.18. Plot of % error in relative velocity versus relative depth for Culvert #1.

**Chiu Equation Sensitivity Analysis for Culvert #2. Calculated
M=2.76.**

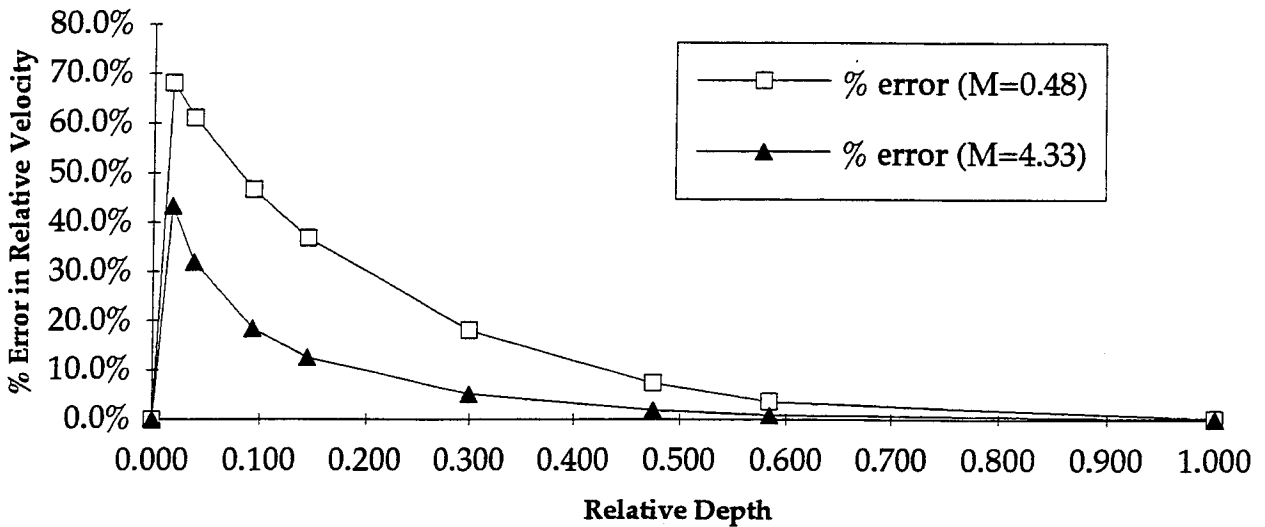


Figure 4.19. Plot of % error in relative velocity versus relative depth for Culvert #2.

**Chiu Equation Sensitivity Analysis for Culvert #3. Calculated
M=2.43.**

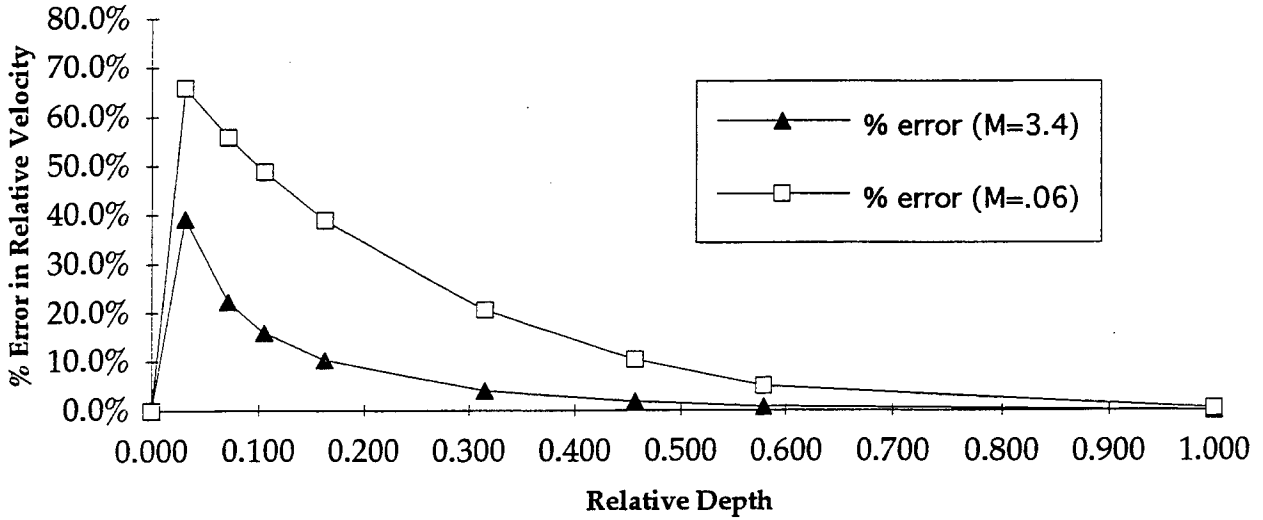


Figure 4.20. Plot of % error in relative velocity versus relative depth for Culvert #3.

**Chiu Equation Sensitivity Analysis for Culvert #4. Calculated
M=6.13.**

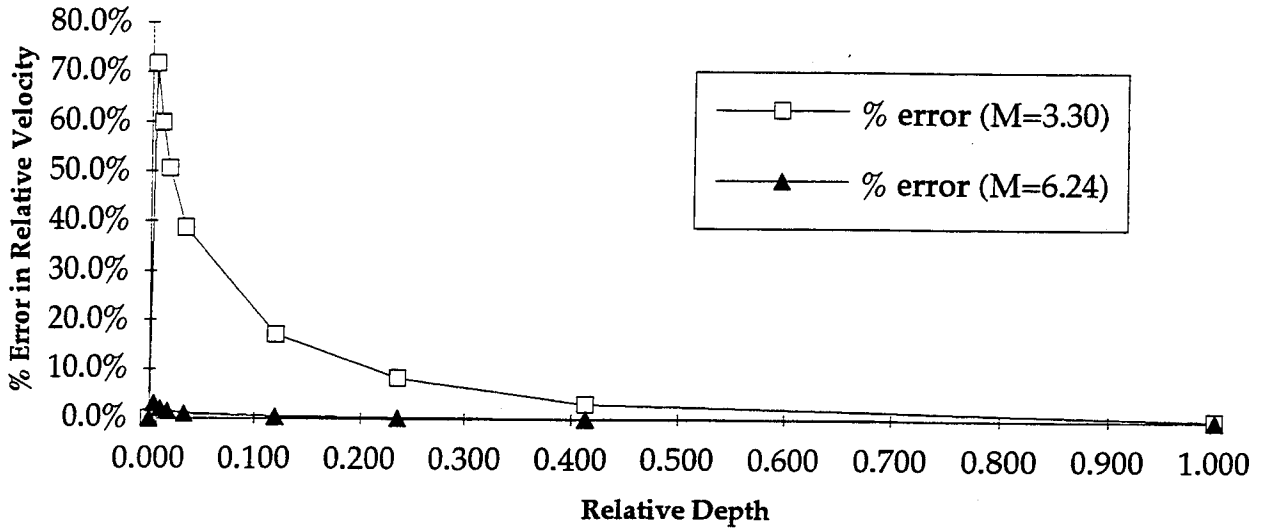


Figure 4.21. Plot of % error in relative velocity versus relative depth for Culvert #4.

4.5.2 Mountjoy Equation Sensitivity Analysis

The values for Manning's n used in the Mountjoy equation to predict effective velocity cross-sections were taken from the American Iron and Steel Institute (1980). However, as was discussed in Section 2.2.2, the Manning n can vary for a given cross-section. For Culvert #1 and Culvert #2 the Manning's n was assumed to be 0.024, for Culvert #3 the Manning's n was assumed to be 0.027, and for Culvert #4 the Manning's n was assumed to be 0.012.

Given a relative depth the Mountjoy equation predicts a velocity at that depth. For a typical experimental run from each of the four culverts, the impact of varying the Manning's $n \pm 0.002$ was examined. Three curves were produced for each analysis, one for each of the three Manning's n values used. The percentage differences between the relative velocities predicted using the assumed value of n and the varied values of n were calculated. A plot was made for each of the four culverts showing the percentage error in the calculated velocity versus the relative depth. These plots show how much difference is produced in the velocity prediction by varying the Manning's $n \pm 0.002$. The plots for Culverts #1, #2, #3, and #4 are shown in Figures 4.22, 4.23, 4.24, and 4.25 respectively.

Mountjoy Method Sensitivity Analysis for Culvert #1. Assumed $n=0.027$

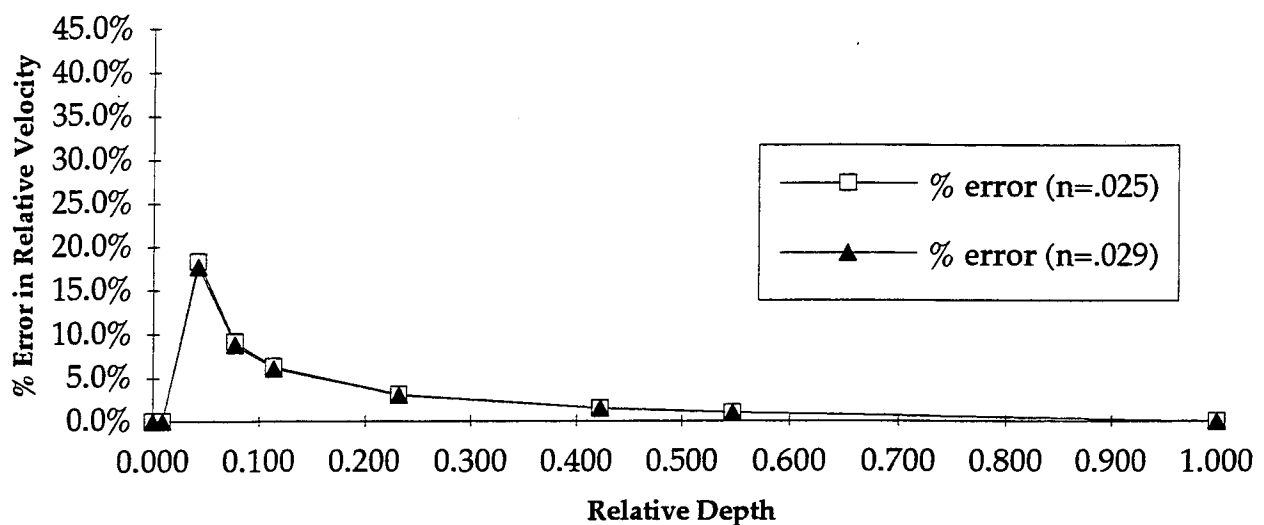


Figure 4.22. Plot of % error in velocity versus relative depth for a typical experimental run in Culvert #1.

**Mountjoy Method Sensitivity Analysis for Culvert #2. Assumed
n=0.027**

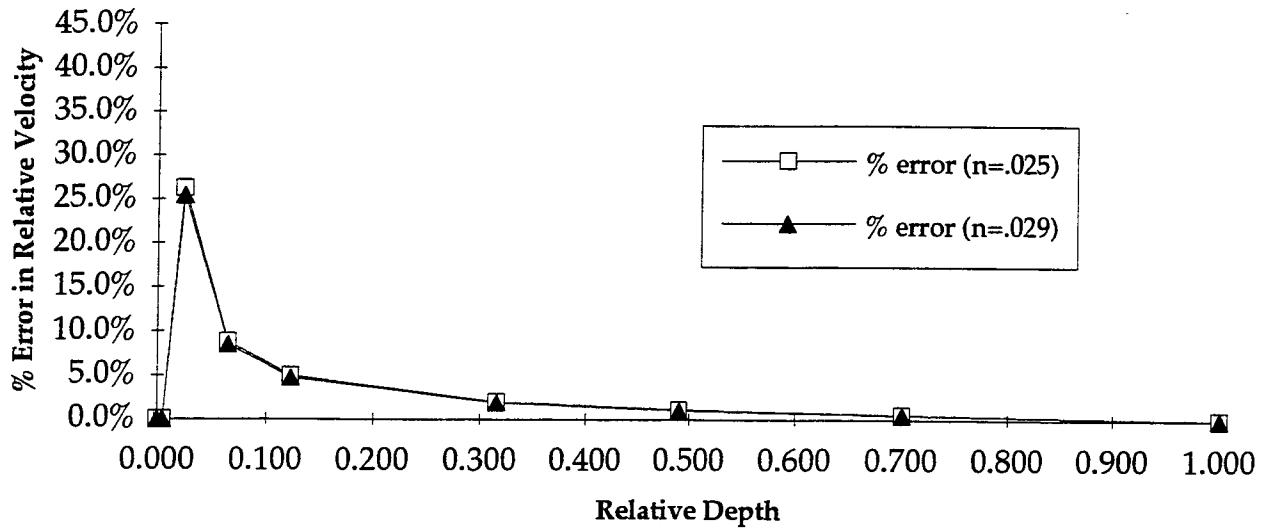


Figure 4.23. Plot of % error in velocity versus relative depth for a typical experimental run in Culvert #2.

**Mountjoy Method Sensitivity Analysis for Culvert #3. Assumed
n=0.030**

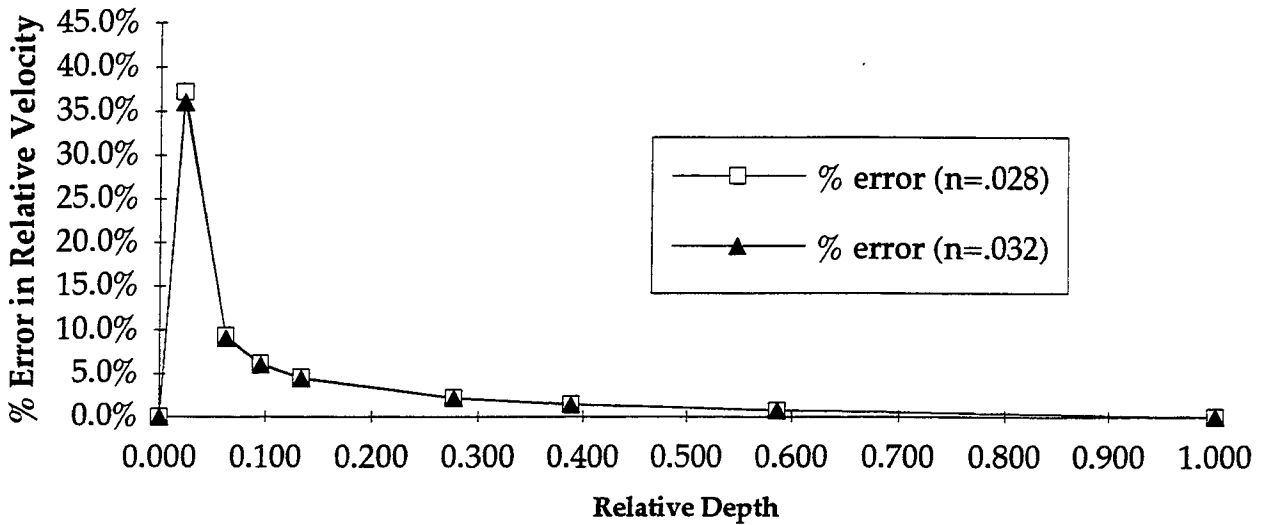


Figure 4.24 Plot of % error in velocity versus relative depth for a typical experimental run in Culvert #3.

Mountjoy Method Sensitivity Analysis for Culvert #4. Assumed $n=0.012$

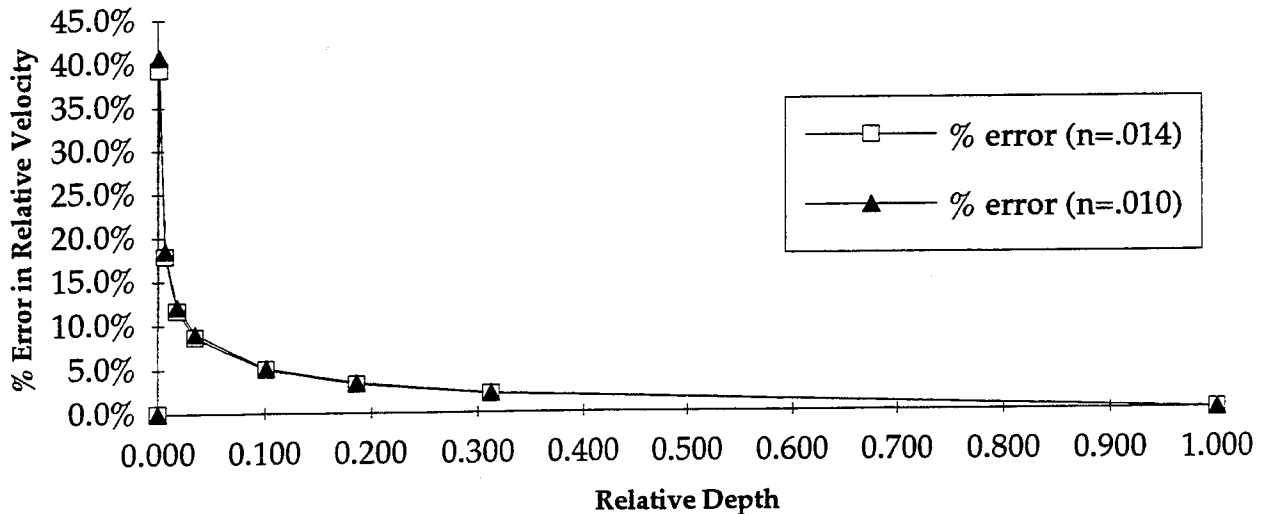


Figure 4.25 Plot of % error in velocity versus relative depth for a typical experimental run in Culvert #4.

4.6 Horizontal Velocity Profiles

Preliminary results from the tests being conducted by WDFW revealed that juvenile fish will in fact find the low velocity regions within the cross-sectional area. In their hatchery experiments, WDFW observed juvenile fish swimming in the low velocity boundary layers in the upper corners of the pipe. Moreover, the juvenile fish traveled near the surface within 0.3 times the depth of flow. These migration zones are shown as shaded regions in Figure 4.26. This observation is consistent with the research findings of investigators studying other species of fish.

4.6.1 Effective Width Calculation

As a result of these observations, attempts were made to determine the horizontal velocity profile at $0.8*d$ with the ultimate goal of determining the width of the migration area.

The horizontal velocity profiles were scaled from the original velocity contour plots and are presented in Appendix D. Various attempts were made to fit this data with known velocity distributions including the Mountjoy and Chiu equations. However, since all of the equations were based on previous studies of longitudinal velocity profile, the measured versus computed results showed a considerable amount of variation.

Since neither the Mountjoy or Chiu equations adequately predicted the velocity along the horizontal profile, an empirical method was examined which computed the effective width from the effective area calculation proposed in this research. The effective area is converted to an equivalent area on each side of the pipe. A trial and error iteration procedure is used to determine the width required to produce that area. A program converts the effective area determined by the previous method into assumed symmetric areas. Through the use of a Downs Correction Factor (DCF), the widths are scaled down to match those measured in the hydraulic testing program. A range of DCF values from 1 to 4 is plotted Figure 4.27 although the designer is free to choose any positive value depending on the level of safety factor required and the certainty of the design requirements. It will be up to the biological constraints as to whether or not this width is acceptable.

A DCF of 1.0 for tail water conditions provides conservative estimates of widths for nearly all the flow cases tested. As would be expected, measurements of these values were dependent upon the downstream tail water depth, and therefore, varied significantly. However, in most every case (2 exceptions) the correction factor was less than one.

An interesting point must be made concerning the concept of tail water or backwater control. In most instances, no attempt was made to insure backwater conditions existed throughout the pipe. Situations where the outfall is partially submerged but the culvert resumes near uniform flow conditions at an upstream location within the pipe may produce more severe conditions with respect to fish passage. Consequently, in designs where backwater conditions are expected to dominate the outlet, the designer should make sure that such controls exist throughout the culvert.

A program called JUFIPP - JUvenile FIsh Passage Program was developed to compute the effective widths. JUFIPP was developed using Visual Basic 4.0 and comes on three diskettes. There is a setup module loaded on disk 1 of 3 which allows for easy installation. A graphical user interface (GUI) prompts data from the designer for ease of use. The user provides information concerning the discharge, slope, diameter, roughness, DCF, and error tolerance (typically 0.001 meters), and the program computes the width. Using the example provided in Appendix E, the input data requirements are quite simple. Default values and limited error checking have also been provided.

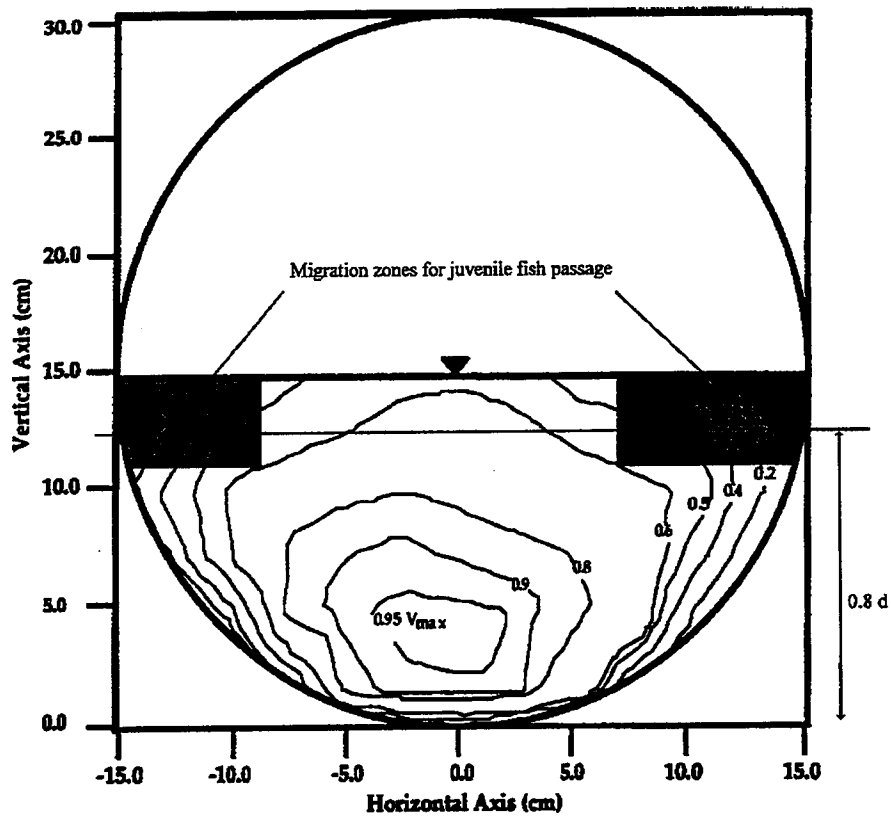


Figure 4.26 Migration zones for juvenile fish passage

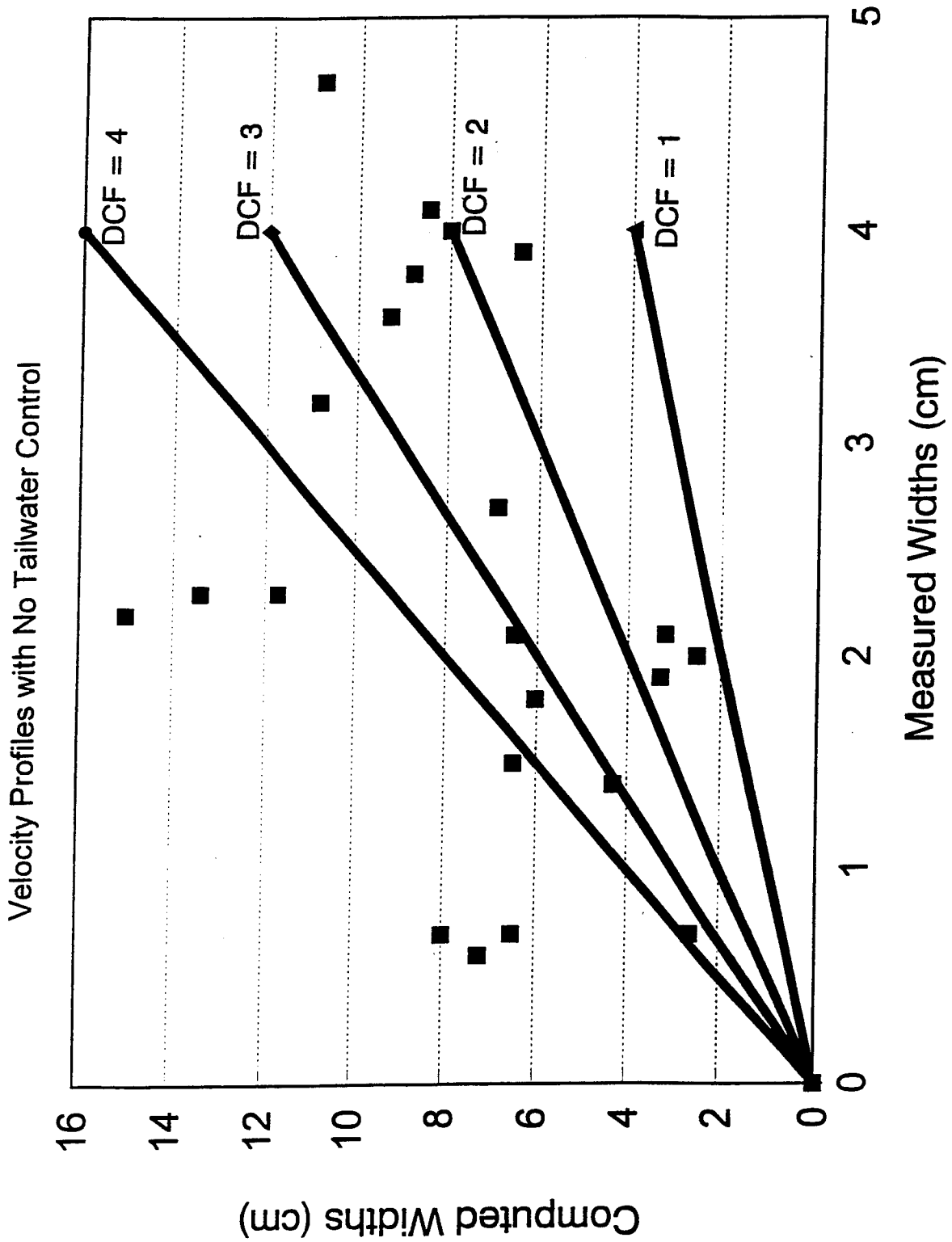


Figure 4.27 Downs Correction Factor for width adjustment

Chapter 5

SUMMARY AND CONCLUSIONS

5.1 Summary

The primary objectives of this research were to: (1) measure the cross-sectional velocity distributions in four metal culverts of different diameters and corrugations; and (2) to develop an empirical method of predicting velocity distributions in larger diameter culverts.

Because the velocity distributions measured for the experimental culverts were often non-symmetrical about the centerline, it was not possible to predict the exact two-dimensional velocity distributions. Because of this asymmetry, the areas between the velocity contour lines were converted to symmetrical ring-shaped bands which were then used to create an "effective" two-dimensional velocity distribution. This effective velocity distribution represents average band widths of a given velocity range that could be expected in the culvert, which may be the important design parameter in juvenile fish passage.

Two equations were used to predict the thicknesses of the bands in the effective cross-section. The first equation was the Chiu equation (Equation 2.21) and the second equation was the Mountjoy equation (Equation 2.16). Each of these equations was used to predict the one-dimensional velocity distribution at the centerline. And because the effective band widths were symmetrical this enabled the effective velocity distribution cross-section to be predicted.

The selection of the equation which provides the best fit allows for the effective velocity distribution in a larger diameter, annular corrugated, circular culvert to be predicted. This method of scaling is based on the fit provided by the selected equation being verified by the experimental results from the four test culverts.

By expanding the original concept, effective widths may be estimated from the effective area calculations. Once biological criteria have been set, these widths may be useful in establishing proper design guidelines.

5.2 Conclusions

The Mountjoy equation was selected as the more accurate method of predicting the effective band widths. The Mountjoy equation provided a better fit to the experimental data than did the Chiu equation for many of the experimental runs. For most of the runs in which the Chiu equation was more accurate, the fit provided by the Mountjoy equation was not significantly worse.

It must be noted that the fit provided by the Chiu equation was improved with the selection of a best fit entropy parameter (M). However, according to Chiu (1995) the value of M is constant for a channel section regardless of discharge and flow depth. Because no relationship was found which would enable the prediction of the best fit M , the constant calculated value of M was used for the Chiu equation.

The fits provided by each of the equations did not appear to be affected by the downstream control. The experimental runs covered a wide range of discharge (0.0052 to 0.1274 m³/s (0.1836 cfs to 4.499 cfs)), relative depth (0.17* D_o to 0.79* D_o), and slope (0.5% to 5.0%) combinations for each of the test culverts. Both the Mountjoy equation and the Chiu equation provided reasonable fits to the experimental data regardless of the experimental condition experienced.

5.2.1 Limitations of Conclusions

This research investigated only circular, annular corrugated, metal culverts. Thus, the results that were obtained and the conclusions that were drawn from these results are valid only for circular, metal culverts with annular corrugations. This research also concentrated solely on the hydraulic conditions in the culvert. It is important to note that only hydraulic characteristics were taken into consideration for this research and that juvenile fish passage may be impacted by a number of other factors, for example, high sediment load and temperature. These other factors may impact the swimming capability of juvenile fish.

5.3 Recommendations for Further Studies

The WDFW is currently conducting research related to the swimming capabilities of juvenile fish in highway culverts. This research will provide a better understanding of the size of the required low velocity region for juvenile fish, and what are the limiting flow velocities and slopes. Preliminary results indicate juvenile salmon, approximately 63 mm (2.5 in) long, will not pass in velocities greater than 36.6-39.6 cm/s (14.4-15.6 in/s) or slopes greater than 1% (Powers, 1995). The final results should be combined with this study to provide better design criteria.

It is also recommended that research be performed into ways of providing acceptable velocities for juvenile fish in existing culverts. This may include the following: (1) Installation of baffles in the culvert barrel to increase roughness and reduce velocities in the boundary layer; (2) Development of a corrugated culvert with large amplitude corrugations (i.e. 6.6 cm x 5.0 cm (2.6 in x 2.0 in), 7.6 cm x 7.6 cm (3 in x 3 in)). Finally, field studies could be conducted in cooperation with the WDFW to examine the juvenile fish in their natural habitat. The hydraulic effects of approach velocities, downstream conditions, and unsteady flow could be examined.

References

- AISI. 1980. Modern Sewer Design. New York, NY. American Iron and Steel Institute.
- Baker, C.O. and F.E. Votapka. 1990. Fish Passage Through Culverts. USDA-Forest Service.
- Bates, K. 1994. Juvenile Fish Passage Through Culverts. Washington Department of Fish and Wildlife Study Notes.
- Bates, K. 1992. Excerpts from: Fishway Design for Pacific Salmon. Washington Department of Transportation Fish Passage Workshop. June 17, 1992.
- Behlke, C.E.; D.L. Kane; R.F. McLean; and M.D. Travis. 1989. Field observation of arctic grayling passage through highway culverts. Transportation Research Record 1224. 63-66.
- Bell, M.C. 1973. Fisheries Handbook of Engineering Requirements and Biological Criteria. Portland, OR, U.S. Corps of Engineers, North Pacific Division.
- Blaxter, J.H.S. 1969. Swimming Speeds of Fish. FAO Fisheries Report. 62(2). Rome, Italy. 62-100.
- Cederholm, C.J. and W.J. Scarlett. 1981. Seasonal immigrations of juvenile salmonids into four small tributaries of the Clearwater River, Washington. 1977-1981. Salmon and Trout Migratory Behavior Symposium, June 1981. Seattle, WA. 98-110.
- Chaudhry, M. H. 1993. Open Channel Flow. Prentice-Hall, Inc. Englewood Cliffs, N.J.
- Chiu, C-L. 1988. Entropy and 2-D velocity distribution in open channels. Journal of Hydraulic Engineering, ASCE, Vol. 114, No. 7. 738-756.
- Chiu, C-L. 1989. Velocity distribution in open-channel flow. Journal of Hydraulic Engineering, ASCE, Vol. 115, No. 5. 615-628.
- Chiu, C-L and D.W. Murray. 1992. Variation of velocity distribution along non-uniform open channel flow. Journal of Hydraulic Engineering, ASCE, Vol. 118, No. 7. 989-1001.
- Chiu, C-L, G-F Lin, and J-M Lu. 1993. Application of Probability and Entropy Concepts in Pipe-Flow Study. Journal of Hydraulic Engineering, ASCE, Vol. 119, No. 6, June 1993. 742-755.
- Chiu, C-L and C.A.A. Said. 1995. Maximum and Mean Velocities and Entropy in Open Channel Flow. Journal of Hydraulic Engineering, ASCE. Vol. 121. No. 1. January, 1995. 26-35.
- Chow, V.T. 1959. Open-Channel Hydraulics. McGraw-Hill Book Company. New York, NY.
- Chow, V.T. 1964. Handbook of Applied Hydrology. A Compendium of Water-resource Technology. McGraw-Hill Book Company. New York, NY.

- Dane, B.G. 1978. A review and resolution of fish passage problems at culvert sites in British Columbia. Department of Fisheries and Environment, Pacific Region. Fisheries and Marine Service Technical Report No. 810.
- Evans, W.A. and F. B. Johnston. 1980. Fish Migration and Fish Passage. A Practical Guide to Solving Fish Passage Problems. U.S. Department of Agriculture-Forest Service Region 5 report. June 1972. Revised March 1974. Revised 1980. 63 pages.
- Gebhards, S. and J. Fischer 1972. Fish passage and culvert installations. Idaho Fish and Game Report. 12 p.
- Grant, D.M. 1979. ISCO Open Channel Flow Measurement Handbook. First edition. Second printing. Instrumentations Specialties Company, Environmental Division. Lincoln, Nebraska.
- Henderson, F.M. 1966. Open Channel Flow. Macmillian Publishing Company, Inc. New York, NY.
- Jones, D.R., O.S. Bamford, and V.W. Kiceniuk. 1974. An evaluation of the swimming performance of several fish species from the MacKenzie River. University of British Columbia, Zoology Department.
- Kane, D.L. and P.M. Wellen. 1985. A hydraulic evaluation of fish passage through roadway culverts in Alaska. Institute of Water Resources, University of Alaska-Fairbanks, Fairbanks, AK; State of Alaska, Department of Transportation and Public Facilities, Research Section, Fairbanks, AK. August 1985. 54 p.
- Katopodis, C., P.R. Robinson and B. G. Sutherland. 1978. A Study of Model and Prototype Culvert Baffling for Fish Passage. Fisheries & Marine Service Technical Report No. 828. 78 p.
- Kennedy, R.J. and J.F. Fulton. 1961. The effects of secondary currents upon the capacity of a straight open channel. ASME-EIC. Hydraulics Conference Paper No. 61-EIC-1. Montreal, Canada.
- MacPhee, C. and F.J. Watts. 1976. Swimming performance of arctic grayling in highway culverts. Final report to U.S. Fish and Wildlife Service. Anchorage, Alaska. June, 1976. 42 p.
- Morsel, J., J. Houghton, M. Bell, and R. Costello. 1981. Fish protection strategies for the design and construction of the Alaska segment of the natural gas transportation system. Report prepared by Dames and Moore for Northwest Alaskan Pipeline Company, Anchorage, AK.
- Mountjoy, P.K. 1986. Velocity profile prediction in culverts for fish passage design considerations. MS Thesis. University of Alaska, Fairbanks. May 1986.

- Normann, J.N. 1980. Hydraulic flow resistance factors for corrugated metal conduits. U.S. Federal Highway Administration report. McLean, Virginia. January 1980. 94 p.
- Normann, J.N., R.J. Houghtalen, and W.J. Johnston. 1985. Hydraulic design of highway culverts. U.S. Department of Transportation. Federal Highway Administration. September 1985. 272 p.
- Powers, P.D. and J.F. Orsborn. 1986. Analysis of barriers to upstream fish migration. An Investigation of the physical and biological conditions affective fish passage success at culverts and waterfalls. Prepared by Washington State University for Bonneville Power Administration. Portland, OR. January 1986.
- Powers, P.D. 1995. Preliminary results of Department of Fisheries research. Personal communication. May 18, 1995.
- Replogle, J.A. and V.T. Chow. 1966. Tractive-force distribution in open channels. Journal of the Hydraulics Division, Proceedings of the ASCE. Vol. 92. No. HY2. 169-191.
- Roberson, J.A. and C.T. Crowe. 1990. Engineering Fluid Mechanics. Houghton Mifflin Company. Boston, MA.
- Skeesick, D.G. 1970. The fall immigration of juvenile coho salmon into a small tributary. Fish Commission of Oregon, Research Division. Research Reports of the Fish Commission of Oregon. 90-95.
- Schlichting, H. 1979. Boundary Layer Theory. McGraw-Hill Book Company. New York, NY.
- Shukry, A. 1950. Flow around bends in an open flume. Transactions, ASCE. Vol. 115. 751-779.
- U.S. Department of Agriculture-Forest Service. 1978. Fish/culvert roadway drainage guide. USDA-Forest Service. Alaska Region. September 1978.
- Washington Department of Fisheries. 1990. Fish Passage Guidelines: Culvert Installations.
- Washington Department of Fish and Wildlife. 1995. Reviewer comments of draft WSDOT technical report submitted by Barber and Downs September 5, 1995.
- Ziemer, G.L. 1965. Culvert design. Alaska Department of Fish and Game.

Appendix A

Manning Roughness Coefficient Plots

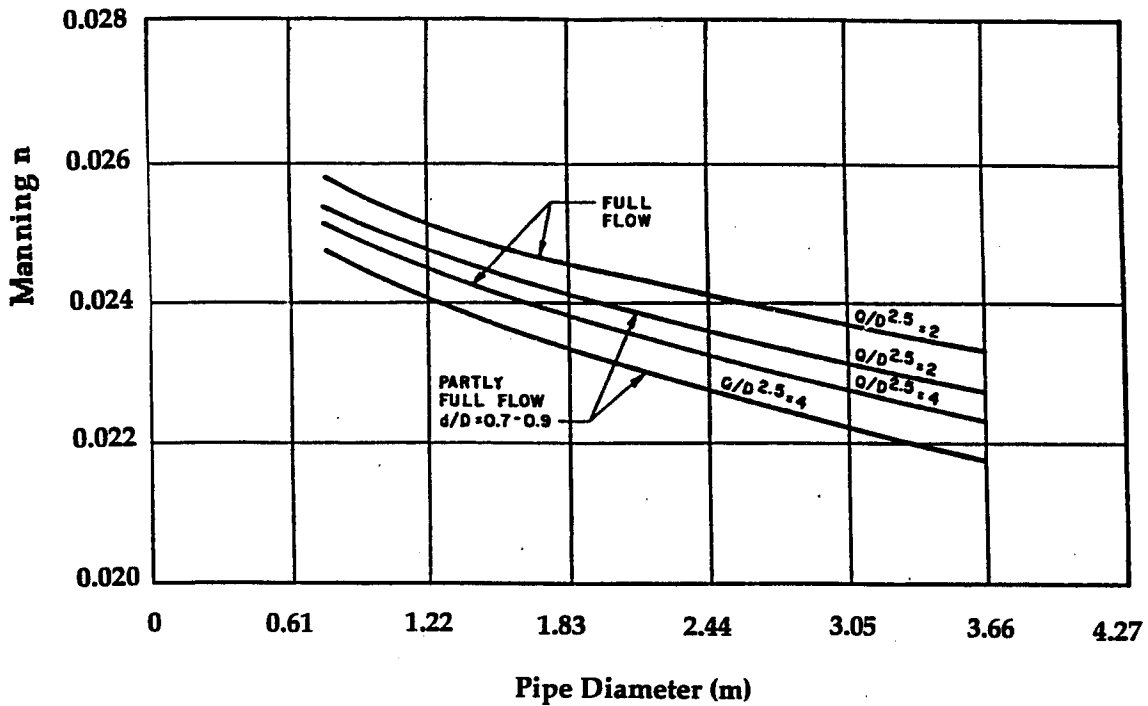


Figure A2.1. Manning roughness coefficient (n) versus Diameter for 14.9 x 2.5 cm annular corrugated metal pipe. (Modified from Normann, 1980).

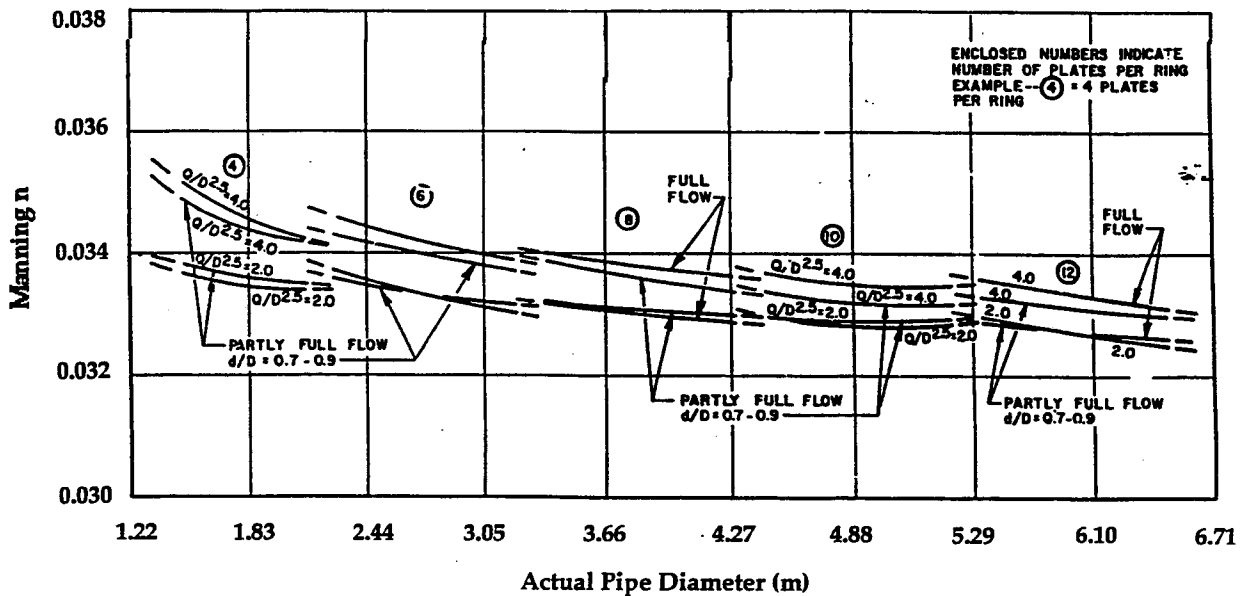


Figure A2.2. Manning roughness coefficient (n) versus Diameter for 14.9 x 5.0 cm annular structural plate corrugated metal pipe. (Modified from Normann, 1980).

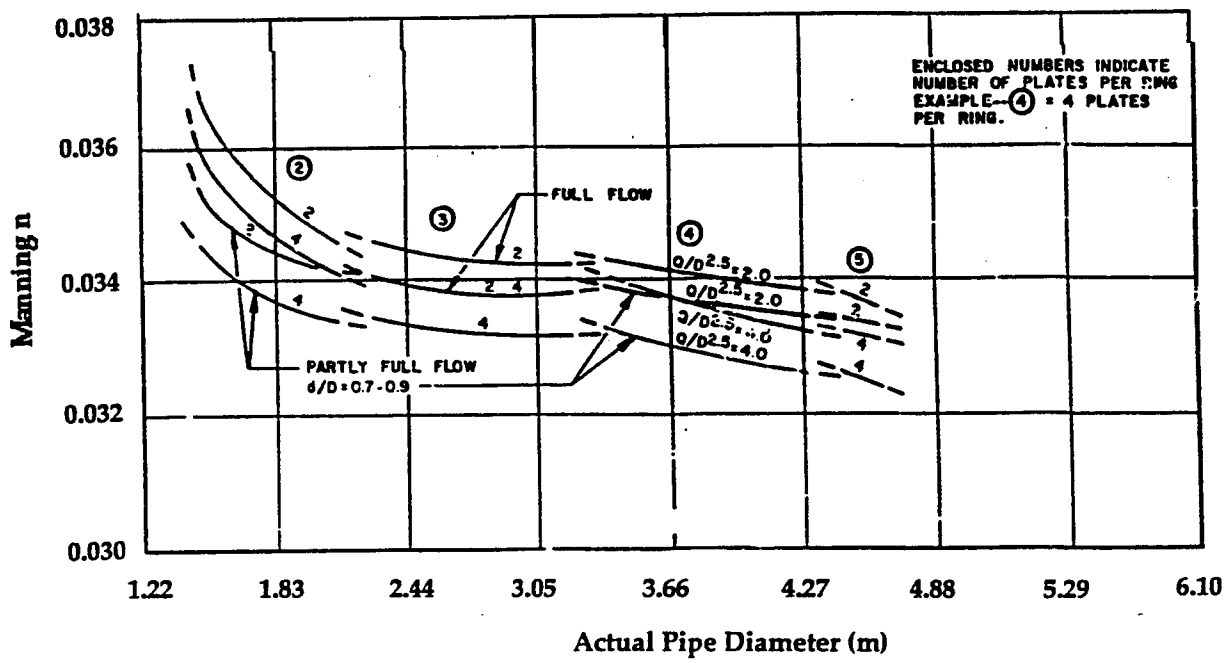


Figure A2.3. Manning roughness coefficient (n) versus Diameter for 22.3 x 6.2 cm annular structural plate corrugated metal pipe.

Appendix B

Velocity Contour Plots (shown looking downstream)

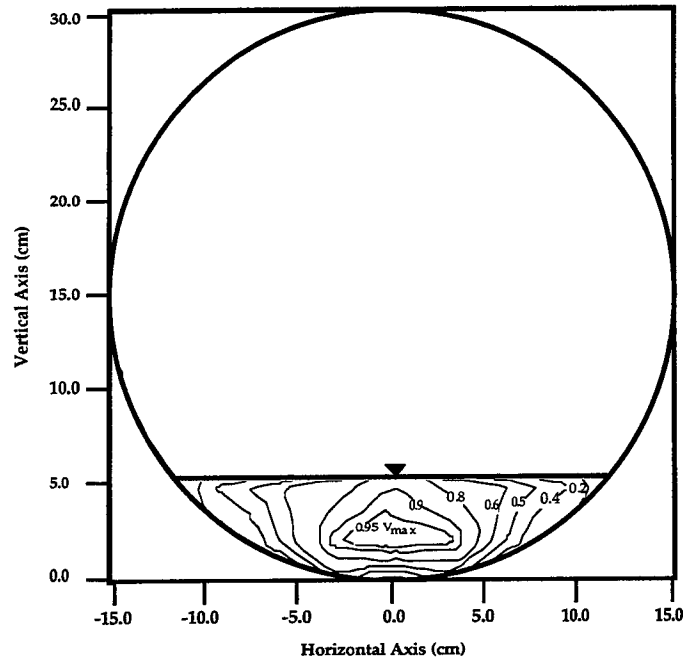


Figure B4.1. Velocity contour plot for Culvert #1 at $Q = 0.0052$ cms, 5% slope, $0.17D_o$, $L/D = 14$, no downstream control, $V_{max} = 101.9$ cm/sec.

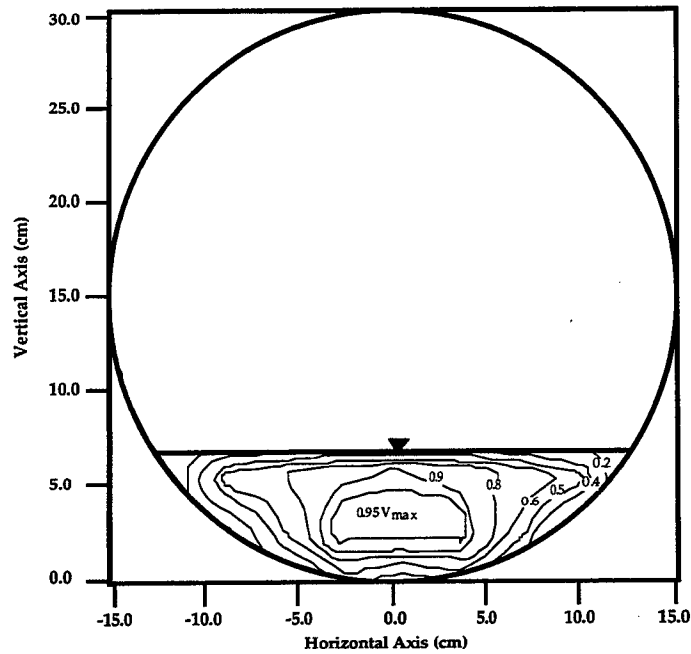


Figure B4.2. Velocity contour plot for Culvert #1 at $Q = 0.0064$ cms, 3% slope, $0.23D_o$, $L/D = 14$, no downstream control, $V_{max} = 82.0$ cm/sec.

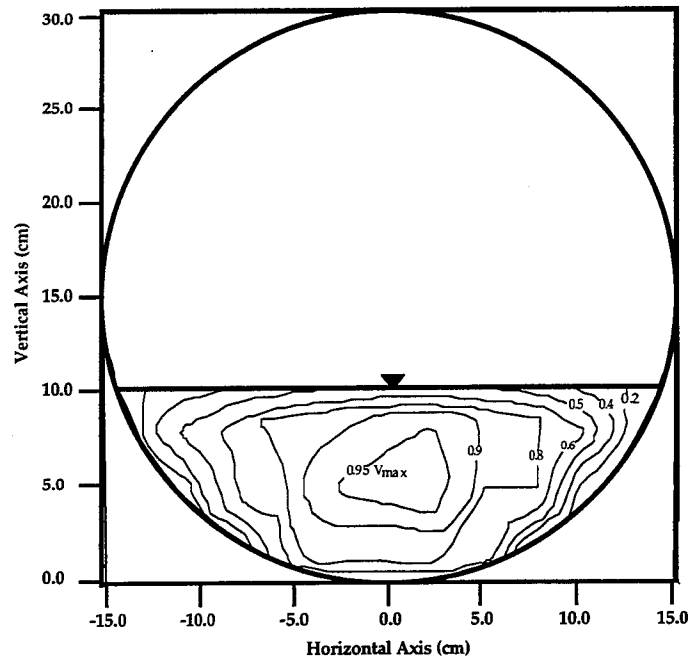


Figure B4.3. Velocity contour plot for Culvert #1 at $Q = 0.0082$ cms, 1% slope, $0.34D_0$, $L/D = 14$, no downstream control, $V_{max} = 61.2$ cm/sec.

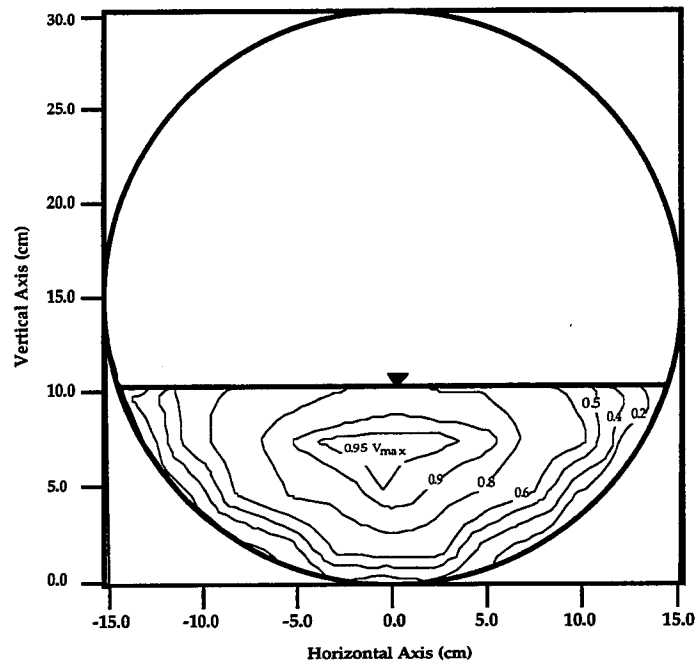


Figure B4.4. Velocity contour plot for Culvert #1 at $Q = 0.0094$ cms, 1/2% slope, $0.34D_0$, $L/D = 14$, no downstream control, $V_{max} = 59.9$ cm/sec.

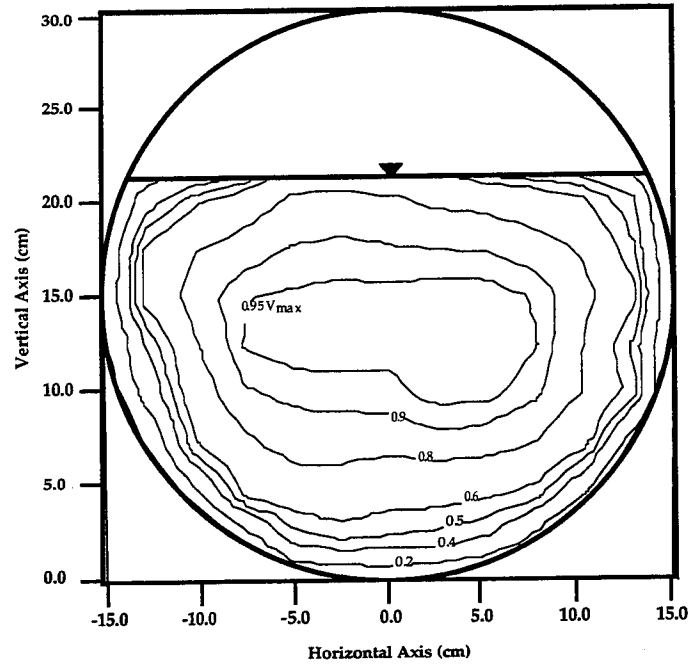


Figure B4.5. Velocity contour plot for Culvert #1 at $Q = 0.0124$ cms, 1/2% slope, $0.68D_o$, $L/D = 14$, downstream control, $V_{max} = 34.5$ cm/sec.

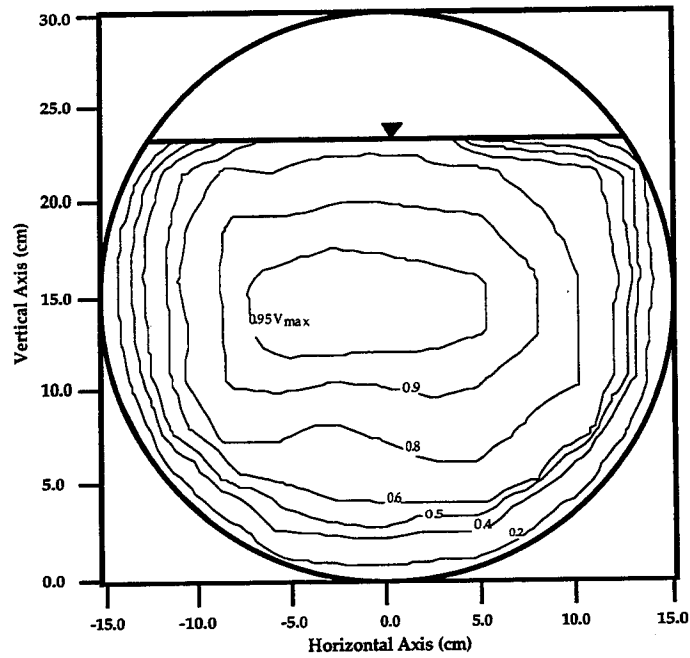


Figure B4.6. Velocity contour plot for Culvert #1 at $Q = 0.0124$ cms, 1% slope, $0.76D_o$, $L/D = 14$, downstream control, $V_{max} = 33.2$ cm/sec.

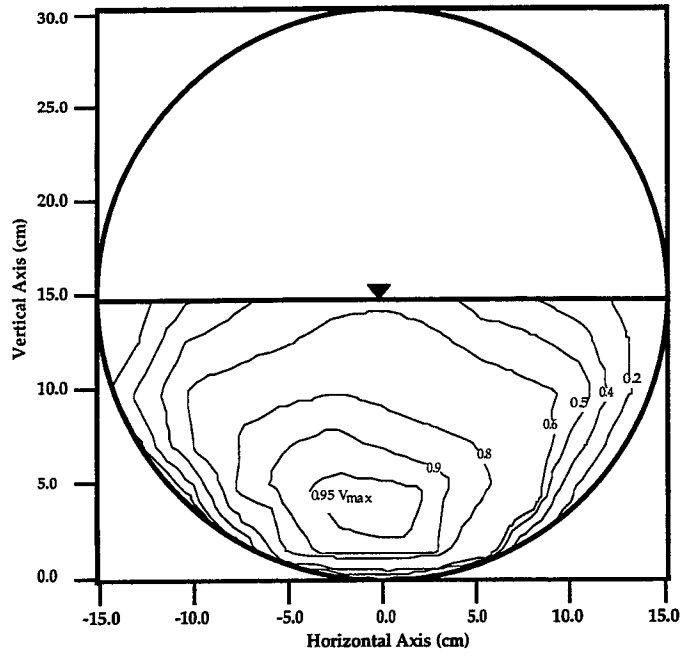


Figure B4.7. Velocity contour plot for Culvert #1 at $Q = 0.0142$ cms, 5% slope, $0.49D_0$, $L/D = 14$, downstream control, $V_{max} = 63.1$ cm/sec.

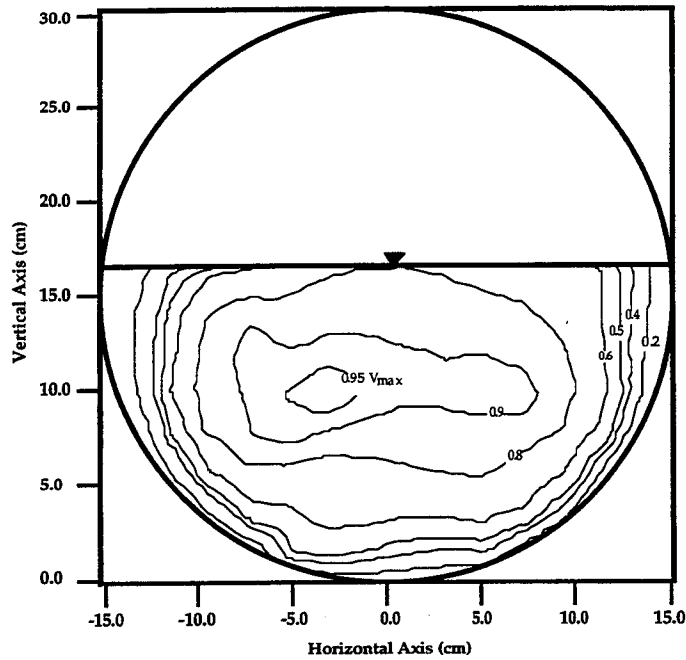


Figure B4.8. Velocity contour plot for Culvert #1 at $Q = 0.0213$ cms, 1/2% slope, $0.56D_0$, $L/D = 14$, downstream control, $V_{max} = 85.1$ cm/sec.

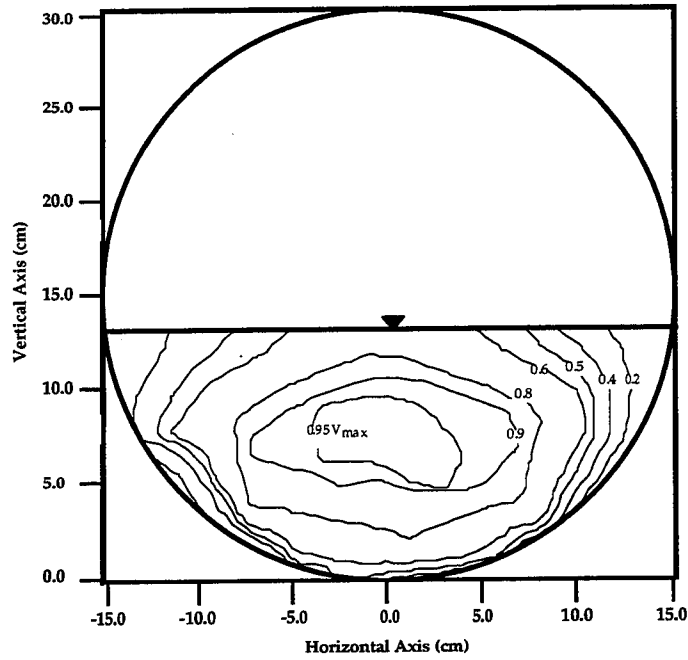


Figure B4.9. Velocity contour plot for Culvert #1 at $Q = 0.0278$ cms, 3% slope, $0.43D_0$, $L/D = 14$, no downstream control, $V_{\max} = 125.9$ cm/sec.

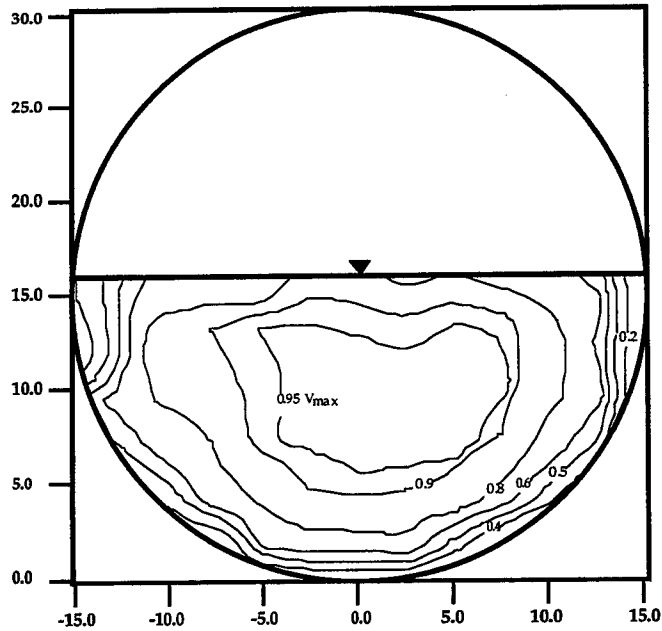


Figure B4.10. Velocity contour plot for Culvert #1 at $Q = 0.0284$ cms, 1% slope, $0.52D_0$, $L/D = 14$, no downstream control, $V_{\max} = 92.7$ cm/sec.

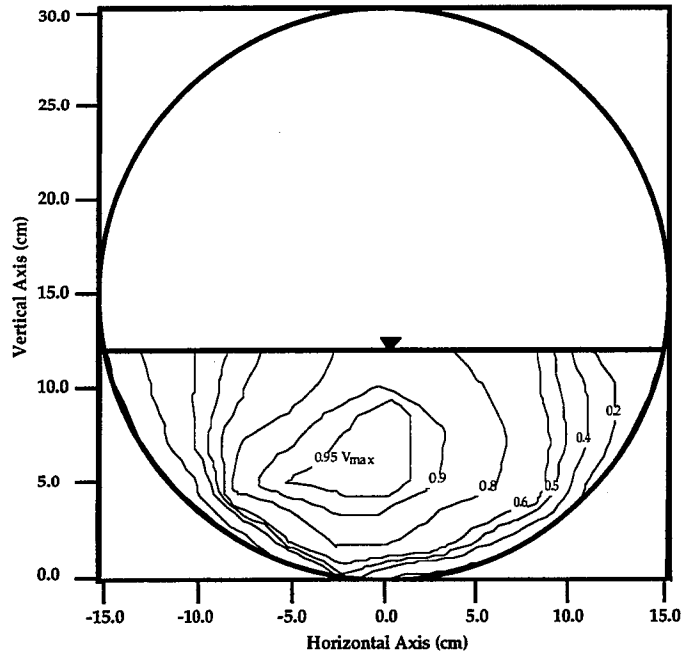


Figure B4.11. Velocity contour plot for Culvert #1 at $Q = 0.0290$ cms, 5% slope, $0.39D_0$, $L/D = 14$, no downstream control, $V_{max} = 169.3$ cm/sec.

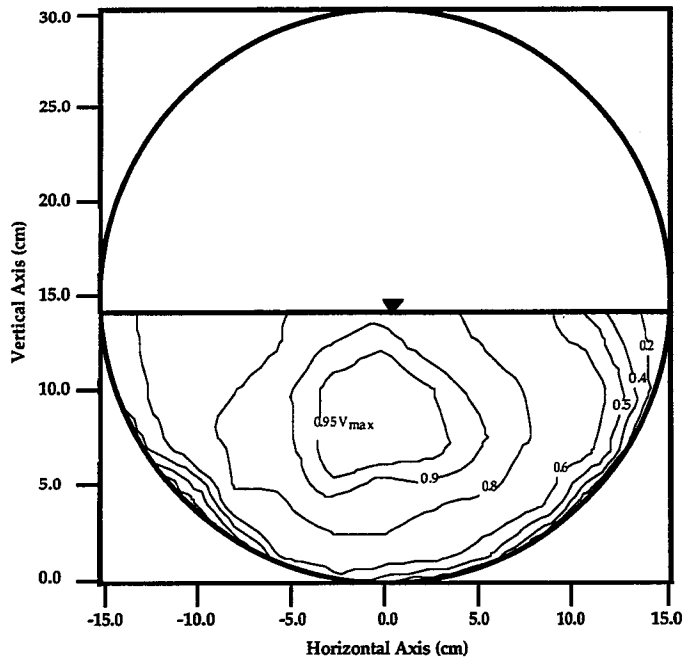


Figure B4.12. Velocity contour plot for Culvert #1 at $Q = 0.0438$ cms, 5% slope, $0.46D_0$, $L/D = 14$, no downstream control, $V_{max} = 178.0$ cm/sec.

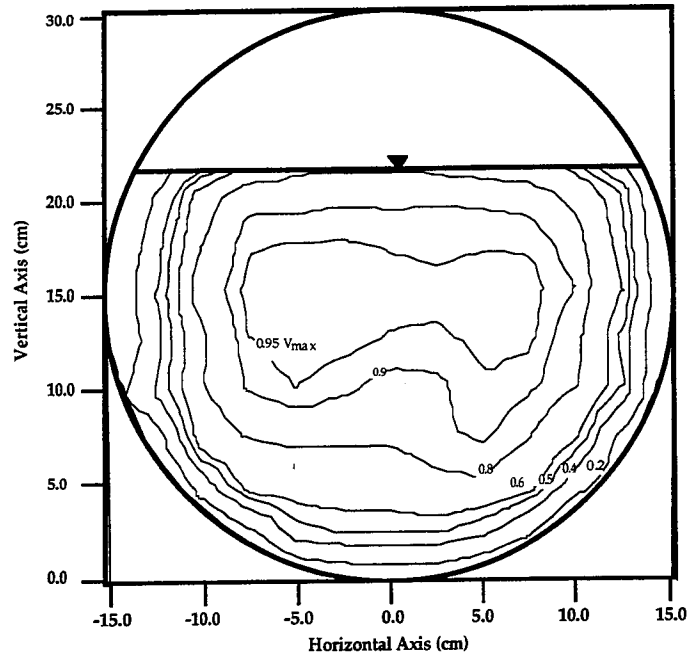


Figure B4.13. Velocity contour plot for Culvert #1 at $Q = 0.0456$ cms, 1/2% slope, $0.72D_0$, $L/D = 14$, no downstream control, $V_{max} = 108.5$ cm/sec.

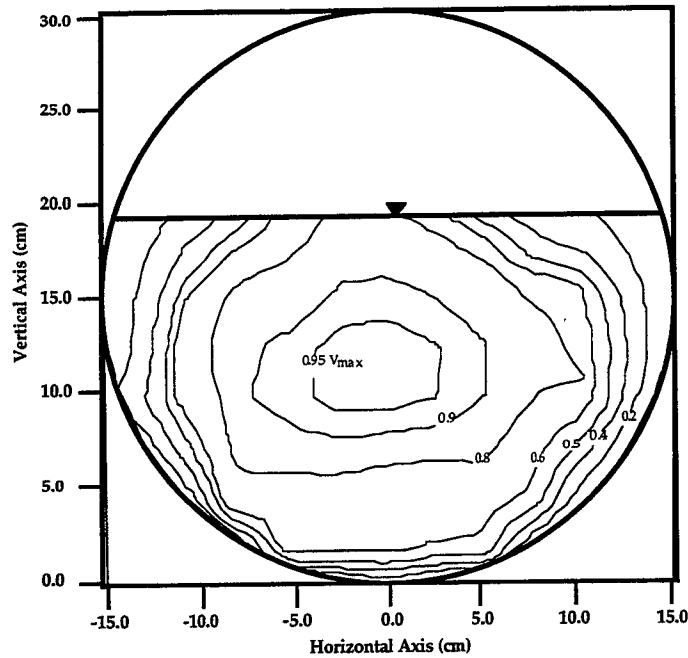


Figure B4.14. Velocity contour plot for Culvert #1 at $Q = 0.0527$ cms, 3% slope, $0.62D_0$, $L/D = 14$, no downstream control, $V_{max} = 159.6$ cm/sec.

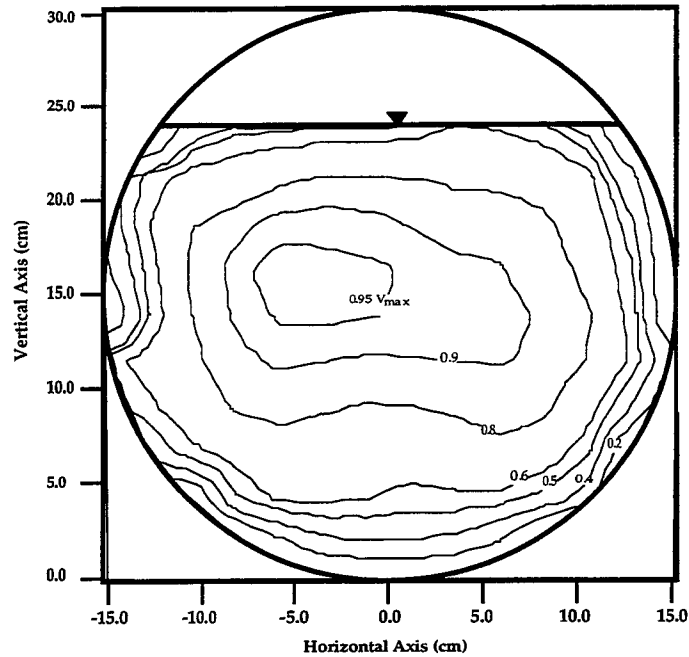


Figure B4.15. Velocity contour plot for Culvert #1 at $Q = 0.0539$ cms, 1% slope, $0.79D_o$, $L/D = 14$, no downstream control, $V_{max} = 124.4$ cm/sec. .

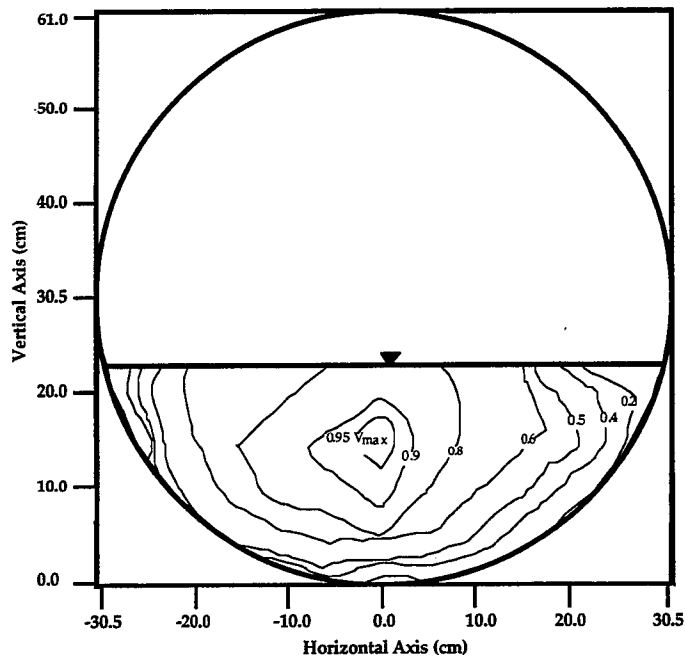


Figure B4.16. Velocity contour plot for Culvert #2 at $Q = 0.0153$ cms, 1/2% slope, $0.38D_o$, $L/D = 14$, downstream control, $V_{max} = 26.4$ cm/sec.

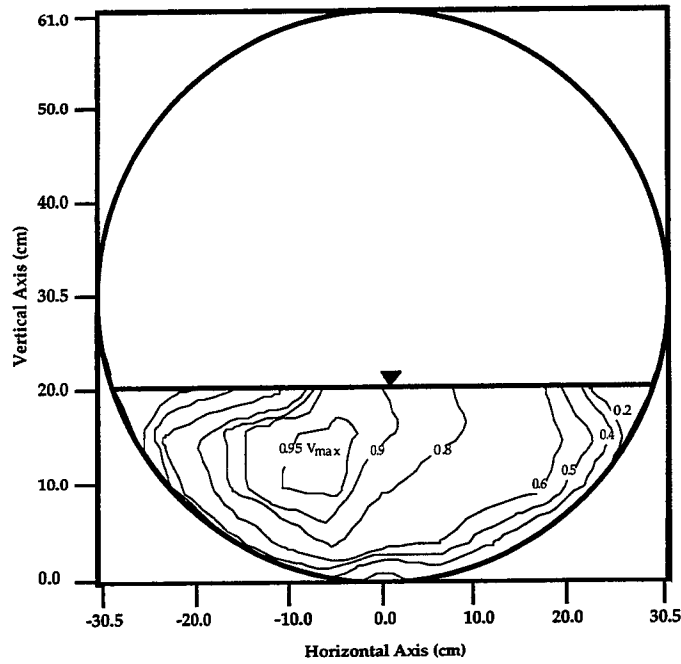


Figure B4.17. Velocity contour plot for Culvert #2 at $Q = 0.0153$ cms, $1/2\%$ slope, $0.33D_0$, $L/D = 8$, downstream control, $V_{max} = 29.2$ cm/sec.

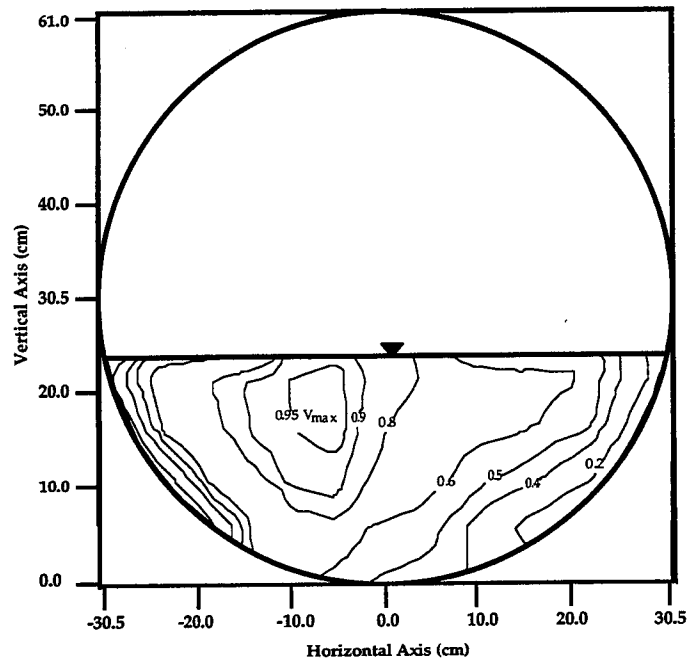


Figure B4.18. Velocity contour plot for Culvert #2 at $Q = 0.0153$ cms, 1% slope, $0.39D_0$, $L/D = 14$, downstream control, $V_{max} = 25.2$ cm/sec.

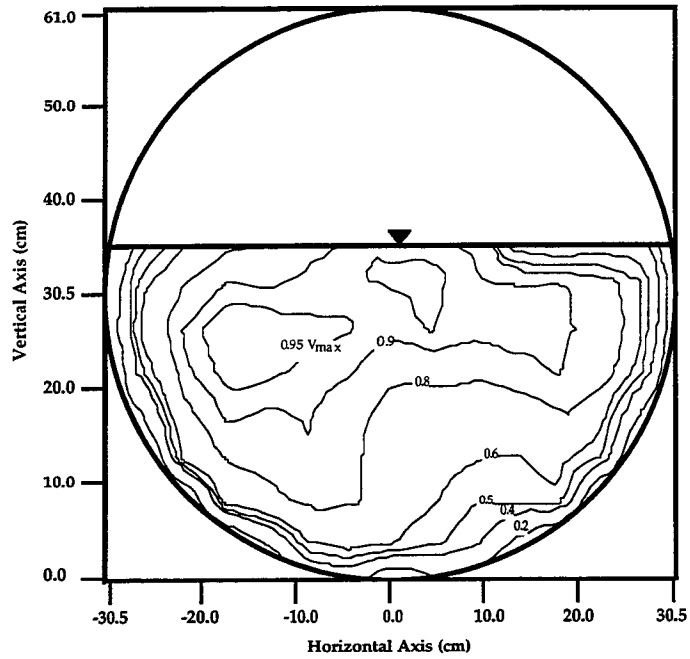


Figure B4.19. Velocity contour plot for Culvert #2 at $Q = 0.0283$ cms, $1/2\%$ slope, $0.58D_o$, $L/D = 14$, downstream control, $V_{max} = 22.8$ cm/sec.

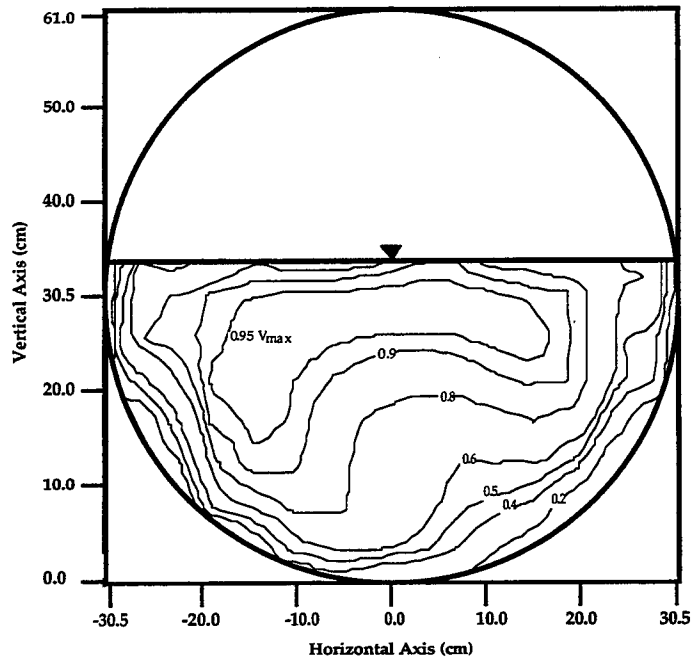


Figure B4.20. Velocity contour plot for Culvert #2 at $Q = 0.0283$ cms, $1/2\%$ slope, $0.56D_o$, $L/D = 8$, downstream control, $V_{max} = 26.6$ cm/sec.

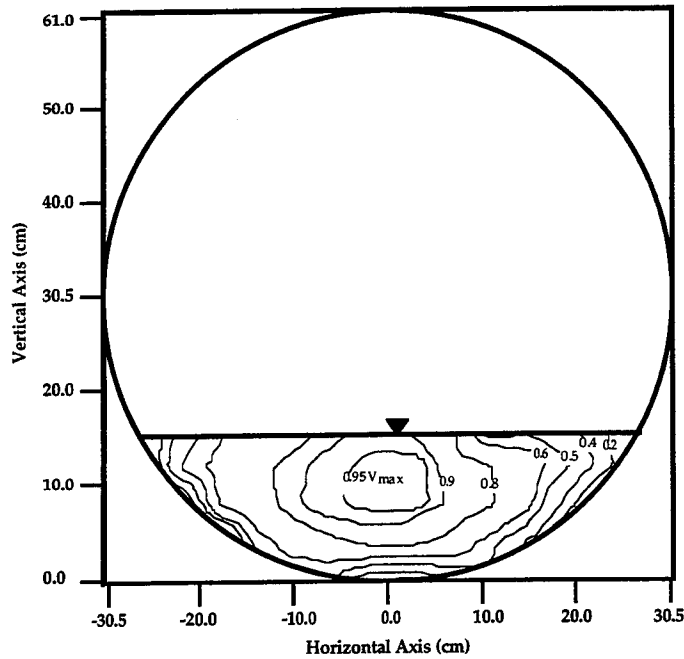


Figure B4.21. Velocity contour plot for Culvert #2 at $Q = 0.0396$ cms, $1/2\%$ slope, $0.25D_0$, $L/D = 14$, no downstream control, $V_{max} = 90.1$ cm/sec.

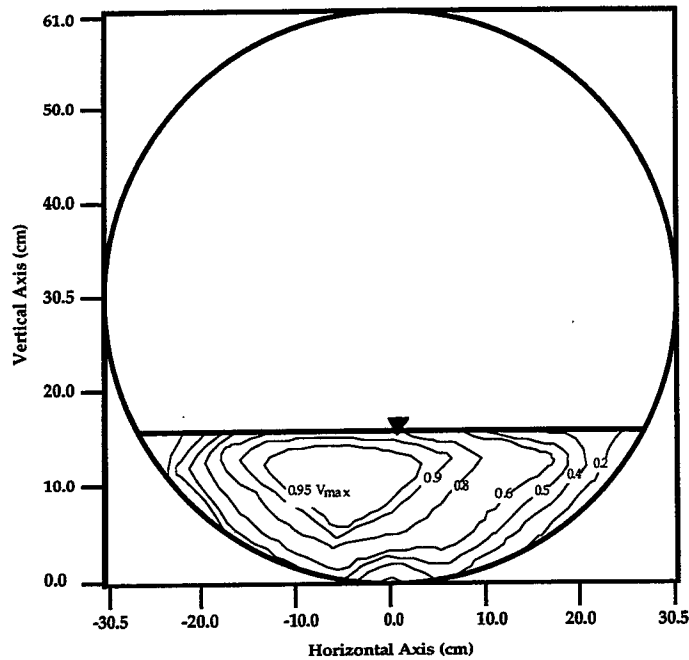


Figure B4.22. Velocity contour plot for Culvert #2 at $Q = 0.0396$ cms, $1/2\%$ slope, $0.25D_0$, $L/D = 8$, downstream control, $V_{max} = 84.9$ cm/sec.

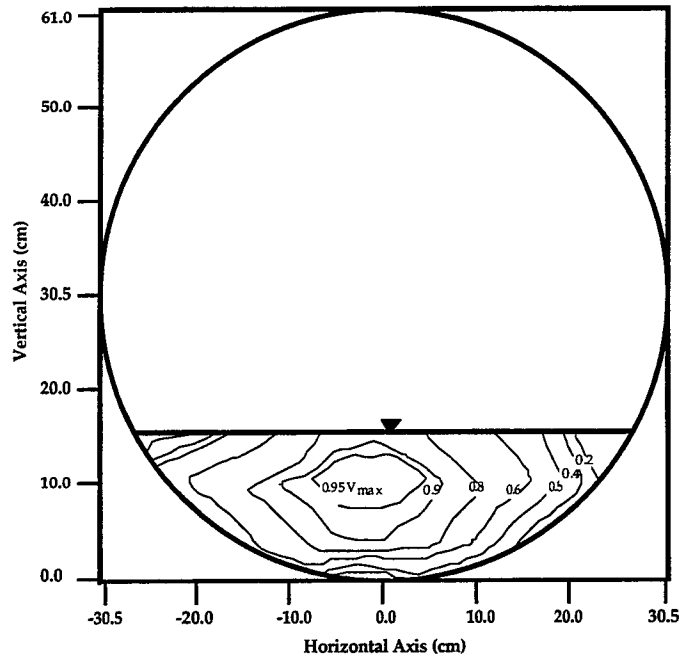


Figure B4.23. Velocity contour plot for Culvert #2 at $Q = 0.0515$ cms, 1% slope, $0.25D_0$, $L/D = 14$, no downstream control, $V_{\max} = 108.0$ cm/sec.

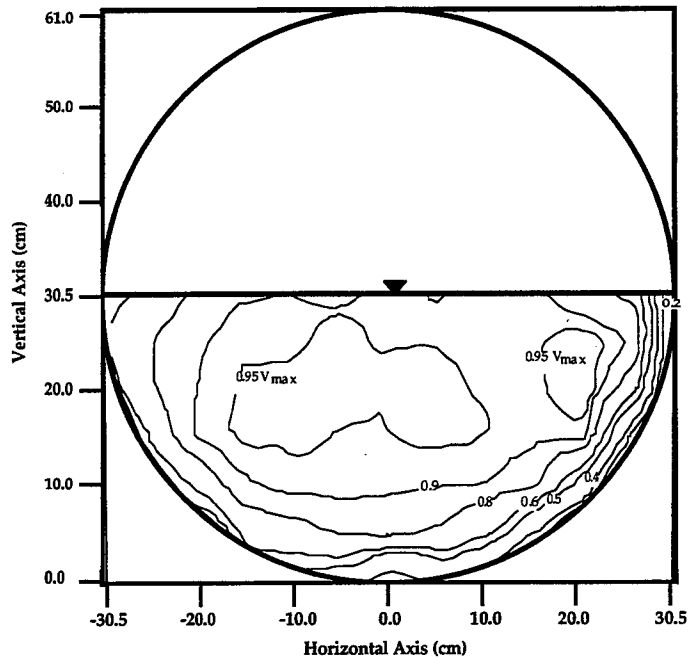


Figure B4.24. Velocity contour plot for Culvert #2 at $Q = 0.0566$ cms, 1/2% slope, $0.50D_0$, $L/D = 1$, downstream control, $V_{\max} = 51.3$ cm/sec.

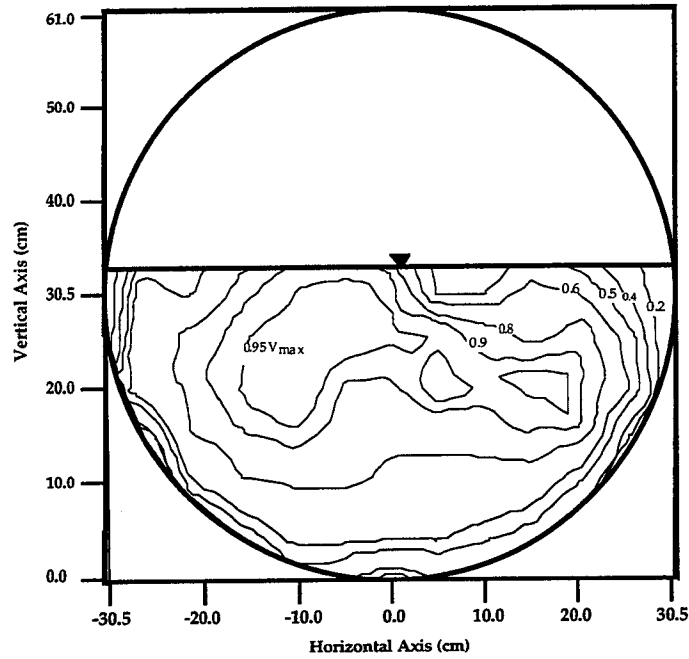


Figure B4.25. Velocity contour plot for Culvert #2 at $Q = 0.0566$ cms, $1/2\%$ slope, $0.55D_o$, $L/D = 12$, downstream control, $V_{max} = 46.3$ cm/sec.

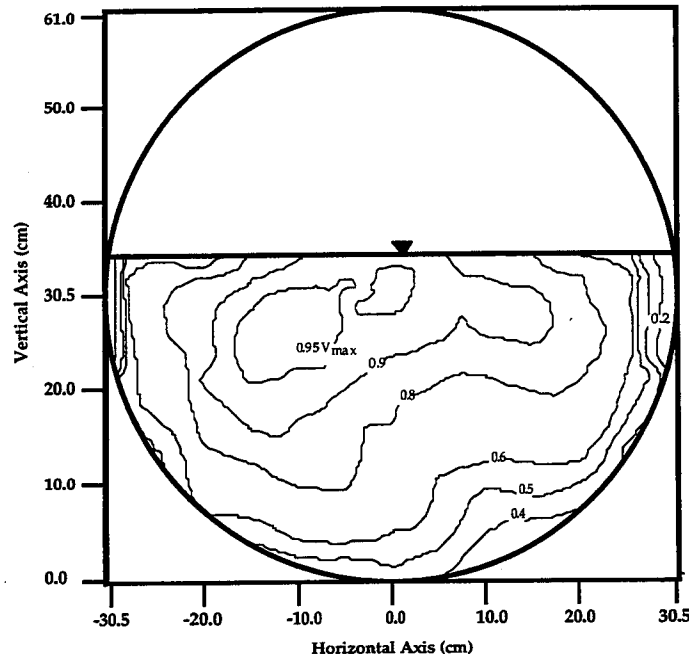


Figure B4.26. Velocity contour plot for Culvert #2 at $Q = 0.0566$ cms, $1/2\%$ slope, $0.57D_o$, $L/D = 14$, downstream control, $V_{max} = 41.8$ cm/sec.

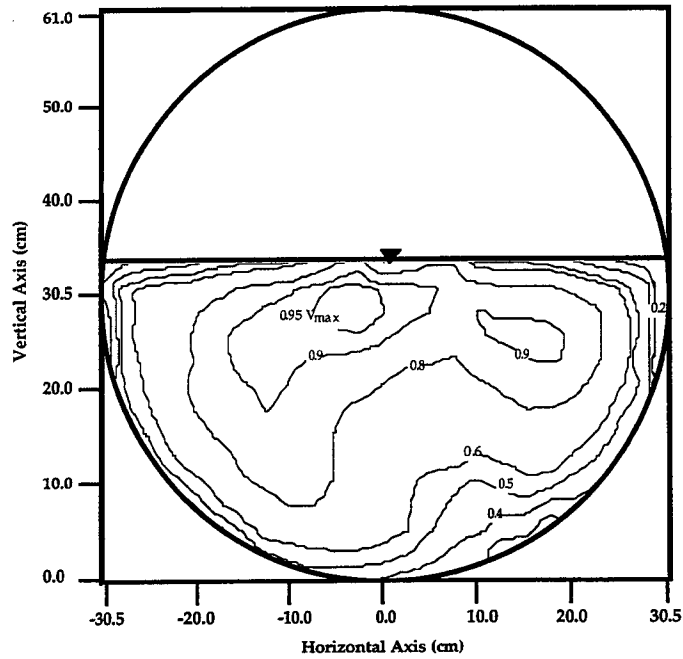


Figure B4.27. Velocity contour plot for Culvert #2 at $Q = 0.0566$ cms, 1/2% slope, $0.56D_0$, $L/D = 8$, downstream control, $V_{max} = 44.9$ cm/sec.

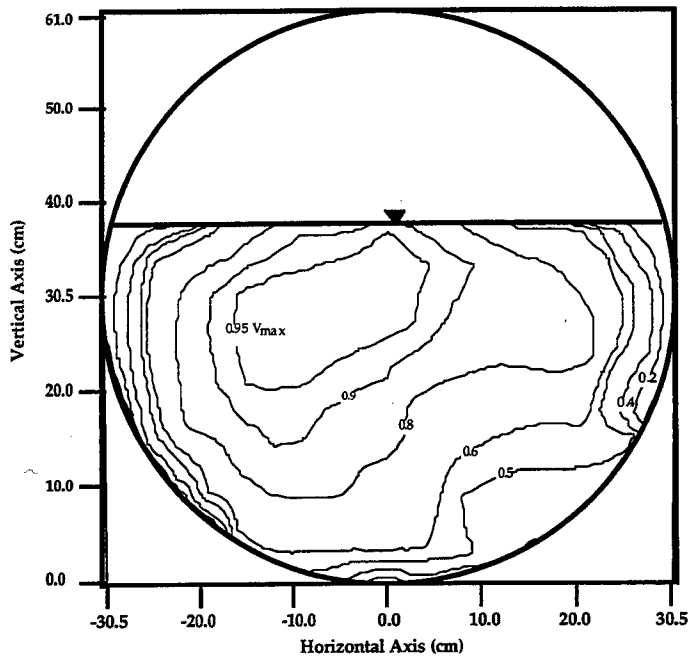


Figure B4.28. Velocity contour plot for Culvert #2 at $Q = 0.0566$ cms, 1% slope, $0.62D_0$, $L/D = 14$, downstream control, $V_{max} = 37.6$ cm/sec.

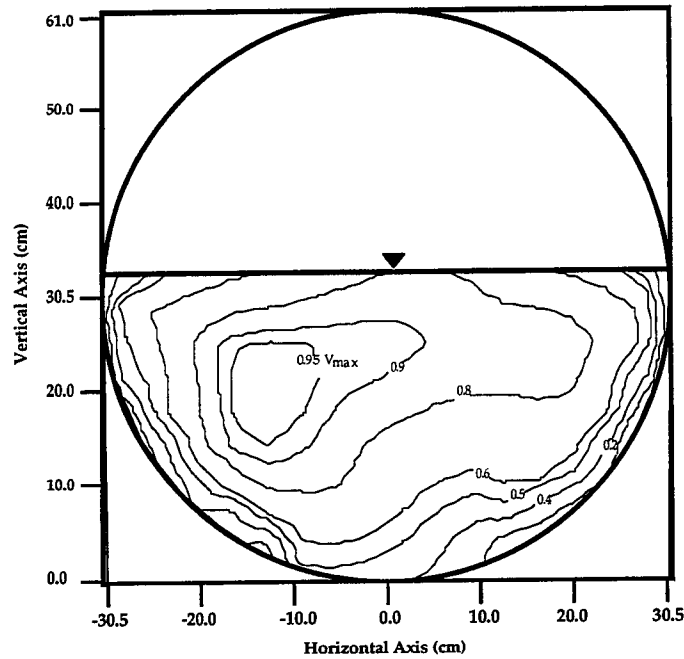


Figure B4.29. Velocity contour plot for Culvert #2 at $Q = 0.0850$ cms, $1/2\%$ slope, $0.54D_o$, $L/D = 12$, downstream control, $V_{max} = 69.1$ cm/sec.

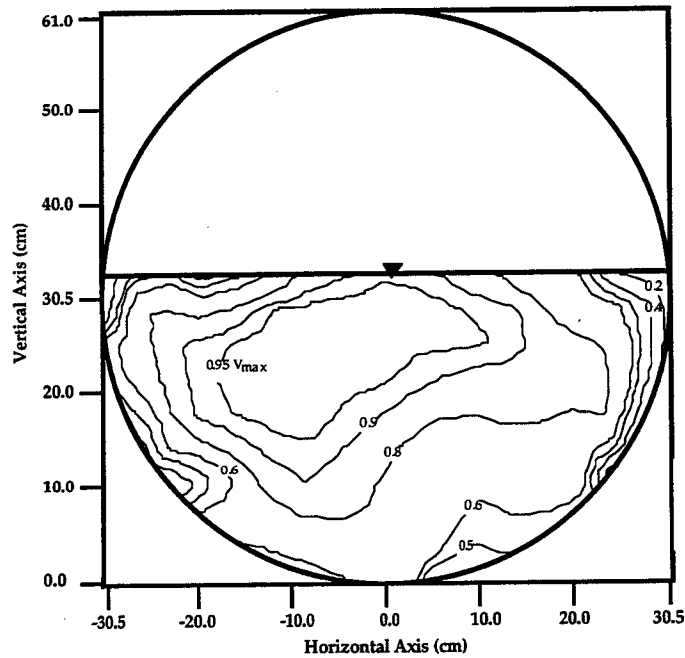


Figure B4.30. Velocity contour plot for Culvert #2 at $Q = 0.0850$ cms, $1/2\%$ slope, $0.54D_o$, $L/D = 14$, downstream control, $V_{max} = 64.2$ cm/sec.

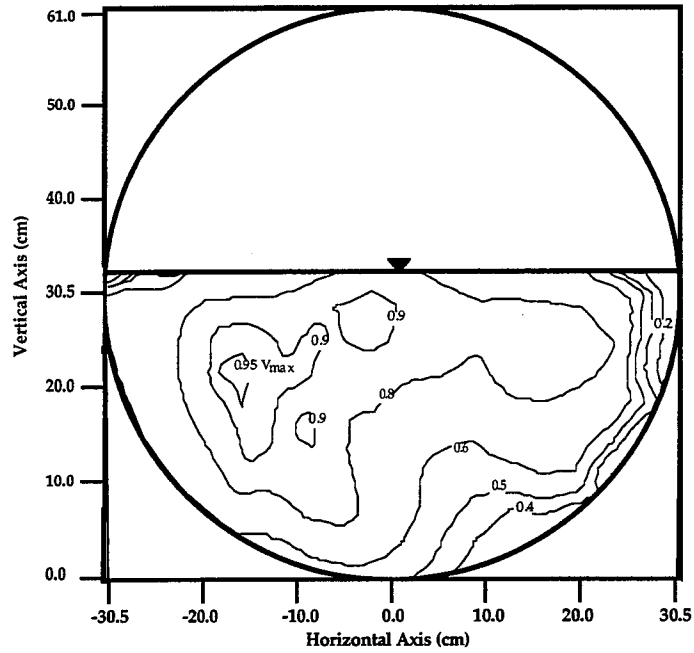


Figure B4.31. Velocity contour plot for Culvert #2 at $Q = 0.0850$ cms, $1/2\%$ slope, $0.54D_0$, $L/D = 8$, downstream control, $V_{max} = 69.8$ cm/sec.

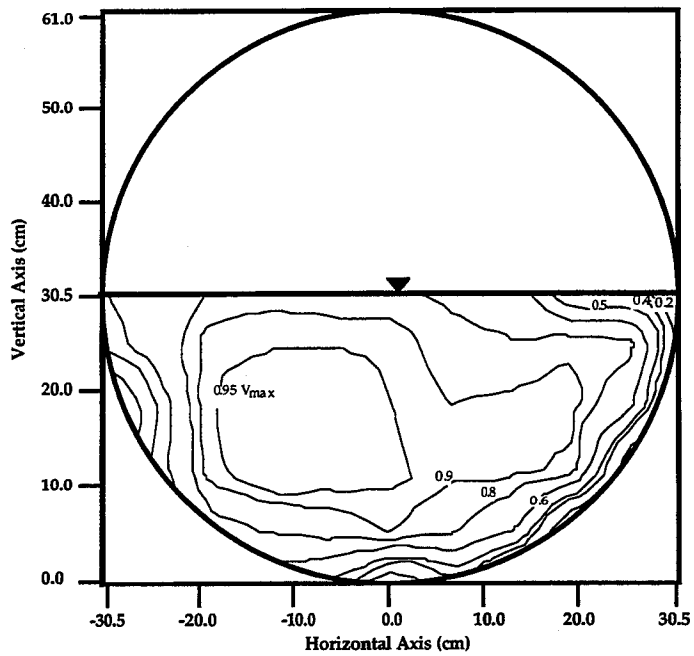


Figure B4.32. Velocity contour plot for Culvert #2 at $Q = 0.0850$ cms, $1/2\%$ slope, $0.50D_0$, at entrance, downstream control, $V_{max} = 71.5$ cm/sec.

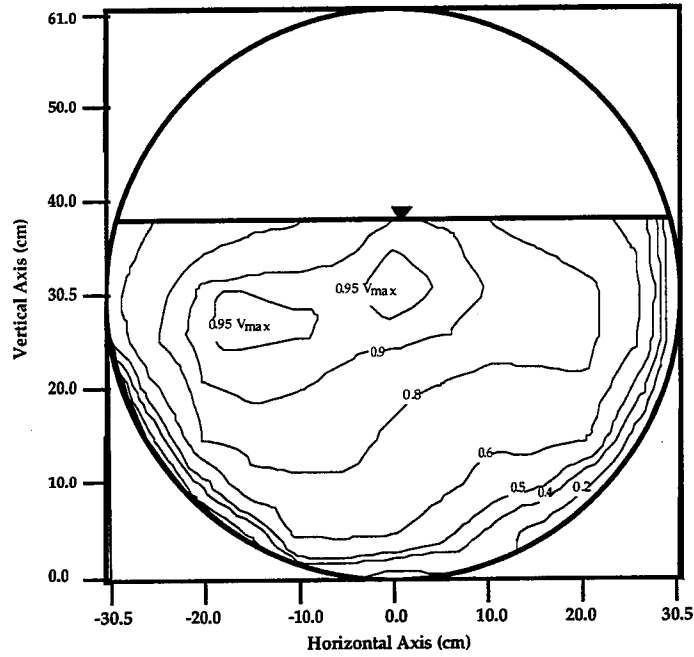


Figure B4.33. Velocity contour plot for Culvert #2 at $Q = 0.0850$ cms, 1% slope, $0.63D_0$, $L/D = 14$, downstream control, $V_{max} = 58.2$ cm/sec.

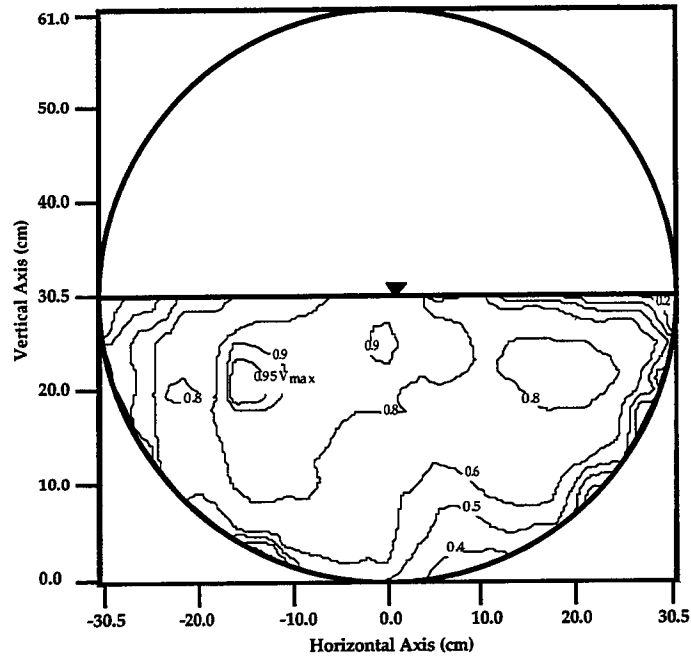


Figure B4.34. Velocity contour plot for Culvert #2 at $Q = 0.1274$ cms, 1/2% slope, $0.50D_0$, $L/D = 8$, no downstream control, $V_{max} = 118.4$ cm/sec.

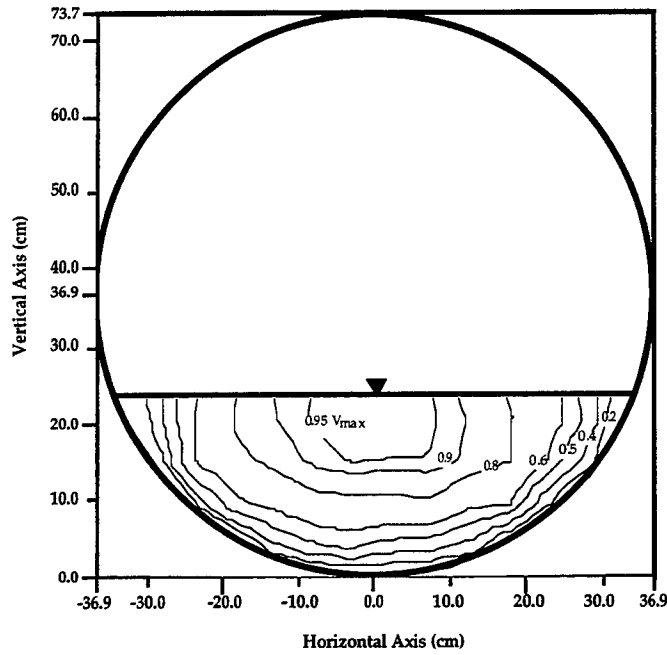


Figure B4.35. Velocity contour plot for Culvert #3 at $Q = 0.0153$ cms, 1/2% slope, $0.31D_0$, $L/D = 8$, downstream control, $V_{max} = 22.2$ cm/sec.

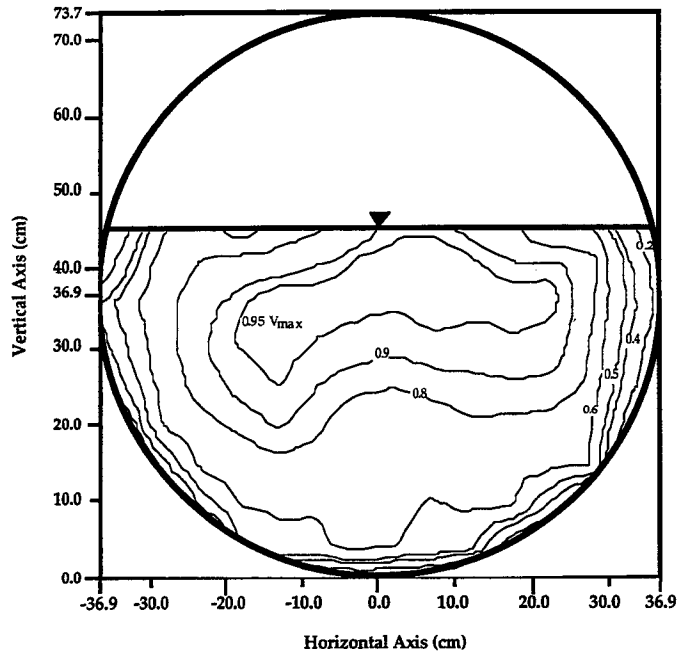


Figure B4.36. Velocity contour plot for Culvert #3 at $Q = 0.0153$ cms, 1% slope, $0.62D_0$, $L/D = 8$, downstream control, $V_{max} = 9.9$ cm/sec.

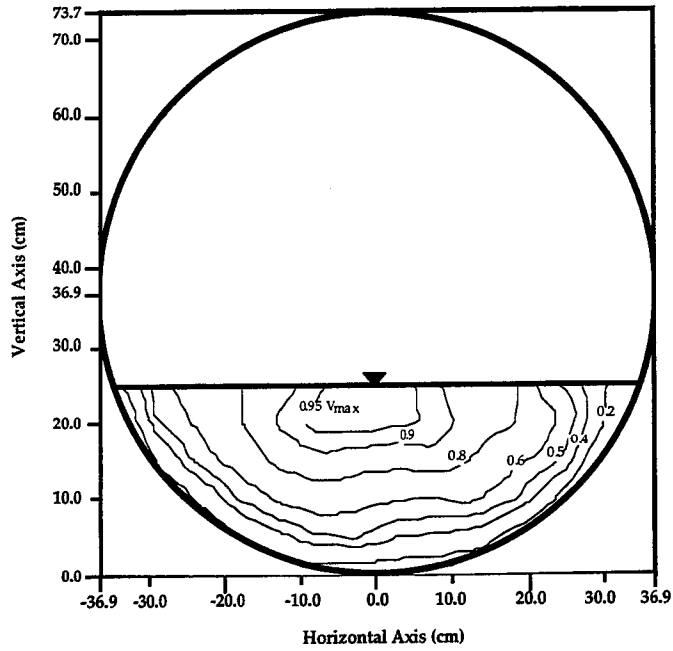


Figure B4.37. Velocity contour plot for Culvert #3 at $Q = 0.0153$ cms, $1/2\%$ slope, $0.33D_0$, $L/D = 8$, downstream control, $V_{max} = 20.5$ cm/sec.

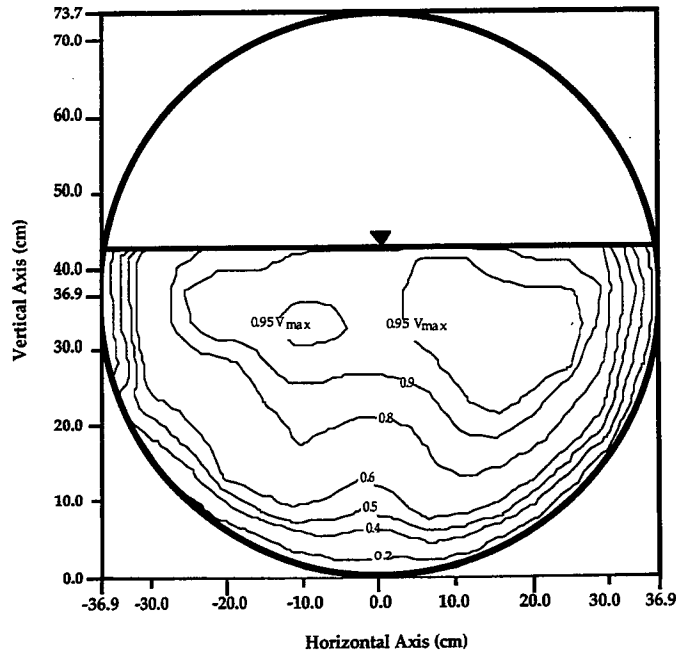


Figure B4.38. Velocity contour plot for Culvert #3 at $Q = 0.0566$ cms, $1/2\%$ slope, $0.57D_0$, $L/D = 8$, downstream control, $V_{max} = 31.2$ cm/sec.

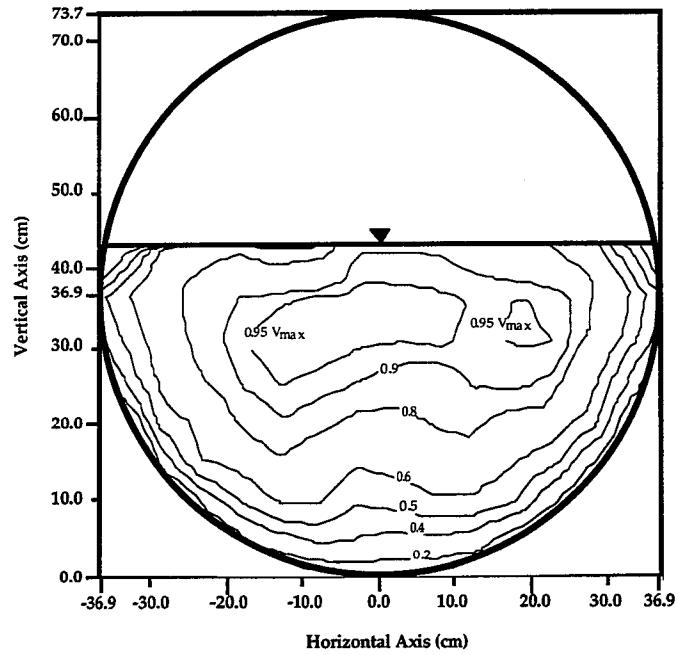


Figure B4.39. Velocity contour plot for Culvert #3 at $Q = 0.0566$ cms, 1% slope, $0.58D_o$, $L/D = 8$, downstream control, $V_{max} = 33.9$ cm/sec.

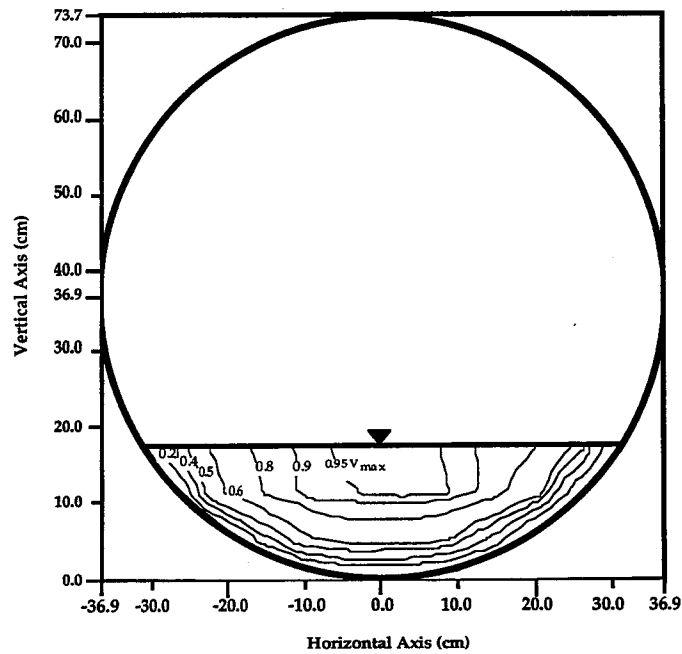


Figure B4.40. Velocity contour plot for Culvert #3 at $Q = 0.0575$ cms, 1/2% slope, $0.24D_o$, $L/D = 8$, no downstream control, $V_{max} = 120.8$ cm/sec.

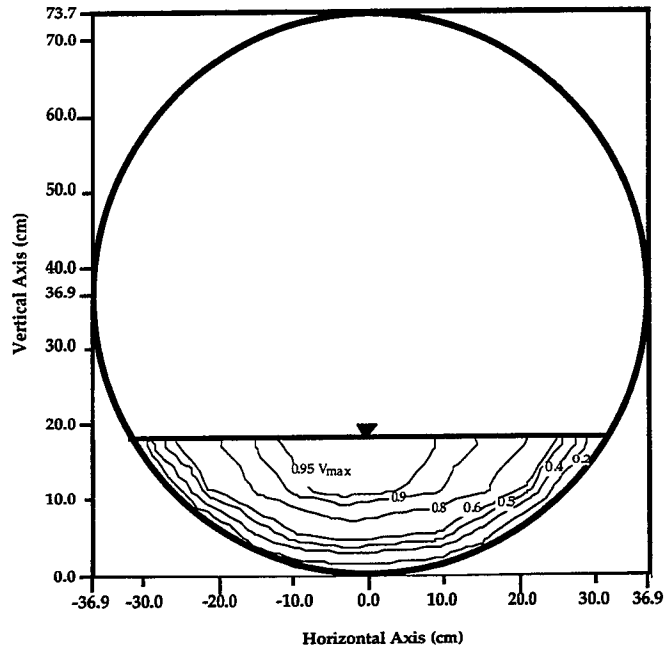


Figure B4.41. Velocity contour plot for Culvert #3 at $Q = 0.0664$ cms, 1% slope, $0.25D_o$, $L/D = 8$, no downstream control, $V_{max} = 135.1$ cm/sec.

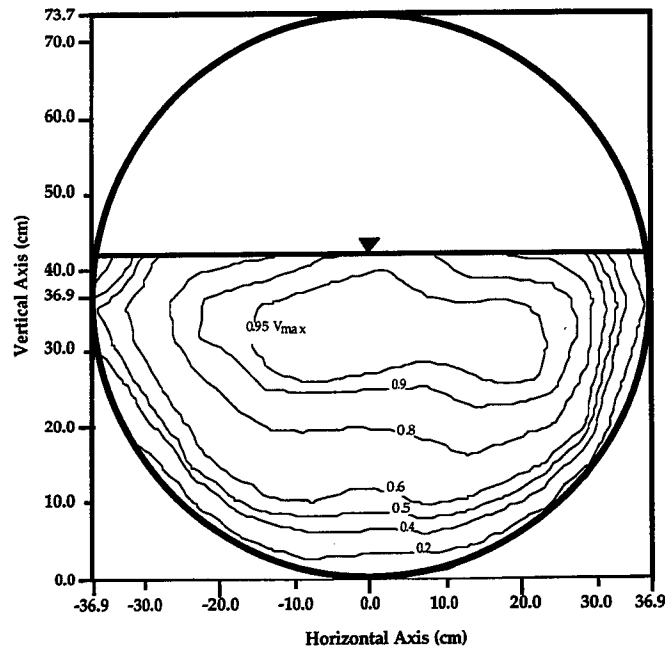


Figure B4.42. Velocity contour plot for Culvert #3 at $Q = 0.0850$ cms, 1/2% slope, $0.57D_o$, $L/D = 8$, downstream control, $V_{max} = 46.6$ cm/sec.

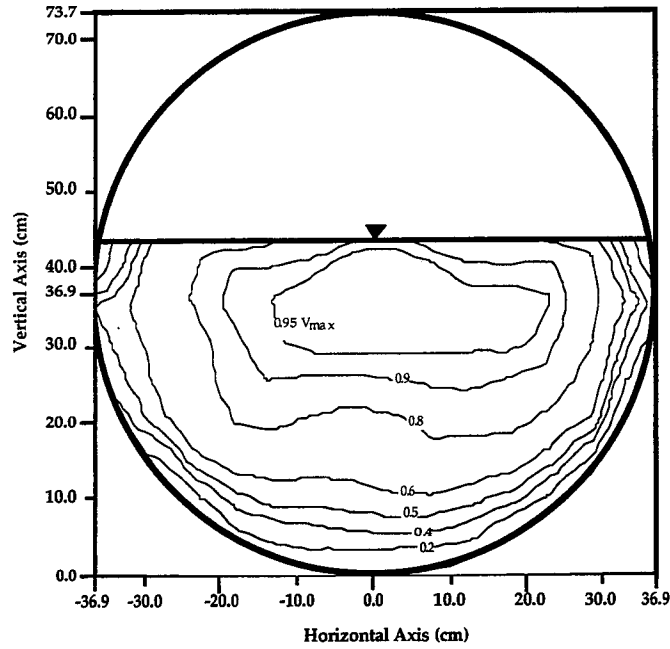


Figure B4.43. Velocity contour plot for Culvert #3 at $Q = 0.0850$ cms, 1% slope, $0.59D_o$, $L/D = 8$, downstream control, $V_{max} = 44.2$ cm/sec.

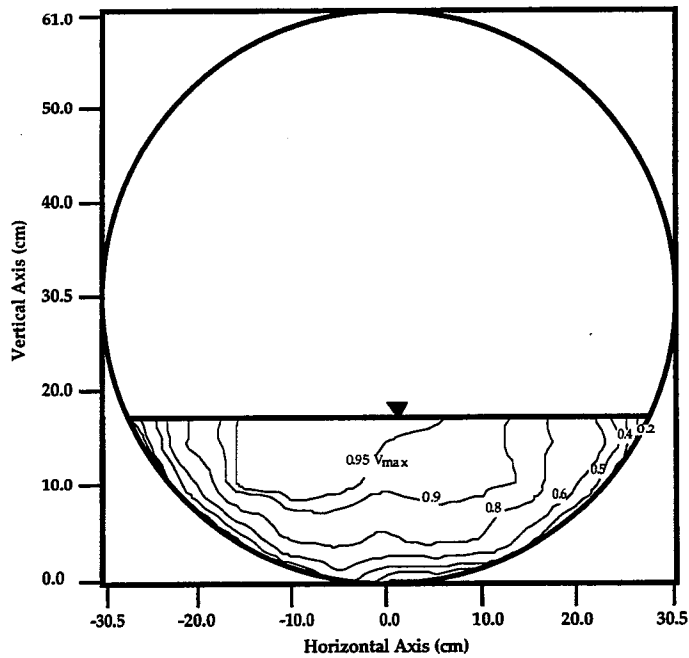


Figure B4.44. Velocity contour plot for Culvert #4 at $Q = 0.0153$ cms, 1/2% slope, $0.28D_o$, $L/D = 7$, downstream control, $V_{max} = 27.4$ cm/sec.

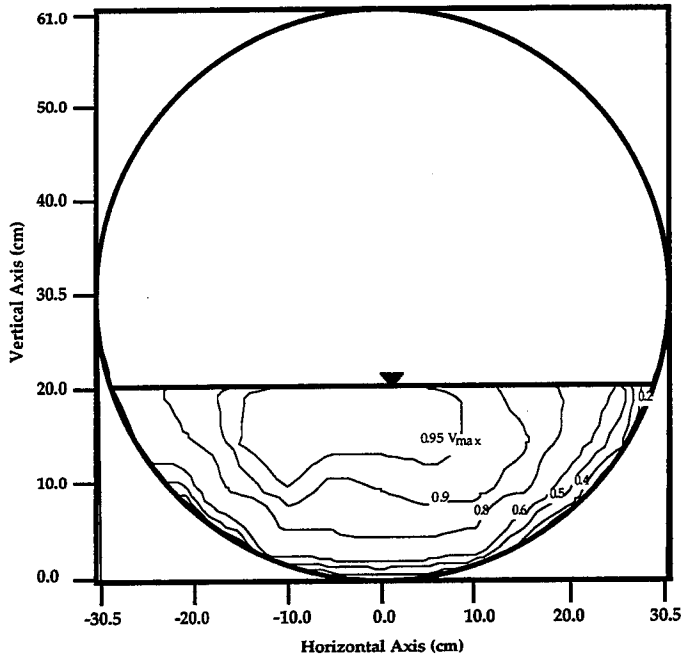


Figure B4.45. Velocity contour plot for Culvert #4 at $Q = 0.0153$ cms, $1/2\%$ slope, $0.33D_0$, $L/D = 7$, downstream control, $V_{\max} = 23.1$ cm/sec.

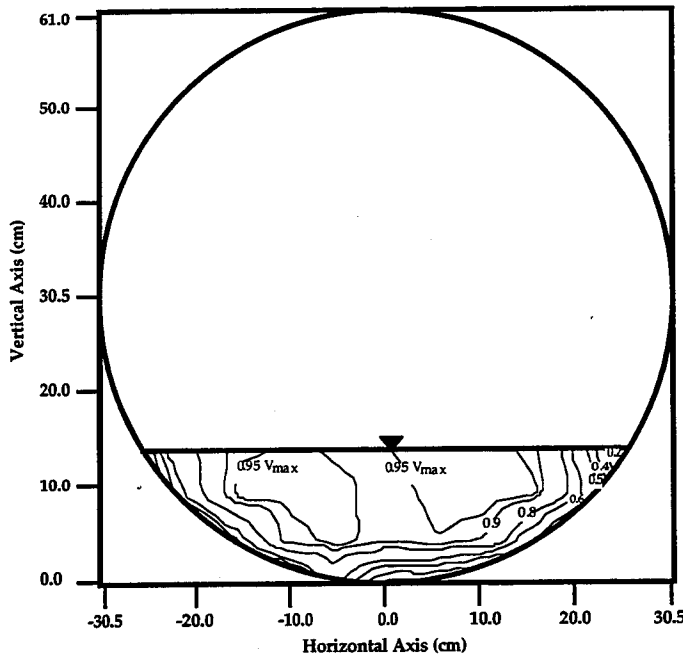


Figure B4.46. Velocity contour plot for Culvert #4 at $Q = 0.0500$ cms, $1/2\%$ slope, $0.23D_0$, $L/D = 7$, no downstream control, $V_{\max} = 127.2$ cm/sec.

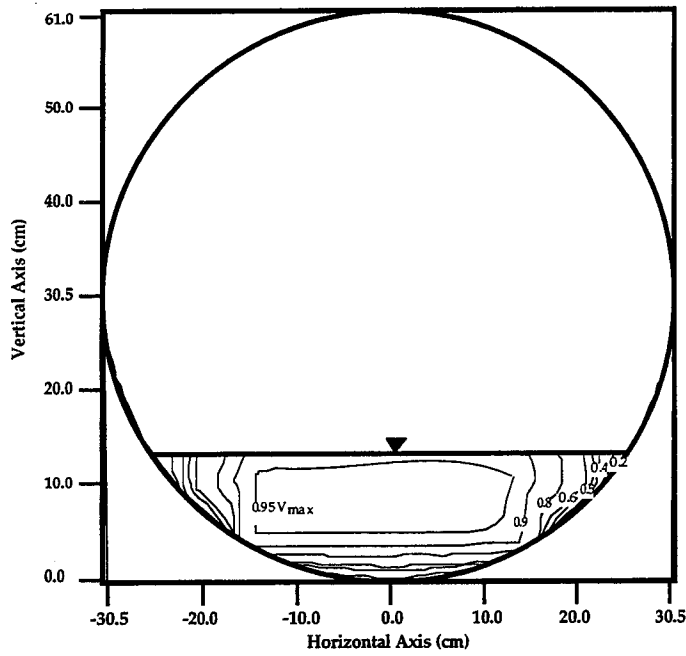


Figure B4.47. Velocity contour plot for Culvert #4 at $Q = 0.0563$ cms, 1% slope, $0.22D_o$, $L/D = 7$, no downstream control, $V_{max} = 140.2$ cm/sec.

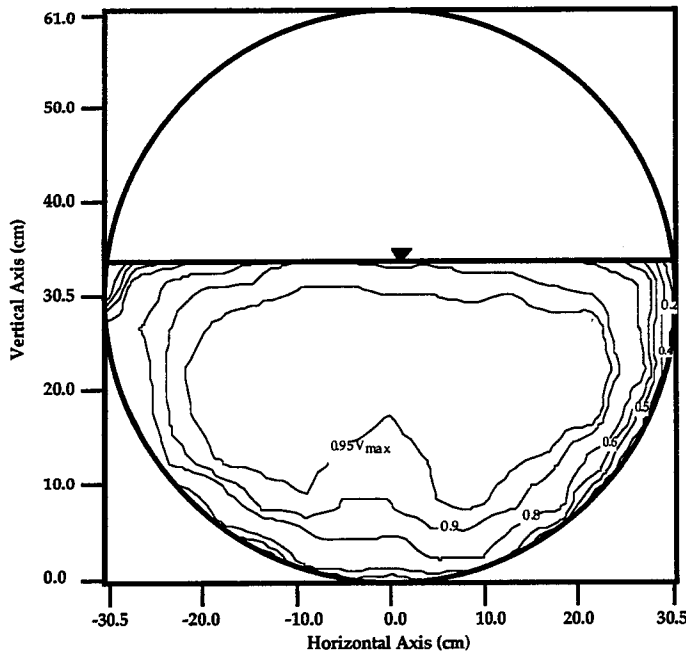


Figure B4.48. Velocity contour plot for Culvert #4 at $Q = 0.0566$ cms, 1/2% slope, $0.57D_o$, $L/D = 7$, downstream control, $V_{max} = 38.9$ cm/sec.

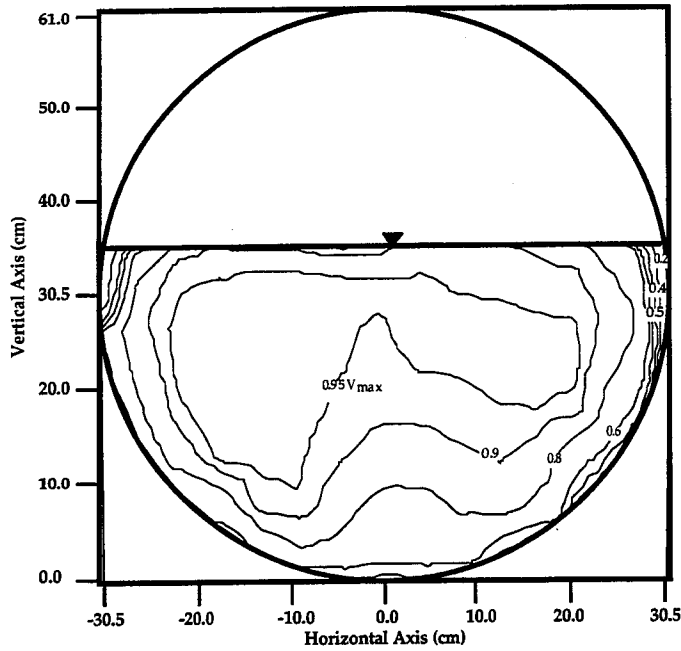


Figure B4.49. Velocity contour plot for Culvert #4 at $Q = 0.0566$ cms, 1% slope, $0.59D_0$, $L/D = 7$, downstream control, $V_{max} = 36.8$ cm/sec.

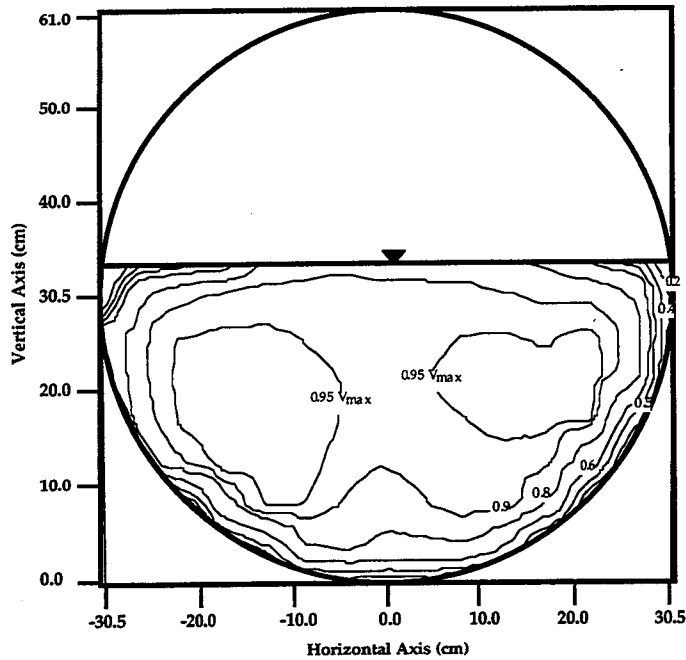


Figure B4.50. Velocity contour plot for Culvert #4 at $Q = 0.0850$ cms, 1/2% slope, $0.56D_0$, $L/D = 7$, downstream control, $V_{max} = 59.7$ cm/sec.

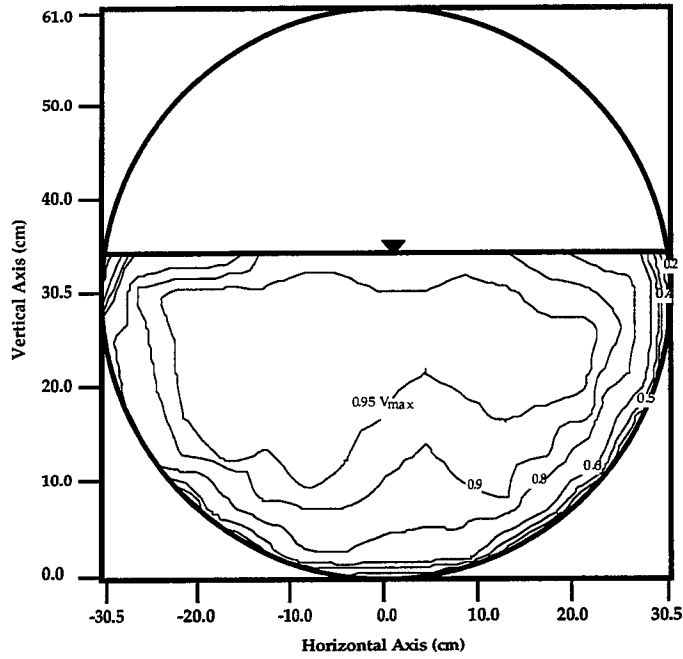


Figure B4.51. Velocity contour plot for Culvert #4 at $Q = 0.0850 \text{ cms}$, 1% slope, $0.58D_0$, $L/D = 7$, downstream control, $V_{\text{max}} = 54.2 \text{ cm/sec}$.

Appendix C

Plots of One-Dimensional Centerline Velocity Contour Plots for:

**Experimental Data
Chiu Equation
Mountjoy Equation**

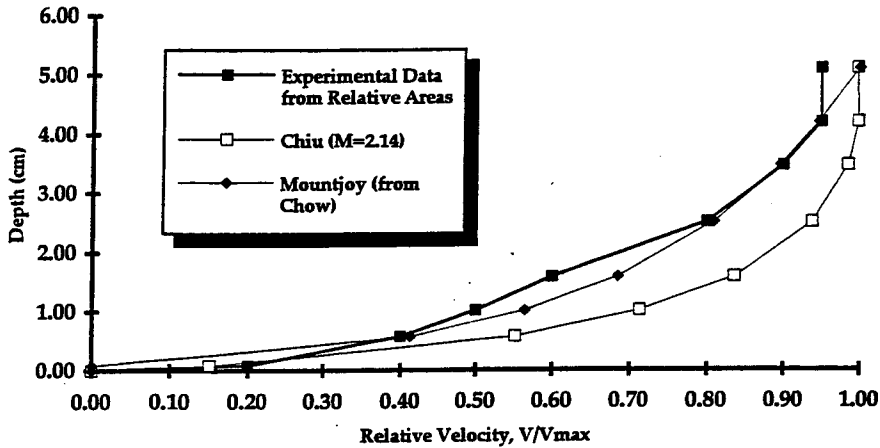


Figure C4.1. One-dimensional centerline velocity plots for Culvert #1 at $Q = 0.0052 \text{ m}^3/\text{s}$, 5% slope, $0.17D_0$, $L/D = 14$, no downstream control, $V_{\text{max}} = 101.9 \text{ cm/s}$.

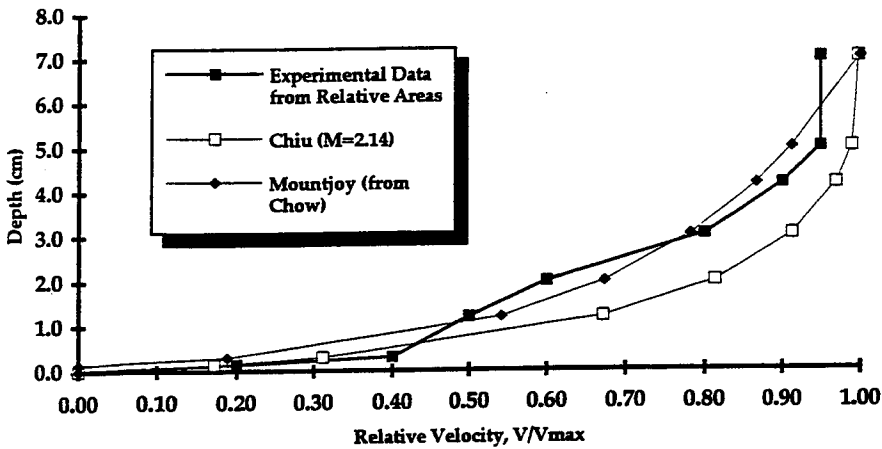


Figure C4.2. One-dimensional centerline velocity plots for Culvert #1 at $Q = 0.0064 \text{ m}^3/\text{s}$, 3% slope, $0.23D_0$, $L/D = 14$, no downstream control, $V_{\text{max}} = 82.0 \text{ cm/s}$.

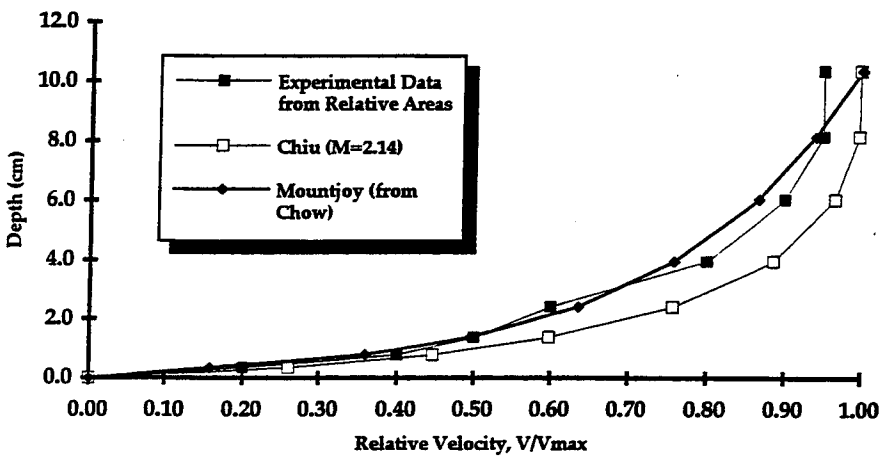


Figure C4.3. One-dimensional centerline velocity plots for Culvert #1 at $Q = 0.0082 \text{ m}^3/\text{s}$, 1% slope, $0.34D_0$, $L/D = 14$, no downstream control, $V_{\text{max}} = 61.2 \text{ cm/s}$.

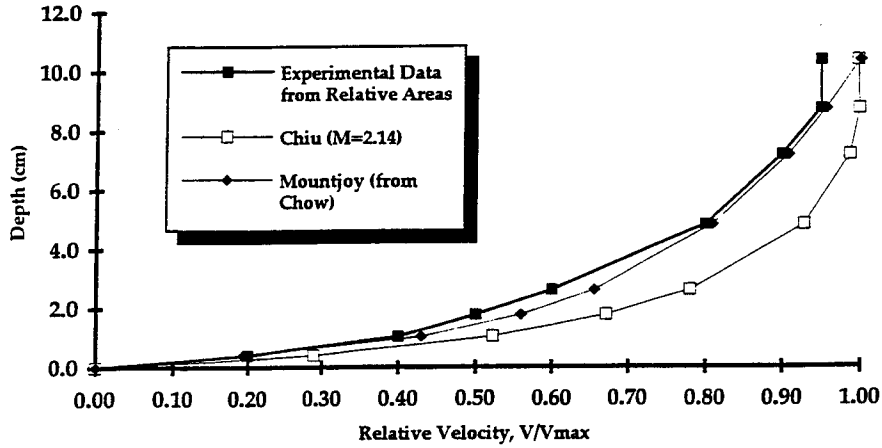


Figure C4.4. One-dimensional centerline velocity plots for Culvert #1 at $Q = 0.0094 \text{ m}^3/\text{s}$, $1/2\%$ slope, $0.34D_0$, $L/D = 14$, no downstream control, $V_{\text{max}} = 59.9 \text{ cm/s}$.

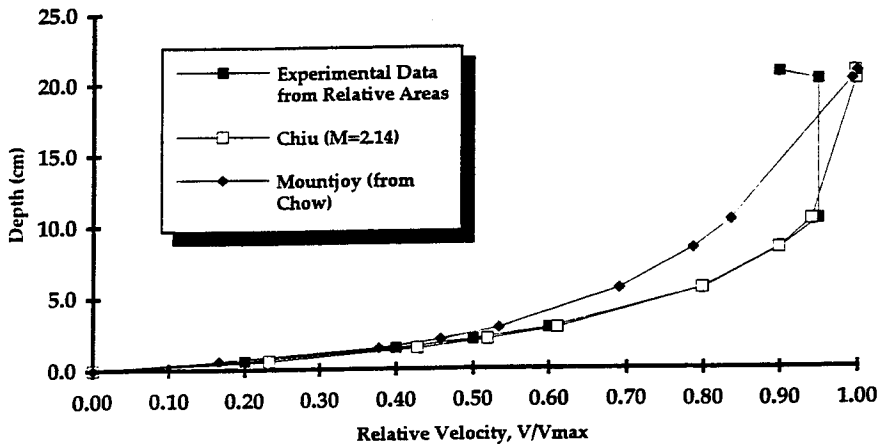


Figure C4.5. One-dimensional centerline velocity plots for Culvert #1 at $Q = 0.0124 \text{ m}^3/\text{s}$, $1/2\%$ slope, $0.68D_0$, $L/D = 14$, downstream control, $V_{\text{max}} = 34.5 \text{ cm/s}$.

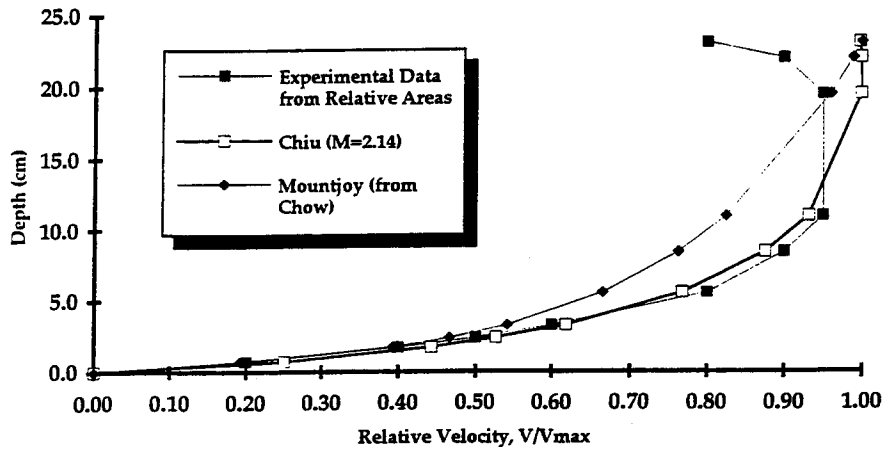


Figure C4.6. One-dimensional centerline velocity plots for Culvert #1 at $Q = 0.0124 \text{ m}^3/\text{s}$, 1% slope, $0.76D_0$, $L/D = 14$, downstream control, $V_{\text{max}} = 33.2 \text{ cm/s}$.

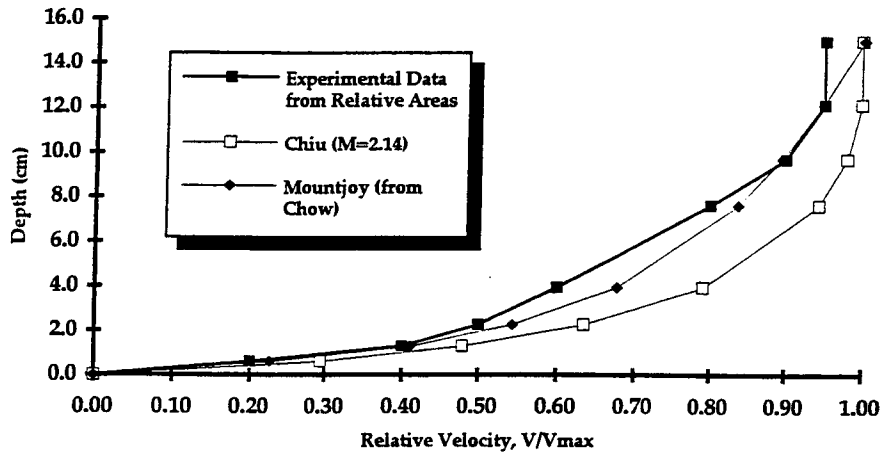


Figure C4.7. One-dimensional centerline velocity plots for Culvert #1 at $Q = 0.0142 \text{ m}^3/\text{s}$, 5% slope, $0.49D_0$, $L/D = 14$, downstream control, $V_{\text{max}} = 63.1 \text{ cm/s}$.

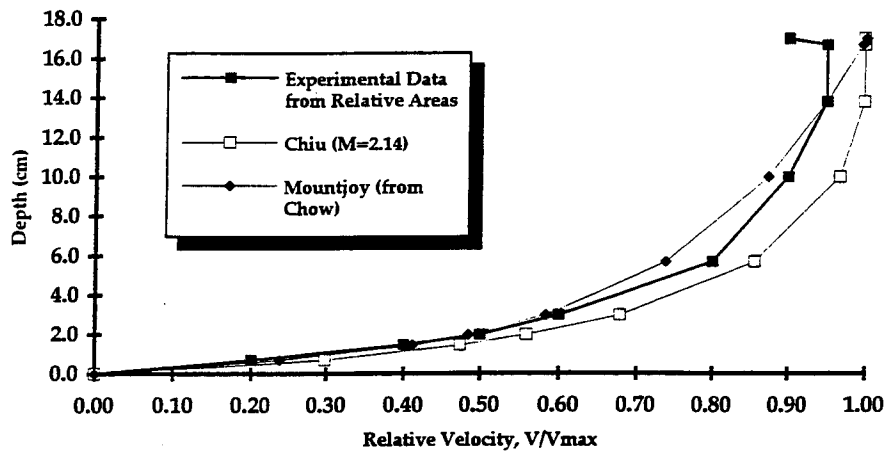


Figure C4.8. One-dimensional centerline velocity plots for Culvert #1 at $Q = 0.0213 \text{ m}^3/\text{s}$, 1/2% slope, $0.56D_0$, $L/D = 14$, downstream control, $V_{\text{max}} = 85.1 \text{ cm/s}$.

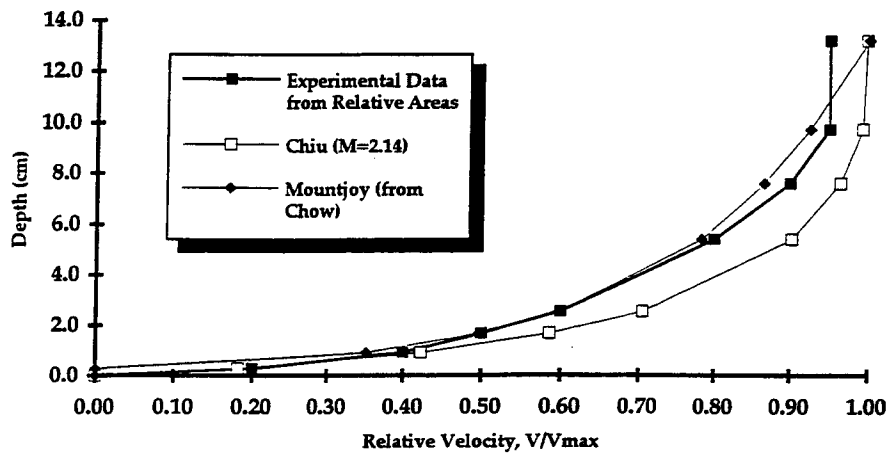


Figure C4.9. One-dimensional centerline velocity plots for Culvert #1 at $Q = 0.0278 \text{ m}^3/\text{s}$, 3% slope, $0.43D_0$, $L/D = 14$, no downstream control, $V_{\text{max}} = 125.9 \text{ cm/s}$.

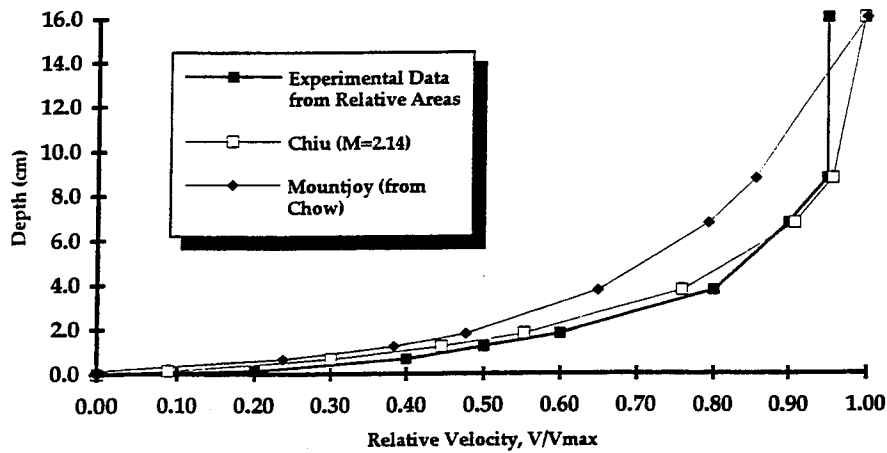


Figure C4.10. One-dimensional centerline velocity plots for Culvert #1 at $Q = 0.0284 \text{ m}^3/\text{s}$, 1% slope, $0.52D_0$, $L/D = 14$, no downstream control, $V_{\text{max}} = 92.7 \text{ cm/s}$.

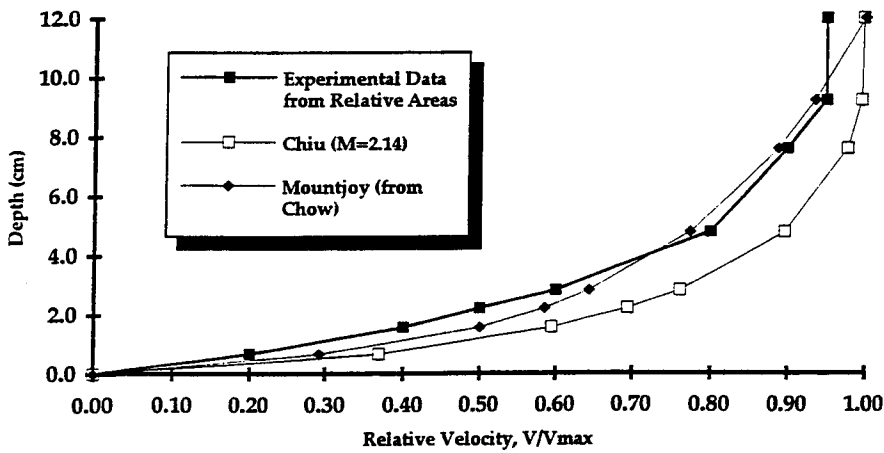


Figure C4.11. One-dimensional centerline velocity plots for Culvert #1 at $Q = 0.0290 \text{ m}^3/\text{s}$, 5% slope, $0.39D_0$, $L/D = 14$, no downstream control, $V_{\text{max}} = 169.3 \text{ cm/s}$.

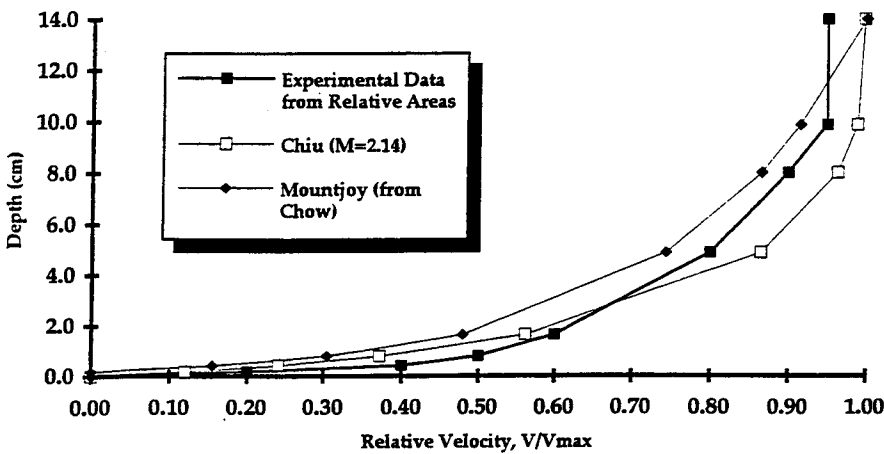


Figure C4.12. One-dimensional centerline velocity plots for Culvert #1 at $Q = 0.0438 \text{ m}^3/\text{s}$, 5% slope, $0.46D_0$, $L/D = 14$, no downstream control, $V_{\text{max}} = 178.0 \text{ cm/s}$.

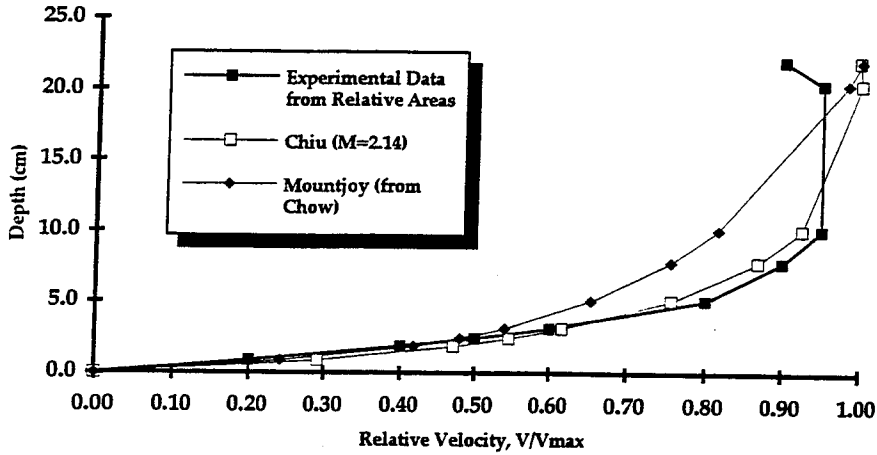


Figure C4.13. One-dimensional centerline velocity plots for Culvert #1 at $Q = 0.0456 \text{ m}^3/\text{s}$, 1/2% slope, $0.72D_0$, $L/D=14$, no downstream control, $V_{\text{max}} = 108.5 \text{ cm/s}$.

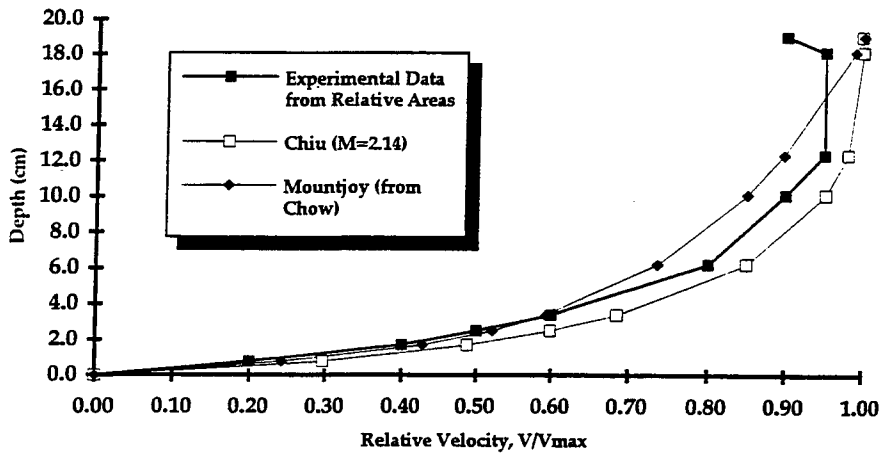


Figure C4.14. One-dimensional centerline velocity plots for Culvert #1 at $Q = 0.0527 \text{ m}^3/\text{s}$, 3% slope, $0.62D_0$, $L/D = 14$, no downstream control, $V_{\text{max}} = 159.6 \text{ cm/s}$.

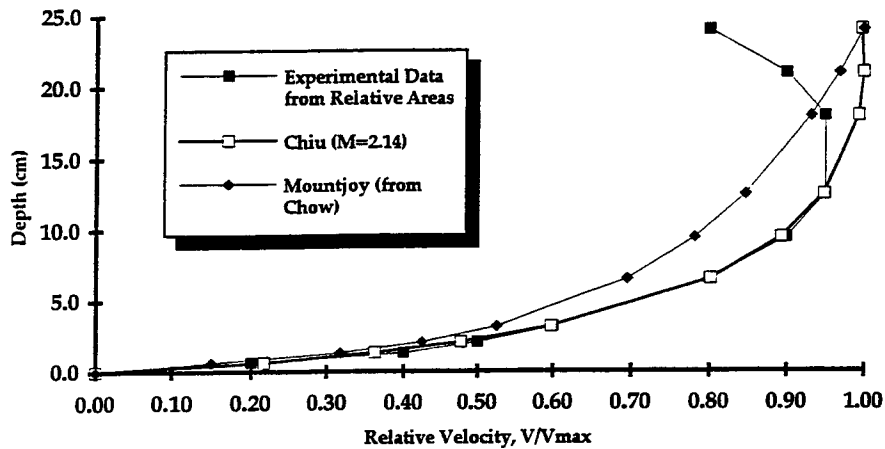


Figure C4.15. One-dimensional centerline velocity plots for Culvert #1 at $Q = 0.0539 \text{ m}^3/\text{s}$, 1% slope, $0.79D_0$, $L/D = 14$, no downstream control, $V_{\text{max}} = 124.4 \text{ cm/s}$.

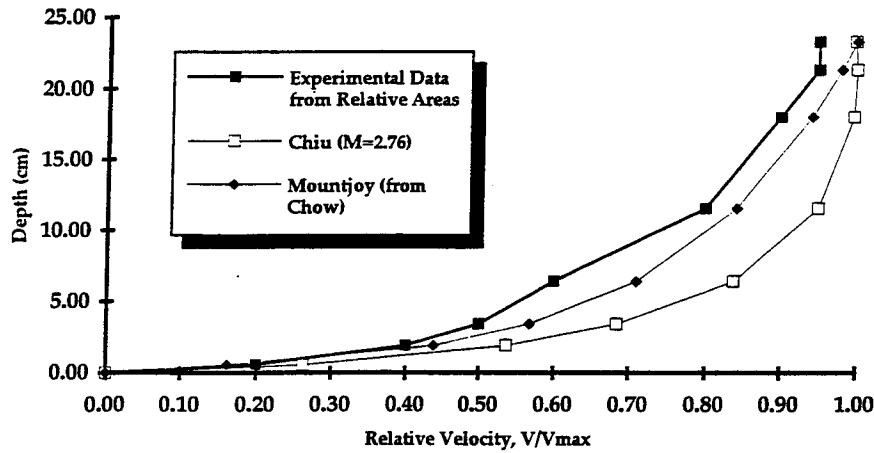


Figure C4.16. One-dimensional centerline velocity plots for Culvert #2 at $Q = 0.0153 \text{ m}^3/\text{s}$, 1/2% slope, $0.38D_0$, $L/D = 14$, downstream control, $V_{\text{max}} = 26.4 \text{ cm/s}$.

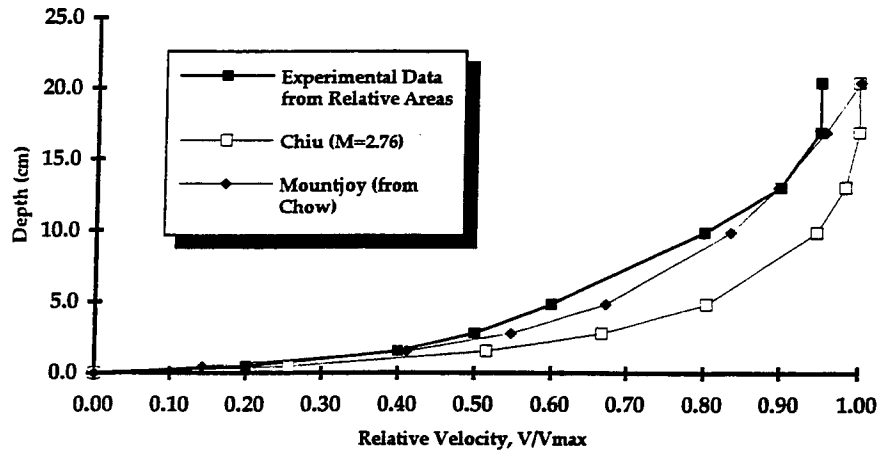


Figure C4.17. One-dimensional centerline velocity plots for Culvert #2 at $Q = 0.0153 \text{ m}^3/\text{s}$, 1/2% slope, $0.33D_0$, $L/D = 8$, downstream control, $V_{\text{max}} = 29.2 \text{ cm/s}$.

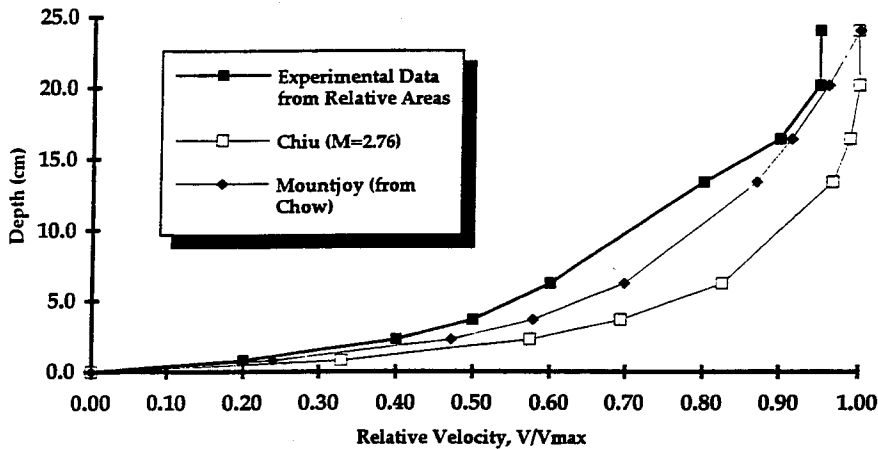


Figure C4.18. One-dimensional centerline velocity plots for Culvert #2 at $Q = 0.0153 \text{ m}^3/\text{s}$, 1% slope, $0.39D_0$, $L/D = 14$, downstream control, $V_{\text{max}} = 25.2 \text{ cm/s}$.

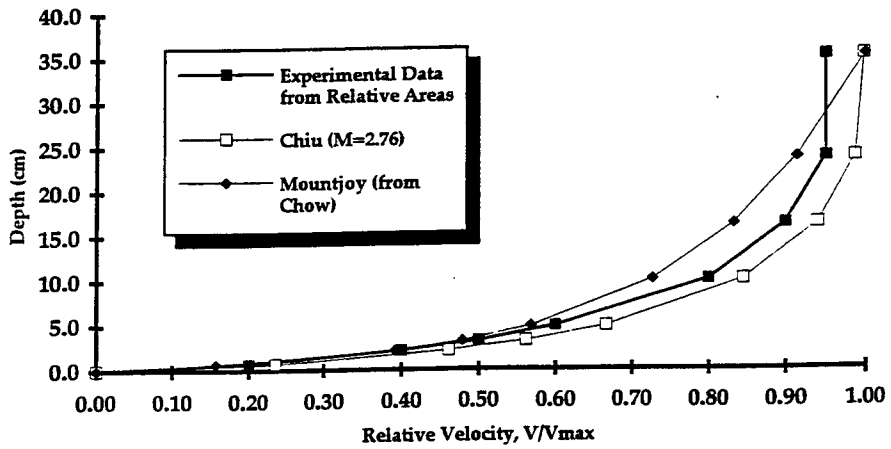


Figure C4.19. One-dimensional centerline velocity plots for Culvert #2 at $Q = 0.0283 \text{ m}^3/\text{s}$, $1/2\%$ slope, $0.58D_0$, $L/D = 14$, downstream control, $V_{\text{max}} = 22.8 \text{ cm/s}$.

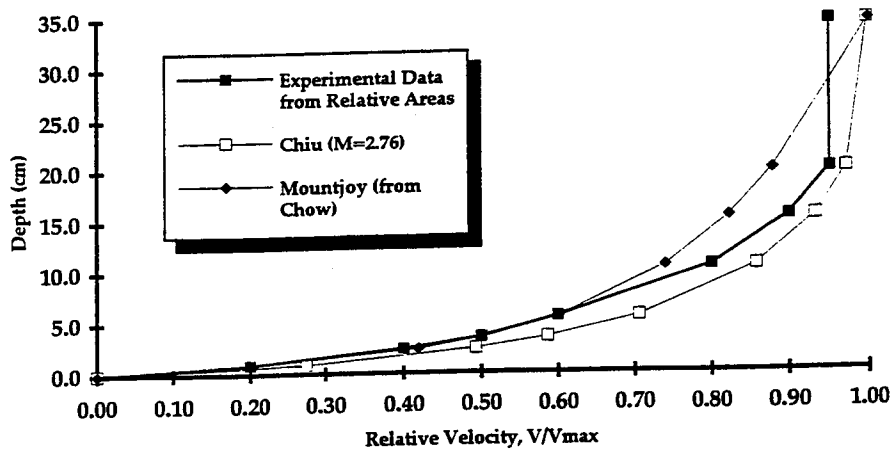


Figure C4.20. One-dimensional centerline velocity plots for Culvert #2 at $Q = 0.0283 \text{ m}^3/\text{s}$, $1/2\%$ slope, $0.56D_0$, $L/D = 8$, downstream control, $V_{\text{max}} = 26.6 \text{ cm/s}$.

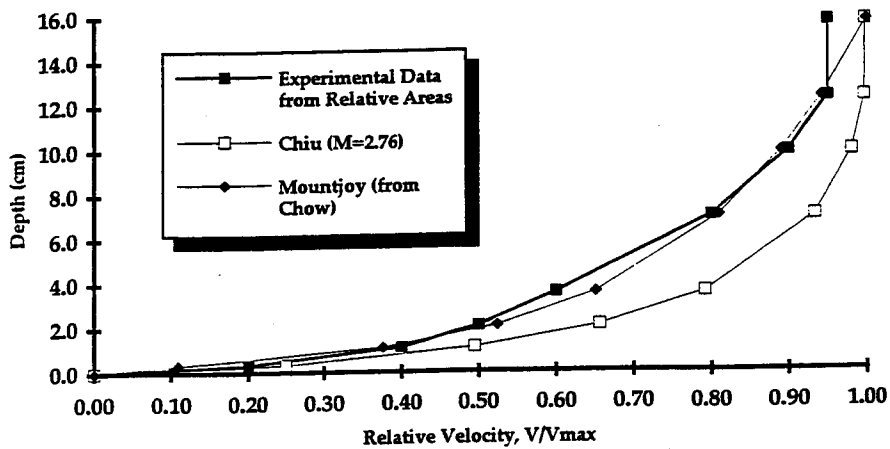


Figure C4.21. One-dimensional centerline velocity plots for Culvert #2 at $Q = 0.0396 \text{ m}^3/\text{s}$, $1/2\%$ slope, $0.25D_0$, $L/D = 14$, no downstream control, $V_{\text{max}} = 90.1 \text{ cm/s}$.

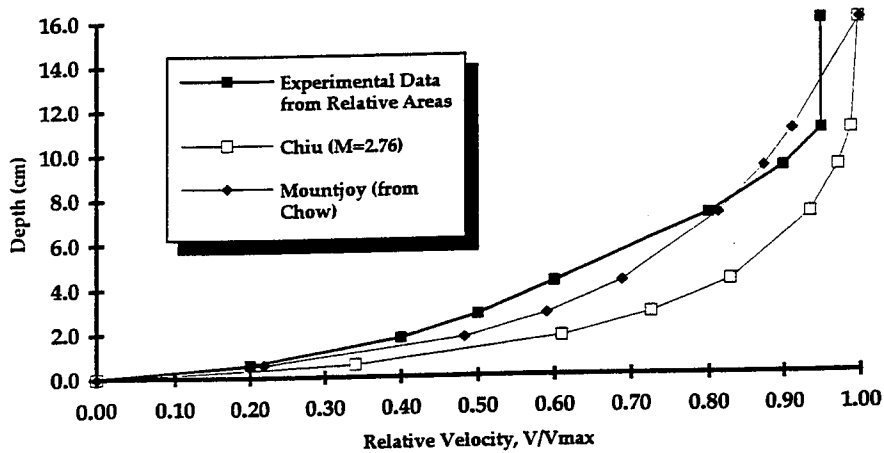


Figure C4.22. One-dimensional centerline velocity plots for Culvert #2 at $Q = 0.0396 \text{ m}^3/\text{s}$, $1/2\%$ slope, $0.25D_0$, $L/D = 8$, downstream control, $V_{\text{max}} = 84.9 \text{ cm/s}$.

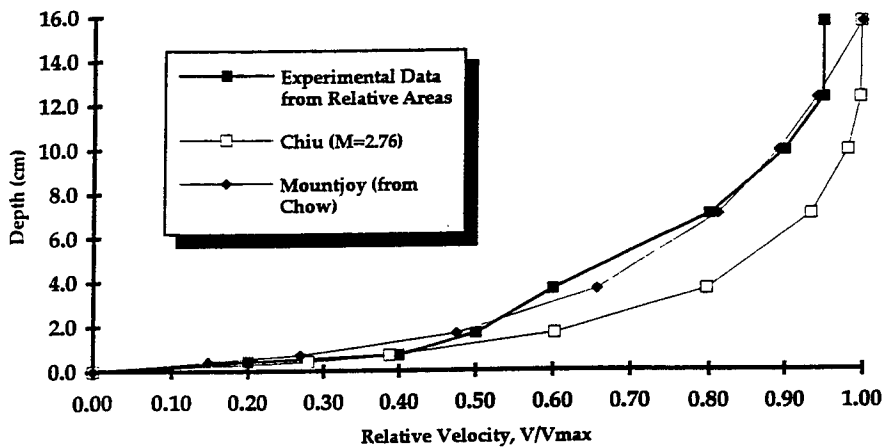


Figure C4.23. One-dimensional centerline velocity plots for Culvert #2 at $Q = 0.0515 \text{ m}^3/\text{s}$, 1% slope, $0.25D_0$, $L/D = 14$, no downstream control, $V_{\text{max}} = 108.0 \text{ cm/s}$.

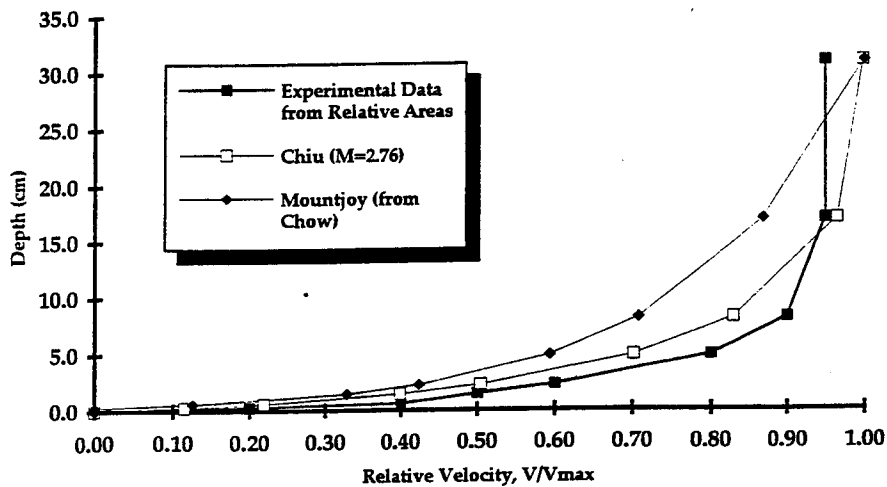


Figure C4.24. One-dimensional centerline velocity plots for Culvert #2 at $Q = 0.0566 \text{ m}^3/\text{s}$, $1/2\%$ slope, $0.50D_0$, $L/D = 1$, downstream control, $V_{\text{max}} = 51.3 \text{ cm/s}$.

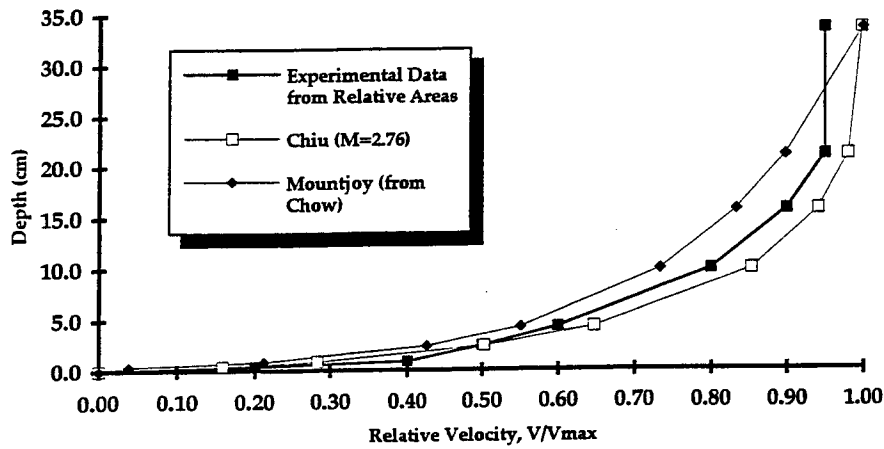


Figure C4.25. One-dimensional centerline velocity plots for Culvert #2 at $Q = 0.0566 \text{ m}^3/\text{s}$, $1/2\%$ slope, $0.55D_0$, $L/D = 12$, downstream control, $V_{\text{max}} = 46.3 \text{ cm/s}$.

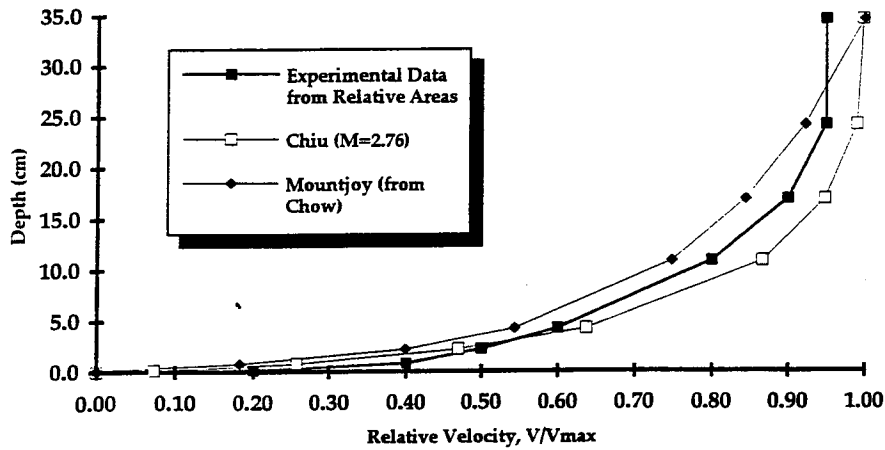


Figure C4.26. One-dimensional centerline velocity plots for Culvert #2 at $Q = 0.0566 \text{ m}^3/\text{s}$, $1/2\%$ slope, $0.57D_0$, $L/D = 14$, downstream control, $V_{\text{max}} = 41.8 \text{ cm/s}$.

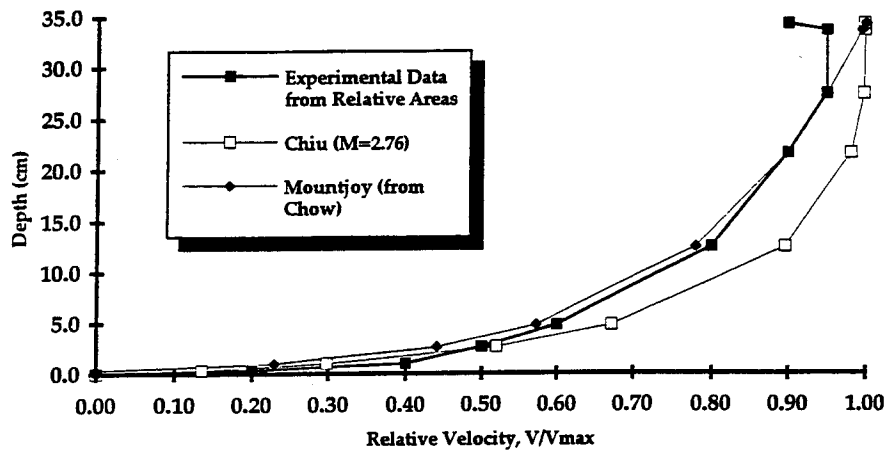


Figure C4.27. One-dimensional centerline velocity plots for Culvert #2 at $Q = 0.0566 \text{ m}^3/\text{s}$, $1/2\%$ slope, $0.56D_0$, $L/D = 8$, downstream control, $V_{\text{max}} = 44.9 \text{ cm/s}$.

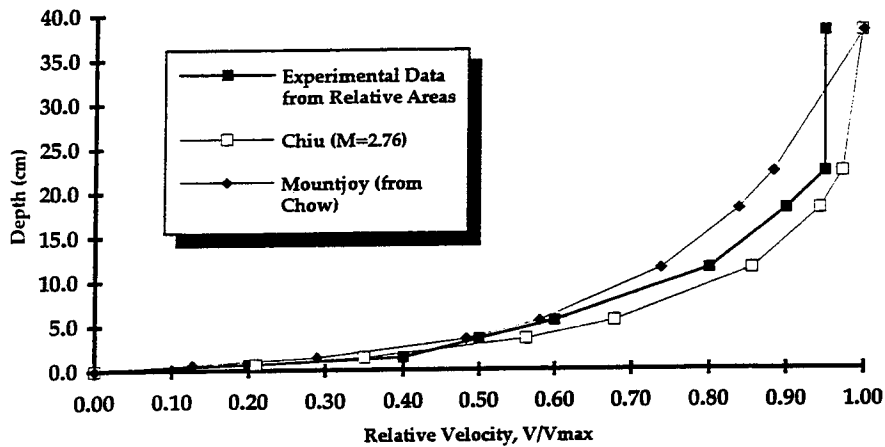


Figure C4.28. One-dimensional centerline velocity plots for Culvert #2 at $Q = 0.0566 \text{ m}^3/\text{s}$, 1% slope, $0.62D_0$, $L/D = 14$, downstream control, $V_{\text{max}} = 37.6 \text{ cm/s}$.

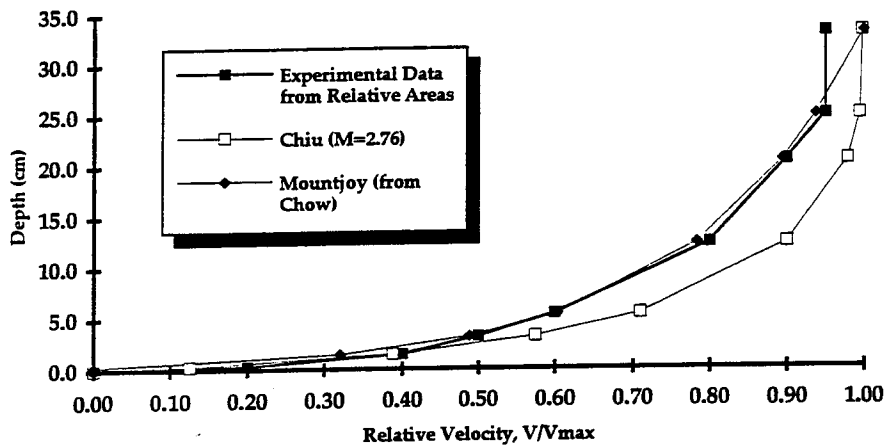


Figure C4.29. One-dimensional centerline velocity plots for Culvert #2 at $Q = 0.0850 \text{ m}^3/\text{s}$, 1/2% slope, $0.54D_0$, $L/D = 12$, downstream control, $V_{\text{max}} = 69.1 \text{ cm/s}$.

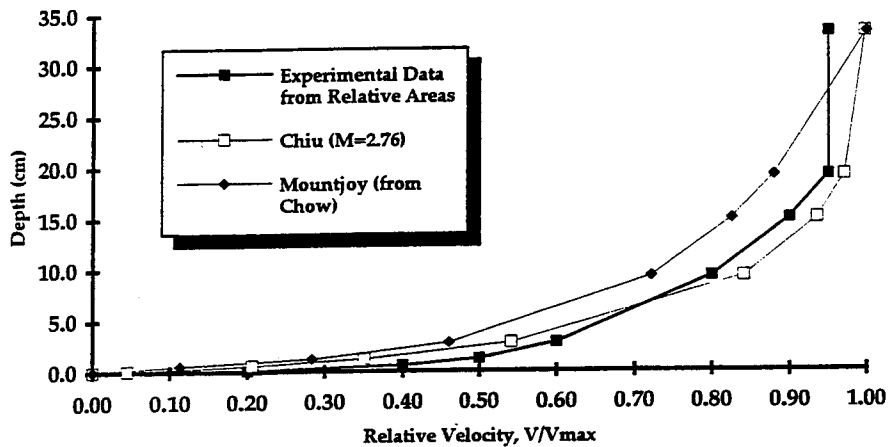


Figure C4.30. One-dimensional centerline velocity plots for Culvert #2 at $Q = 0.0850 \text{ m}^3/\text{s}$, 1/2% slope, $0.54D_0$, $L/D = 14$, downstream control, $V_{\text{max}} = 64.2 \text{ cm/s}$.

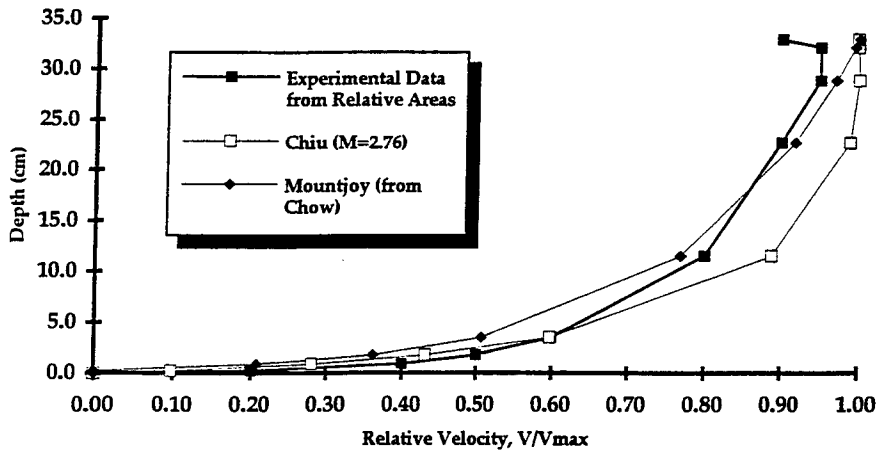


Figure C4.31. One-dimensional centerline velocity plots for Culvert #2 at $Q = 0.0850 \text{ m}^3/\text{s}$, $1/2\%$ slope, $0.54D_0$, $L/D = 8$, downstream control, $V_{\text{max}} = 69.8 \text{ cm/s}$.

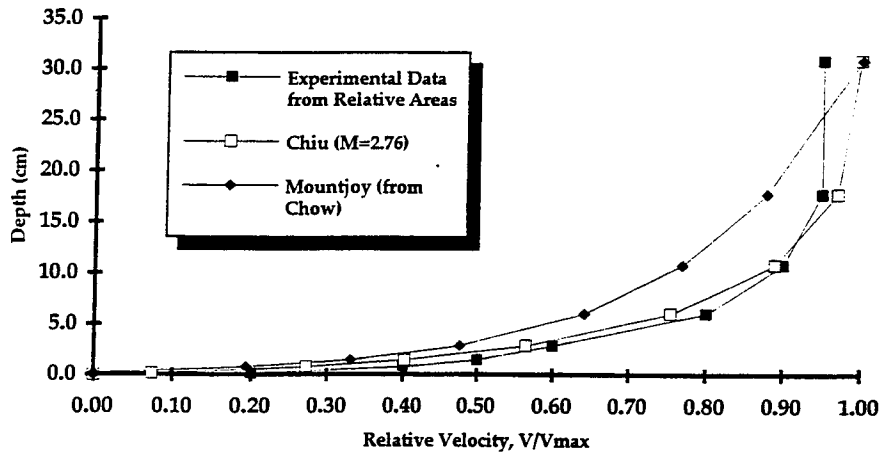


Figure C4.32. One-dimensional centerline velocity plots for Culvert #2 at $Q = 0.0850 \text{ m}^3/\text{s}$, $1/2\%$ slope, $0.50D_0$, at entrance, downstream control, $V_{\text{max}} = 71.5 \text{ cm/s}$.

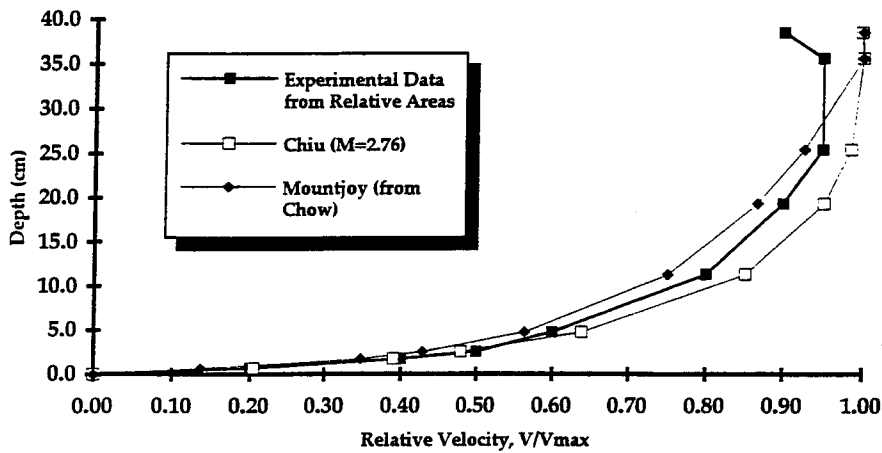


Figure C4.33. One-dimensional centerline velocity plots for Culvert #2 at $Q = 0.0850 \text{ m}^3/\text{s}$, 1% slope, $0.63D_0$, $L/D = 14$, downstream control, $V_{\text{max}} = 58.2 \text{ cm/s}$.

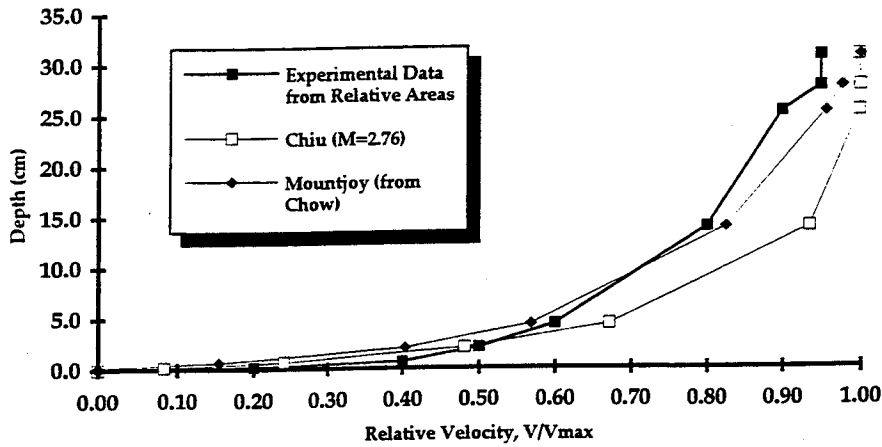


Figure C4.34. One-dimensional centerline velocity plots for Culvert #2 at $Q = 0.1274 \text{ m}^3/\text{s}$, $1/2\%$ slope, $0.50D_o$, $L/D = 8$, no downstream control, $V_{\text{max}} = 118.4 \text{ cm/s}$.

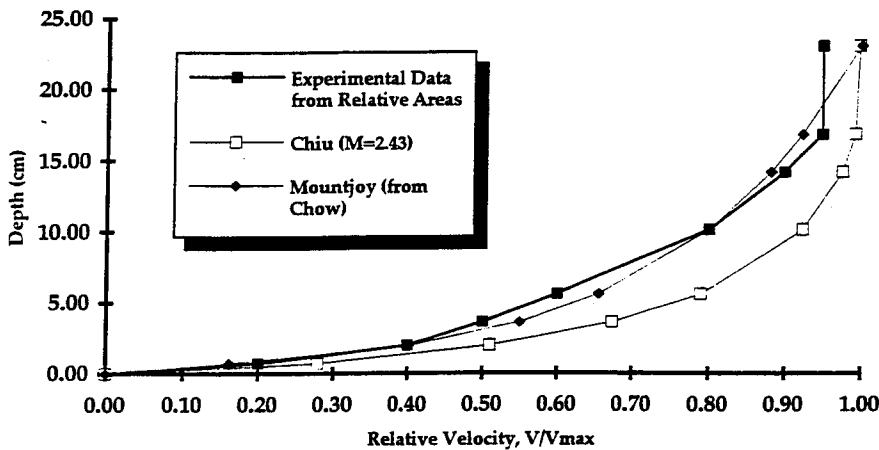


Figure C4.35. One-dimensional centerline velocity plots for Culvert #3 at $Q = 0.0153 \text{ m}^3/\text{s}$, $1/2\%$ slope, $0.31D_o$, $L/D = 8$, downstream control, $V_{\text{max}} = 22.2 \text{ cm/s}$.

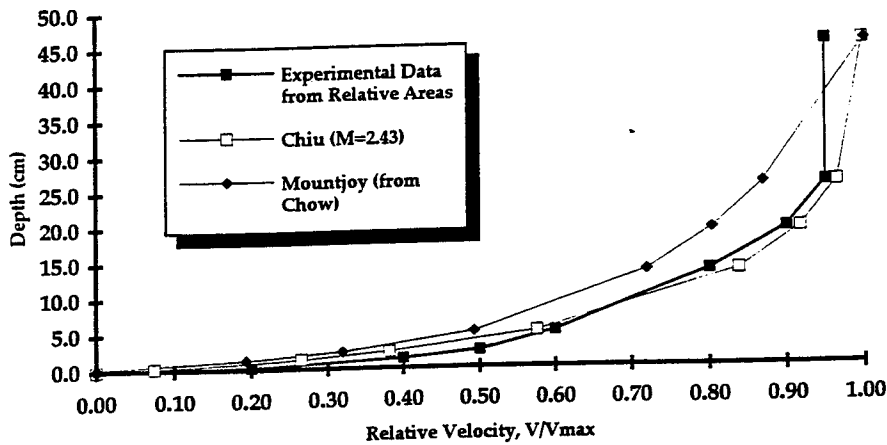


Figure C4.36. One-dimensional centerline velocity plots for Culvert #3 at $Q = 0.0153 \text{ m}^3/\text{s}$, 1% slope, $0.62D_o$, $L/D = 8$, downstream control, $V_{\text{max}} = 9.9 \text{ cm/s}$.

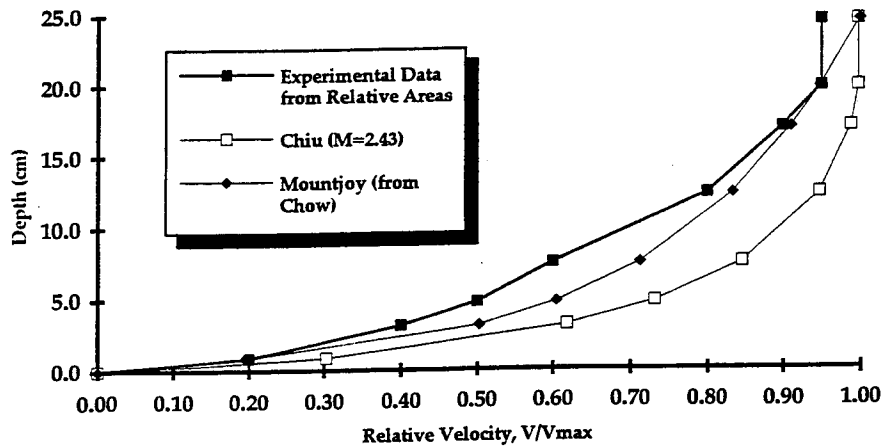


Figure C4.37. One-dimensional centerline velocity plots for Culvert #3 at $Q = 0.0153 \text{ m}^3/\text{s}$, $1/2\%$ slope, $0.33D_0$, $L/D = 8$, downstream control, $V_{\text{max}} = 20.5 \text{ cm/s}$.

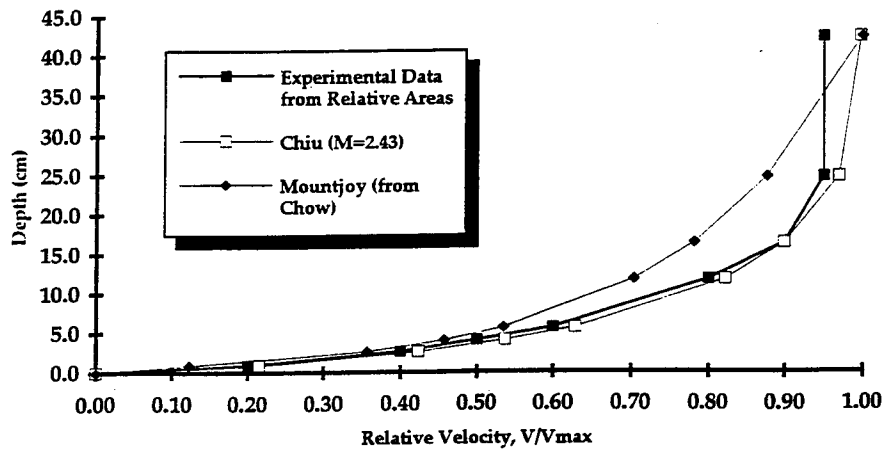


Figure C4.38. One-dimensional centerline velocity plots for Culvert #3 at $Q = 0.0566 \text{ m}^3/\text{s}$, $1/2\%$ slope, $0.57D_0$, $L/D = 8$, downstream control, $V_{\text{max}} = 31.2 \text{ cm/s}$.

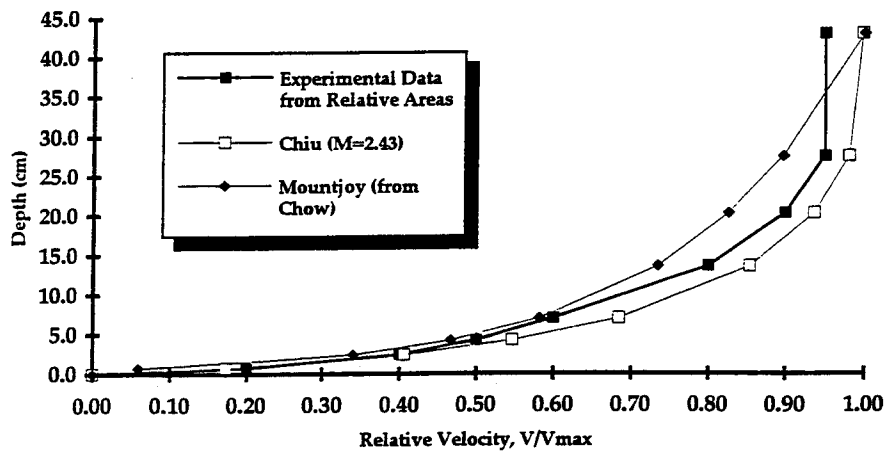


Figure C4.39. One-dimensional centerline velocity plots for Culvert #3 at $Q = 0.0566 \text{ m}^3/\text{s}$, 1% slope, $0.58D_0$, $L/D = 8$, downstream control, $V_{\text{max}} = 33.9 \text{ cm/s}$.

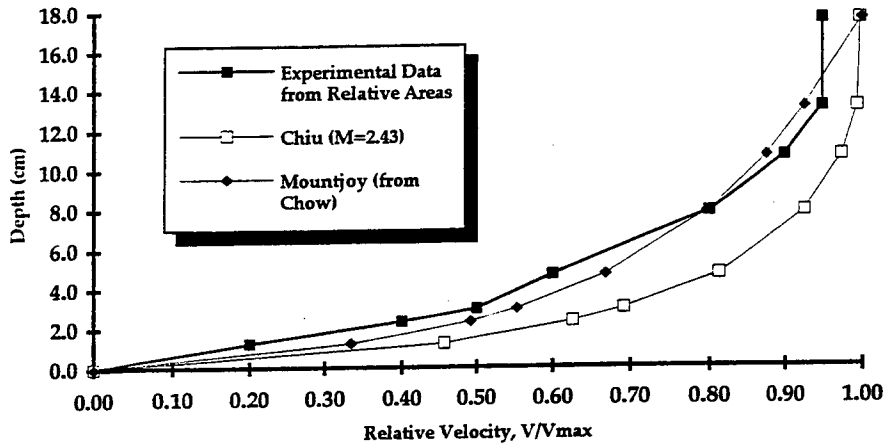


Figure C4.40. One-dimensional centerline velocity plots for Culvert #3 at $Q = 0.0575 \text{ m}^3/\text{s}$, $1/2\%$ slope, $0.24D_0$, $L/D = 8$, no downstream control, $V_{\text{max}} = 120.8 \text{ cm/s}$.

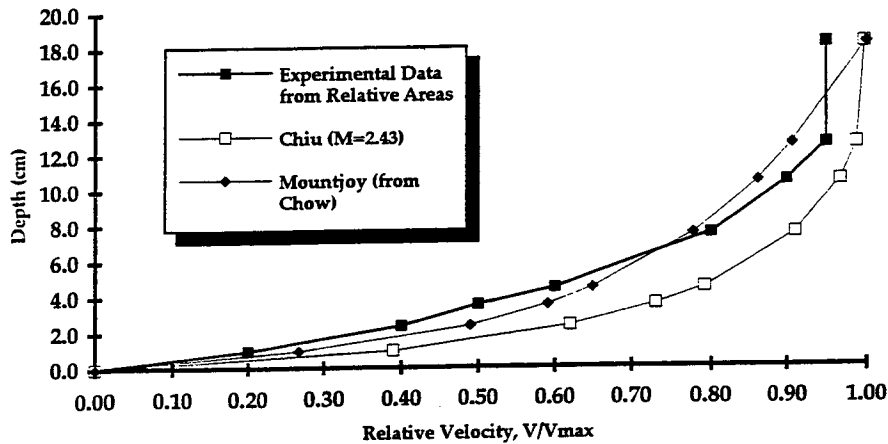


Figure C4.41. One-dimensional centerline velocity plots for Culvert #3 at $Q = 0.0664 \text{ m}^3/\text{s}$, 1% slope, $0.25D_0$, $L/D = 8$, no downstream control, $V_{\text{max}} = 135.1 \text{ cm/s}$.

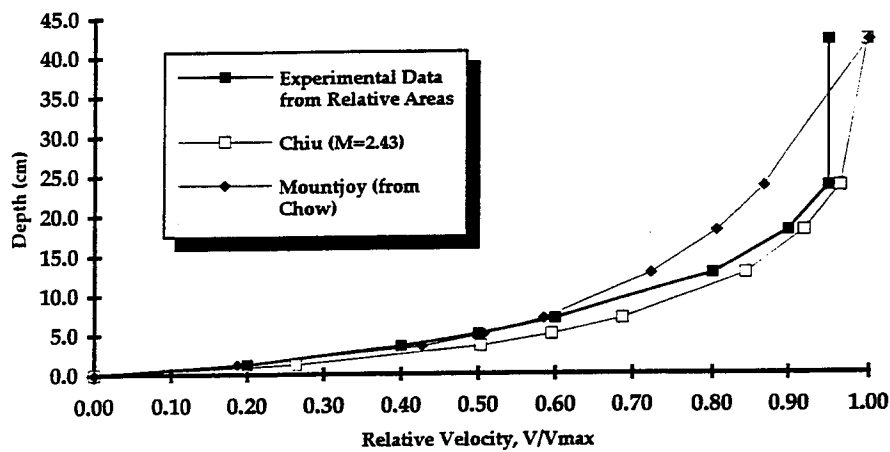


Figure C4.42. One-dimensional centerline velocity plots for Culvert #3 at $Q = 0.0850 \text{ m}^3/\text{s}$, $1/2\%$ slope, $0.57D_0$, $L/D = 8$, downstream control, $V_{\text{max}} = 46.6 \text{ cm/s}$.

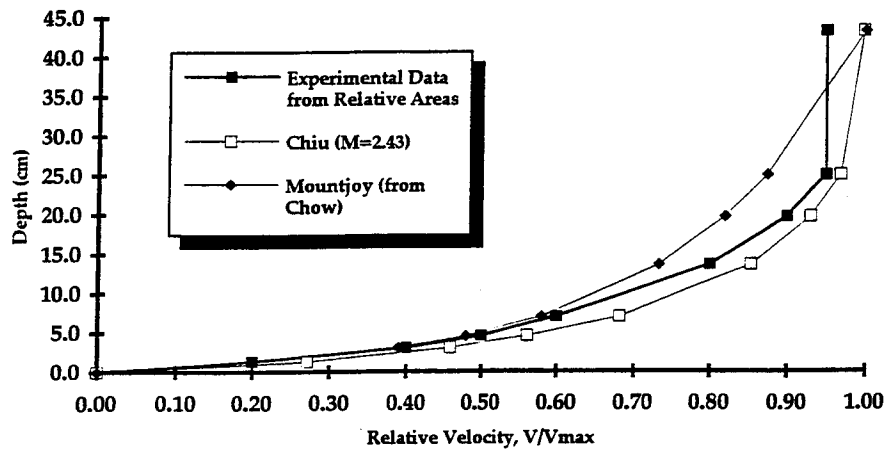


Figure C4.43. One-dimensional centerline velocity plots for Culvert #3 at $Q = 0.0850 \text{ m}^3/\text{s}$, 1% slope, $0.59D_o$, $L/D = 8$, downstream control, $V_{\text{max}} = 44.2 \text{ cm/s}$.

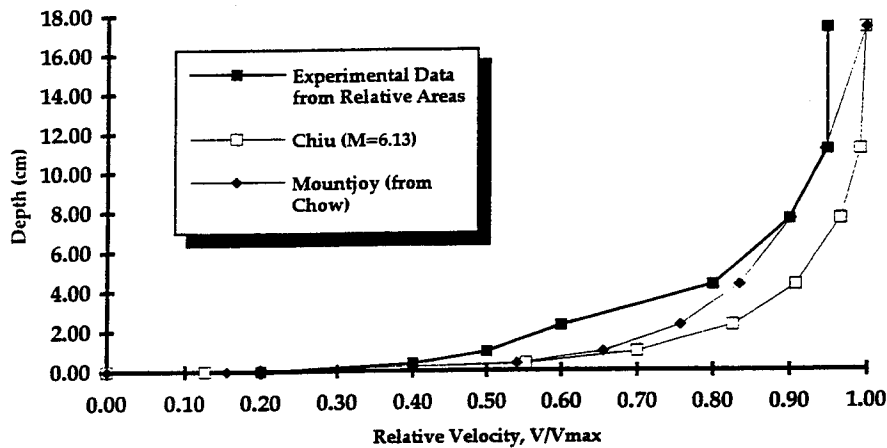


Figure C4.44. One-dimensional centerline velocity plots for Culvert #4 at $Q = 0.0153 \text{ m}^3/\text{s}$, 1/2% slope, $0.28D_o$, $L/D = 7$, downstream control, $V_{\text{max}} = 27.4 \text{ cm/s}$.

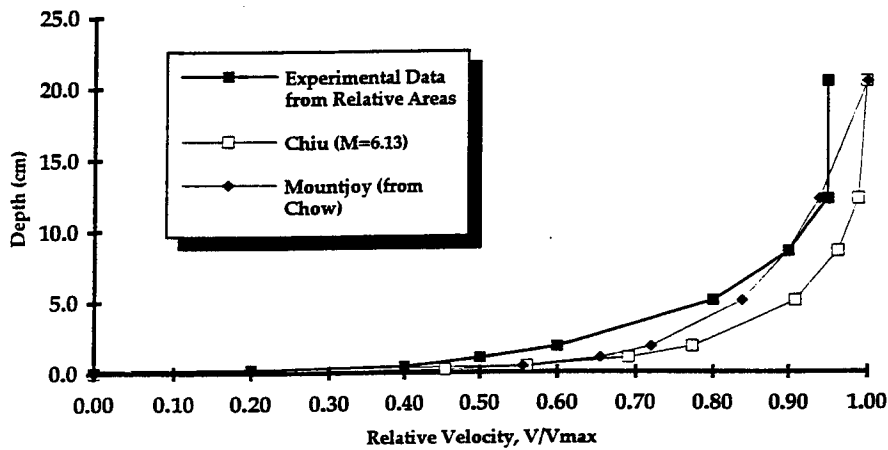


Figure C4.45. One-dimensional centerline velocity plots for Culvert #4 at $Q = 0.0153 \text{ m}^3/\text{s}$, 1/2% slope, $0.33D_o$, $L/D = 7$, downstream control, $V_{\text{max}} = 23.1 \text{ cm/s}$.

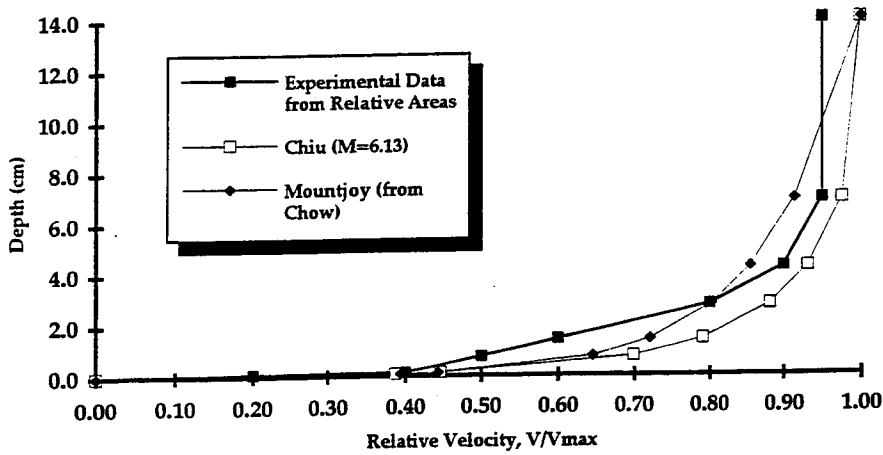


Figure C4.46. One-dimensional centerline velocity plots for Culvert #4 at $Q = 0.0500 \text{ m}^3/\text{s}$, $1/2\%$ slope, $0.23D_0$, $L/D = 7$, no downstream control, $V_{\text{max}} = 127.2 \text{ cm/s}$.

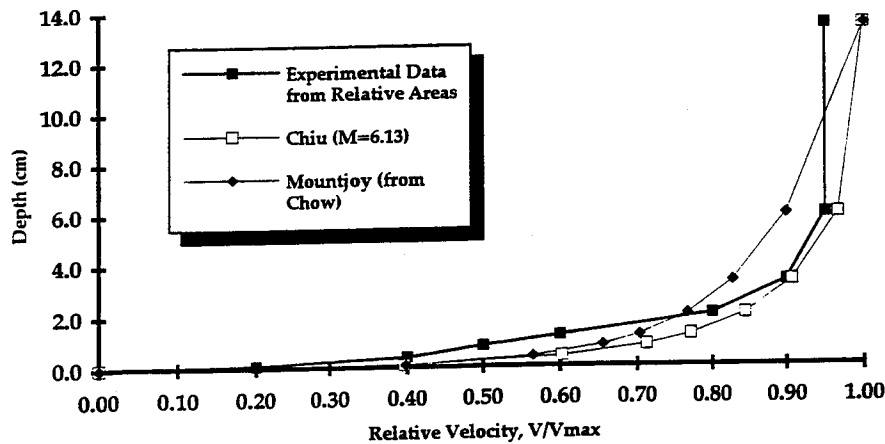


Figure C4.47. One-dimensional centerline velocity plots for Culvert #4 at $Q = 0.0563 \text{ m}^3/\text{s}$, 1% slope, $0.22D_0$, $L/D = 7$, no downstream control, $V_{\text{max}} = 140.2 \text{ cm/s}$.

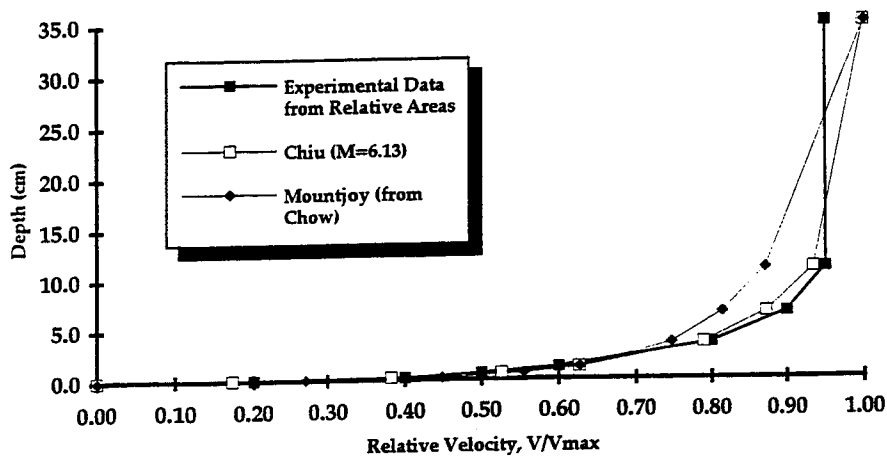


Figure C4.48. One-dimensional centerline velocity plots for Culvert #4 at $Q = 0.0566 \text{ m}^3/\text{s}$, $1/2\%$ slope, $0.57D_0$, $L/D = 7$, downstream control, $V_{\text{max}} = 38.9 \text{ cm/s}$.

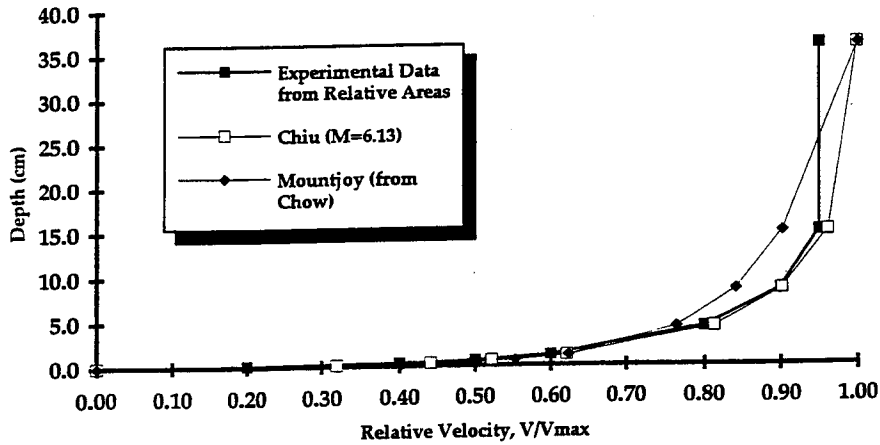


Figure C4.49. One-dimensional centerline velocity plots for Culvert #4 at $Q = 0.0566 \text{ m}^3/\text{s}$, 1% slope, $0.59D_0$, $L/D = 7$, downstream control, $V_{\text{max}} = 36.8 \text{ cm/s}$.

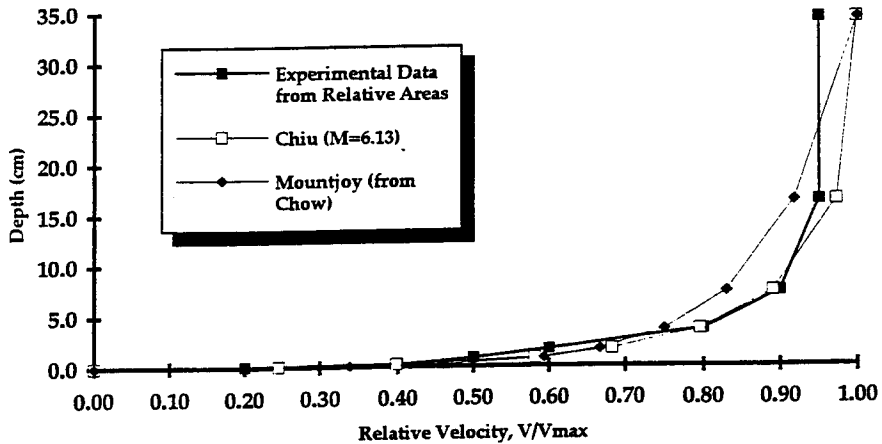


Figure C4.50. One-dimensional centerline velocity plots for Culvert #4 at $Q = 0.0850 \text{ m}^3/\text{s}$, 1/2% slope, $0.56D_0$, $L/D = 7$, downstream control, $V_{\text{max}} = 59.7 \text{ cm/s}$.

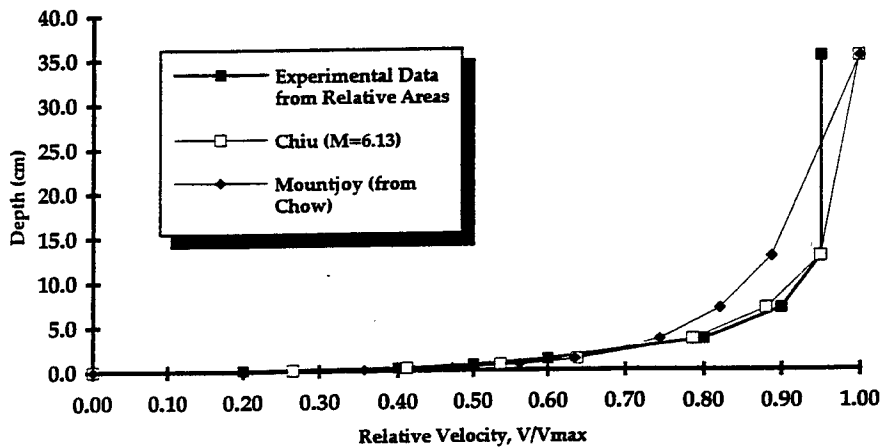


Figure C4.51. One-dimensional centerline velocity plots for Culvert #4 at $Q = 0.0850 \text{ m}^3/\text{s}$, 1% slope, $0.58D_0$, $L/D = 7$, downstream control, $V_{\text{max}} = 54.2 \text{ cm/s}$.

Appendix D
Horizontal Velocity Profiles

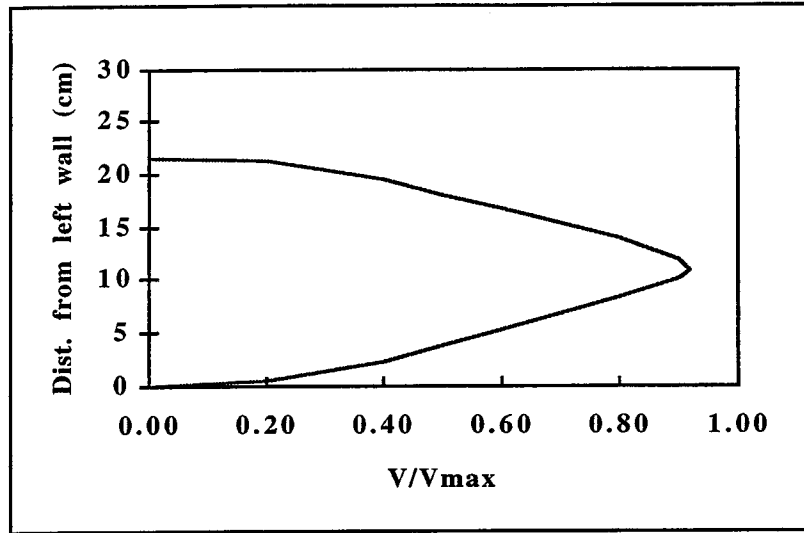


Figure D4.1. Velocity profile for Culvert #1 at $Q = 0.0052$ cms, 5% slope, $0.136D_0$, $L/D = 14$, no downstream control, $V_{max} = 101.9$ cm/sec.

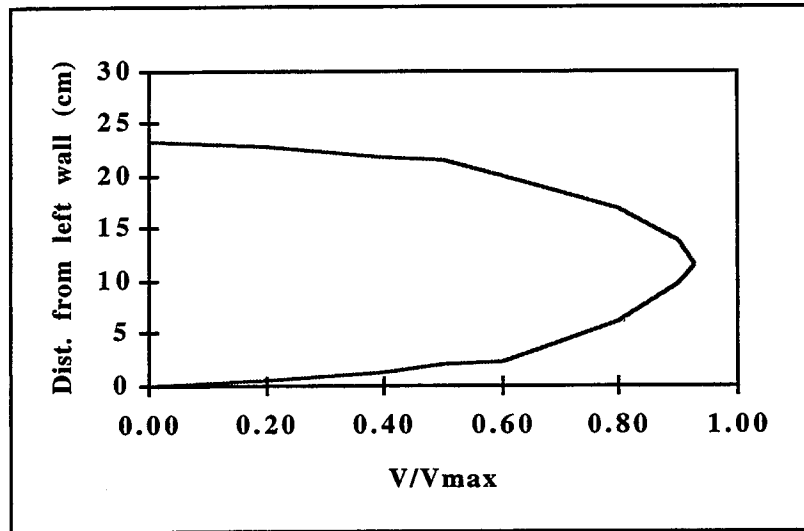


Figure D4.2. Velocity profile for Culvert #1 at $Q = 0.0064$ cms, 3% slope, $0.184D_0$, $L/D = 14$, no downstream control, $V_{max} = 82.0$ cm/sec.

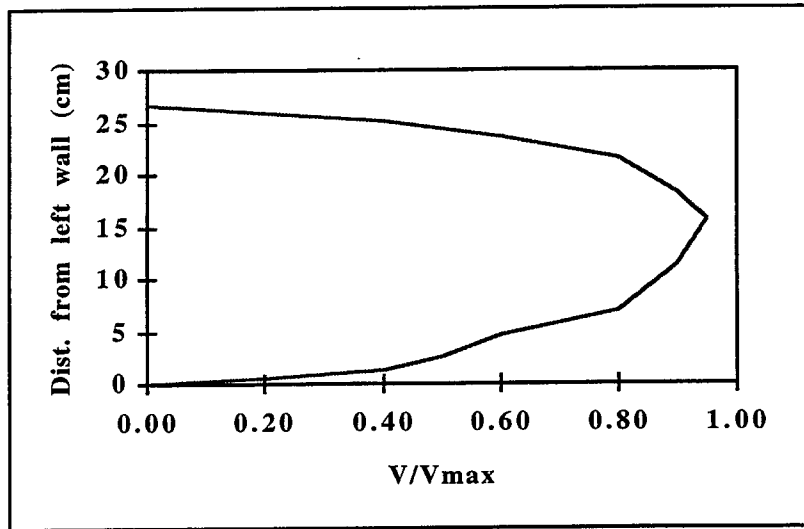


Figure D4.3. Velocity profile for Culvert #1 at $Q = 0.0082$ cms, 1% slope, $0.272D_0$, $L/D = 14$, no downstream control, $V_{max} = 61.2$ cm/sec.

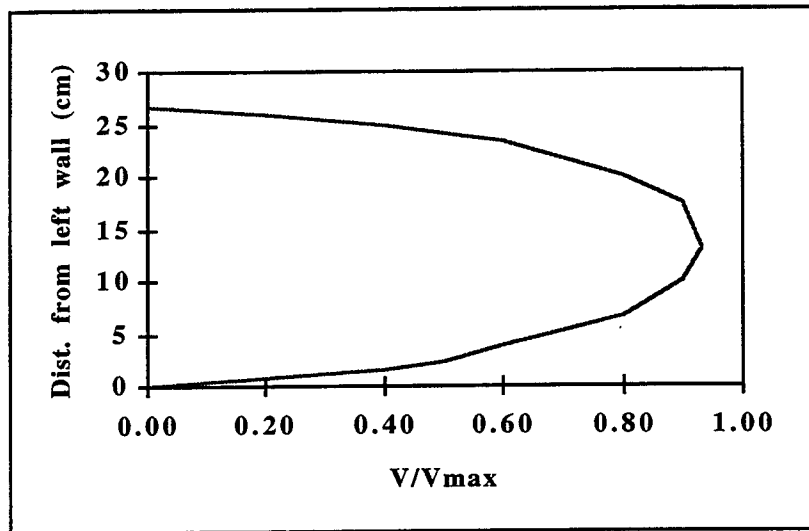


Figure D4.4. Velocity profile for Culvert #1 at $Q = 0.0094$ cms, 1/2% slope, $0.272D_0$, $L/D = 14$, no downstream control, $V_{max} = 59.9$ cm/sec.

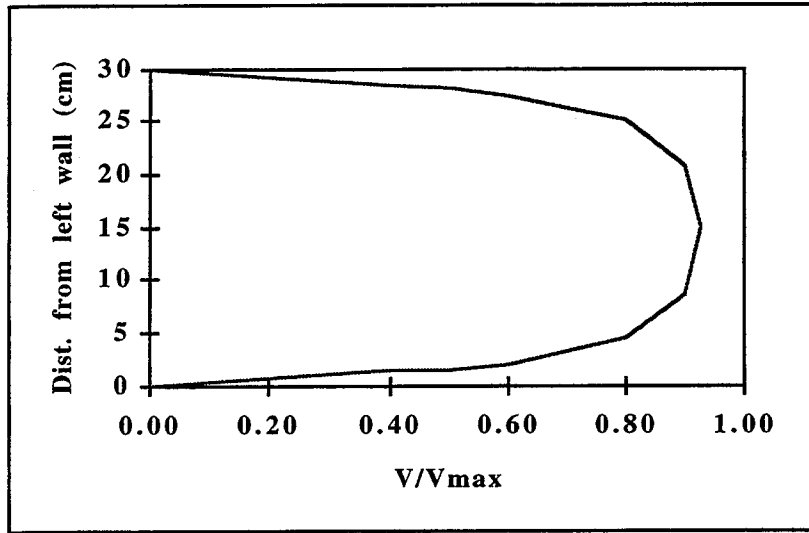


Figure D4.5. Velocity profile for Culvert #1 at $Q = 0.0124$ cms, 1/2% slope, $0.544D_0$, $L/D = 14$, downstream control, $V_{max} = 34.5$ cm/sec.

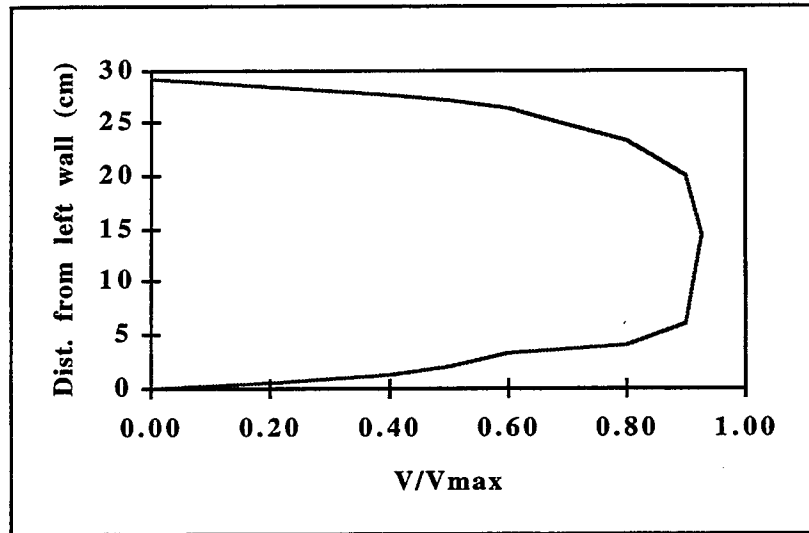


Figure D4.6. Velocity profile for Culvert #1 at $Q = 0.0124$ cms, 1% slope, $0.608D_0$, $L/D = 14$, downstream control, $V_{max} = 33.2$ cm/sec.

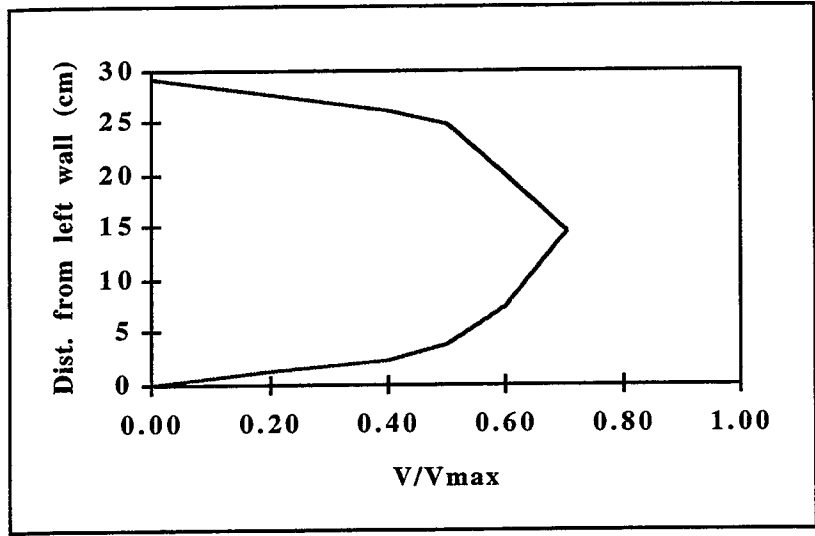


Figure D4.7. Velocity profile for Culvert #1 at $Q = 0.0142$ cms, 5% slope, $0.392D_0$, $L/D = 14$, downstream control, $V_{max} = 63.1$ cm/sec.

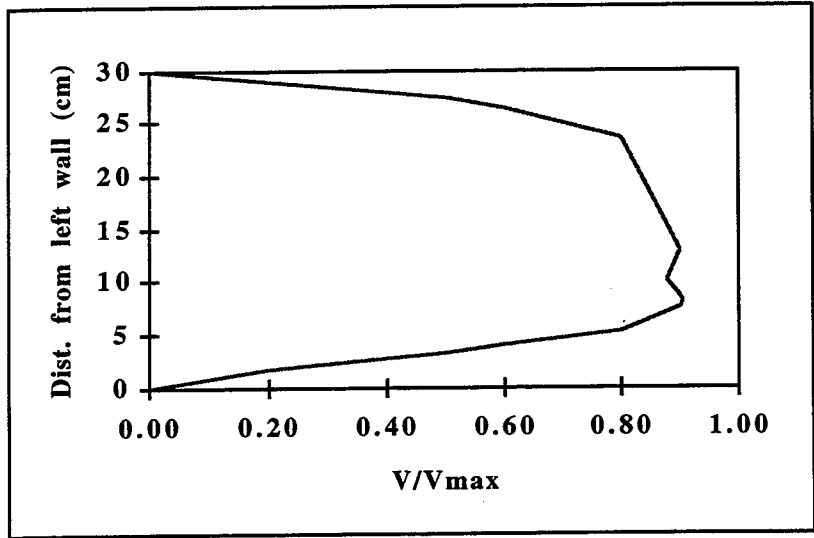


Figure D4.8. Velocity profile for Culvert #1 at $Q = 0.0213$ cms, 1/2% slope, $0.448D_0$, $L/D = 14$, downstream control, $V_{max} = 85.1$ cm/sec.

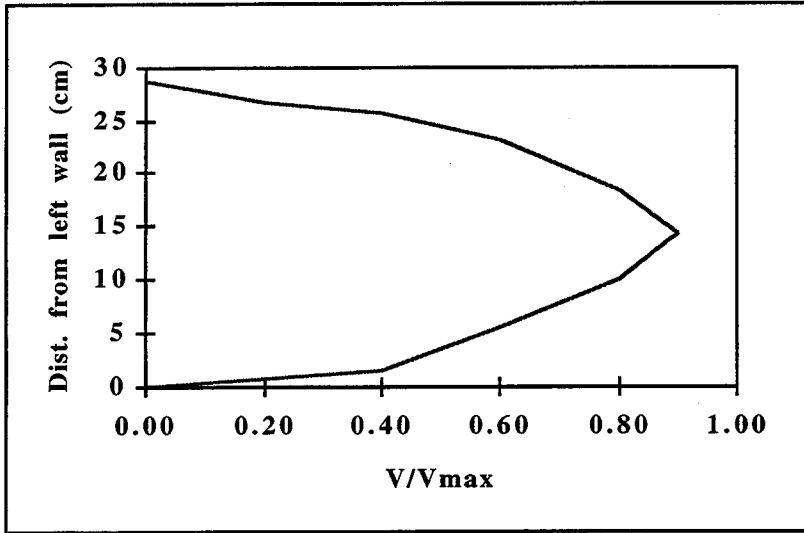


Figure D4.9. Velocity profile for Culvert #1 at $Q = 0.0278$ cms, 3% slope, $0.344D_0$, $L/D = 14$, no downstream control, $V_{max} = 125.9$ cm/sec.

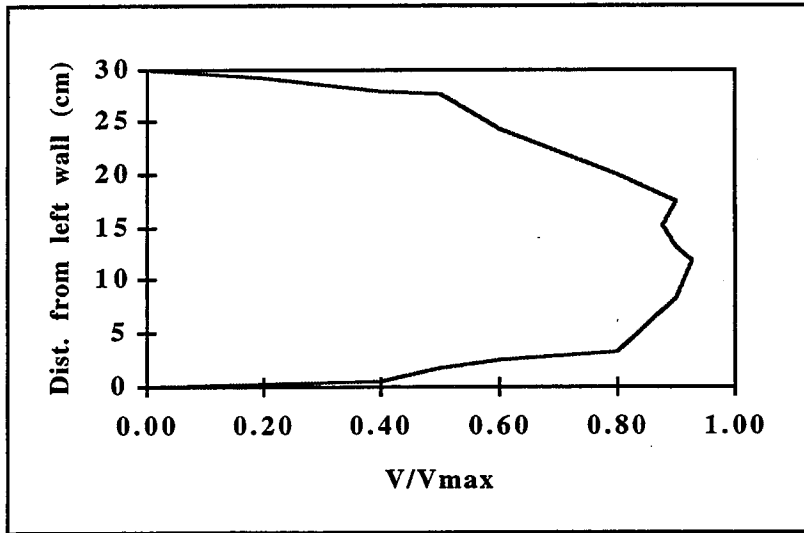


Figure D4.10. Velocity profile for Culvert #1 at $Q = 0.0284$ cms, 1% slope, $0.416D_0$, $L/D = 14$, no downstream control, $V_{max} = 92.7$ cm/sec.

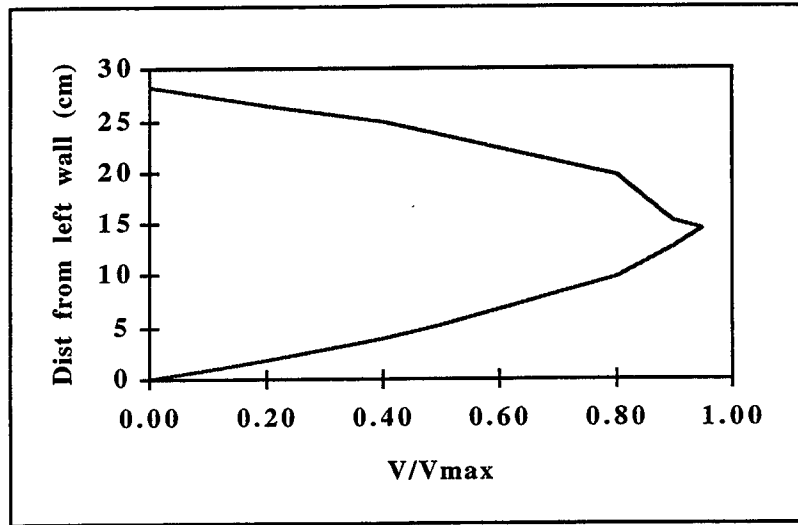


Figure D4.11. Velocity profile for Culvert #1 at $Q = 0.0290$ cms, 5% slope, $0.312D_0$, $L/D = 14$, no downstream control, $V_{max} = 169.3$ cm/sec.

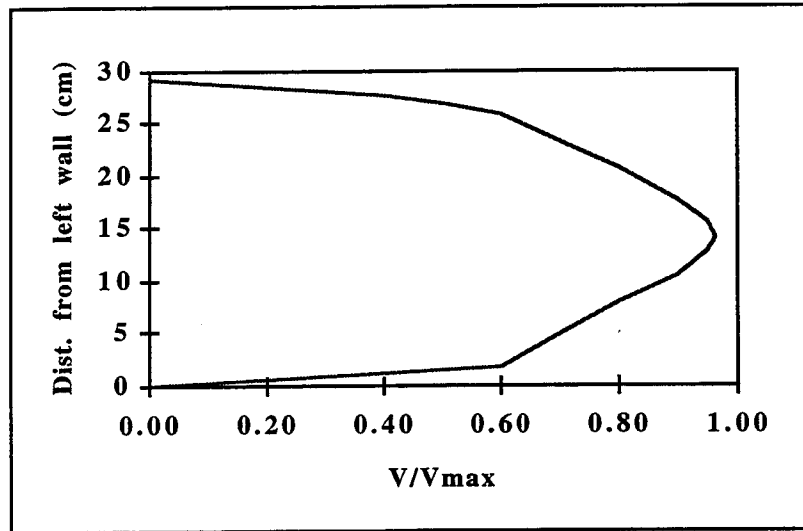


Figure D4.12. Velocity profile for Culvert #1 at $Q = 0.0438$ cms, 5% slope, $0.368D_0$, $L/D = 14$, no downstream control, $V_{max} = 178.0$ cm/sec.

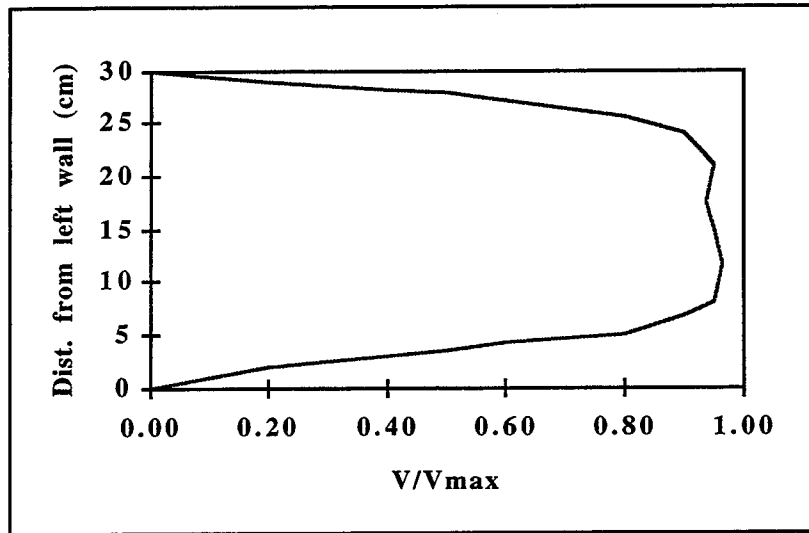


Figure D4.13. Velocity profile for Culvert #1 at $Q = 0.0456$ cms, 1/2% slope, $0.576D_0$, $L/D = 14$, no downstream control, $V_{\max} = 108.5$ cm/sec.

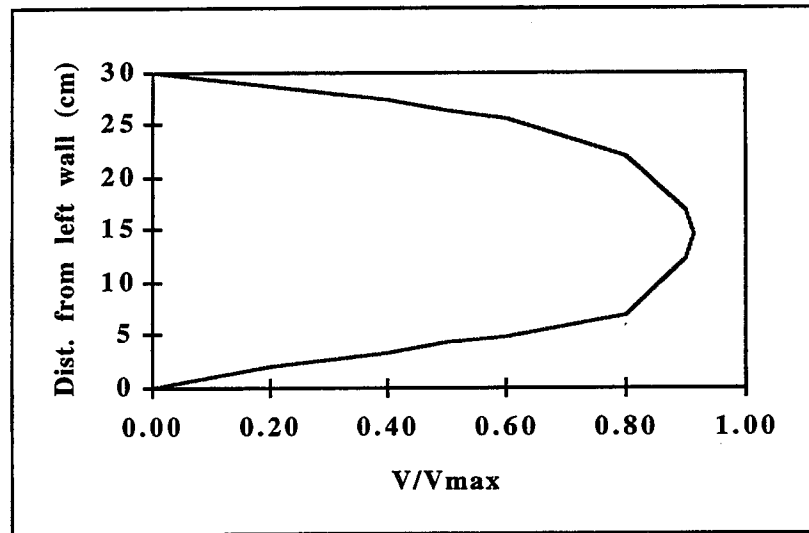


Figure D4.14. Velocity profile for Culvert #1 at $Q = 0.0527$ cms, 3% slope, $0.496D_0$, $L/D = 14$, no downstream control, $V_{\max} = 159.6$ cm/sec.

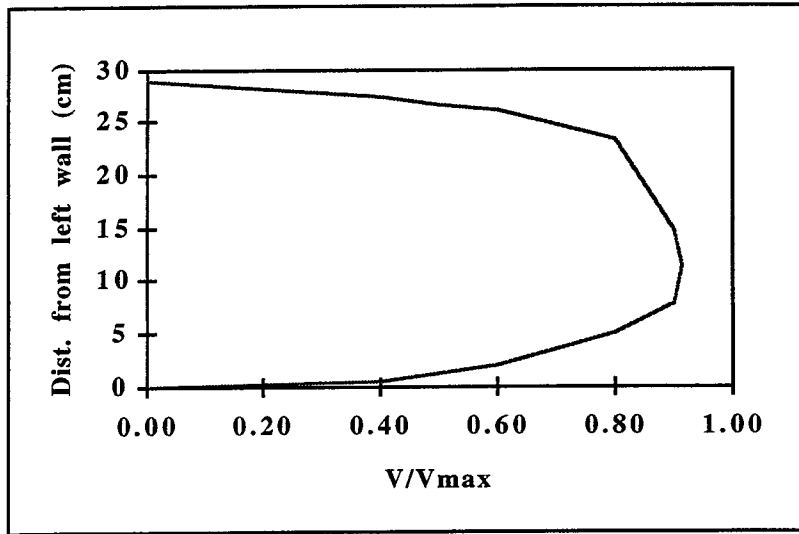


Figure D4.15. Velocity profile for Culvert #1 at $Q = 0.0539 \text{cms}$, 1% slope, $0.632D_o$, $L/D = 14$, no downstream control, $V_{\text{max}} = 124.4 \text{ cm/sec}$.

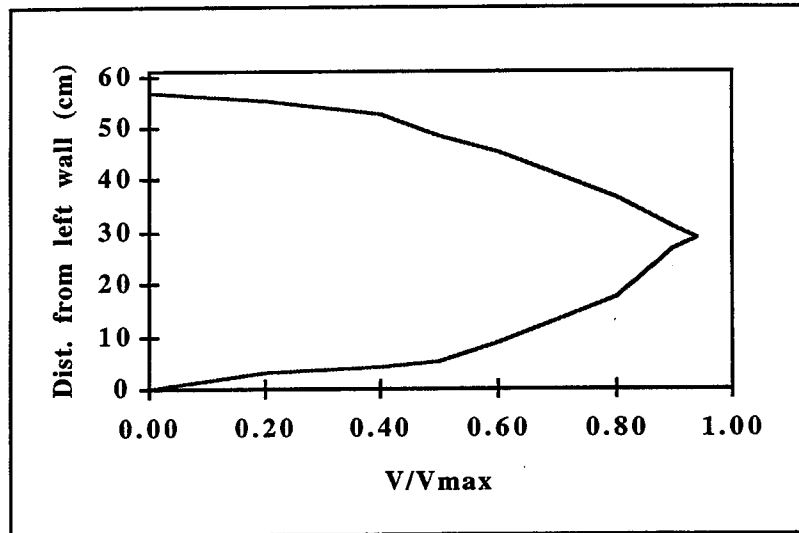


Figure D4.16. Velocity profile for Culvert #2 at $Q = 0.0153 \text{cms}$, 1/2% slope, $0.304D_o$, $L/D = 14$, downstream control, $V_{\text{max}} = 26.4 \text{ cm/sec}$.

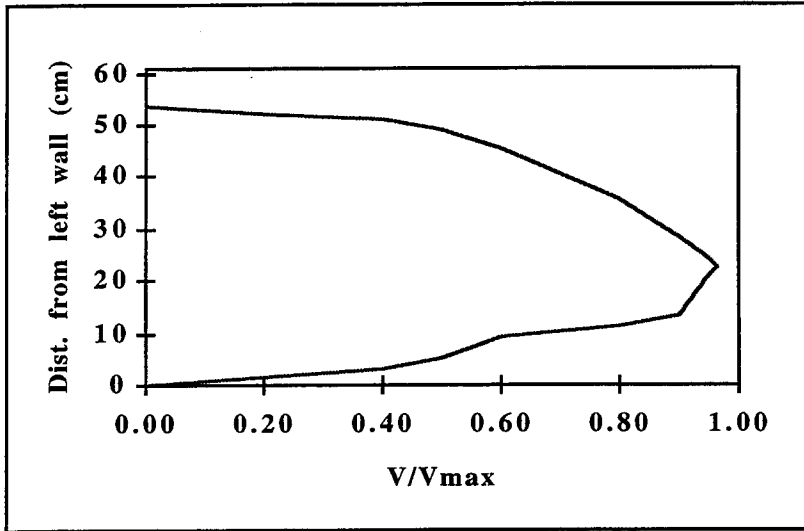


Figure D4.17. Velocity profile for Culvert #2 at $Q = 0.0153$ cms, $1/2\%$ slope, $0.264D_0$, $L/D = 8$, downstream control, $V_{max} = 29.2$ cm/sec.

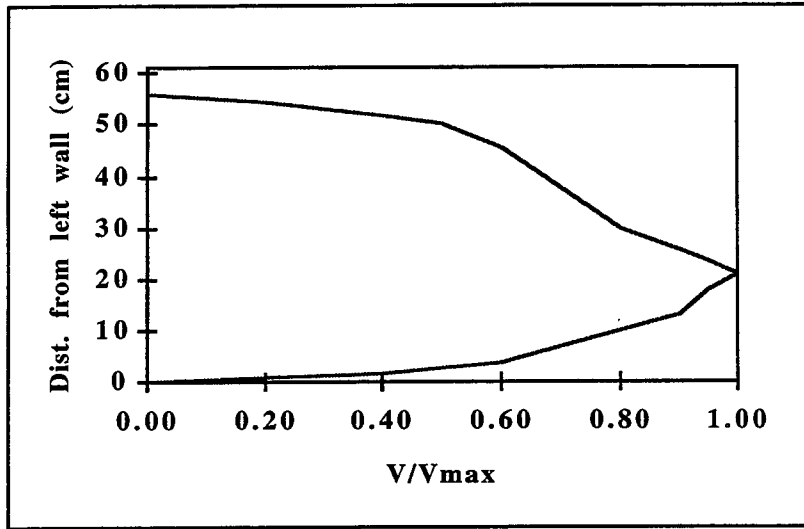


Figure D4.18. Velocity profile for Culvert #2 at $Q = 0.0153$ cms, 1% slope, $0.312D_0$, $L/D = 14$, downstream control, $V_{max} = 25.2$ cm/sec.

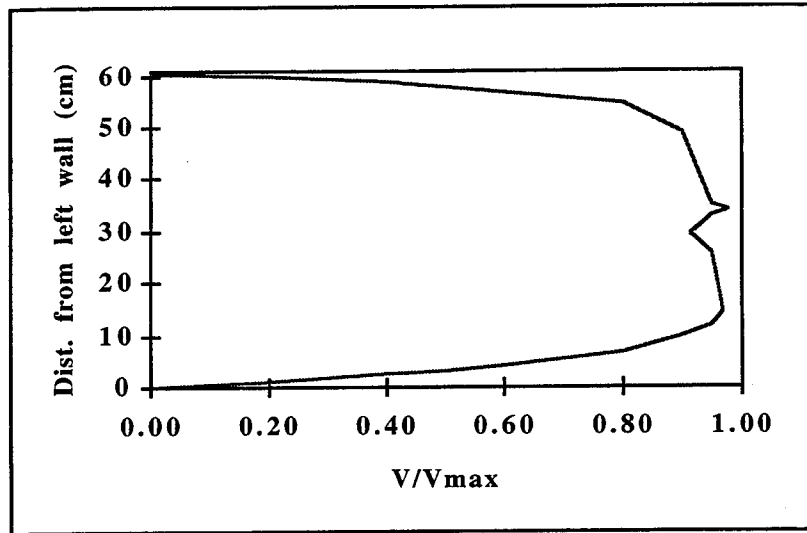


Figure D4.19. Velocity profile for Culvert #2 at $Q = 0.0283$ cms, $1/2\%$ slope, $0.464D_0$, $L/D = 14$, downstream control, $V_{max} = 22.8$ cm/sec.

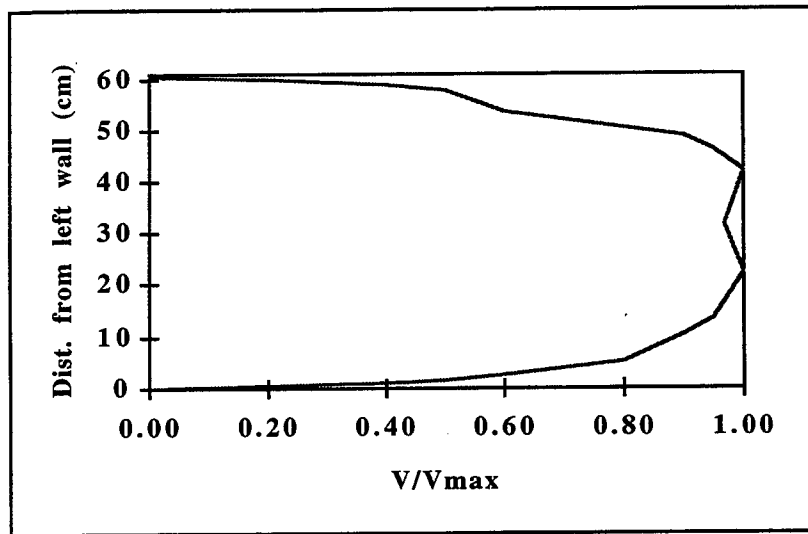


Figure D4.20. Velocity profile for Culvert #2 at $Q = 0.0283$ cms, $1/2\%$ slope, $0.448D_0$, $L/D = 8$, downstream control, $V_{max} = 26.6$ cm/sec.

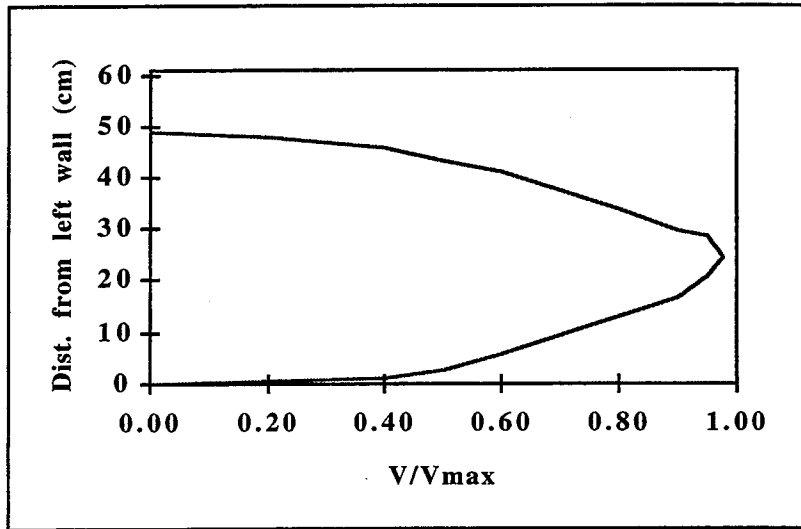


Figure D4.21. Velocity profile for Culvert #2 at $Q = 0.0396$ cms, 1/2% slope, $0.20D_0$, $L/D = 14$, no downstream control, $V_{\max} = 90.1$ cm/sec.

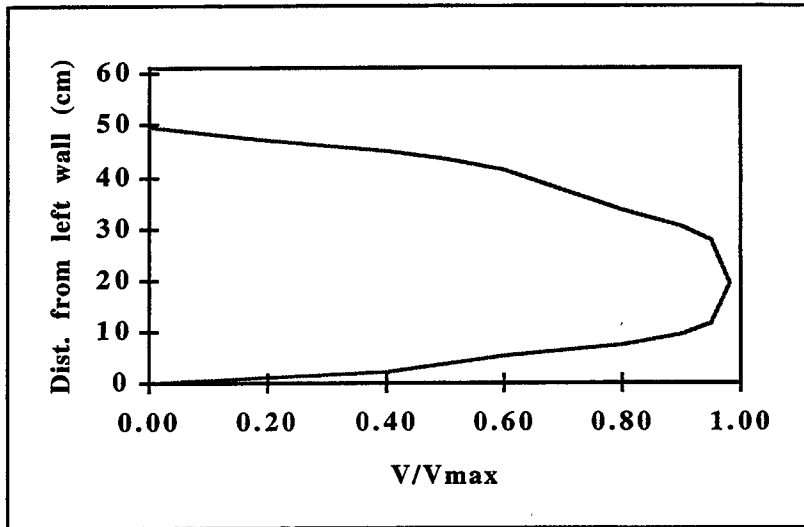


Figure D4.22. Velocity profile for Culvert #2 at $Q = 0.0396$ cms, 1/2% slope, $0.20D_0$, $L/D = 8$, downstream control, $V_{\max} = 84.9$ cm/sec.

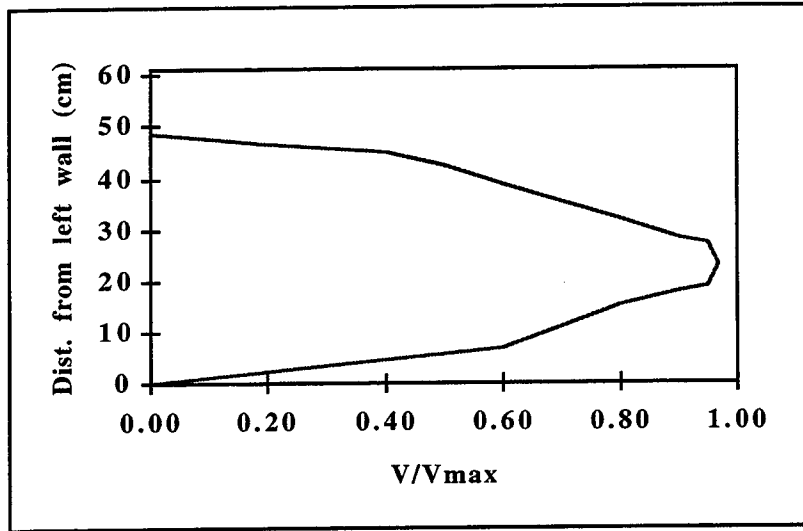


Figure D4.23. Velocity profile for Culvert #2 at $Q = 0.0515$ cms, 1% slope, $0.20D_0$, $L/D = 14$, no downstream control, $V_{max} = 108.0$ cm/sec.

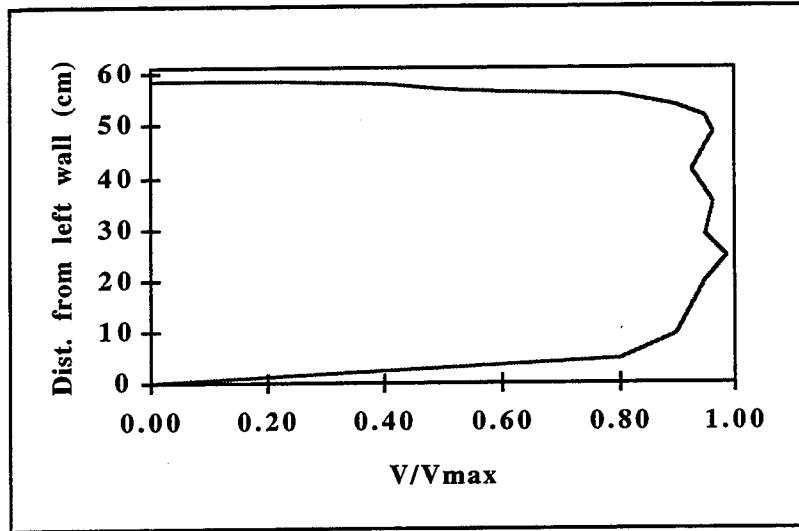


Figure D4.24. Velocity profile for Culvert #2 at $Q = 0.0566$ cms, 1/2% slope, $0.40D_0$, $L/D = 1$, downstream control, $V_{max} = 51.3$ cm/sec.

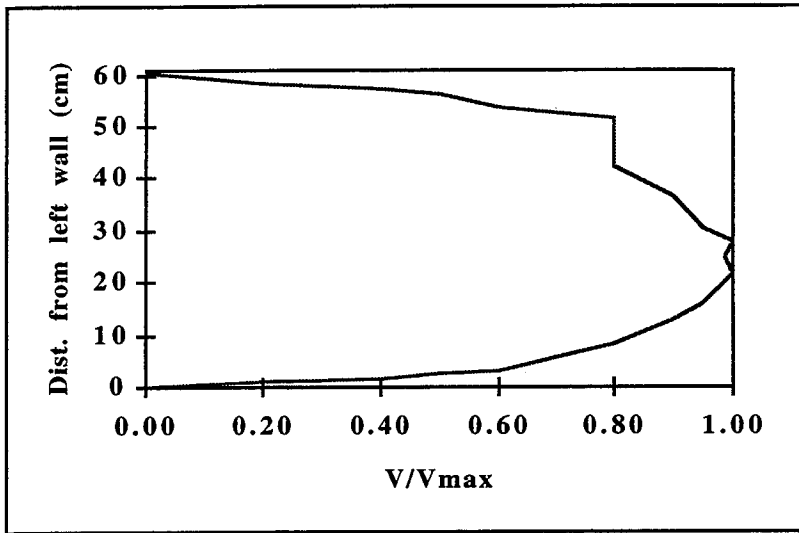


Figure D4.25. Velocity profile for Culvert #2 at $Q = 0.0566$ cms, $1/2\%$ slope, $0.44D_0$, $L/D = 12$, downstream control, $V_{max} = 46.3$ cm/sec.

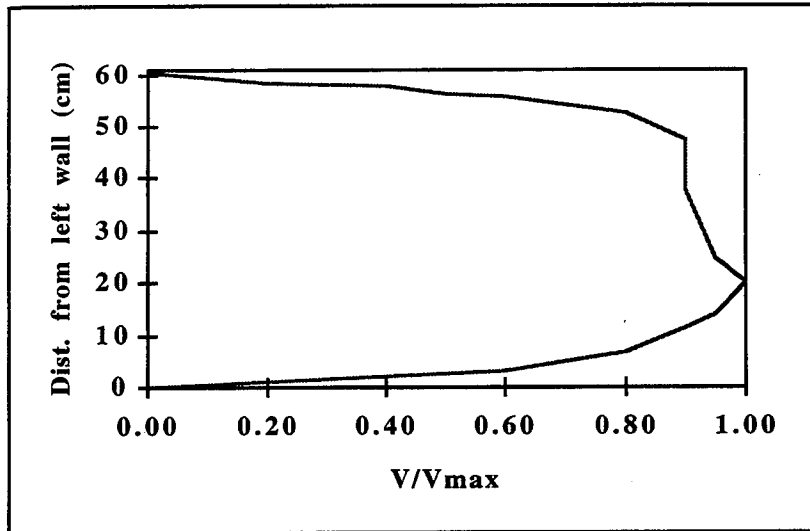


Figure D4.26. Velocity profile for Culvert #2 at $Q = 0.0566$ cms, $1/2\%$ slope, $0.456D_0$, $L/D = 14$, downstream control, $V_{max} = 41.8$ cm/sec.

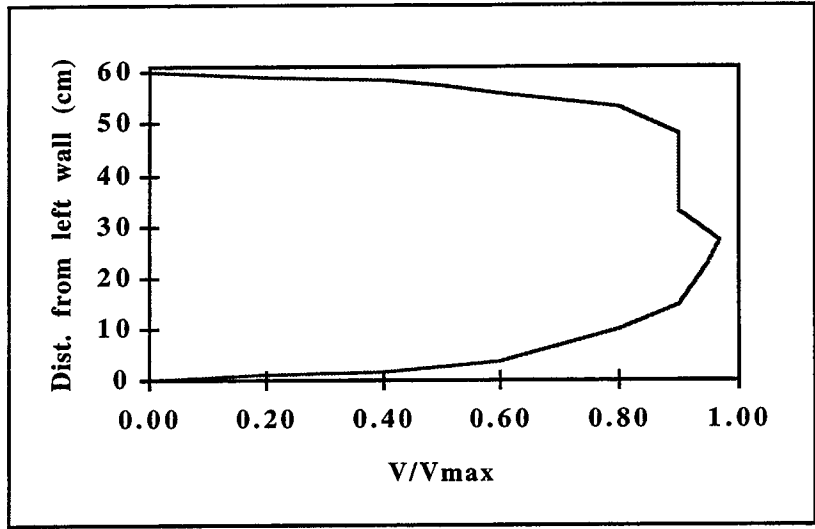


Figure D4.27. Velocity profile for Culvert #2 at $Q = 0.0566$ cms, 1/2% slope, $0.448D_0$, $L/D = 8$, downstream control, $V_{max} = 44.9$ cm/sec.

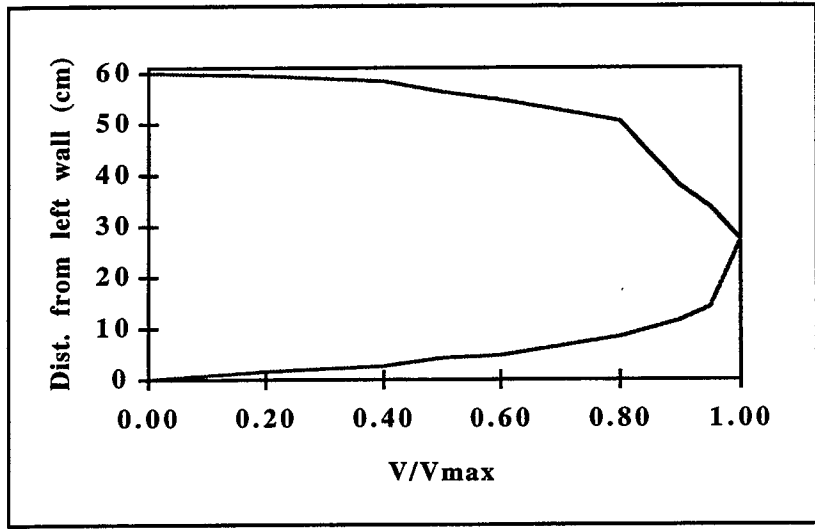


Figure D4.28. Velocity profile for Culvert #2 at $Q = 0.0566$ cms, 1% slope, $0.496D_0$, $L/D = 14$, downstream control, $V_{max} = 37.6$ cm/sec.

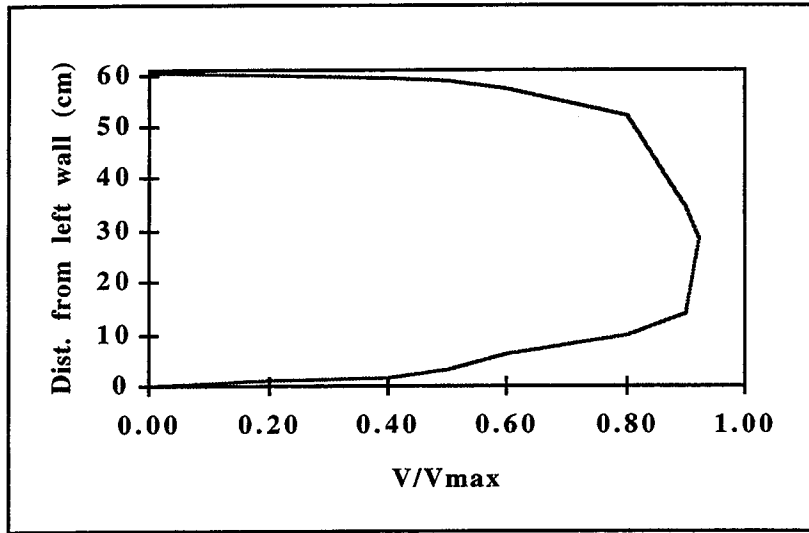


Figure D4.29. Velocity profile for Culvert #2 at $Q = 0.0850$ cms, 1/2% slope, $0.432D_0$, $L/D = 12$, downstream control, $V_{max} = 69.1$ cm/sec.

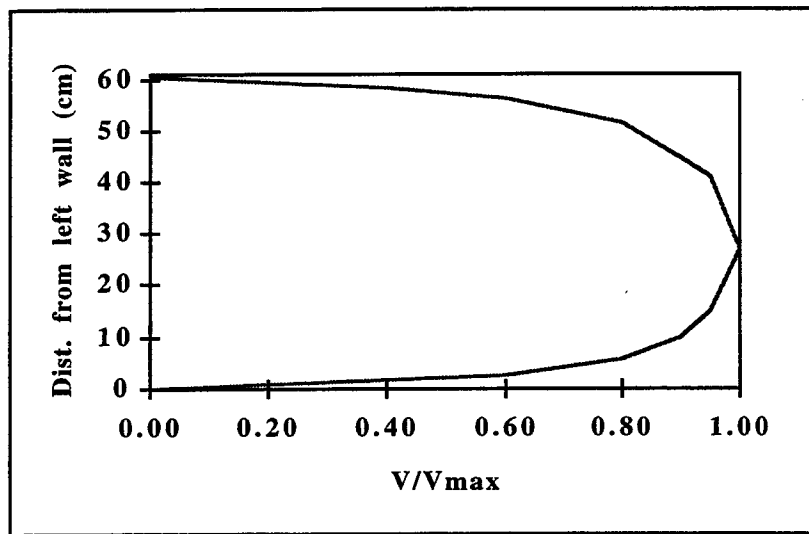


Figure D4.30. Velocity profile for Culvert #2 at $Q = 0.0850$ cms, 1/2% slope, $0.432D_0$, $L/D = 14$, downstream control, $V_{max} = 64.2$ cm/sec.

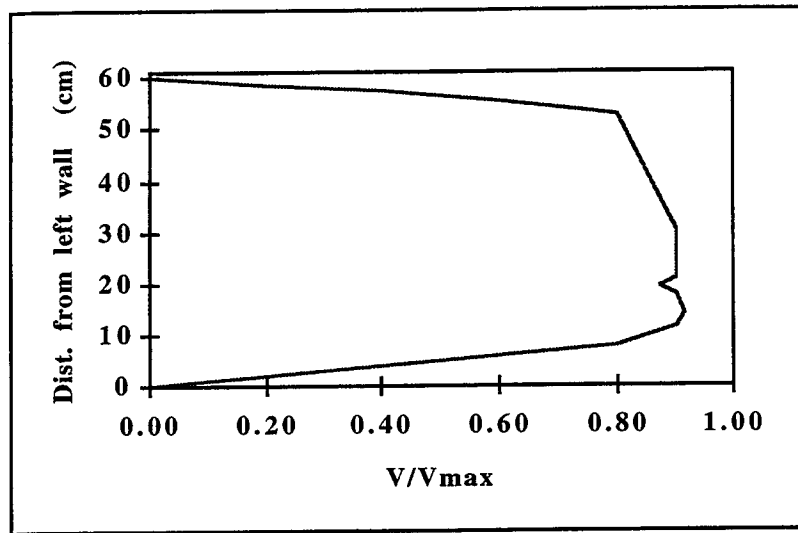


Figure D4.31. Velocity profile for Culvert #2 at $Q = 0.0850$ cms, 1/2% slope, $0.432D_0$, $L/D = 8$, downstream control, $V_{max} = 69.8$ cm/sec.

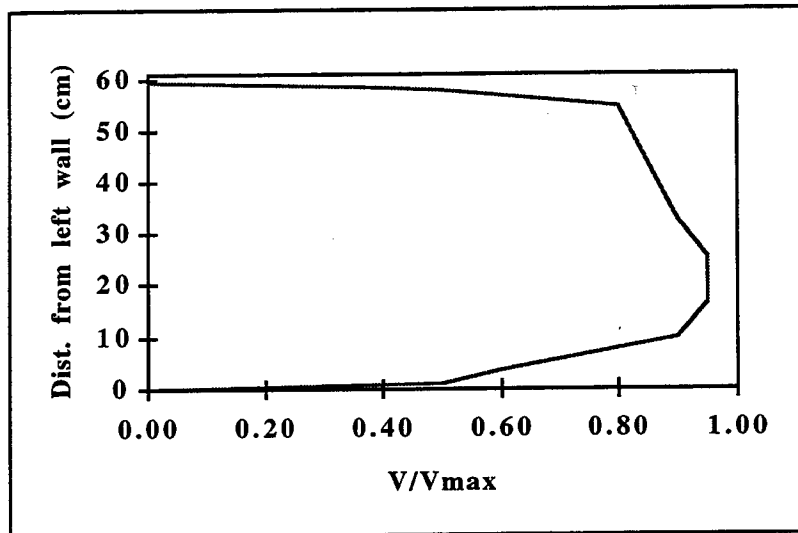


Figure D4.32. Velocity profile for Culvert #2 at $Q = 0.0850$ cms, 1/2% slope, $0.40D_0$, at entrance, downstream control, $V_{max} = 71.5$ cm/sec.

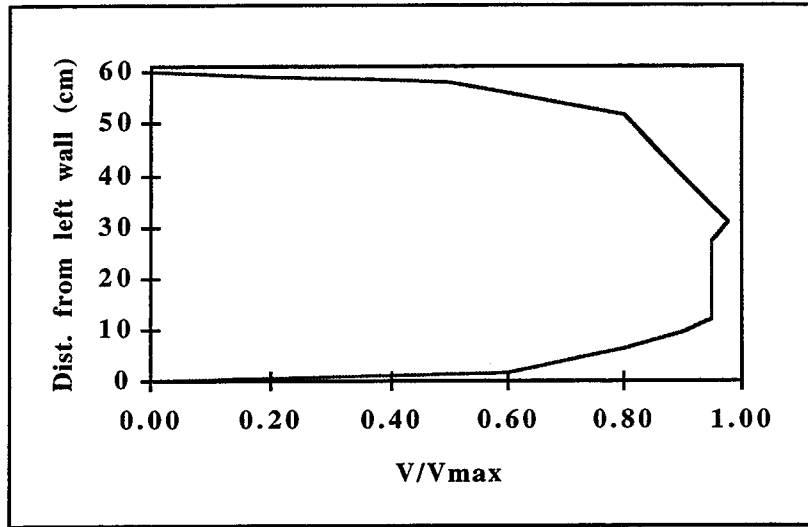


Figure D4.33. Velocity profile for Culvert #2 at $Q = 0.0850$ cms, 1% slope, $0.504D_0$, $L/D = 14$, downstream control, $V_{max} = 58.2$ cm/sec.

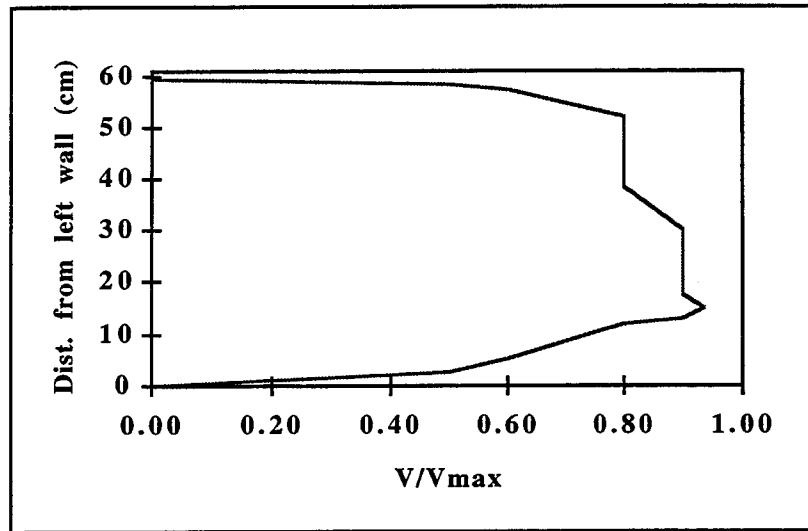


Figure D4.34. Velocity profile for Culvert #2 at $Q = 0.1274$ cms, 1/2% slope, $0.40D_0$, $L/D = 8$, no downstream control, $V_{max} = 118.4$ cm/sec.

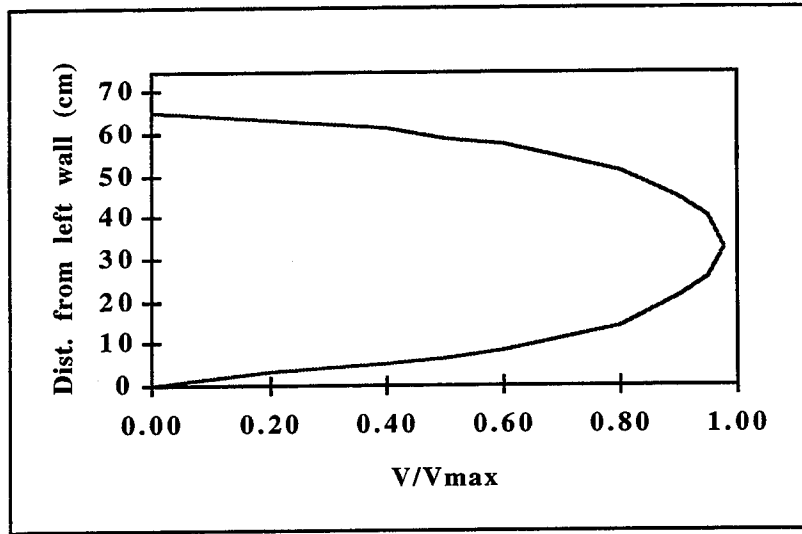


Figure D4.35. Velocity profile for Culvert #3 at $Q = 0.0153$ cms, $1/2\%$ slope, $0.248D_0$, $L/D = 8$, downstream control, $V_{max} = 22.2$ cm/sec.

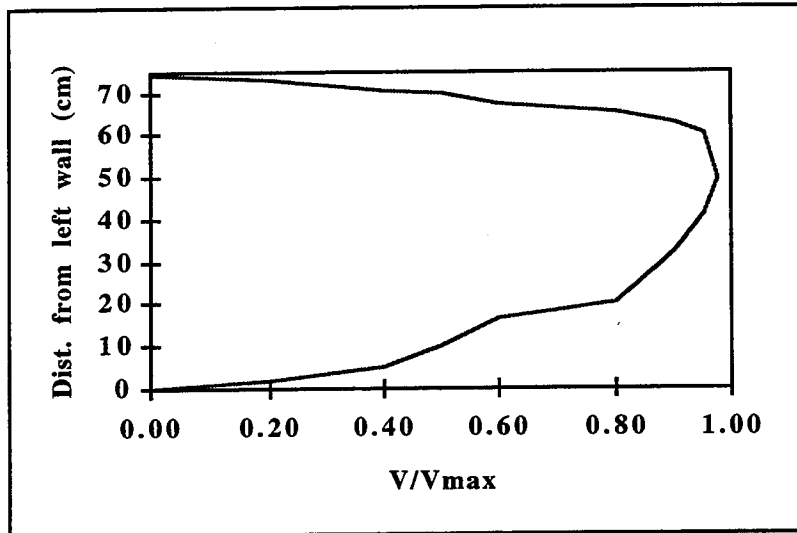


Figure D4.36. Velocity profile for Culvert #3 at $Q = 0.0153$ cms, 1% slope, $0.496D_0$, $L/D = 8$, downstream control, $V_{max} = 9.9$ cm/sec.

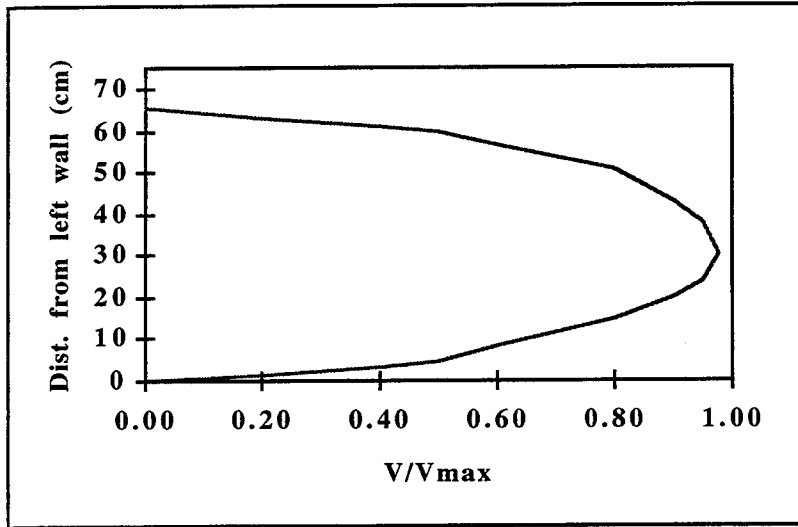


Figure D4.37. Velocity profile for Culvert #3 at $Q = 0.0153$ cms, 1/2% slope, $0.264D_0$, $L/D = 8$, downstream control, $V_{max} = 20.5$ cm/sec.

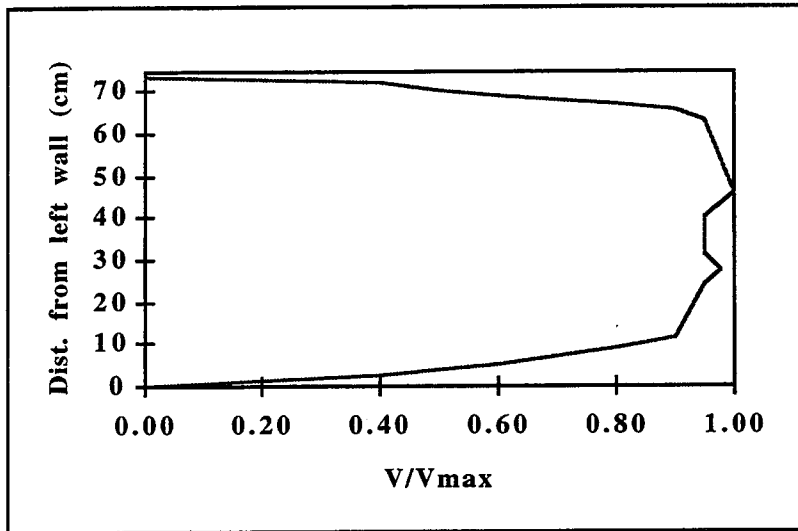


Figure D4.38. Velocity profile for Culvert #3 at $Q = 0.0566$ cms, 1/2% slope, $0.456D_0$, $L/D = 8$, downstream control, $V_{max} = 31.2$ cm/sec.

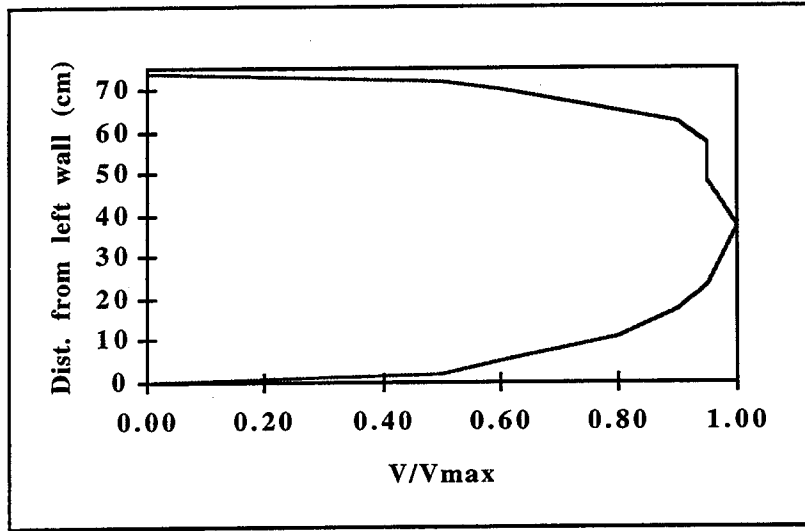


Figure D4.39. Velocity profile for Culvert #3 at $Q = 0.0566$ cms, 1% slope, $0.464D_0$, $L/D = 8$, downstream control, $V_{max} = 33.9$ cm/sec.

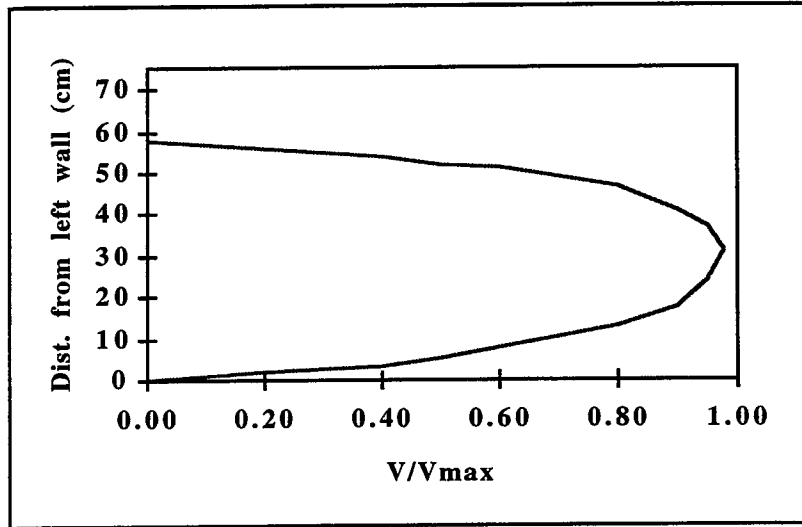


Figure D4.40. Velocity profile for Culvert #3 at $Q = 0.0575$ cms, 1/2% slope, $0.192D_0$, $L/D = 8$, no downstream control, $V_{max} = 120.8$ cm/sec.

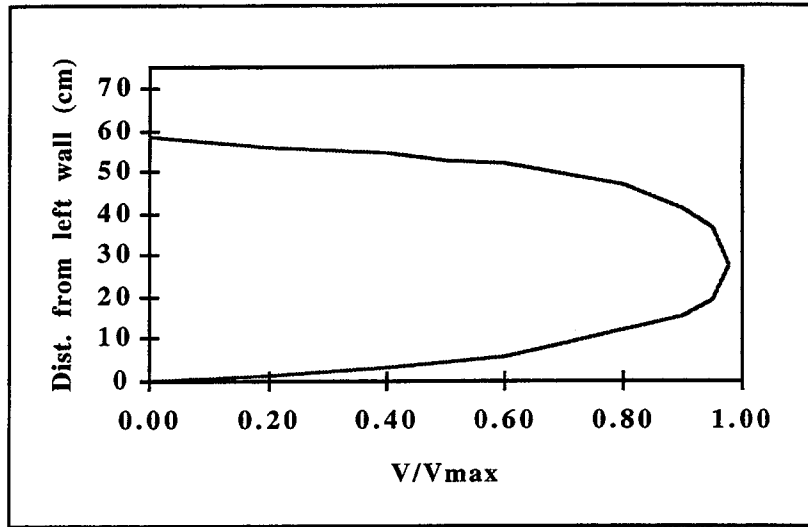


Figure D4.41. Velocity profile for Culvert #3 at $Q = 0.0664$ cms, 1% slope, $0.20D_0$, $L/D = 8$, no downstream control, $V_{max} = 135.1$ cm/sec.

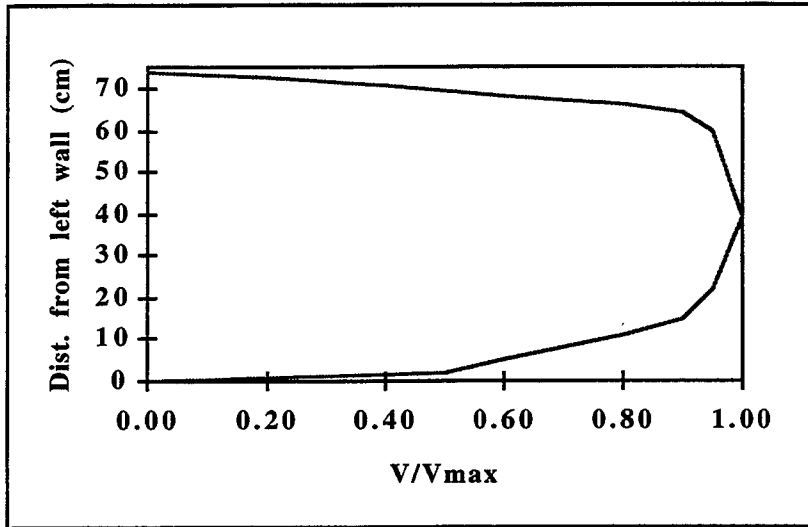


Figure D4.42. Velocity profile for Culvert #3 at $Q = 0.0850$ cms, 1/2% slope, $0.456D_0$, $L/D = 8$, downstream control, $V_{max} = 46.6$ cm/sec.

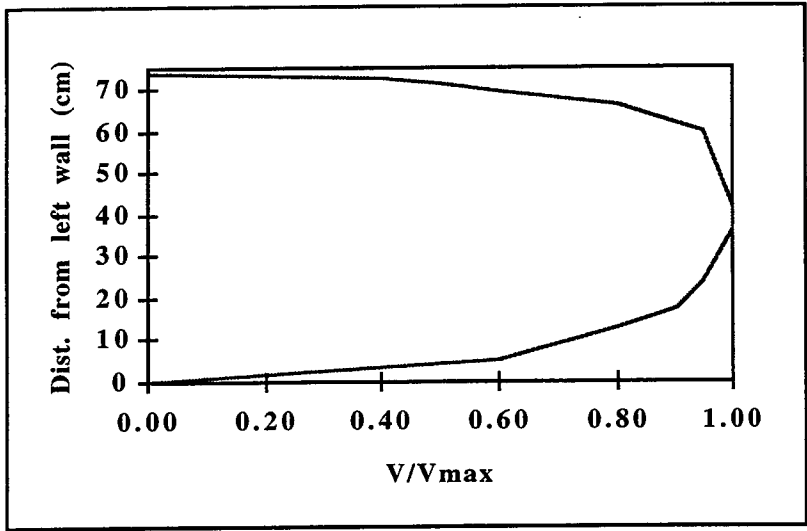


Figure D4.43. Velocity profile for Culvert #3 at $Q = 0.0850$ cms, 1% slope, $0.472D_o$, $L/D = 8$, downstream control, $V_{max} = 44.2$ cm/sec.

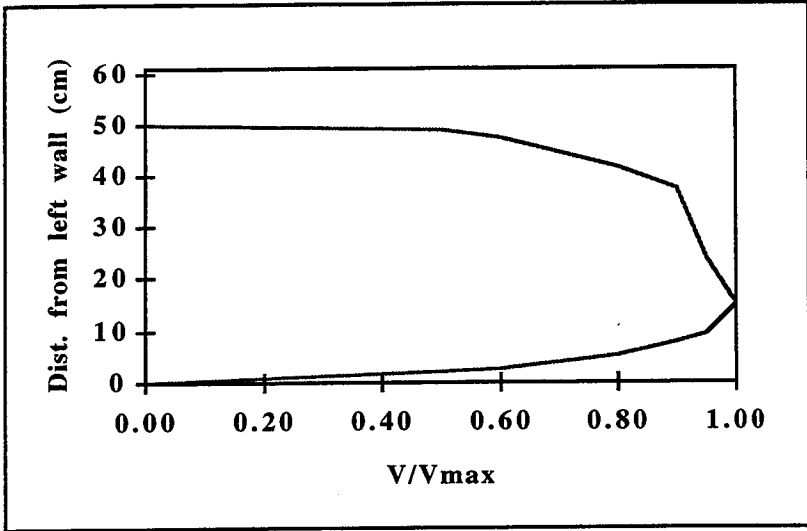


Figure D4.44. Velocity profile for Culvert #4 at $Q = 0.0153$ cms, 1/2% slope, $0.224D_o$, $L/D = 7$, downstream control, $V_{max} = 27.4$ cm/sec.

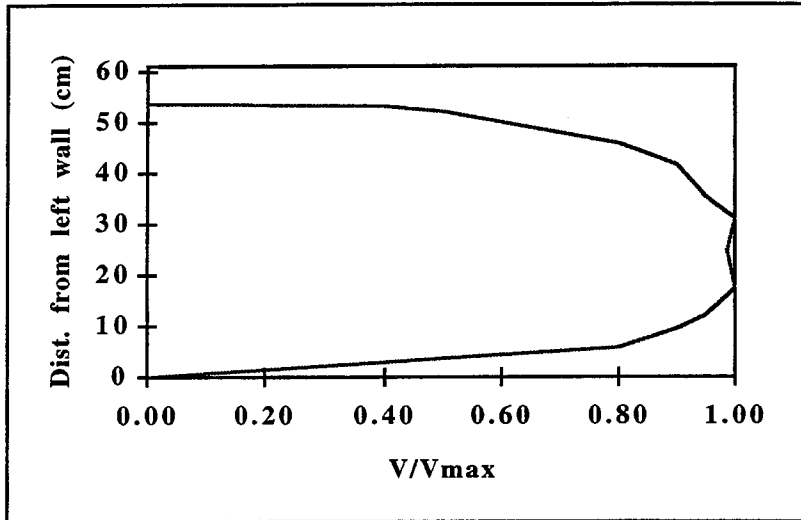


Figure D4.45. Velocity profile for Culvert #4 at $Q = 0.0153$ cms, 1/2% slope, $0.264D_0$, $L/D = 7$, downstream control, $V_{max} = 23.1$ cm/sec.

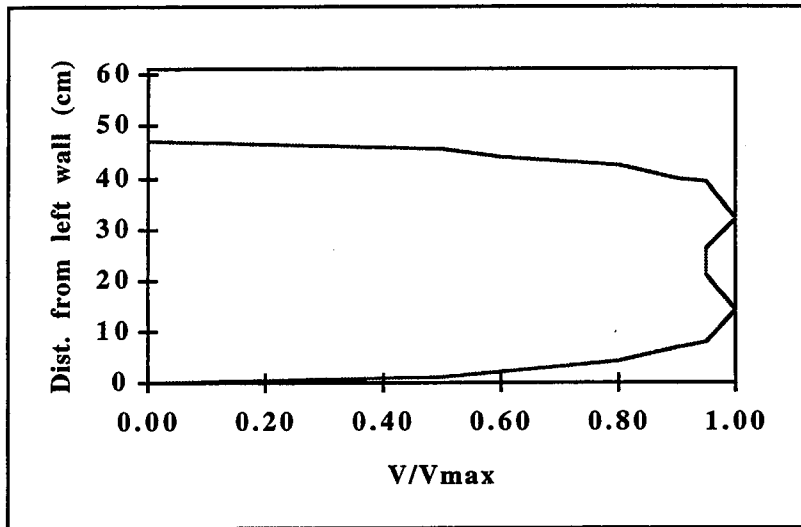


Figure D4.46. Velocity profile for Culvert #4 at $Q = 0.0500$ cms, 1/2% slope, $0.184D_0$, $L/D = 7$, no downstream control, $V_{max} = 127.2$ cm/sec.

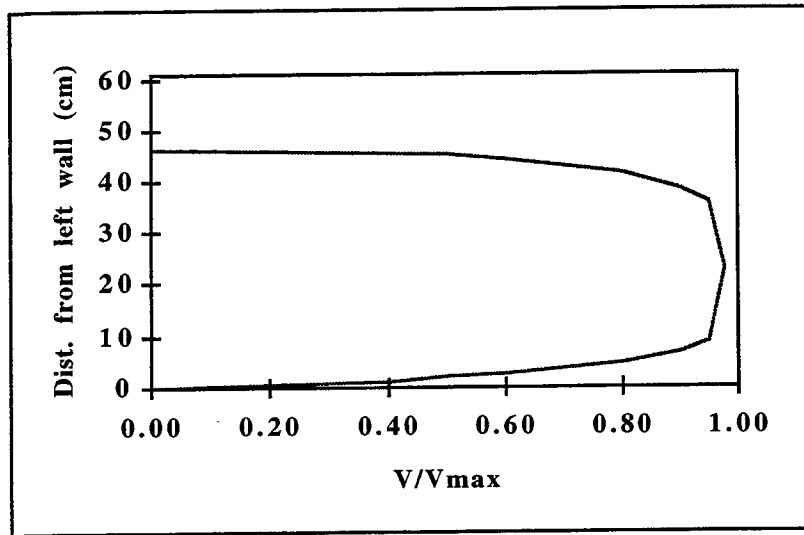


Figure D4.47. Velocity profile for Culvert #4 at $Q = 0.0563$ cms, 1% slope, $0.176D_0$, $L/D = 7$, no downstream control, $V_{max} = 140.2$ cm/sec.

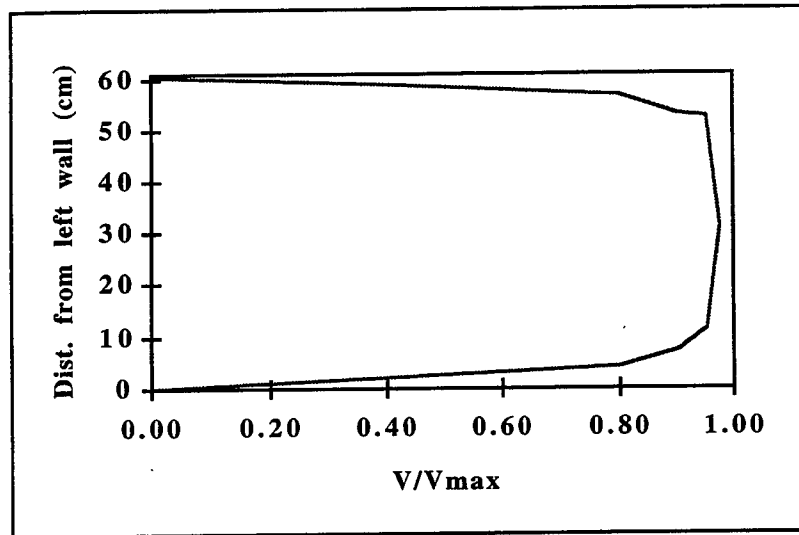


Figure D4.48. Velocity profile for Culvert #4 at $Q = 0.0566$ cms, 1/2% slope, $0.456D_0$, $L/D = 7$, downstream control, $V_{max} = 38.9$ cm/sec.

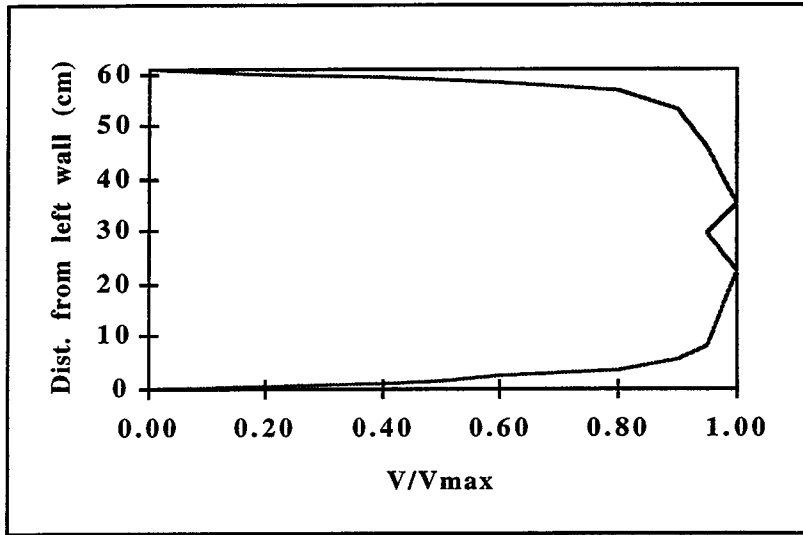


Figure D4.49. Velocity profile for Culvert #4 at $Q = 0.0566\text{cms}$, 1% slope, $0.472D_0$, $L/D = 7$, downstream control, $V_{\text{max}} = 36.8 \text{ cm/sec}$.

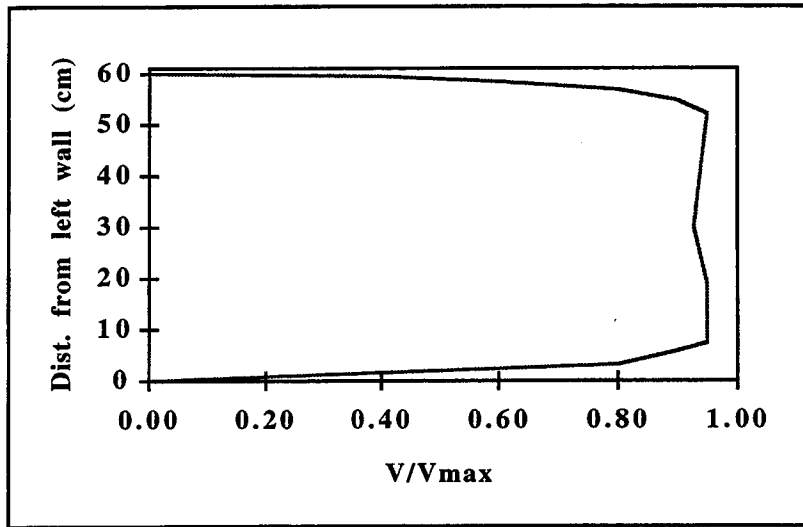


Figure D4.50. Velocity profile for Culvert #4 at $Q = 0.0850\text{cms}$, 1/2% slope, $0.448D_0$, $L/D = 7$, downstream control, $V_{\text{max}} = 59.7 \text{ cm/sec}$.

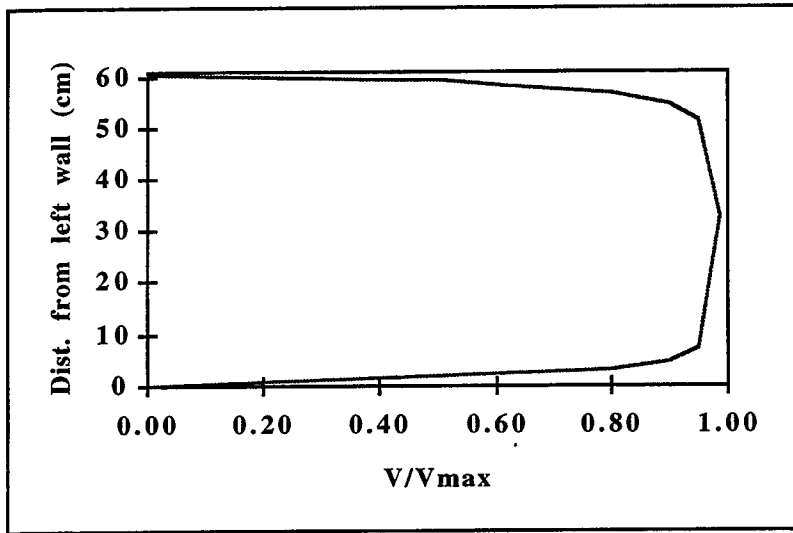


Figure D4.51. Velocity profile for Culvert #4 at $Q = 0.0850 \text{cms}$, 1% slope, $0.464D_o$, $L/D = 7$, downstream control, $V_{\text{max}} = 54.2 \text{ cm/sec}$.

Appendix E
Example Problem

Example Problem

Given the following information, determine the band width and the area of flow with a velocity below the design criteria for juvenile salmon.

Design information:

Design velocity for juvenile fish = 0.5 m/s;
 Discharge (Q) = 1.2 m³/s;
 Pipe slope = 0.25%;
 Culvert diameter (D) = 1.5 m with 7.62 cm x 2.5 cm annular corrugations;
 Manning roughness coefficient (n) = 0.027.

Using an iterative approach with Equation 2.3, the total area of flow and the hydraulic radius can be determined. Recall Equation 2.3:

$$Q = VA = \frac{1}{n} AR^{2/3} S_f^{1/2} \quad (\text{SI Units})$$

For partial pipe flow as shown below in the figure;

$$\text{the flow area (A)} = \frac{1}{8} (\theta - \sin \theta) D_o^2 \quad \text{and the hydraulic radius (R)} = \frac{1}{4} \left(1 - \frac{\sin \theta}{\theta} \right) D_o$$

Choose theta (q) and iterate until desired discharge of 1.2 m³/s is obtained.

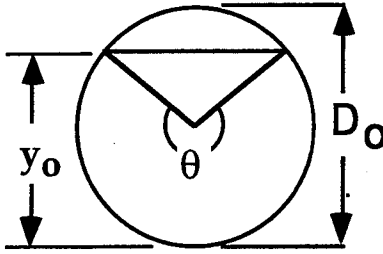
Calculation of flow parameters

Theta radians	n	Slope	Flow Area (m ²)	Hyd. Radius	Calc (Q) (m ³ /s)	Vavg (m/s)
3.40	0.027	0.0025	1.028	0.4031847	1.04	1.01
3.50	0.027	0.0025	1.083	0.4125839	1.11	1.03
3.62	0.027	0.0025	1.148	0.4226898	1.20	1.04
3.70	0.027	0.0025	1.190	0.4286996	1.25	1.05

← OK

Determine the depth of flow (y_o)

$$\text{Depth of flow (y}_o\text{)} = \frac{D_o}{2} + \frac{D_o}{2} \left(\sin \left(\frac{\theta - 3.1416}{2} \right) \right); \quad y_o = 0.93 \text{ m}$$



Partially Full Culvert Cross Section

Using the Mountjoy equation, the bandwidth can be calculated

Recall Equation 2.16:
$$v = A \log_{10} \left(\frac{y}{y_0} \right) + B$$

where v is the velocity at depth y , $A = \frac{(32g)^{1/2} (V_{avg})n}{R^{1/6}}$ and $B = \frac{0.88(8g)^{1/2} (V_{avg})n}{R^{1/6}} + V_{avg}$

Next, calculate A and B using data in the table (all parameters should have consistent units.):

$$g = 9.81 \text{ m/s}^2; V_{avg} = 1.04 \text{ m/s}; n = .027; R = .4227; y_0 = 0.93 \text{ m}$$

Therefore $A = 0.574$ and $B = 1.293$

v = the design velocity for fish passage (0.5 m/s)

Rearranging equation 2.16:
$$\log_{10} \left(\frac{y}{y_0} \right) = \frac{v - B}{A}$$

$$\text{or } y = y_0 10^{\left(\frac{v-B}{A} \right)}$$

Evaluating this equation yields $y = 0.039 \text{ m}$ or **4 cm**.

Thus a band width of 4 cm will have flow velocities lower than 0.5 m/s. The corresponding area of flow with a velocity less than 0.5 m/s is 0.103 m². This is approximately 10% of the total flow cross-sectional area.

Effective Width Calculation:

In their hatchery experiments, WDFW observed juvenile fish swimming in the low velocity boundary layers in the upper corners of the pipe. Moreover, the juvenile fish traveled near the surface within 0.3 times the depth of flow. This observation is consistent with other researchers. As a result of these observations, attempts were made to determine the horizontal velocity profile at $0.8*d$ with the ultimate goal of determining the width of the migration area. The effective area is converted to an equivalent area on each side of the pipe. A trial and error iteration procedure is used to determine the width required to produce that area. The program converts the area determined by the previous method into assumed symmetric areas. Through the use of a Downs Correction Factor (DCF), the widths are scaled down to match those measured in the hydraulic testing program. A range of DCF values from 1 to 4 was plotted Figure 4.27 although the designer is free to choose any positive value depending on the level of safety factor required and the certainty of the design requirements. For example, selecting a value of 3 for a situation with no tail water control produces width estimates which are reasonable or conservative for nearly 67 percent of the cases with an assumed maximum permissible velocity of 38 cm/sec (1.25 feet/second). For the current example problem, this calculation results in a width of approximately 3.0 cm. It will be up to the biological constraints as to whether or not this width is acceptable.

A DCF of 1.0 for tail water conditions provides conservative estimates of widths for nearly all the flow cases tested. As would be expected, measurements of these values were dependent upon the downstream tail water depth, and therefore, varied significantly. However, in most every case (2 exceptions) the correction factor was less than one.

An interesting point must be made concerning the concept of tail water or backwater control. In most instances, no attempt was made to insure backwater conditions existed throughout the pipe. Situations where the outfall is partially submerged but the culvert

resumes near uniform flow conditions at an upstream location within the pipe may produce more severe conditions with respect to fish passage. Consequently, in designs where backwater conditions are expected to dominate the outlet, the designer should make sure that such controls exist throughout the culvert.

A program called JUFIPP - JUvenile FIsh Passage Program was developed to compute the effective widths. The user provides information concerning the discharge, slope, diameter, roughness, DCF, and error tolerance (typically 0.001 meters), and the program computes the width.